Gluonic Excitations in Meson-Meson Systems

Nosheen Akbar

CENTRE FOR HIGH ENERGY PHYSICS
UNIVERSITY OF THE PUNJAB
LAHORE-54590, PAKISTAN

(July, 2011)

Gluonic Excitations in Meson-Meson Systems

By

NOSHEEN AKBAR

Submitted in Partial Fulfillment of the requirements for the Degree of

DOCTOR OF PHILOSOPHY

at

CENTRE FOR HIGH ENERGY PHYSICS
UNIVERSITY OF THE PUNJAB
LAHORE

DECELARATION

This thesis is being submitted to the University of the Punjab, to meet the partial requirements of the "DEGREE OF PHILOSOPHY" in the field of "High Energy Physics". It does not contain any material already submitted for award of any degree or diploma in any university. To the best of my knowledge, there is no material published or written by another person, except with references. If any reference is found missing that would be completely unintentional and I do not pretend to own any credit for that.

Nosheen

Nosheen Akbar

Doctoral Dissertation Certificate

It is certified that I have read this dissertation and that in my opinion; it is adequate in scope and quality as dissertation for the degree of "Doctor of Philosophy" in High Energy Physics.

Associate Prof. Dr. Bilal Masud
(Supervisor)
Centre for High Energy Physics
University of the Punjab
Lahore, Pakistan

Submitted Through:

Prof. Dr. Haris Rashid
(Director)
Centre for High Energy Physics
University of the Punjab
Lahore, Pakistan

To my daughters

Areeba and Nabeeha

Table of Contents

List of Tables

List of Figures

List of Publications

1. Dynamical Implications of Gluonic Excitations in Meson-Meson Systems

(Resubmitted to Physical Review D after minor revisions; Manuscript ID DB10769)

arXiv: 1102.1690v2

2. Wave Function Based Characteristics of Hybrid Mesons

(Submitted to European Physical Journal A; Manuscript ID EPJA-101678)

arXiv: 1106.1690v2

3. Unitarizing the Meson-Meson Phase Shifts with Intermediate Hybrid States

(Manuscript under preparation for Physical Review D)

Abstract

The present work initially describes the gluonic excitations in meson-meson systems by ignoring the spin and flavour. This portion of the work is done by using the $q\bar{q}$ potential in the quadratic potential for ground state mesons, and for hybrid mesons we use an additional smeared $\frac{1}{r}$ potential. For the parameters of this potential, we use values chosen to 1) minimize the error resulting from our use of a quadratic potential and 2) best fit the lattice data for difference of Σ_g and Π_u configurations of the gluonic field between a quark and an antiquark. We use a potential model matrix in the extended $q^2\bar{q}^2$ basis which at quark level is known to provide a good fit to numerical simulations of a $q^2\bar{q}^2$ system in pure gluonic theory for static quarks in a selection of geometries. A combination of resonating group method formalism and Born approximation is used to include the quark motion using wave functions of a $q\bar{q}$ potential within a cluster. At the quark level, including the gluonic excitation was noted to partially replace the need for introducing many-body terms in a multi-quark potential. We study how successful such a replacement is at the (dynamical) hadronic level of relevance to actual hard experiments. Thus we study effects of both gluonic excitations and many-body terms on mesonic transition amplitudes and the energy shifts resulting from the second order perturbation theory (i.e. from the respective hadron loops).

In second portion of thesis work, we go beyond the quadratic potential approximation and use the realistic potential with including the spin and flavour and use the exact wave functions (found by solving the Schrödinger equation numerically) to study relevant characteristics like masses, root mean square radii, and radial wave

functions at the origin. We have done this more accurate and numerically more difficult work only for a $q\overline{q}$ system. The above mentioned characteristics are studied for conventional charmonium mesons as well as for hybrids (with exotic quantum number states with $J^{PC} = 0^{+-}, 1^{-+}$ and 2^{+-} of charmonium hybrid mesons). We use an extension (fitted to the lattice data) of the quark potential model to study the characteristics of hybrids. We treat the ground and excited gluonic field between a quark and an antiquark as in the Born-Oppenheimer expansion, and use the shooting method to numerically solve the required Schrödinger equation for the radial wave functions. From these we calculate the above mentioned quantities; for masses we also check through a Crank Nichelson discretization. We also compare our results with the experimentally observed masses and theoretically predicted results of the other models. Our results have implications for scalar form factors, energy shifts, magnetic polarizabilities, decay constants, decay widths and differential cross sections of conventional and hybrid mesons; we accordingly include some results that can help in experimentally recognizing hybrid mesons.

Acknowledgements

While submitting this thesis for the degree of PhD, I wish to express all praise to Almighty Allah, the Most Merciful, the Most Gracious, for enabling me to carry out this work and all the respects are for the Holy Prophet Muhammad (Peace be upon Him) who enabled me to recognize my Creator. First and foremost, my gratitude goes to my honourable supervisor, Associate Professor Dr. Bilal Masud, University of the Punjab, Lahore, for his guidence, valuable suggestions, sustained encouragement and support during this research.

I am grateful to kind-hearted and compassionate Director of the centre, Prof. Dr. Haris Rashid for providing all the required facilities in the laboratories to complete this work.

I am extremely thankful to all my teachers, laboratory staff, library staff, and office staff of CHEP, University of the Punjab, Lahore, for their devotion and kind co-operation during my course and research work.

I wish to thank my univeristy fellows, Imran Jamil and Ghulam mustafa for their kind cooperation. I will always remember good company of my friends, Sarwat Zahra, Bushra Shafaq and Uzma Ajmal, for all the good and bad times we had together; I shall always remember their collaboration with pleasure.

Finally and most of all, I acknowledge my family to whom I owe a lot more than just thanks for their constant support and encouragement especially my husband, whose admire love and help potentiated me for this work. I am in debt to my loving

parents for all their prayers and good wishes for me. No sentiments are there to express my thanks to my in-laws, who actually encouraged me to enroll for this degree. Without their moral support, care and sustained patience, I would not have been able to complete this work. It is necessary here to say something about my sweetest and the most beloved daughters Areeba and Nabeeha, whose innocent and cute activities, removed all my tensions and made me fresh especially in the hours of stress.

University of the Punjab, Lahore. Nosheen Akbar

July, 2011.

Chapter 1

Introduction

After twelve years of Yukawa's meson hypothesis [1], Powell [2] discovered the first π meson in cosmic rays to understand the nature of the strong force that bounds together the nuclei. In 1960's, a large number of new particles were discovered, and it made sense that all these discovered particles could not be elementary particles. After many years, physicists, Gell-Mann [3] and Zweig [4] introduced quark model that suggested that all hadrons (mesons and baryons) are made of elementary particles called quarks. Mesons with integer spin were modeled as a quark anti-quark pair and baryons with half integer spin made up of three quarks. Now physicists accept that quarks have six flavors; u, d, c, s, t, b. u, c, and t, quarks have fractional electric charge $+2/3e$, and d, s, and b have electric charge $-1/3e$. Another property of quarks was introduced by Greenberg [5] in 1964 , and later by Han and Nambu [6] in 1965 that quarks also have color charge. The colour charge is a conserved quantum number like electric charge. All quarks have an antiparticle with opposite charge and color. An important feature of the quark model is that quarks and antiquarks combine together in such a way that their bound states (called hadrons) should have colour singlet and have integer electric charge.

During 1970's, quark model [3, 4] was considered a complete model for hadron's description. Using this model, many hadron's properties were explained phenomenologically. The great achievement of this model was the prediction of Ω^- (a particle with three $s-$quarks). Quark model [3, 4] can explain meson's properties with certain J^{PC} quantum numbers. But it could not explain the phenomena related to gluon dynamics, such as it could not explain the hybrids (hadrons having gluonic field in the excited state), glue balls (bound states of gluons) [7] that are suggested by QCD.

1.1 Quantum Chromodynamics

Since 1970's, Quantum Chromodynamics (QCD) [8] is considered as the theory of strong interactions. This theory describes interactions between quarks and gluons. Gluons are massless, spin 1 colour charged particles capable of acting as a source of gluonic field. QCD allows colour charge with three types called red, blue, and green. Due to fact of three colours, QCD is an $SU(3)_c$ theory. Quarks interact between each other by exchanging the gluon between them. For the region of large momenta, QCD is well established, where the perturbative methods based on the Feynman diagrams [9] work due to asymptotic freedom [10]. Asymptotic freedom was introduced in 1973 by Gross and Wilczek [10] and Politzer [11] to explain the experiments of deep inelastic scattering (an electron proton scattering). At short interquark distances (or at high energies or momenta), the effective coupling becomes sufficiently small. Therefore higher orders in Feynman diagrams or non-perturbative effects can be neglected as a first approximation, i.e. quarks and gluons interact very weakly. This means that interaction between quarks within hadrons asymptotically converge to zero at short distances.

However, for region of smaller momenta (at large distances, comparable to hadron size (1 fm)), situation is different theoretically and experimentally. In this region, effective coupling becomes large, therefore higher orders in Feynman diagrams cannot be neglected and non-perturbative effects may exist i.e. the interaction between quark and gluon is very strong resulting in quark confinement. Therefore infinite amount of energy is required to separate quarks. In this region another approach is well-established termed as lattice-gauge-theory.

1.2 Lattice-Gauge-Theory

Lattice-gauge-theory was proposed by Wilson [12], Polyakov [13], and Wegner [14]. It is the study of the gauge theories on space time that has been discretised on a lattice. This theory is valid for the study of low energy QCD properties. But this gives only numbers (or numerical results) for selected discrete configurations. These numerical methods are expensive and require much computer time. Thus for an understanding of properties of QCD, models are required.

1.3 QCD Models

The numbers generated by lattice simulations of quantum chromodynamics and continuum models of the hadronic systems can be used to improve models through constraints of getting a least chisquare difference with the numbers for the corresponding discrete quarks and antiquarks configurations. Such lattice-improved models can then be reasonably used for all spatial configurations to eventually give dynamical predictions for experimentally measurable quantities like meson masses, meson-meson bindings and cross-sections and phase shifts (polarization potentials [15]) to meson

masses arising through meson-meson loops, etc. To study the properties of medium and low energy QCD, a large number of models have been developed such as QCD based Potential Model, Flux Tube Model, Sum of two body Potential model, Four body Potential model, etc.

1.3.1 QCD based Potential Model

The most significant model is the potential model in which the quark antiquark interaction (with ground state gluonic field) is modeled by a potential which is given by one gluon exchange mechanism, but is modified to incorporate the confining potential as the limit for large distances. This means that for small inter-quark distance r, the potential is expected to be of the coulomb form (in analogy to the potential between electrically charged particles separated by distance r), and for large inter-quark distances, the quarks are subject to confining forces, and from the linearity of the spin values versus $(mass)^2$ for hadrons, it is deduced that the potential at large r is linear [16]. Thus a favoured QCD potential for ground state gluonic field consists of coulomb plus linear form.

QCD based potential model can be extended to incorporate the gluonic excitations. In the extended QCD potential model an additional term (for excited state potential) is added in the linear plus coulombic potential.

1.3.2 Flux Tube Model

Flux Tube Model [17] for hadrons is based on quarks and flux-tube degrees of freedom. This model is extracted from the strong coupling Hamiltonian lattice formulation of QCD, introduced by John Kogut and Leonard Susskind [18], in which Gauge-invariant

configuration space have a collection of strings with quarks at their ends. The strings are lines of non-abelian electric flux. In this lattice Hamiltonian approach in ref. [18], the full QCD Hamiltonian can be considered as a sum of two pieces; one describes the dynamics of the glue and includes the quark mass term, and other describes the quark dynamics as well as the creation and annihilation of $q\overline{q}$ pair.

In Flux tube model, gluons re-arrange themselves into flux-tubes. In heavy quark limit, these flux tubes adjust their configurations instantaneously in response to quark motion. Thus quarks are constrained to move on adiabatic gluonic energy surfaces. The lowest adiabatic surface corresponds to ground state potential (coulomb plus linear) derivable from lattice gauge theory [19]. States with ground state potential form conventional mesons of quark model, and states with excited state potential correspond to hybrids. Flux tube model [17] is not valid at short inter quark distances.

1.3.3 Potential Models for Multiquark Systems

A successful model of hadrons (strongly interacting particles) should be able to describe possible multiple-quark systems as well [20]. Many models for the study of properties of a multiple quark system properties are developed. The simplest way to extend a two-particle potential model to a few-body is to use the potential for each pair of particles in the few-body system and simply add up such two-body potentials. This approach is used in refs. [21, 22, 23, 24] and is successful in atomic and nucleon systems; the corresponding two-body interaction being described by Coulombic and Yukawa potential, for example. For a hadron (or a system of hadrons) composed of many quarks, antiquarks and the gluonic field, the lowest order perturbative Feynman amplitudes are of this sum-of-pair-wise form. Though Feynman diagrams themselves

become impractical for typical hadronic energies because of larger couplings, models have been tried which simply replace the two-body Coulombic potential (essentially a Fourier transform of the Gluonic propagator) by more general Coulombic-plus-linear form; see refs. [21] [22] [23] [24]. This approach is not free of problems; one phenomenological problem with sum-of-two-body potentials model arises when it is applied to multi-quark systems. It leads to inverse power van der Waals' potentials between separated colour-singlet hadrons [25], which is in contradiction with experimental data. In trying to correct the problems with sum-of-two-body model, in 1990's a four body potential model was proposed [20] [26]. This four body potential model for multi-quark systems is defined by modifying overlap and potential matrices of the weak coupling limit through multiplying their off-diagonal elements by a factor f that depends on the position of all four quarks. f tends to 1 for short distances while it tends to 0 for larger ones. For small distances, this model agrees with two-body potential model results. For distances above 0.5 fermi, it agrees with the flux tube model.

An application of this four-body potential model for meson-meson system ($K\overline{K}$ system)to meson-meson scattering and binding, based on the resonating group method [27], is presented in ref. [20] which includes both the spin and flavor degrees of freedom, extending the formalism presented already in the spin independent situation [26]. This model [20] was applied to $K\overline{K}$ scattering ($K\overline{K} \leftrightarrow \eta\eta$ for isoscalars, and $K\overline{K} \leftrightarrow \pi\eta'$ for isovectors). It is seen that due to four-body modeling of the the gluonic effects in this multi-quark system, the $K\overline{K}$-attraction resulting from the quark exchange mechanism gets appreciably decreased compared to that emerging through the naïve two-body potential approach.

In 1990's A. M. Green and P. Pennanen constructed a potential model [28] for a selection of 6 (static) geometries of a $q^2\bar{q}^2$ system for fixed configuration of two quark two antiquark system in $SU(2)_c$ written in a six states basis with eight parameters $(k_f, f_1^a, f_2^a, k_a, k_c, b_o, a_o, c_o)$. The parameters values proposed by this continuum $qq\bar{q}\bar{q}$ model were chosen to simply minimize

$$\chi^2_A = \frac{1}{N(G)} \sum_{i=1}^{N(G)} (E_i - M_i)^2 / \triangle E_i, \tag{1.3.1}$$

where $N(G)$ is the number of data points for geometry G. $qq\bar{q}\bar{q}$ geometries [28] numerically worked on were squares, rectangles, tetrahedra, etc. with quarks at the corners. For each data point i , the lattice energy E_i was extracted by solving the following eigenvalue equation

$$W^T_{ikl} a^T_{il} = \lambda_i^{(T)} W^{T-1}_{ikl} a^T_{il} \tag{1.3.2}$$

for $\lambda_i^{(T)}$ that approaches to $\exp(-V_i)$ as (Euclidean time) $T \to \infty$, and then subtracting the energy of two separated $q\bar{q}$ clusters from the V_i to get the lattice-generated $qq\bar{q}\bar{q}$ binding energy E_i for the data point. The values of the $\lambda_i^{(T)}$, and thus of E_i, depend only on the numerical values of the elements W^T_{ikl} of the matrix of the Wilson loops. The values of k and l depend on the number of Wilson loops evaluated; for the $qq\bar{q}\bar{q}$ system these were taken to be 1 and 2. Two of the corresponding Wilson operators (whose vacuum expectation values are the Wilson loops W^T_{kl}) are shown in Fig.1.1 [29]. Knowing the Wilson loops, the procedure of getting V_i can be found for example in eqs. 4, 11, 12 and 15 of ref. [30]. The arguments for the continuum limit being achieved before extracting E_i are given in ref. [31]. The M_i in eq.(1.3.1) are obtained by subtracting energy of two separated $q\bar{q}$ clusters from the eigenvalues of

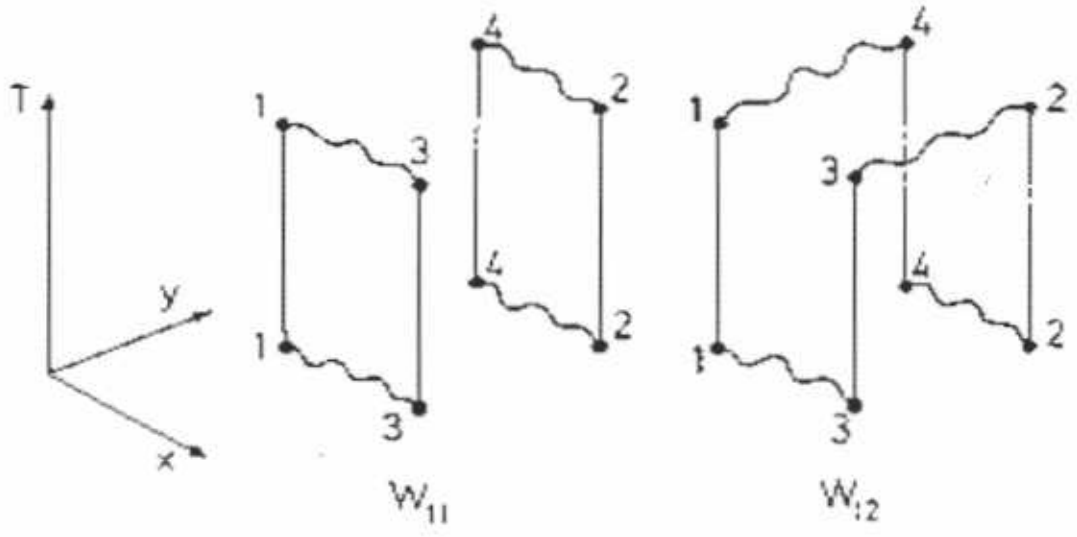

Figure 1.1: Four quark Wilson loops W_{11} and W_{12}

a matrix obtained through a *model* of the $qq\bar{q}\bar{q}$ system. For this, the model has to give a basis and an operator $\widehat{V}$ whose representation with respect to the basis gives a potential matrix V. M_i are obtained by setting the determinant of $V-(M_i+V_{11})N$ equal to zero, with V_{11} being the energy of two separated $q\bar{q}$ clusters and N being the (overlap) matrix (of an identity operator) in the basis. In [28], the dimensionless parameter k_f is used in defining f in eqs.(2.3.1,2.3.2), and its value is mentioned in paragraphs just below these equations and in a paragraph just below eq.(3.3.6). f_1^a, f_2^a, k_a are in eq.(3.0.5), k_c in eq.(3.0.4), b_o, a_o, c_o are parameters used in writing the potential energy matrix elements. In ref. [28], f_1^a and b_o are fixed at 0 and 1, and f_2^a and a_o are related.

To refine the model, both the basis and the operator can be improved. Ref. [28] improve directly the matrix (representation) after writing down the underlying basis.

They do this in a number of ways. One model, termed model II, uses $\{|1\rangle, |2\rangle, |3\rangle\}$ basis but multiplies the off-diagonal elements of overlap and potential energy matrices (that is, the representations of the identity and potential operators

$$\sum_{i<j} v_{ij} \mathbf{F}_i.\mathbf{F}_j$$

respectively) by a few-body gluonic field overlap factor f. Here v_{ij} is the ground state potential energy and $\mathbf{F}_1.\mathbf{F}_2$ are defined in chapter 2 after eq.(2.1.1). This model II was noted to much reduce, at the quark level, the chisquare of eq.(1.3.1). This model has been worked out in [20, 26, 32] till meson-level transition amplitudes. The dynamical calculations require a kinetic energy term as well. That is taken, apart from some technical considerations of hermicity, proportional to the overlap matrix and hence its off-diagonal elements are also multiplied by the overlap f factor. Thus f provides one parametrization that connects QCD simulations with hard experiments.

But model II is not the best model of ref. [28]; the paper continues to then improve the basis by including the gluonic excitations as well. That is, it extends the $\{|1\rangle, |2\rangle, |3\rangle\}$ basis by including the excited states of gluonic field $|1^*\rangle, |2^*\rangle, |3^*\rangle$. (The excited states of gluonic field can, for example, be seen in the QCD numerical simulations; see ref.[33, 19] and others). When the overlap, potential and kinetic energy matrices are written in this extended basis, their order increases to 6×6 rather than previous 3×3. If in addition, we introduce many body terms in this extended model, new kind of gluonic field overlap factors (f^a, f^c) appear in the off diagonal terms resulting in what ref. [28] terms model III giving the least chisqure in ref. [28]; (see eq.(3.3.3) below).

1.4 Brief Sketch of Thesis Work

The purpose of our thesis work is to study the gluonic excitations. In first portion of thesis work, we study these excitations in meson-meson system by ignoring spin and flavour, and using a quadratic $q\bar{q}$ potential. In second portion of thesis, we improve the work by including spin and flavour with realistic potential, but for a quark antiquark system. To study the gluonic excitations in meson-meson system, we work out on the improved model III of ref. [28, 34] till the meson-meson scattering amplitudes and energy shifts. As this improved model III includes the gluonic excitations, it incorporates transitions from four quark ground state to the one having gluonic excitations.

What we add to this series (models introduced in refs. [28, 34]) of works is

1) ourselves writing an analytical quadratic plus exponentially falling expression for the excited state gluonic field potential between a quark and antiquark and fit its parameters to the lattice data for the excited state gluonic field values available for discrete quark antiquark separations in [19] , and

2) use models and fits of ref. [28] to extend the model to a system of diquark, diantiquark and to its gluonic excitations. Precisely, we replace the numerically fitted $0.562 + 0.0696r - \frac{0.255}{r} - \frac{0.045}{r^2}$ ground state quark antiquark potential used in ref. [28] by a constant plus quadratic confining potential term and the *additional* $\frac{\pi}{r} - \frac{4.24}{r^2} + \frac{3.983}{r^4}$ potential for the $q\bar{q}$ gluonic excitation by one of the form $A\exp(-Br^2)$. We have to do this, because we are doing a full meson level dynamical calculations for transition amplitudes from one set of quark-antiquark clusterings (mesons) to the other. From these amplitudes we also calculate polarization potentials [15] for a meson-meson

system. Thus we incorporate quark motion (precisely, wave functions for different $qq\bar{q}\bar{q}$ spatial configurations) as well, whereas the model of ref. [28] specializes to a fixed configuration of the two quarks and two antiquarks. We have to replace the resulting potential formulas of ref. [28] by simpler ones that can be symbolically integrated at a later stage, after necessary multiplications by wave functions of $qq\bar{q}\bar{q}$ positions, to complete the adiabatic-approximation-based treatment of a $qq\bar{q}\bar{q}$ system. In adiabatic approximation, in first step quarks and antiquarks are considered fixed at definite points (or ignore the kinetic energy term), so that only gluonic part of wave function is discussed. Then consider the slow motion as compared to gluonic dynamics.

A worth-mentioning aspect we have studied is the hadron-level implications of the differences of the gluonic-excitation-including model III and the sum-of-pair-wise approach. The quark-level work in ref. [28] can be interpreted to mean that with suitable extensions and modifications something like a sum-of-pairs approach can be a good approximation for a tetraquark system as well. It writes "At the shortest distances, upto about 0.2fm, perturbation theory is reasonable with the binding being given mainly by the $|1\rangle$, $|2\rangle$, and $|3\rangle$ states inter-acting simply through the two-quark potentials with little effect from four-quark potentials". However, ref. [28] tells, "for large inter-quark distance (greater than 0.5 fermi), quark-pair creation can no longer be neglected. However, in the intermediate energy range, from about 0.2 to 0.5 fm, the four-quark potentials act in such a way as to reduce the effect of the $|1\rangle$, $|2\rangle$, and $|3\rangle$ states so that the binding is dominated by the $|1^*\rangle$, $|2^*\rangle$, and $|3^*\rangle$ states, which now interact among themselves again simply through the two-quark potentials with little effect from four-quark potentials." This suggests that a model involving only

two-quark potentials could be justified provided excited gluon states (such as $|1^*\rangle$, $|2^*\rangle$, $|3^*\rangle$) are included on the same footing as the standard states $|1\rangle$, $|2\rangle$,$|3\rangle$. We have checked if such features survive at the experimentally meaningful hadron level, by comparing the dynamical implications of

(1) a model extended to the gluonic excitations but otherwise sharing many features with the sum-of-pair-wise approach, with

(2) a model that includes explicit many-body terms but does not include gluonic excitations.

Thus we report if after including the gluonic excitations a sum-of-two-body potential model can replace to some extent many-body potential terms in a tetraquark system *even at a hadronic level.* Specifically, we have calculated in both kind of models meson-meson transition amplitudes T_{ij} from (i) a ground state meson-meson clustering to (j) a different ground-state clustering and to a clustering of gluonic-excited mesons. T_{ij} are elements of the meson-meson scattering theory T-matrix, can be termed as phase shifts, transition potentials or meson-meson coupling, and their absolute squares give meson-meson differential cross sections [23]. Moreover, using these transition amplitudes in the second order perturbation theory we calculate shifts in a ground state meson-meson energy due to coupling to a different ground-state clustering and due to coupling to an excited state meson-meson system (i.e. to *hybrid loops*). These energy shifts are what are also termed polarization potentials [15].

To reach the hadronic level, we have included quark motion through quark wave functions. To solve for quark position wave functions, there are a number of methods used such as variational method [21, 22], Born-order diagrams [23], and resonating group method [10]. Variational approach is used by Weinstein and Isgur [21, 22] to

optimize a meson-meson wave function in a quadratic (and later coulomb plus linear) potential and a hyperfine term combined with a sum-of-two-body approach. Then they projected the meson-meson state onto free meson wave functions to estimate a relative two meson wave function which gives the equivalent meson-meson potential and obtained the meson-meson phase shifts. The similar results can be obtained by using Born-order quark exchange diagrams [23] in a non-relativistic potential model to describe low energy scattering of $q\bar{q}$ mesons. In the present paper, a formalism of resonating group method is used as used in [26]. In resonating group method, dependence on the internal co-ordinates of the system is specified before solving the problem to integrate out the degrees of freedom corresponding to the internal coordinates of clusters of the system. At a later stage, because of the complexity of the calculations we also specify the dependence on the vectors connecting the centers of masses of our mesonic clusters, something that is done in a Born approximation. Moreover, we have not included in our basis an explicit diquark-diantiquark state. In the weak coupling limit such a state is a linear combination of the meson-meson states and thus cannot be included in a basis. Away from the weak coupling this can be included. But its inclusion in the basis did not affect the lattice simulations that based the work in ref. [28] and thus we have expanded our two-quark two antiquark wave function in a basis that is limited to four meson-meson states: ground and excited states for each of the two possible $qq\bar{q}\bar{q}$ clusterings shown in fig. 2.2.

In this work, we have taken all the constituent quark masses to be same as that of a charm quark. Without incorporating flavor and spin dependence, the purpose of this chapter is to study certain features of including the gluonic excitations in

our basis. But the calculations may be relevant to properties of open charm meson-meson systems in limit of mass of other quark approaching that of the charm quarks and antiquark in the system. Or, without incorporating antisymmetrization of the identical quarks and antiquarks, This chapter may indicate certain features of the couplings of some suggested mesons like $\psi(4040)$, $\psi(4415)$,$\psi(3770)$ and $\psi(4160)$ as reported in ref. [35] [36]. These particles are suggested to have the flavor content of $(cc\overline{c}\overline{c})$.

In this thesis work, some characteristics (masses, root mean square radii and wave functions at the origin) obtainable through the numerically generated solutions of non-relativistic Schrödinger equation (also used in ref. [19]) for conventional and hybrid mesons are studied by including the spin and flavour degrees of freedom. Reviews of the spectrum of these excited states can be found in ref. [37] [38]. An advantage of considering the charmonium mesons is indicated in ref. [39] as

> "The best systems for a hybrid search may be $c\bar{c}$ or $b\bar{b}$ where there is a large gap between the lowest states and the $D\overline{D}$ and $B\overline{B}$ threshod respectively."

To find the wave functions of conventional charmonium mesons, we use the realistic columbic plus linear potential model to solve the Schrödinger equation numerically by taking the corresponding quantum numbers of mesons. To study hybrids, we repeat the numerical work with the columbic plus linear potential plus exponentially falling potential. From the numerically found wave functions, we calculate the root mean square radii. These radii can be used to find scalar form factors [40] for charmonium mesons, along with energy shifts [41] and magnetic polarizabilities [41]. Thus we have reported some predictions about these quantities for conventional and

hybrid charmonium mesons. We have also found the numerical value of radial wave function square at the origin ($|R(0)|^2$), which can be used to calculate the decay constants [42], decay rates [42], and differential cross sections [43] for quarkonium states. The predictions about these quantities are also reported in chapter 5 for conventional and hybrid charmonium mesons.

In Chapter 2, the potential models (sum of two body potential model and four body potential model) in three gluonic basis is introduced for the static quarks. Basically, in this chapter we incorporate the quark motion through a resonating group method formalism which means pre-specifying quark-antiquark wave functions within $q\bar{q}$ clusters. The coupled integral equations for the remaining inter-cluster wave function $\chi_K(\mathbf{R}_K)$ are also written in this chapter, and $\mathbf{R}_K$ is defined in eq.(2.3.5). In Chapter 3, the potential model in six basis in the pure gluonic theory is introduced for the static quarks. We tell where does the model of ref. [28] fits in our full scheme that incorporates the quark motion through a resonating group method formalism which means pre-specifying quark-antiquark wave functions within $q\bar{q}$ clusters. Then coupled integral equations for inter-cluster wave functions $\chi_K(\mathbf{R}_K)$ and $\chi^*_K(\mathbf{R}_K)$ are derived. These integral equations are solved to calculate the transition amplitudes and energy shifts. In previous chapters, Hamiltonians (matrix representation) are written for multiquark system (without spin and flavour basis states) with quadratic potential. But in Chapter 4, the Hamiltonians are written for realistic coulombic plus linear potential and improved by incorporating spin and flavour degrees of freedom but limited to a $q\bar{q}$ system for the conventional and hybrid mesons. Then shooting method-based numerical procedure is described to find the solution of the Schrödinger equation for conventional charmonium mesons. The expressions used to find masses,

root mean square radii, and square of radial wave functions at the origin ($|R(0)|^2$) of conventional and hybrid charmonium mesons are also written in this chapter. The numerical results for meson-meson system transition amplitudes and energy shifts with concluding remarks are given in chapter 5. The partial wave analysis for meson-meson scattering results are also reported in chapter 5. Results (for $q\overline{q}$ or $q\overline{q}(g)$) for the masses, root mean square radii and $|R(0)|^2$ of conventional and hybrid mesons are also reported in this chapter for systems composed of charm quarks and antiquarks. Based on these results, some results related to experimentally measurable quantities are also reported.

Chapter 2

The Potential Model for Meson-Meson Systems in Three Gluonic Basis (Ignoring Spin and Flavour)

In this chapter the potential model for the meson-meson systems is described as already introduced in refs. [26, 20]. For this the $q^2\overline{q}^2$ hamiltonian is written in the gluonic basis using the quark antiquark potential model ignoring the spin and flavour. Due to the neglect of spin, isospin, and flavour, spin and flavour basis are not mentioned. Therefore hyperfine term in the potential is also neglected that leaves us with only the gluonic basis and quark spatial dependent part of the wave function. Introducing overlap, potential, and kinetic energy matrices in the gluonic basis, and using the formalism of resonating group method [27], coupled integral equations are derived in this chapter.

2.1 Sum-of-Two-Body Potential Model for Meson-Meson Systems

In sum-of-two-body potential model, potential part of the hamiltonian of the $q^2\overline{q}^2$ is a sum of two-body potentials between each pair (i,j) of quarks antiquarks [20, 22]. Using the two-body potential model, the Hamiltonian [22] for meson-meson systems in a sum-of-pair-wise interaction form, described as

$$H = -\sum_{i=1}^{4}\left[m_i + \frac{\widehat{P}_i^2}{2m_i}\right] + \sum_{i<j} v_{ij}\mathbf{F}_i.\mathbf{F}_j. \tag{2.1.1}$$

In the above equation, m_i is the mass and $\widehat{P}_i$ is the momentum of the ith particle (quark or anti-quark) and $\hat{V} = \sum_{i<j} v_{ij}\mathbf{F}_i.\mathbf{F}_j$ is the potential energy operator. v_{ij} is the quark-antiquark potential mentioned below in eqs.(2.3.17,2.3.18). Here $\mathbf{F}_i$ (operating on i_{th} particle) has eight components. Each component is equal to $\frac{\lambda_i}{2}$, where λ_i are the Gell-Mann matrices. For quarks $\mathbf{F} = \frac{\lambda}{2}$, and for antiquarks $\frac{-\lambda^*}{2}$ [22]. The matrix elements of $\mathbf{F}_i.\mathbf{F}_j$ are written in Appendix with colour basis $\mid 1\rangle, \mid 2\rangle$, and $\mid 3\rangle$. In four quark system, the basis corresponding to three different topologies (shown in Fig.2.2 as in ref. [20]) are defined as

$$\mid 1\rangle_g = (q_1q_3)(q_2q_4), \quad \mid 2\rangle_g = (q_1q_4)(q_2q_3), \text{ and } \quad \mid 3\rangle_g = (q_1q_2)(q_3q_4). \tag{2.1.2}$$

In this basis, the overlap matrix N is written in ref. [26, 20] as

$$N = {}_g\langle k \mid l\rangle_g = \begin{bmatrix} 1 & 1/3 & 1/\sqrt{3} \\ 1/3 & 1 & -1/\sqrt{3} \\ 1/\sqrt{3} & -1/\sqrt{3} & 1 \end{bmatrix}, \tag{2.1.3}$$

with $k, l = 1, 2, 3$.

Using the matrix elements of $\mathbf{F}_i.\mathbf{F}_j$ in basis $\mid 1\rangle, \mid 2\rangle$, and $\mid 3\rangle$ listed in Appendix, the matrix elements of operator $\hat{V}$ (introduced above just after eq.(2.1.1)) becomes

$$\hat{V} =_g \langle k \mid V \mid l \rangle_g = \begin{bmatrix} V_{11} & V_{12} & V_{13} \\ V_{21} & V_{22} & V_{23} \\ V_{31} & V_{32} & V_{33} \end{bmatrix}, \tag{2.1.4}$$

where

$$\begin{aligned} V_{11} &= -\frac{4}{3}(v_{1\bar{3}} + v_{2\bar{4}}) \\ V_{12} = V_{21} &= \frac{4}{9}(v_{12} + v_{\bar{3}\bar{4}} - v_{1\bar{3}} - v_{2\bar{4}} - v_{1\bar{4}} - v_{2\bar{3}}) \\ V_{13} = V_{31} &= \frac{2}{3\sqrt{3}}\big(- 2(v_{1\bar{3}} + v_{2\bar{4}}) + v_{1\bar{4}} + v_{2\bar{3}} - v_{12} - v_{\bar{3}\bar{4}}\big) \\ V_{23} = V_{32} &= \frac{2}{3\sqrt{3}}\big(2(v_{1\bar{4}} + v_{2\bar{3}}) + v_{12} + v_{\bar{3}\bar{4}} - v_{2\bar{4}} - v_{1\bar{3}}\big) \\ V_{22} &= -\frac{4}{3}(v_{1\bar{4}} + v_{2\bar{3}}) \\ V_{33} &= -\frac{1}{3}\big(2(v_{12} + v_{\bar{3}\bar{4}}) + v_{1\bar{3}} + v_{2\bar{4}} + v_{1\bar{4}} + v_{2\bar{3}}\big) \end{aligned} \tag{2.1.5}$$

This sum-of-pair-wise interaction approach has many phenomenological successes, but it is not free of problems; for example it leads to inverse power van der Waals' potentials [25] between separated colour-singlet hadrons, which are in contradiction with experimental data. Nevertheless this model has many phenomenological successes and it is worthwhile inquiring if

1) it provides a basis and operator to generate a potential matrix, and

2) how good is the chisquare (defined in eq.(1.3.1)) if the eigenvalues (E_i) of the resulting matrix are used as M_i in eq.(1.3.1).

The answer provided by ref. [28] and earlier related works is that the model does generate a matrix of the required kind. But the resulting chisquare, defined by eq.(1.3.1), is too bad; see Fig.2.1 (Fig.4 of ref.[44]).

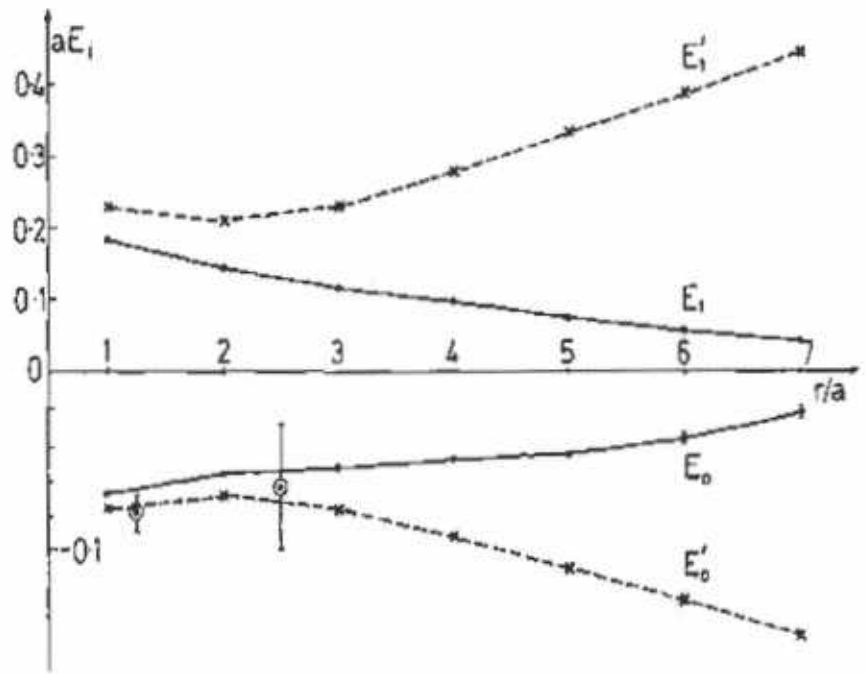

Figure 2.1: $E_{0,1}$ from Monte Carlo simulation and $E'_{0,1}(f = 1)$ from the 2×2 model as shown in Fig.4 of ref. [44].

2.2 Modified Potential Model for Meson-Meson Systems

In trying to correct the problems with the sum-of-two-body potential model, in 1990's four body potential model named f-model was proposed [26] [20]. This four body potential model for multiquark systems is defined by modifying the overlap and potential matrices (in eqs.(2.1.3,2.1.4)) of weak coupling limits through multiplying their off-diagonal elements by a factor f. In this four body potential model [26, 20] overlap, potential and kinetic energy matrices are defined as

$$N =_g \langle k \mid l \rangle_g = \begin{bmatrix} 1 & f/3 & f/\sqrt{3} \\ f/3 & 1 & -f/\sqrt{3} \\ f/\sqrt{3} & -f/\sqrt{3} & 1 \end{bmatrix}, \tag{2.2.1}$$

$$V =_g \langle k \mid V \mid l \rangle_g = \begin{bmatrix} V_{11} & V_{12} & V_{13} \\ V_{21} & V_{22} & V_{23} \\ V_{31} & V_{32} & V_{33} \end{bmatrix}, \tag{2.2.2}$$

where

$$\begin{aligned}
V_{11} &= -\frac{4}{3}(v_{1\bar{3}} + v_{2\bar{4}}) \\
V_{12} = V_{21} &= \frac{4}{9} f(v_{12} + v_{\bar{3}\bar{4}} - v_{1\bar{3}} - v_{2\bar{4}} - v_{1\bar{4}} - v_{2\bar{3}}) \\
V_{13} = V_{31} &= \frac{2}{3\sqrt{3}} f\big(-2(v_{1\bar{3}} + v_{2\bar{4}}) + v_{1\bar{4}} + v_{2\bar{3}} - v_{12} - v_{\bar{3}\bar{4}}\big) \\
V_{23} = V_{32} &= \frac{2}{3\sqrt{3}} f\big(2(v_{1\bar{4}} + v_{2\bar{3}}) + v_{12} + v_{\bar{3}\bar{4}} - v_{2\bar{4}} - v_{1\bar{3}}\big) \\
V_{22} &= -\frac{4}{3} f(v_{1\bar{4}} + v_{2\bar{3}}) \\
V_{33} &= -\frac{1}{3} f\big(2(v_{12} + v_{\bar{3}\bar{4}}) + v_{1\bar{3}} + v_{2\bar{4}} + v_{1\bar{4}} + v_{2\bar{3}}\big)
\end{aligned} \tag{2.2.3}$$

and

$$KE =_g \langle k \mid KE \mid l \rangle_g = N^{\frac{1}{2}}_{k,l} \Big(\frac{-1}{2m} \sum_{i=1}^{4} \nabla_i^2\Big) N^{\frac{1}{2}}_{k,l}. \tag{2.2.4}$$

2.3 The Gluon Field Overlap Factor

The best form of the gluonic field overlap factor, f, is suggested by ref. [28] as

$$f = exp[-b_s k_f S], \tag{2.3.1}$$

with S being minimal surface area bounded by external lines obtained by joining the position of quarks and anti-quarks, and b_s is string tension [17]. k_f is a dimensionless parameter and in ref. [28] $k_f = 0.57$ is obtained by a fit of simplest two state area-based model (named as I_a) to numerical results for a selection of meson-meson geometries.

In ref. [45] the gluonic field overlap factor f is used in Gaussian form as

$$f = exp[-k_f b_s \sum_{i<j} r_{ij}^2], \tag{2.3.2}$$

employed in $SU(3)_c$ for interpreting results in terms of the potential for the corresponding heavy-light meson. In ref. [45], the simulations are fitted by using f when the gluonic field is in the ground state i.e. overlap matrix is a 2×2 matrix. For a particular geometry, the above mentioned forms of f are related. Therefore parameter k_f in eq.(2.3.1) and corresponding k_f in eq.(2.3.2) can be compared for a particular geometry. It is noted that, after corrections for a ratio of 8 between sum of square of distance (including two diagonals) and area for square geometry, the relative difference is just 5%; $k_f = 0.6$ [45] for the sum of square of distances in eq.(2.3.2) and $k_f = 0.57$ [28] in case of minimal area in eq.(2.3.1). We used k_f multiplying sum of area form of f (written in eq.(2.3.2)) with $k_f = 0.6$ (as used in [45]) for numerical convenience.

2.3.1 The Quark Motion and Overlap, Potential Energy, Kinetic Energy Matrices

In the adiabatic approximation the quarks antiquarks are considered fixed at definite points in first stage, so that only gluonic part of the wave function is discussed, then considered the slower motion as well. Using this approximation, the total state vector of a system containing two quarks, two anti-quarks and gluonic field between them can be written as sum of product of quark position dependence function $\phi_k(\mathbf{r}_1, \mathbf{r}_2, \mathbf{r}_{\overline{3}}, \mathbf{r}_{\overline{4}})$ and gluonic field states $\mid k\rangle_g$. (The gluonic state $\mid k\rangle_g$ is defined as a state approaching to colour state $\mid k\rangle_c$ in the limit of quark anti-quark separation approaching to zero.)

The function $\phi_k(\mathbf{r}_1, \mathbf{r}_2, \mathbf{r}_{\overline{3}}, \mathbf{r}_{\overline{4}})$ can be written as

$$\phi_k(\mathbf{r}_1, \mathbf{r}_2, \mathbf{r}_{\overline{3}}, \mathbf{r}_{\overline{4}}) = \phi_k(\mathbf{R}_c, \mathbf{R}_K, \mathbf{y}_K, \mathbf{z}_K),$$

with $k, K = 1, 2, 3$. R_c is overall center of mass co-ordinate of the whole system. Here two different symbols k and K are used just for convenience in using these equations in the next chapter in which the similar work is done in extended basis (ground and excited state gluonic basis). In chapter 3, $k = 1, 2, 3, 1^*, 2^*, 3^*$ but K values remains unchanged.

With notation of Fig.2.2, the relative co-ordinates $\mathbf{R}_1, \mathbf{R}_2$, and $\mathbf{R}_3$ are defined as

$$\mathbf{R}_1 = \frac{1}{2}(\mathbf{r}_1 + \mathbf{r}_{\overline{3}} - \mathbf{r}_2 - \mathbf{r}_{\overline{4}}),\ \mathbf{y}_1 = \mathbf{r}_1 - \mathbf{r}_{\overline{3}},\ \mathbf{z}_1 = \mathbf{r}_2 - \mathbf{r}_{\overline{4}} \tag{2.3.3}$$

$$\mathbf{R}_2 = \frac{1}{2}(\mathbf{r}_1 + \mathbf{r}_{\overline{4}} - \mathbf{r}_2 - \mathbf{r}_{\overline{3}}),\ \mathbf{y}_2 = \mathbf{r}_1 - \mathbf{r}_{\overline{4}},\ \mathbf{z}_2 = \mathbf{r}_2 - \mathbf{r}_{\overline{3}} \tag{2.3.4}$$

$$\mathbf{R}_3 = \frac{1}{2}(\mathbf{r}_1 + \mathbf{r}_2 - \mathbf{r}_{\overline{3}} - \mathbf{r}_{\overline{4}}),\ \mathbf{y}_3 = \mathbf{r}_1 - \mathbf{r}_2,\ \mathbf{z}_3 = \mathbf{r}_{\overline{3}} - \mathbf{r}_{\overline{4}}, \tag{2.3.5}$$

$\mathbf{R}_1$ is vector joining centers of masses of mesonic clusters $(1, \overline{3})$ and $(2, \overline{4})$; similarly about $\mathbf{R}_2$ and $\mathbf{R}_3$. Now using the formalism of resonating group method [27], the

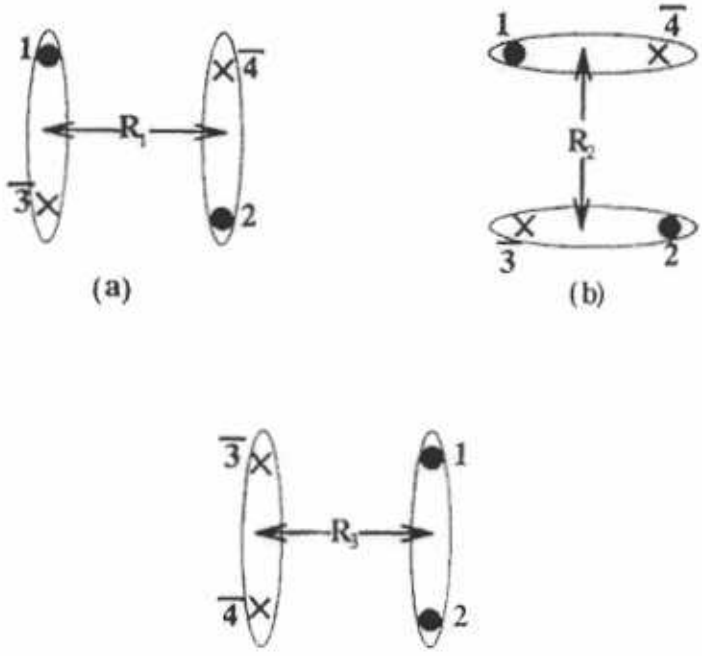

Figure 2.2: Three different topologies of diquark and diantiquark systems

quark position dependence function can be written as a product of known dependence ψ on $\mathbf{R}_c$,$\mathbf{y}_K$,$\mathbf{z}_K$ and unknown dependence χ on $\mathbf{R}_K$. i.e.

$$\phi_K(\mathbf{R}_c, \mathbf{R}_K, \mathbf{y}_K, \mathbf{z}_K) = \psi_c(\mathbf{R}_c)\chi_k(\mathbf{R}_K)\psi_K(\mathbf{y}_K, \mathbf{z}_K). \tag{2.3.6}$$

Thus, the total state vector of the $q^2\overline{q}^2$ system can be written as

$$\mid \Psi(q_1 q_2 q_{\overline{3}} q_{\overline{4}})\rangle = \sum_k \mid k\rangle_g \psi_c(\mathbf{R}_c)\chi_k(\mathbf{R}_K)\psi_k(\mathbf{y}_K, \mathbf{z}_K), \tag{2.3.7}$$

where $\chi_k(\mathbf{R}_K)$ being treated as variational functions to be determined by solving the approximate coupled Schrödinger equations in the relative coordinates $\mathbf{R}_1$ and $\mathbf{R}_2$ (In the beginning $\mathbf{R}_3$ also enters into the formalism, but later it is integrated out. Then the remaining coupled equations depend only on $\mathbf{R}_1$ and $\mathbf{R}_2$). $\psi_K(\mathbf{y}_K, \mathbf{z}_K)$ is a product of two functions $\xi_k(\mathbf{y}_K)$ and $\xi_k(\mathbf{z}_K)$ corresponding to the two mesonic clusters

of the channel k, i.e,

$$\psi_k(\mathbf{y}_K, \mathbf{z}_K) = \xi_k(\mathbf{y}_K)\xi_k(\mathbf{z}_K), \tag{2.3.8}$$

$\xi_k(\mathbf{y}_K)$ and $\xi_k(\mathbf{z}_K)$ being the normalized solutions of the Schrödinger equation for quadratic confining potential (written in eq.(2.3.18)) for a pair of quark-anti-quark within a cluster. We take

$$\begin{aligned} \xi_K(\mathbf{y}_K) &= \frac{1}{(2\pi d^2)^{\frac{3}{4}}} exp(-\frac{y_K^2}{4d^2}), \\ \xi_K(\mathbf{z}_K) &= \frac{1}{(2\pi d^2)^{\frac{3}{4}}} exp(-\frac{z_K^2}{4d^2}), \end{aligned} \tag{2.3.9}$$

as in ref.[26]. Here d is the size of meson (detail is written after eq.(2.3.18)) and m being the constituent quark mass. In our case, m is the mass of c-quark and equal to 1.4794 GeV as used in [46].

In above, the potential and wave function was for a pair of quarks. Now we write the Schrödinger equation for the meson-meson system, starting from noting that the overlap of $(\mathbf{H} - E_c) \mid \Psi\rangle$ with an arbitrary variation $\mid \delta\Psi\rangle$ of state vector $\mid \Psi\rangle$ vanishes where $\mid \Psi\rangle$ is the state vector of whole diquark-diantiquark system written in eq.(2.3.7). In $\mid \delta\Psi\rangle$, we consider only variation in χ_k, as in resonating group method [27]. Thus we write

$$\begin{aligned} \langle \delta\Psi \mid \mathbf{H} - E_c \mid \Psi\rangle = \sum_{k,l} \int d^3R_c d^3R_K d^3y_K d^3z_K \psi_c(\mathbf{R}_c)\delta\chi_k(\mathbf{R}_K)\xi_k(\mathbf{y}_K)\xi_k(\mathbf{z}_K)_g \\ \langle k \mid \mathbf{H} - E_c \mid l\rangle_g \psi_c(\mathbf{R}_c)\chi_l(\mathbf{R}_L)\xi_l(\mathbf{y}_L)\xi_l(\mathbf{z}_L) = 0, \end{aligned} \tag{2.3.10}$$

for$K, L, k, l = 1, 2, 3$. The arbitrary variations $\delta\chi_k(\mathbf{R}_K)$'s for different values of R_K are linearly independent and hence their co-efficient in eq.(2.3.10) should be zero.

With the trivial R_c integration performed to give a finite result, this leads to

$$\sum_l \int d^3y_K d^3z_K \xi_k(\mathbf{y}_K)\xi_k(\mathbf{z}_K)_g\langle k \mid \mathbf{H} - E_c \mid l\rangle_g \chi_l(\mathbf{R}_L)\xi_l(\mathbf{y}_L)\xi_l(\mathbf{z}_L) = 0, \quad (2.3.11)$$

where

$$_g\langle k \mid \mathbf{H} - E_c \mid l\rangle_g =_g \langle k \mid KE + V + 4m - E_c \mid l\rangle_g.$$

For $K = L$, in eq.(2.3.11), $\chi_l(\mathbf{R}_L)$ is independent of $\mathbf{y}_K$ and $\mathbf{z}_K$ therefore can be taken out of integrations. After integration, the result is an $\mathbf{R}_K$ dependent co-efficient of $\chi_k(\mathbf{R}_K)$. For $K \neq L$, $\mathbf{y}_K$ and $\mathbf{z}_K$ are replaced by their linear combinations with one of them as identical to $\mathbf{R}_L$ and other one independent of it. The jacobian of transformation from $\mathbf{y}_K, \mathbf{z}_K$ to $\mathbf{R}_K$ is equal to 8. Only the latter (independent $\mathbf{R}$) can be integrated out because of, yet, unknown functional dependence of χ_l on $\mathbf{R}_l$. After integration w.r.t $\mathbf{R}$ (independent of χ_l, we get

$$\sum_{l=1}^{3} \int d^3\mathbf{R}_L \Big[(\mathcal{KE})_{k,l}(\mathbf{R}_K, \mathbf{R}_L) + \mathcal{V}_{k,l}(\mathbf{R}_K, \mathbf{R}_L) - \big(E_c - \sum_{i=1}^{\overline{4}} m_i\big)\mathcal{N}_{k,l}(\mathbf{R}_k, \mathbf{R}_l)\Big]\chi_l(\mathbf{R}_L) = 0. \quad (2.3.12)$$

the $\mathcal{N}, \mathcal{V}$, and $\mathcal{KE}$ matrices [26] with basis $\mid 1\rangle_g, \mid 2\rangle_g, \mid 3\rangle_g$ are written as

$$\mathcal{N} = \begin{bmatrix} 1 & \frac{1}{3}E(R_1, R_2) & \frac{1}{\sqrt{3}}E(R_1, R_3) \\ \frac{1}{3}E(R_2, R_1) & 1 & -\frac{1}{\sqrt{3}}E(R_2, R_3) \\ \frac{1}{\sqrt{3}}E(R_3, R_1) & -\frac{1}{\sqrt{3}}E(R_3, R_2) & 1 \end{bmatrix}, \quad (2.3.13)$$

where $E(R_a, R_b) = F(R_a)F(R_b)$ with

$$F(R) = \left[\frac{1}{\pi d^2(1 + 4\overline{k}d^2)}\right]^{3/4} exp\left[-\frac{(1 + 8\overline{k}d^2)}{2d^2}R^2\right], \quad (2.3.14)$$

and $\mathcal{KE}$ is the kinetic energy matrix. As we considered that all quarks have same

mass, m, so integration gives the following result,

$$\mathcal{KE} = \begin{bmatrix} \frac{3}{2}\omega - \frac{1}{2m}\nabla_{R_1^2} & \frac{1}{3}\frac{\omega}{2}E(R_1,R_2)P(R_1,R_2) & \frac{1}{\sqrt{3}}\frac{\omega}{2}E(R_1,R_3)P(R_1,R_3) \\ \frac{1}{3}\frac{\omega}{2}E(R_1,R_2)P(R_1,R_2) & \frac{3}{2}\omega - \frac{1}{2m}\nabla_{R_2^2} & -\frac{1}{\sqrt{3}}E(R_2,R_3) \\ \frac{1}{\sqrt{3}}E(R_3,R_1) & -\frac{1}{\sqrt{3}}E(R_3,R_2) & \frac{3}{2}\omega - \frac{1}{2m}\nabla_{R_3^2} \end{bmatrix}, \tag{2.3.15}$$

where $\omega = 1/md^2$, and

$$P(R_a,R_b) = (1+4\overline{k}d^2)\left[\frac{15}{2} - \frac{1+4\overline{k}d^2}{d^2}(R_a^2+R_b^2)\right] \tag{2.3.16}$$

In the potential models, the confining potential for $Q\overline{Q}$ system in the the ground state gluonic field is mostly used in the form of

$$v_{ij} = \frac{-4\alpha_s}{3r} + br + c, \tag{2.3.17}$$

with inter-quark distance r. Here α_s is quark-gluon coupling constant, b is string tension, c is constant, and $-4/3$ is due to the color factor $\mathbf{F.F}$ (see eq. (5.1.5)). As already mentioned in introduction that linear term arises from confinement and Coulomb term describes quark interaction due to the one gluon exchange. This term is dominant at short inter-quark distance. When we used the potential with the colour structure of one gluon exchange in the form mentioned above, it becomes impossible for us to solve the integral equations appearing below in eq.(2.4.1-2.4.3). Therefore we use the parametrization of the static two quark potential as

$$v_{ij} = Cr_{ij}^2 + \overline{C}, \qquad \text{with} \quad i,j = 1,2,\overline{3},\overline{4} \tag{2.3.18}$$

This was also used in quark description of NN scattering [47, 48], and in pseudo scalar meson-meson scattering [49]. The potential in quadratic form has also been used in ref. [50, 26] and recently used in ref. [32] to explain the dynamics of meson-meson

system. In this simple harmonic potential, the parameters C and ω are related to size (d) of wave function (ξ_k) through the relations $\omega = \frac{1}{md^2}$ and $C = -\frac{3}{16}m\omega^2$, and for consistency of the diagonal term of the integral eq.(3.4.3) $\overline{C} = \frac{3}{8}(4m + 3\omega - 2M)$ GeV [26] with M being the mass of a meson. In ref. [26], the above expression for C is obtained for light quark-antiquark system, but we used it for heavy quark-antiquark system (charmonium meson system) with $M = 2m = 2.9588$GeV. The parameter d is chosen in such a way to reduce the error resulting from a use of this quadratic potential instead of the realistic one. The error may be both in the wave functions of the distance between a quark and antiquark within cluster ($\psi_k(\mathbf{y}_k, \mathbf{z}_k)$ of eq.(2.3.7)) and χ of eq.(2.3.7) of the vector joining the centers of masses of two clusters. As for the first dependence, we found that the maximum overlap integral of each of the wave functions $\xi_K(\mathbf{y}_K)$ and $\xi_K(\mathbf{z}_K)$ of the quadratic potential and that of a more realistic coulombic plus linear potential is 99% at $d = 1.16\text{GeV}^{-1}$. (For the parameters of the realistic potential we used values $\alpha_s = 0.5461$GeV [46] and $b_s = 0.1425$GeV [46] for mesons composed of charm quarks). This overlap is shown in Fig.2.3. A similar work was done in ref. [51] for lighter quarks. They found that the overlap wave function of SHO (quadratic potential) and that of coulombic plus linear can be made as large as 99.4% with the suitable adjustment of parameters. Now using the potential in the quadratic form, the $\mathcal{V}$ matrix becomes

$$\mathcal{V} = \begin{bmatrix} 24C_0d^2 & 8GC_0E(R_1,R_2) & \frac{2\sqrt{3}}{3}C_0E(R_1,R_3)H \\ 8GC_0E(R_2,R_1) & 24C_0d^2 & \frac{2\sqrt{3}}{3}C_0E(R_2,R_3)H \\ \frac{2\sqrt{3}}{3}C_0E(R_3,R_1)H & \frac{2\sqrt{3}}{3}C_0E(R_3,R_2)H & D(R_3) + 18C_0d^2 \end{bmatrix}, \quad (2.3.19)$$

as in ref. [26]. For the convenience in writing, we define

$$H = (2R_3^2 + 9G), G = d^2/(1 + 4\overline{k}d^2), C_0 = -\frac{1}{3}C = 1/16md^4,$$

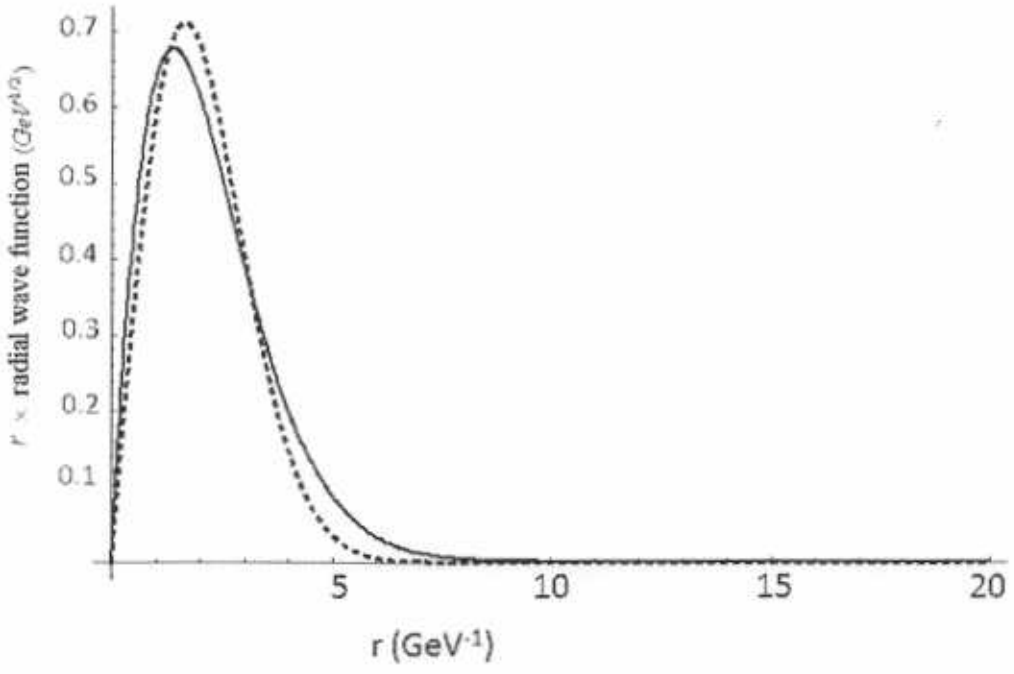

Figure 2.3: Overlap of the (ground state) wave function of the realistic linear plus Coulombic potential and that of the quadratic potential. The solid line represents linear plus coulombic potential wave function and the dashed line represents quadratic potential wave function.

and

$$D(R_3) = 4C_0R_3^2 + \frac{5}{2}Dexp(-4\overline{k}R_3^2)[(1+4\overline{k}d^2)^{-3} - (1+8\overline{k}d^2)^{-3}exp(-4\overline{k}R_3^2)]$$

2.4 Coupled Integral Equations

Using these $\mathcal{N}, \mathcal{V}$, and $\mathcal{KE}$ matrices in eq.(2.3.11), we obtained the following three coupled equations (as in ref. [26]

$$\begin{aligned}
&(-E_c - 8Cd^2 - \frac{8}{3}\overline{C} - \frac{\nabla^2_{\mathbf{R}_1}}{2m} + \frac{3}{2}\omega + 4m)\chi_1(\mathbf{R}_1) + \\
&\left(\frac{1}{\pi d^2(1+4\overline{k}d^2)}\right)^{\frac{3}{2}} \int d^3\mathbf{R}_2 exp\left(\frac{-(1+8\overline{k}d^2)(\mathbf{R}_1^2+\mathbf{R}_2^2)}{2d^2}\right)[-\frac{E_c}{3} - \frac{8Cd^2}{3(1+4\overline{k}d^2)} + \\
&\frac{4m}{3} - \frac{8}{9}\overline{C} + \frac{1+4\overline{k}d^2}{6md^2}\left(\frac{15}{2} - (\mathbf{R}_1^2+\mathbf{R}_2^2)(\frac{1+4\overline{k}d^2}{d^2})\right)]\chi_2(\mathbf{R}_2) + \\
&\frac{1}{\sqrt{3}}\left(\frac{1}{\pi d^2(1+4\overline{k}d^2)}\right)^{\frac{3}{2}} \int d^3\mathbf{R}_3 exp\left(\frac{-(1+8\overline{k}d^2)(\mathbf{R}_1^2+\mathbf{R}_3^2)}{2d^2}\right)[-E_c - \frac{6Cd^2}{(1+4\overline{k}d^2)} \\
&+ 4m - \frac{8}{3}\overline{C} + \frac{1+4\overline{k}d^2}{2md^2}\left(\frac{15}{2} - (\mathbf{R}_1^2+\mathbf{R}_3^2)(\frac{1+4\overline{k}d^2}{d^2})\right)]\chi_3(\mathbf{R}_3),
\end{aligned} \tag{2.4.1}$$

$$\begin{aligned}
&(-E_c - 8Cd^2 - \frac{8}{3}\overline{C} - \frac{\nabla^2_{\mathbf{R}_2}}{2m} + \frac{3}{2}\omega + 4m)\chi_2(\mathbf{R}_2) + \\
&\left(\frac{1}{\pi d^2(1+4\overline{k}d^2)}\right)^{\frac{3}{2}} \int d^3\mathbf{R}_1 exp\left(\frac{-(1+8\overline{k}d^2)(\mathbf{R}_2^2+\mathbf{R}_1^2)}{2d^2}\right)[-\frac{E_c}{3} - \frac{8Cd^2}{3(1+4\overline{k}d^2)} + \\
&\frac{4m}{3} - \frac{8}{9}\overline{C} + \frac{1+4\overline{k}d^2}{6md^2}\left(\frac{15}{2} - (\mathbf{R}_2^2+\mathbf{R}_1^2)(\frac{1+4\overline{k}d^2}{d^2})\right)]\chi_1(\mathbf{R}_1) + \\
&\frac{1}{\sqrt{3}}\left(\frac{1}{\pi d^2(1+4\overline{k}d^2)}\right)^{\frac{3}{2}} \int d^3\mathbf{R}_3 exp\left(\frac{-(1+8\overline{k}d^2)(\mathbf{R}_2^2+\mathbf{R}_3^2)}{2d^2}\right)[-E_c - \frac{6Cd^2}{(1+4\overline{k}d^2)} \\
&+ 4m - \frac{8}{3}\overline{C} + \frac{1+4\overline{k}d^2}{2md^2}\left(\frac{15}{2} - (\mathbf{R}_2^2+\mathbf{R}_3^2)(\frac{1+4\overline{k}d^2}{d^2})\right)]\chi_3(\mathbf{R}_3),
\end{aligned} \tag{2.4.2}$$

and

$$(-E_c - 8Cd^2 - \frac{8}{3}\overline{C} - \frac{\nabla^2_{\mathbf{R}_3}}{2m} + \frac{3}{2}\omega + 4m)\chi_3(\mathbf{R}_3) +$$
$$\frac{1}{\sqrt{3}}\left(\frac{1}{\pi d^2(1+4\overline{k}d^2)}\right)^{\frac{3}{2}} \int d^3\mathbf{R}_1 exp\left(\frac{-(1+8\overline{k}d^2)(\mathbf{R}_1^2+\mathbf{R}_3^2)}{2d^2}\right)[-E_c - \frac{6Cd^2}{(1+4\overline{k}d^2)}$$
$$+ 4m - \frac{8}{3}\overline{C} + \frac{1+4\overline{k}d^2}{2md^2}\left(\frac{15}{2} - (\mathbf{R}_1^2+\mathbf{R}_3^2)(\frac{1+4\overline{k}d^2}{d^2})\right)]\chi_1(\mathbf{R}_1)$$
$$- \frac{1}{\sqrt{3}}\left(\frac{1}{\pi d^2(1+4\overline{k}d^2)}\right)^{\frac{3}{2}} \int d^3\mathbf{R}_2 exp\left(\frac{-(1+8\overline{k}d^2)(\mathbf{R}_2^2+\mathbf{R}_3^2)}{2d^2}\right)[-E_c - \frac{6Cd^2}{(1+4\overline{k}d^2)}$$
$$+ 4m - \frac{8}{3}\overline{C} + \frac{1+4\overline{k}d^2}{2md^2}\left(\frac{15}{2} - (\mathbf{R}_2^2+\mathbf{R}_3^2)(\frac{1+4\overline{k}d^2}{d^2})\right)]\chi_2(\mathbf{R}_2) \tag{2.4.3}$$

These three coupled integral equations are solved in ref. [26] to find the transition matrix elements. These equations are derived when the gluonic field is in the ground state. In the next chapter we will derive the integral equations in the modified basis with the incorporation of excited state gluonic field.

Chapter 3

Potential Model in Extended Basis

In the previous chapter, we introduced the sum of two body potential model and modified it to include QCD effects through multiplying the off-diagonal elements of overlap, potential and kinetic energy matrices in the basis $|1\rangle_g, |2\rangle_g, |3\rangle_g$(defined in eq.(2.1.2)) of weak coupling limit by the gluon field overlap factor f . In this chapter, we further modify this potential model by extending the basis into six states by including those corresponding to the excited state gluonic field. These new excited state basis are defined as

$$|1^*\rangle = (q_1q_3)_g(q_2q_4)_g, \quad |2^*\rangle = (q_1q_4)_g(q_2q_3)_g, \text{ and } \quad |3^*\rangle = (q_1q_2)_g(q_3q_4)_g. \tag{3.0.1}$$

Here $(q_1q_3)_g$ denotes a state where gluonic field is in lowest excited state. (Excited states of gluonic field can, for example, be seen in the QCD numerical simulations; see ref.[19] and others.)

By extending the basis to six states, the N, V, and KE matrices becomes 6×6 matrices with gluonic field overlap factors f^a and f^c in addition to the above mentioned f. These factors are parametrized in ref. [28] so as to agree the $SU(2)_c$

simulations reported in this work. In $SU(3)_c$, these overlap factors have the following definitions:

$$\langle 1^*|2^*\rangle = \langle 1^*|3^*\rangle = \langle 2^*|3^*\rangle = -\frac{f^c}{3}, \tag{3.0.2}$$

and

$$\langle 1^*|2\rangle = \langle 1^*|3\rangle = \langle 2^*|3^*\rangle = ... = -\frac{f^a}{3}, \tag{3.0.3}$$

According to ref. [28] f^c is defined in ref. [28] in a form similar to f as

$$f^c = \exp(-b_s k_c S), \tag{3.0.4}$$

and

$$f^a = (f_1^a + b_s f_2^a S \exp(-b_s k_c S), \tag{3.0.5}$$

with $f_1^a = 0$ [28]. It is also mentioned in ref. [28] that $\langle 1|1^*\rangle = \langle 2|2^*\rangle = \langle 3|3^*\rangle = 0$ because of the orthogonality of gluonic excited state with ground state.

In the six basis (or the extended basis) with $f = f^a = f^c = 1$, the Hamiltonian have the following form

$$H = -\sum_{i=1}^{4}[m_i + \frac{\widehat{P}_i^2}{2m_i}] + \sum_{i<j}(v_{ij} + \epsilon \triangle v_{ij}^*)\mathbf{F}_i.\mathbf{F}_j, \tag{3.0.6}$$

where v_{ij} is the potential energy of a $q\overline{q}$ pair ij for ground state gluonic field and $\triangle v_{ij}^*$ is the difference between ground and excited state gluonic field potential for that pair. We take the kinetic energy in the non-relativistic limits. This limit is also used in a recent work by Vijande ref. [50] that deals with multiquark system (two quarks and two antiquarks) to study the spectrum using a string model for the potential. In ref. [28], potential energy matrix elements are written so that the potential energy for each pair ij is equal to v_{ij} for the matrix elements of the Hamiltonian between

gluonic ground states, and it is equal to $v_{ij} + \triangle v^*_{ij}$ for the matrix elements between the gluonic-excited states. We have modeled these two forms by taking $\epsilon = 0$ for the ground state matrix elements and $\epsilon = 1$ for the elements between gluonic-excited states. For the elements between ground and excited state gluonic field, the ϵ value that results from the parameter a_0 of ref. [28] being fitted to 4 (in their Table 1) is surprisingly 2 and not any value between 0 and 1. A possibility is that this is a result of them taking the area S, we mentioned in chapter 2 in eq.(2.3.2), in the form of average of the sum of triangle areas instead of a theoretically motivated minimal surface area. Thus we have somewhat explored $\epsilon = \frac{1}{2}$ between 0 and 1 and $\epsilon = 1$ in addition to $\epsilon = 2$ which we have mainly studied.

$\mathbf{F}_i$ (operating on i_{th} particle) is already defined after eq.(2.1.1). m is mass of quark (or anti-quark). We are considering that all the four quarks have same mass, m which is equal to the mass of c-quark and thus $m = 1.4794$ GeV as used in ref. [46]. The matrix elements of $\mathbf{F}_i.\mathbf{F}_j$ are written in Appendix between the ground state gluonic field basis $\mid 1\rangle_g, \mid 2\rangle_g, \mid 3\rangle_g$, and excited state gluonic field basis $\mid 1^*\rangle$, and $\mid 2^*\rangle$.

3.1 Overlap of Linear plus Columbic plus Gluonic Excited Potential and Quadratic plus Gluonic Excited Potential Functions

For the additional term in the $q\bar{q}$ potential for the gluonic excitation, the usual flux tube (π/r [17]) or string based analytical expressions become impractical for us. Thus for that we tried an *ansätz* of the form of

$$\triangle v^*_{ij} = Ae^{-Br^2_{ij}}, \tag{3.1.1}$$

as mentioned in the introduction. This gaussian gluonic potential is a smeared form of $\frac{constant}{r}$ as written in appendix of ref. [22]. From the Fig.3.1 (Fig.3 of [19]), we get the potential energy difference ε_i between ground and excited states for different r values (r_i). We choose A and B for which χ^2 becomes minimum. χ^2 is defined as

$$\chi^2 = \sum_{i=1}^{n} (\varepsilon_i - A\exp[-Br_{ij}^2])^2, \tag{3.1.2}$$

with n being the number of data points. This gives

$$A = 1.8139\,\text{GeV}, \qquad B = 0.0657\,\text{GeV}^2.$$

For finding the wave function corresponding to our total potential $Cr_{ij}^2 + \overline{C} + Ae^{-Br_{ij}^2}$, we used the variational method with an *ansätz* wave function

$$\xi_K^*(\mathbf{y}_K) = ny_K^2 \exp(-py_K^2). \tag{3.1.3}$$

The normalization of this $\xi_K^*(\mathbf{y}_K)$ w.r.t y_K gives

$$n = (42^{\frac{3}{4}} p^{\frac{7}{4}})(15^{\frac{1}{2}} \pi^{\frac{3}{4}}).$$

This leaves us with one variational parameter p chosen to minimize the expectation value of the two body Hamiltonian for $q\bar{q}$ pair in the excited state gluonic field wave function. This gave $p = 0.048\text{GeV}^2$. For this value of p, the overlap of wave function of the quadratic potential plus $\triangle v_{ij}^*$ and that of coulombic plus linear plus $\triangle v_{ij}^*$ within a hybrid cluster became 99.9%. Both wave functions (of ground plus excited state potential) are shown in in Fig.3.2. The wave functions of the ground state potential are shown in Fig.2.3. Having much reduced the errors in the in-cluster factors ψ_k of the total wave function (of eq.(2.3.7)), the question remains how much the inter-cluster factors χ_k of the (terms of the) total state vector are affected by our use of convenient

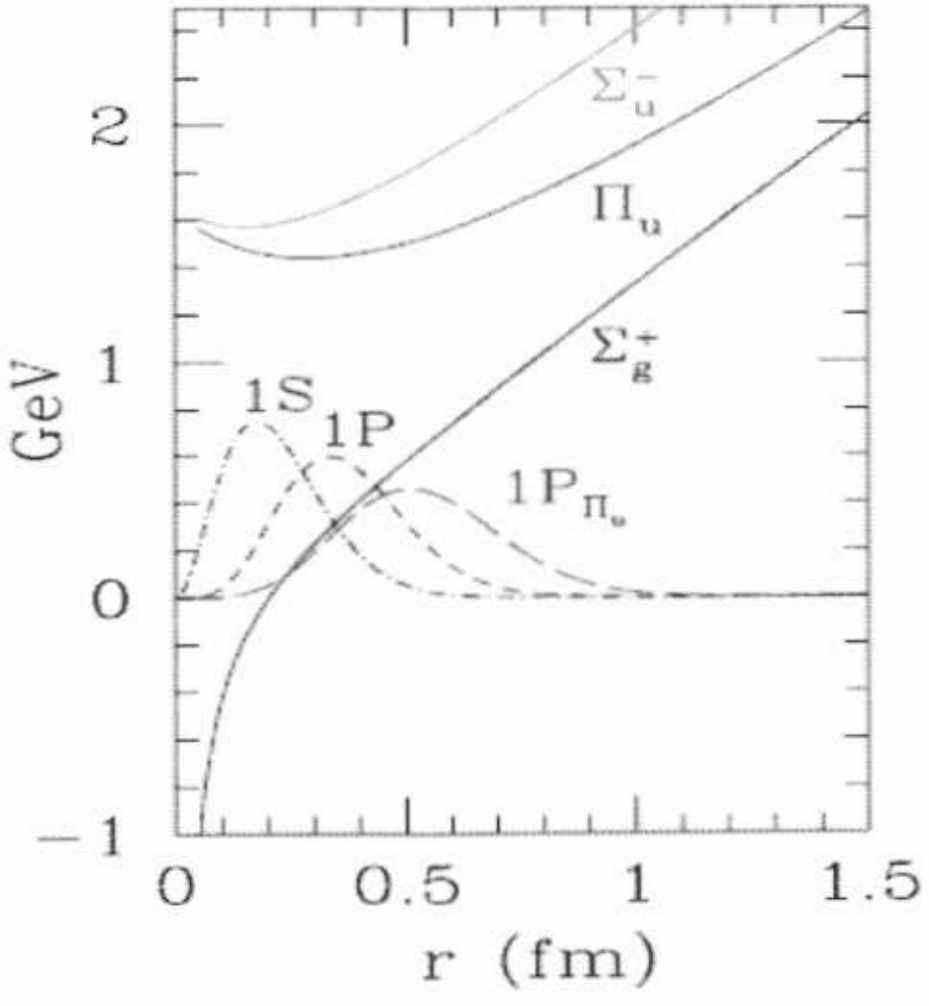

Figure 3.1: Ground and excited state potential.

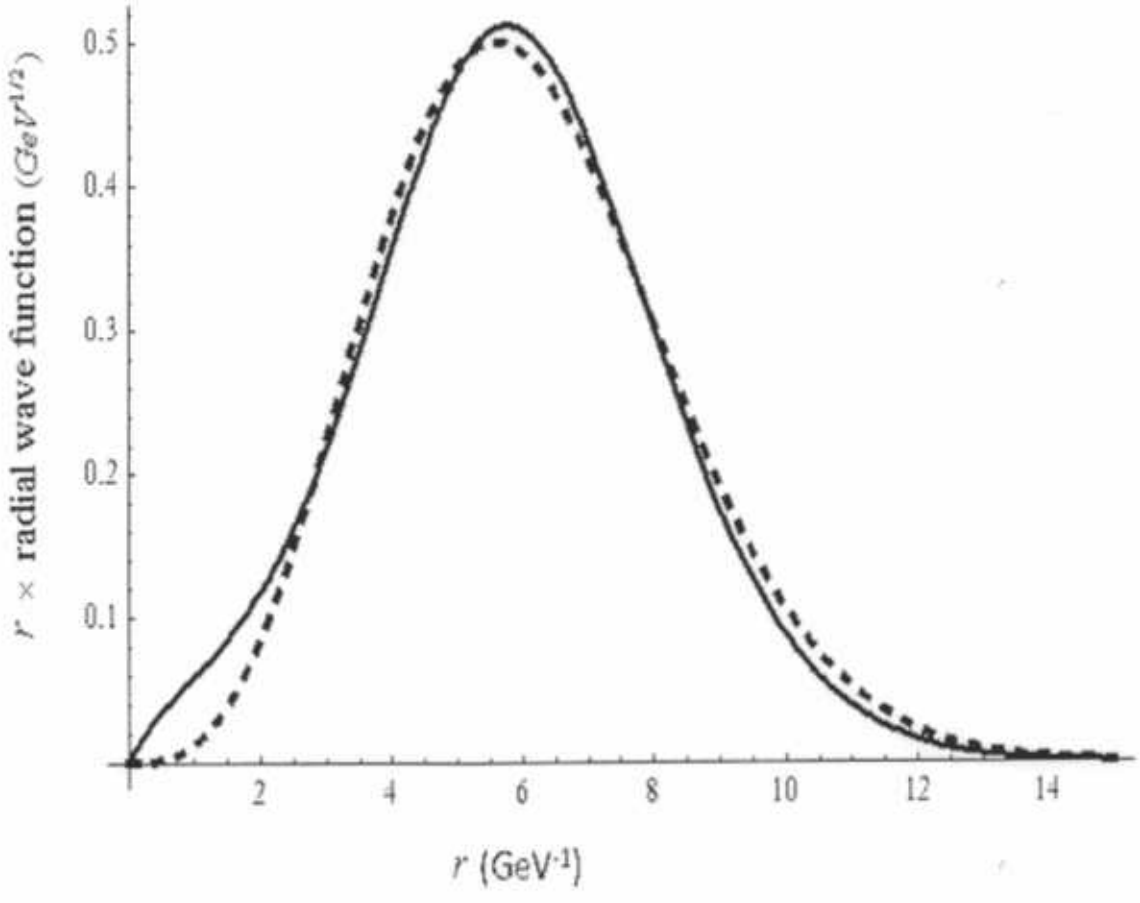

Figure 3.2: Excited state wave functions of realistic linear plus columbic plus $A\exp(-Br^2)$ and quadratic plus $A\exp(-Br^2)$ potential. Solid line represent linear plus columbic plus $A\exp(-Br^2)$ potential and dashed line represent quadratic plus $A\exp(-Br^2)$ potential wave function.

but not realistic $q\bar{q}$ potentials. For the inter-cluster wave functions, eventually we use below in eq. (3.5.11) plane wave forms which get their justifications from the validity of Born approximation for our problem regardless of potential expressions we use. This plane wave form has only one usual parameter (the wave number) and eq.(3.5.10) below relates its value for the ground as well as excited state inter-cluster wave functions to the very good values of d and p that almost give realistic ground state and excited state wave functions within $q\bar{q}$ clusters. But the relations between the inter-cluster wave numbers and the d and p do assume a quadratic confinement. This may affect our numerical results, but hopefully not at least the qualitative features we are pointing out. Perhaps it is worth mentioning here that properties of $q^2\bar{q}^2$ systems were calculated using quadratic confinement in ref. [21], and then with the realistic potential in ref. [22] and both the works favoured the existence of meson-meson molecules. That is, their results for $q^2\bar{q}^2$ systems were not much different.

3.2 The Approximations Used

Now all the necessary ingredients have been discussed to write the multi-channel Schrödinger equation in our extended basis. Before generalizing the Schrödinger equation of eq.(2.3.11) to the extended basis, all necessary approximations are written in this section that are used in the thesis work, for the simplicity and numerical convenience of the work. Most of them have already been mentioned above. Here all of them are collected that are mentioned above or used at a later stage in the solution of integral equations resulting from resonating group method and Schrödinger equation.

1-Quadratic Confinement

In the Hamiltonian of the meson-meson system (written in eq.(3.0.6)), the space dependent coefficient of $\mathbf{F}_i.\mathbf{F}_j$ operator represents the quark confinement. This coefficient is taken in the quadratic form instead of the theoretically better motivated coulombic plus linear form. This approximation is already discussed in the paragraph after eq.(2.3.18).

Non-Relativistic Kinetic Energy

The kinetic energy is also considered in the non-relativistic limits. This is valid for heavy quarks. The non-relativistic limits are also used in ref. [50] that deals with multiquark system (two quarks and two antiquarks) to study the spectrum using a string model for the potential.

The Cluster Wave Function Pre-specified

Because of large number of quark coordinates, it becomes difficult to solve them exactly. Rather the dependence is specified on the vectors joining particles inside a mesonic cluster before solving the Schrödinger equation, which is solved just for the dependence on the vectors joining the centers of mass of the mesonic clusters.

Neglect of the Third Gluonic Channel

This two level approximation is not mentioned in the above text. This approximation is related to the neglect of the third gluonic channel (that is involve explicitly diquark and diantiquark mesonic channels). Justification of this approximation is given below after eq.(3.3.2).

Born Approximation

Born Approximation is also used below in solving the integral equations. This approximation is valid if interaction (T-matrix elements or phase shifts) are small [55].

3.3 Setting up the Coupled Integral Equations

Now we re-write the Schrödinger equation (already written in eq.(2.3.10)) in the six basis states ($\mid 1\rangle, \mid 2\rangle, \mid 3\rangle, \mid 2^*\rangle, , \mid 3^*\rangle$) by combining the Hamiltonian (defined in eq.(3.0.6)) and all the wave functions mentioned above. Thus we wrote

$$\langle \delta\Psi \mid \mathbf{H} - E_c \mid \Psi\rangle = \sum_{k,l} \int d^3R_c d^3R_K d^3y_K d^3z_K \psi_c(\mathbf{R}_c)\delta\chi_k(\mathbf{R}_K)\xi_k(\mathbf{y}_K)\xi_k(\mathbf{z}_K)_g$$
$$\langle k \mid \mathbf{H} - E_c \mid l\rangle_g \psi_c(\mathbf{R}_c)\chi_l(\mathbf{R}_L)\xi_l(\mathbf{y}_L)\xi_l(\mathbf{z}_L) = 0 \tag{3.3.1}$$

for$k, l = 1, 2, 3, 1^*, 2^*, 3\star$ and $K, L = 1, 2, 3$. The difference between this eq.(3.3.1) and the eq.2.3.10 (written in previous chapter) is that eq.(3.3.1) is written in six basis but eq.2.3.10 is written in three basis states. The arbitrary variations $\delta\chi_k(\mathbf{R}_K)$'s for different values of R_K are linearly independent as before and hence their co-efficient in eq.(3.3.1) should be zero similar to eq.(2.3.11). With the trivial R_c integration performed to give a finite result, this leads to

$$\sum_l \int d^3y_K d^3z_K \xi_k(\mathbf{y}_K)\xi_k(\mathbf{z}_K)_g\langle k \mid \mathbf{H} - E_c \mid l\rangle_g \chi_l(\mathbf{R}_L)\xi_l(\mathbf{y}_L)\xi_l(\mathbf{z}_L) = 0, \tag{3.3.2}$$

where

$$_g\langle k \mid \mathbf{H} - E_c \mid l\rangle_g =_g \langle k \mid KE + V + 4m - E_c \mid l\rangle_g.$$

Elements of enlarged V and KE matrices (similar to eqs.(2.2.1-2.2.4)) are defined below in eq.(3.3.5) and eq.(3.3.6). In ref. [28] it is stated that,

> "In some of our earlier work this was interpreted to mean that it was unnecessary to include all three states and so the symmetry was broken by keeping the two states with the lowest energy, let us say A and B. A similar thing also occurred in the lattice simulations. There it was found that the energy of the lowest state was always the same in both a 2×2 and 3×3 description, providing A or B had the lowest energy. In addition the energy of the second state was, in most cases, more or less the same."

This two level approximation is also used in the model of a later work [52] for the tetraquark system. Considering this, we include only two topologies(1,2), meaning four states($|\,1\rangle, |\,2\rangle, |\,1^*\rangle, |\,2^*\rangle$). According to the model of ref. [28] the overlap matrix N in this truncated 4-basis is given by

$$N(f) =_g \langle k \mid l \rangle_g = \begin{bmatrix} 1 & f/3 & 0 & -f^a/3 \\ f/3 & 1 & -f^a/3 & 0 \\ 0 & -f^a/3 & 1 & -f^c/3 \\ -f^a/3 & 0 & -f^c/3 & 1 \end{bmatrix}. \tag{3.3.3}$$

For potential matrix $V(f)$ the matrix elements are

$$V(f) =_g \langle k \mid V \mid l \rangle_g = \begin{bmatrix} V_{11} & V_{12} & V_{11^*} & V_{12^*} \\ V_{21} & V_{22} & V_{21^*} & V_{22^*} \\ V_{1^*1} & V_{1^*2} & V_{1^*1^*} & V_{1^*2^*} \\ V_{2^*1} & V_{2^*2} & V_{2^*1^*} & V_{2^*2^*} \end{bmatrix}. \tag{3.3.4}$$

Here,

$$
\begin{aligned}
V_{11} &= -\frac{4}{3}(v_{1\bar{3}} + v_{2\bar{4}}) \\
V_{12} = V_{21} &= \frac{4}{9}f(v_{12} + v_{\bar{3}\bar{4}} - v_{1\bar{3}} - v_{2\bar{4}} - v_{1\bar{4}} - v_{2\bar{3}}) \\
V_{22} &= -\frac{4}{3}(v_{1\bar{4}} + v_{2\bar{3}}) \\
V_{21^*} = V_{2^*1} &= -\frac{f^a}{18}\left(\sqrt{2}(v^*_{1\bar{3}} + v^*_{2\bar{4}}) - \frac{16}{\sqrt{2}}(v^*_{1\bar{4}} + v^*_{2\bar{3}}) - \sqrt{2}(-v^*_{12} - v^*_{\bar{3}\bar{4}})\right) \\
V_{1^*2} = V_{12^*} &= -\frac{f^a}{18}\left(\sqrt{2}(v^*_{1\bar{4}} + v^*_{2\bar{3}}) - \frac{16}{\sqrt{2}}(v^*_{1\bar{3}} + v^*_{2\bar{4}}) - \sqrt{2}(-v^*_{12} - v^*_{\bar{3}\bar{4}})\right) \\
V_{1^*1^*} &= \frac{1}{6}(v^*_{1\bar{3}} + v^*_{2\bar{4}}) \\
V_{1^*2^*} = V_{2^*1^*} &= -\frac{1}{18}f^c\Big(- (v^*_{1\bar{3}} + v^*_{2\bar{4}} + v^*_{1\bar{4}} + v^*_{2\bar{3}}) + 10(v^*_{12} + v^*_{\bar{3}\bar{4}})\Big) \\
V_{2^*2^*} &= \frac{1}{6}(v^*_{1\bar{4}} + v^*_{2\bar{3}}) \\
V_{1^*1} = V_{11^*} &= V_{2^*2} = V_{22^*} = 0,
\end{aligned}
\tag{3.3.5}
$$

with $v^*_{ij} = v_{ij} + \epsilon\triangle v^*_{ij}$, ϵ being defined above (after eq.(3.0.6)). The coefficients of v_{ij} and v^*_{ij}, resulting from the **F.F** operator, are given in the Appendix. The kinetic energy matrix of the two quarks two anti-quarks is taken to be

$$
KE =_g \langle k \mid KE \mid l\rangle_g = N(f)^{\frac{1}{2}}_{k,l}\left(\frac{-1}{2m}\sum_{i=1}^{4}\nabla_i^2\right)N(f)^{\frac{1}{2}}_{k,l}. \tag{3.3.6}
$$

The kinetic energy in the same form is also used in ref. [26]. When we are observing dynamical effects for ground state, our overlap, potential and kinetic energy matrices are 2×2 matrices and we use f with $k_f = 0.6$ as used in ref. [30](detail is already written in chapter 2 after eq.(2.3.2)). But when we incorporate the excited state gluonic field states, our overlap, potential and kinetic energy matrices become 4×4 matrices. In the upper left 2×2 block of these matrices, the form of f remains the same but the value of k_f is changed to 1.51 according to a conclusion of ref. [28]. In

the other blocks f^a, f^c [28] [53] are also used. If we take f^a as a function of area as defined in [28], it becomes unmanageable to solve the integral equations (3.4.3-3.4.6) below and hence we have taken f^a to be a constant. But we have tried a variety of its values to explore how much our conclusions depend on its value. As for f^c, the fit in refs. [53] [28] of the model of these worksto the lattice data favours $k_c = 0$ (introduced above in eq.(3.0.4)) which implies that $f^c = 1$ i.e. excited configurations interact amongst themselves in the way expected from perturbation theory. Thus we have used $f^c = 1$.

3.4 Coupled Integral Equations

Using "N"," V" and "KE" elements in eq.(3.3.2), we got four integral equations for four different values of k or l. Then we do the $\mathbf{y}_K$ and $\mathbf{z}_K$ integrations. Most of the integrations in the above equation are in the Gaussian form. For $K = L = 1, 2$, in eq.(3.3.2), $\chi_l(\mathbf{R}_L)$ is independent of $\mathbf{y}_K$ and $\mathbf{z}_K$ and, thus, can be taken out of integrations. After the integration, the result is $\mathbf{R}_K$ dependent co-efficient of $\chi_k(\mathbf{R}_K)$.

Few integration formula's used are:

$$\begin{aligned}
&\int \exp(-\lambda y^2 + J.y)dy = (\frac{\pi}{\lambda})^{1/2}\exp(\frac{J^2}{4\lambda}) \\
&\int (y)\exp(-\lambda y^2 + J.y)dy = (\frac{\pi}{\lambda})^{1/2}\frac{J}{4\lambda}\exp(\frac{J^2}{4\lambda}) \\
&\int y^2\exp(-\lambda y^2 + J.y)dy = (\frac{\pi}{\lambda})^{1/2}(\frac{J^2}{4\lambda^2} + \frac{1}{2\lambda})\exp(\frac{J^2}{4\lambda}) \\
&\int y^3\exp(-\lambda y^2 + J.y)dy = (\frac{\pi}{\lambda})^{1/2}\frac{J}{4\lambda^2}(3 + \frac{J^2}{2\lambda}\exp(\frac{J^2}{4\lambda}) \\
&\int y^4\exp(-\lambda y^2 + J.y)dy = (\frac{\pi}{\lambda})^{1/2}(\frac{3J^2}{4\lambda^3} + \frac{J^4}{16\lambda^4} + \frac{3}{4\lambda^2})\exp(\frac{J^2}{4\lambda}) \\
&\int y^5\exp(-\lambda y^2 + J.y)dy = (\frac{\pi}{\lambda})^{1/2}(\frac{J^5}{(2\lambda)^5} + \frac{10J^3}{16\lambda^4} + \frac{15J}{8\lambda^3})\exp(\frac{J^2}{4\lambda}) \\
&\int y^6\exp(-\lambda y^2 + J.y)dy = (\frac{\pi}{\lambda})^{1/2}(\frac{J^6}{(64\lambda)^6} + \frac{15J^4}{32\lambda^5} + \frac{45J^2}{16\lambda^4} + \frac{15}{8\lambda^3})\exp(\frac{J^2}{4\lambda}).
\end{aligned} \tag{3.4.1}$$

For $K \neq L$, $\mathbf{y}_K$ and $\mathbf{z}_K$ are replaced by their linear combinations with one of them as identical to $\mathbf{R}_L$ and other one independent of it as $\mathbf{R}_3$. The jacobian of transformation from $\mathbf{y}_K, \mathbf{z}_K$ to $\mathbf{R}_K$ is equal to 8. Then we integrate the equation w.r.t $\mathbf{R}_3$. Few

integration formula's used are:

$$\int \exp(-\lambda R^2 + \mathbf{J}.\mathbf{R}) d^3\mathbf{R} = (\frac{\pi}{\lambda})^{3/2} \exp(\frac{J^2}{4\lambda})$$

$$\int R^2 \exp(-\lambda R^2 + \mathbf{J}.\mathbf{R}) d^3\mathbf{R} = (\frac{\pi}{\lambda})^{3/2} (\frac{J^2}{4\lambda^2} + \frac{3}{2\lambda}) \exp(\frac{J^2}{4\lambda})$$

$$\int R^4 \exp(-\lambda R^2 + \mathbf{J}.\mathbf{R}) d^3\mathbf{R} = (\frac{\pi}{\lambda})^{3/2} (\frac{J^4}{16\lambda^4} + \frac{5J^2}{4\lambda^3} + \frac{15}{4\lambda^2}) \exp(\frac{J^2}{4\lambda})$$

$$\int R^6 \exp(-\lambda R^2 + \mathbf{J}.\mathbf{R}) d^3\mathbf{R} = (\frac{\pi}{\lambda})^{3/2} (\frac{J^6}{2^6\lambda^6} + \frac{7 \times 3J^4}{2^5\lambda^5} + \frac{105J^2}{16\lambda^4} + \frac{7 \times 5 \times 3}{8\lambda^3}) \exp(\frac{J^2}{4\lambda})$$

$$\int R^8 \exp(-\lambda R^2 + \mathbf{J}.\mathbf{R}) d^3\mathbf{R} = (\frac{\pi}{\lambda})^{3/2} \left(\frac{J^8}{2^8\lambda^8} + \frac{36J^6}{2^7\lambda^7} + \frac{(7 \times 3 \times 13) + 105J^4}{2^6\lambda^6} + \right.$$
$$\left. \frac{(7 \times 5 \times 3)(105 \times 11)J^2}{32\lambda^5} + \frac{9 \times 7 \times 5 \times 3}{16\lambda^4} \right) \exp(\frac{J^2}{4\lambda})$$

$$\int \mathbf{R}_1.\mathbf{R}_3 \exp(-\lambda R_3^2 + a\mathbf{J}.\mathbf{R}_3) d^3\mathbf{R}_3 = (\frac{\pi}{\lambda})^{3/2} (a/\lambda) R_1^2 \exp(\frac{J^2}{4\lambda})$$

$$\int (\mathbf{R}_1.\mathbf{R}_3)^2 \exp(-\lambda R_3^2 + \mathbf{J}.\mathbf{R}_3) d^3\mathbf{R}_3 = (\frac{\pi}{\lambda})^{3/2} \left(\frac{J^2}{4\lambda^2} R_1^4 + \frac{R_1^2}{2\lambda} \right) \exp(\frac{J^2}{4\lambda})$$

$$\int R_3^2 (\mathbf{R}_1.\mathbf{R}_3) \exp(-\lambda R_3^2 + a\mathbf{J}.\mathbf{R}_3) d^3\mathbf{R}_3 = (\frac{\pi}{\lambda})^{3/2} \left((a^3/\lambda^3) R_1^4 + 5a/\lambda^2 R_1^2 \right) R_1^2 \exp(\frac{J^2}{4\lambda})$$

$$\int R_3^4 (\mathbf{R}_1.\mathbf{R}_3)^2 \exp(-\lambda R_3^2 + 2b\mathbf{R}_2.\mathbf{R}_3) d^3\mathbf{R}_3 = (\frac{\pi}{\lambda})^{3/2} \left\{ \frac{b^6}{\lambda^6} (\mathbf{R}_1.\mathbf{R}_2)^2 R_2^4 + \frac{b^4}{\lambda^5} \left(R_1^2 R_2^4 \right.\right.$$
$$\left. + 18 R_2^2 (\mathbf{R}_1.\mathbf{R}_3)^2 \right) + \frac{b^2}{\lambda^4} (63(\mathbf{R}_1.\mathbf{R}_2)^2 + 14 R_1^2 R_2^2 + x_1^2 x_2^2 + y_1^2 y_2^2 + z_1^1 z_2^2)$$
$$\left. + \frac{35}{(2\lambda)^3} R_1^2 \right\} \exp(\frac{J^2}{4\lambda}).$$

(3.4.2)

Integration, as described above, leaves the following four equations:

$$\Delta_1(\mathbf{R}_1)\chi_1(\mathbf{R}_1) + \left(\frac{1}{\pi d^2(1+4\bar{k}d^2)}\right)^{\frac{3}{2}} \int d^3\mathbf{R}_2 exp\left(\frac{-(1+8\bar{k}d^2)(\mathbf{R}_1^2+\mathbf{R}_2^2)}{2d^2}\right)\Big[-\frac{E_c}{3} - \frac{8Cd^2}{3(1+4\bar{k}d^2)} + \frac{4m}{3} - \frac{8}{9}\overline{C} + \frac{1+4\bar{k}d^2}{6md^2}\left(\frac{15}{2} - (\mathbf{R}_1^2+\mathbf{R}_2^2)(\frac{1+4\bar{k}d^2}{d^2})\right)\Big]\chi_2(\mathbf{R}_2) + \frac{8f^2n^2}{18\sqrt{2}(2\pi d^2)^{\frac{3}{2}}}\int d^3\mathbf{R}_2 \exp(\frac{-\mathbf{R}_2^2}{2d^2})\exp(-2p\mathbf{R}_1^2)[(\frac{\pi}{\frac{1}{2d^2}+2p})^{\frac{3}{2}}F_1(\mathbf{R}_1,\mathbf{R}_2) - 2AE(\mathbf{R}_1,\mathbf{R}_2)]\chi_2^*(\mathbf{R}_2) = 0, \tag{3.4.3}$$

$$\Delta_2(\mathbf{R}_2)\chi_2(\mathbf{R}_2) + \left(\frac{1}{\pi d^2(1+4\bar{k}d^2)}\right)^{\frac{3}{2}} \int d^3\mathbf{R}_1 exp\left(\frac{-(1+8\bar{k}d^2)(\mathbf{R}_1^2+\mathbf{R}_2^2)}{2d^2}\right)\Big[-\frac{E_c}{3} - \frac{8Cd^2}{3(1+4\bar{k}d^2)} + \frac{4m}{3} - \frac{8}{9}\overline{C} + \frac{1+4\bar{k}d^2}{6md^2}\left(\frac{15}{2} - (\mathbf{R}_1^2+\mathbf{R}_2^2)(\frac{1+4\bar{k}d^2}{d^2})\right)\Big]\chi_1(\mathbf{R}_1) + \frac{8f^2n^2}{18\sqrt{2}(2\pi d^2)^{\frac{3}{2}}}\int d^3\mathbf{R}_1 \exp(\frac{-\mathbf{R}_1^2}{2d^2})\exp(-2p\mathbf{R}_2^2)[(\frac{\pi}{\frac{1}{2d^2}+2p})^{\frac{3}{2}}F_1(\mathbf{R}_2,\mathbf{R}_1) - 2AE(\mathbf{R}_2,\mathbf{R}_1)]\chi_1^*(\mathbf{R}_1) = 0, \tag{3.4.4}$$

$$F_4(\mathbf{R}_1)\chi_1^*(\mathbf{R}_1) + \frac{8f^4n^2}{18\sqrt{2}(2\pi d^2)^{\frac{3}{2}}}\int d^3\mathbf{R}_2\exp(\frac{-\mathbf{R}_1^2}{2d^2})\exp(-2p\mathbf{R}_2^2)[(\frac{\pi}{\frac{1}{2d^2}+2p})^{\frac{3}{2}}F_3(\mathbf{R}_1,\mathbf{R}_2)-$$
$$2AE(\mathbf{R}_2,\mathbf{R}_1)]\chi_2(\mathbf{R}_2) + \frac{8n^4f^4}{3}\int d^3\mathbf{R}_2\exp(-2p\mathbf{R}_1^2-2p\mathbf{R}_2^2)\Big[(\frac{\pi}{4p})^{\frac{3}{2}}\big(E_cF_5(\mathbf{R}_1,\mathbf{R}_2)$$
$$+F_6(\mathbf{R}_1,\mathbf{R}_2)\big)+2A\big[\exp(-B\mathbf{R}_2^2)\{D(\mathbf{R}_1,\mathbf{R}_2)D_1(\mathbf{R}_2)+\mathbf{R}_1^4\mathbf{R}_2^4+2(\mathbf{R}_1^6+\mathbf{R}_1^4\mathbf{R}_2^2)$$
$$D_2(\mathbf{R}_1)+2(\mathbf{R}_1^2+\mathbf{R}_2^2)D_3(\mathbf{R}_2)+D_4(\mathbf{R}_2)-4\mathbf{R}_2^4D_5(\mathbf{R}_1,\mathbf{R}_2)-4D_6(\mathbf{R}_1,\mathbf{R}_2)-$$
$$8\mathbf{R}_2^2D_7(\mathbf{R}_1,\mathbf{R}_2)-4\mathbf{R}_1^4D_8(\mathbf{R}_2)-4D_9(\mathbf{R}_2)-8\mathbf{R}_1^2D_{10}(\mathbf{R}_2)+16D_{11}(\mathbf{R}_1,\mathbf{R}_2)\}$$
$$\exp(\frac{(2B)^2\mathbf{R}_2^2}{4(B+4p)})+\exp(-B\mathbf{R}_1^2)\{D(\mathbf{R}_1,\mathbf{R}_2)D_1(\mathbf{R}_1)+\mathbf{R}_1^4\mathbf{R}_2^4+2(\mathbf{R}_1^6+\mathbf{R}_1^4\mathbf{R}_2^2)$$
$$D_2(\mathbf{R}_1)+2(\mathbf{R}_1^2+\mathbf{R}_2^2)D_3(\mathbf{R}_1)+D_4(\mathbf{R}_1)-4\mathbf{R}_1^4D_5(\mathbf{R}_2,\mathbf{R}_1)-4D_6(\mathbf{R}_2,\mathbf{R}_1)-$$
$$8\mathbf{R}_1^2D_7(\mathbf{R}_2,\mathbf{R}_1)-4\mathbf{R}_1^4D_8(\mathbf{R}_1)-4D_9(\mathbf{R}_1)-8\mathbf{R}_2^2D_{10}(\mathbf{R}_1)+16D_{11}(\mathbf{R}_2,\mathbf{R}_1)\}$$
$$\exp(\frac{(2B)^2\mathbf{R}_1^2}{4(B+4p)})\big]+\frac{1}{2m}(\frac{\pi}{4p})^{\frac{3}{2}}D_{12}(\mathbf{R}_1,\mathbf{R}_2)\Big]\chi_2^*(\mathbf{R}_2)=0, \tag{3.4.5}$$

and

$$F_4(\mathbf{R}_2)\chi_2^*(\mathbf{R}_2) + \frac{8f^4n^2}{18\sqrt{2}(2\pi d^2)^{\frac{3}{2}}}\int d^3\mathbf{R}_1\exp(\frac{-\mathbf{R}_2^2}{2d^2})\exp(-2p\mathbf{R}_1^2)[(\frac{\pi}{\frac{1}{2d^2}+2p})^{\frac{3}{2}}F_3(\mathbf{R}_2,\mathbf{R}_1)-$$
$$2AE(\mathbf{R}_1,\mathbf{R}_2)]\chi_1(\mathbf{R}_1) + \frac{8f^4n^4}{3}\int d^3\mathbf{R}_1\exp(-2p\mathbf{R}_2^2-2p\mathbf{R}_1^2)\Big[(\frac{\pi}{4p})^{\frac{3}{2}}\big(E_cF_5(\mathbf{R}_2,\mathbf{R}_1)$$
$$+F_6(\mathbf{R}_2,\mathbf{R}_1)\big)+2A\big[\exp(-B\mathbf{R}_2^1)\{D(\mathbf{R}_2,\mathbf{R}_1)D_1(\mathbf{R}_1)+\mathbf{R}_2^4\mathbf{R}_1^4+2(\mathbf{R}_2^6+\mathbf{R}_2^4\mathbf{R}_1^2)$$
$$D_2(\mathbf{R}_2)+2(\mathbf{R}_2^2+\mathbf{R}_1^2)D_3(\mathbf{R}_1)+D_4(\mathbf{R}_1)-4\mathbf{R}_1^4D_5(\mathbf{R}_2,\mathbf{R}_1)-4D_6(\mathbf{R}_2,\mathbf{R}_1)-$$
$$8\mathbf{R}_1^2D_7(\mathbf{R}_2,\mathbf{R}_1)-4\mathbf{R}_2^4D_8(\mathbf{R}_1)-4D_9(\mathbf{R}_1)-8\mathbf{R}_2^2D_{10}(\mathbf{R}_1)+16D_{11}(\mathbf{R}_2,\mathbf{R}_1)\}$$
$$\exp(\frac{(2B)^2\mathbf{R}_2^2}{4(B+4p)})+\exp(-B\mathbf{R}_2^2)\{D(\mathbf{R}_2,\mathbf{R}_1)D_1(\mathbf{R}_2)+\mathbf{R}_2^4\mathbf{R}_1^4+2(\mathbf{R}_2^6+\mathbf{R}_2^4\mathbf{R}_1^2)$$
$$D_2(\mathbf{R}_2)+2(\mathbf{R}_2^2+\mathbf{R}_1^2)D_3(\mathbf{R}_2)+D_4(\mathbf{R}_2)-4\mathbf{R}_2^4D_5(\mathbf{R}_1,\mathbf{R}_2)-4D_6(\mathbf{R}_1,\mathbf{R}_2)-$$
$$8\mathbf{R}_2^2D_7(\mathbf{R}_1,\mathbf{R}_2)-4\mathbf{R}_2^4D_8(\mathbf{R}_2)-4D_9(\mathbf{R}_2)-8\mathbf{R}_1^2D_{10}(\mathbf{R}_2)+16D_{11}(\mathbf{R}_1,\mathbf{R}_2)\}$$
$$\exp(\frac{(2B)^2\mathbf{R}_1^2}{4(B+4p)})\big](\frac{\pi}{B+4p})^{\frac{3}{2}}+\frac{1}{2m}(\frac{\pi}{4p})^{\frac{3}{2}}D_{12}(\mathbf{R}_2,\mathbf{R}_1)\Big]\chi_1^*(\mathbf{R}_1)=0. \tag{3.4.6}$$

Here,

$$\Delta_i(\mathbf{R}_i) = -E_c - 8Cd^2 - \frac{8}{3}\overline{C} - \frac{\nabla^2_{\mathbf{R}_i}}{2m} + \frac{3}{2}\omega + 4m,$$

$$F_1(\mathbf{R}_i, \mathbf{R}_j) = (\mathbf{R}_i^4 + \frac{15}{4(\frac{1}{2d^2}+2p)^2} + \frac{\mathbf{R}_i^2}{\frac{1}{2d^2}+2p})\{E_c - 24\overline{C} - 28C\mathbf{R}_j^2 - 28C\frac{3}{2(\frac{1}{2d^2}+2p)}$$
$$+ 2A\exp(-B\mathbf{R}_i^2 - B\mathbf{R}_j^2) + 2A\exp(-B\mathbf{R}_i^2 + B\mathbf{R}_j^2)\} - 28C(\frac{3\mathbf{R}_i^4}{2(\frac{1}{2d^2}+2p)} +$$
$$\frac{105}{8(\frac{1}{2d^2}+2p)^3} + \frac{5\mathbf{R}_i^2}{2(\frac{1}{2d^2}+2p)^2}) + \frac{1}{2m}\{24\mathbf{R}_i^2 - 56p\mathbf{R}_i^4 + 16p^2\mathbf{R}_i^6 - R_i^4(\frac{3}{d^2} + \frac{\mathbf{R}_j^2}{d^4}) +$$
$$\frac{1}{2(\frac{1}{2d^2}+2p)}(72 - 112p\mathbf{R}_i^2 + 80p^2\mathbf{R}_i^4) + \frac{1}{(\frac{1}{2d^2}+2p)^2}(400p^2\mathbf{R}_i^2 - 840p) +$$
$$\frac{1680p^2}{8(\frac{1}{2d^2}+2p)^3}\},$$

$$E(\mathbf{R}_i) = \exp(-B\mathbf{R}_i^2)\exp(\frac{B^2\mathbf{R}_i^2}{\frac{1}{2d^2}+2p+B}),$$

$$F_2(\mathbf{R}_i, \mathbf{R}_j) = 2\mathbf{R}_i^4 + \frac{10B^2\mathbf{R}_j^2}{(\frac{1}{2d^2}+2p+B)^3} + \frac{2B^4\mathbf{R}_j^4}{(\frac{1}{2d^2}+2p+B)^4} + \frac{15}{2(\frac{1}{2d^2}+2p+B)^2} +$$
$$\frac{4B^2\mathbf{R}_i^2\mathbf{R}_j^2}{(\frac{1}{2d^2}+2p+B)^2} + \frac{2(\mathbf{R}_i^2)}{(\frac{1}{2d^2}+2p+B)} - \frac{8B^2(\mathbf{R}_i.\mathbf{R}_j)^2}{(\frac{1}{2d^2}+2p+B)^2},$$

$$E(\mathbf{R}_i, \mathbf{R}_j) = (\frac{\pi}{\frac{1}{2d^2}+2p+B})^{\frac{3}{2}}\{16E(\mathbf{R}_j)F_2(\mathbf{R}_i, \mathbf{R}_j) + 2E(\mathbf{R}_i)F_2(\mathbf{R}_i, \mathbf{R}_i)\},$$

$$F_3(\mathbf{R}_i, \mathbf{R}_j) = (\mathbf{R}_j^4 + \frac{15}{4(\frac{1}{2d^2}+2p)^2} + \frac{\mathbf{R}_j^2}{\frac{1}{2d^2}+2p})\{E_c - 24\overline{C} - 28C\mathbf{R}_i^2 - 28C\frac{3}{2(\frac{1}{2d^2}+2p)}$$
$$+ 2A\exp(-B\mathbf{R}_i^2 - B\mathbf{R}_j^2) + 2A\exp(-B\mathbf{R}_i^2 + B\mathbf{R}_j^2)\} - 28C(\frac{3\mathbf{R}_j^4}{2(\frac{1}{2d^2}+2p)} +$$
$$\frac{105}{8(\frac{1}{2d^2}+2p)^3} + \frac{5\mathbf{R}_j^2}{2(\frac{1}{2d^2}+2p)^2}) + \frac{1}{2m}\{20\mathbf{R}_j^2 - 44p\mathbf{R}_j^4 + 16p^2\mathbf{R}_j^6 - \frac{6\mathbf{R}_j^4}{d^2} + \frac{\mathbf{R}_j^4\mathbf{R}_i^2}{d^4}$$
$$+ \frac{3}{2(\frac{1}{2d^2}+2p)}(42 - 56p\mathbf{R}_j^2 + 32p^2\mathbf{R}_j^4 - \frac{12R_j^2}{d^2} + \frac{2R_j^2R_i^2}{d^4} + \frac{R_2^4}{d^4}) + \frac{15}{4(\frac{1}{2d^2}+2p)^2}$$
$$(-12p + 16p^2\mathbf{R}_j^2 - \frac{6}{d^2} + \frac{\mathbf{R}_j^2}{d^4} + \frac{2\mathbf{R}_j^2}{d^4}) + \frac{1}{d^4}\frac{35\times 3}{(\frac{1}{2d^2}+2p)^3} + (112p$$
$$- 64p^2\mathbf{R}_j^2 + \frac{24}{d^2} - \frac{4\mathbf{R}_i^2}{d^4})\frac{\mathbf{R}_j^2}{2(\frac{1}{2d^2}+2p)} - \frac{20\mathbf{R}_j^2}{d^4(\frac{1}{2d^2}+2p)^2}\},$$

$$F_4(\mathbf{R}_i) = 4m + n^4\{\frac{225E_c}{(4p)^4}(\frac{\pi}{2p})^3 - \frac{\pi^3}{3}\left(\frac{225A}{16(2p+B)^{\frac{7}{2}}(2p)^{\frac{7}{2}}} + \frac{225\bar{c}}{16(2p)^7} + \frac{1575c}{32(2p)^8}\right) +$$
$$\frac{8}{2m}\left(\frac{105}{(8p)^3}\frac{31}{2} - \frac{15}{64p^2}\frac{299}{16p} + \frac{3}{8p}\frac{685}{256p^2} - \frac{39690}{8p^3} + 32p^2\frac{10395}{(8p)^5} + \frac{315}{p^3} - \frac{6615}{(8p)^3}\right)$$
$$(\frac{\pi}{4p})^3 + \frac{8\nabla^2_{\mathbf{R}_i}}{2m}\frac{225\pi^3}{16384p^7}\},$$

$$F_5(\mathbf{R}_i, \mathbf{R}_j) = \mathbf{R}_i^4\mathbf{R}_j^4 + \frac{945}{(8p)^4} + \frac{1}{(8p)^2}(15\mathbf{R}_i^4 + 15\mathbf{R}_j^4 - 36\mathbf{R}_i^2\mathbf{R}_j^2 - 32(\mathbf{R}_i.\mathbf{R}_j)^2) +$$
$$\frac{1}{8p}(2\mathbf{R}_j^4\mathbf{R}_i^2 + 2\mathbf{R}_i^4\mathbf{R}_j^2) + \frac{70}{(8p)^3}(\mathbf{R}_i^2 + \mathbf{R}_j^2),$$

$$F_6(\mathbf{R}_i, \mathbf{R}_j) = (-10A\exp(-B\overline{\mathbf{R}_i + \mathbf{R}_j}^2) - 10A\exp(-B\overline{\mathbf{R}_i - \mathbf{R}_j}^2))\{\frac{15}{(8p)^2}(\mathbf{R}_j^4 + \mathbf{R}_i^4$$
$$+ 4\mathbf{R}_i^2\mathbf{R}_j^2) + \mathbf{R}_i^4\mathbf{R}_j^4 + \frac{6}{8p}(\mathbf{R}_i^6 + \mathbf{R}_i^4\mathbf{R}_j^2) + \frac{210}{(8p)^3}(\mathbf{R}_i^2 + \mathbf{R}_j^2) + \frac{945}{(8p)^4} - \frac{\mathbf{R}_j^4\mathbf{R}_i^2}{2p}$$
$$- \frac{140\mathbf{R}_i^2}{(8p)^3} - 80\frac{\mathbf{R}_i^2\mathbf{R}_i^2}{(8p)^2} - \frac{\mathbf{R}_i^4\mathbf{R}_j^2}{2p} - \frac{140\mathbf{R}_j^2}{(8p)^3} + \frac{32(\mathbf{R}_i.\mathbf{R}_j)^2}{(8p)^2} + \frac{16R_i^2R_j^2}{(8p)^2}\},$$

$$D(\mathbf{R}_i,\mathbf{R}_j)=\mathbf{R}_j^4+\mathbf{R}_i^4+4\mathbf{R}_i^2\mathbf{R}_j^2,$$

$$D_1(\mathbf{R}_j)=\frac{10(2B\mathbf{R}_j)^2}{(2B+8p)^3}+\frac{(2B\mathbf{R}_j)^4}{(2B+8p)^4}+\frac{15}{(2B+8p)^2},$$

$$D_2(\mathbf{R}_i)=\frac{(2B\mathbf{R}_i)^2}{(2B+8p)^2}+\frac{3}{(2B+8p)},$$

$$D_3(\mathbf{R}_i)=\frac{(2B\mathbf{R}_i)^6}{(2B+8p)^6}+\frac{21(2B\mathbf{R}_i)^4}{(2B+8p)^5}+\frac{105}{(2B+8p)^3}+\frac{105(2B\mathbf{R}_i)^2}{(2B+8p)^4},$$

$$D_4(\mathbf{R}_i)=\frac{(2B\mathbf{R}_i)^8}{(2B+8p)^8}+\frac{36(2B\mathbf{R}_i)^6}{(2B+8p)^7}+\frac{378(2B\mathbf{R}_i)^4}{(2B+8p)^6}+\frac{1260(2B\mathbf{R}_i)^2}{(2B+8p)^5}+\frac{945}{(2B+8p)^4},$$

$$D_5(\mathbf{R}_i,\mathbf{R}_j)=\frac{(2B)^2(\mathbf{R}_i.\mathbf{R}_j)^2}{(2B+8p)^2}+\frac{3\mathbf{R}_i^2}{(2B+8p)},$$

$$D_6(\mathbf{R}_i,\mathbf{R}_j)=\frac{(2B)^6(\mathbf{R}_i.\mathbf{R}_j)^2\mathbf{R}_j^4}{(2B+8p)^6}+\frac{(2B)^4}{(2B+8p)^5}(18\mathbf{R}_j^2(\mathbf{R}_i.\mathbf{R}_j)^2+\mathbf{R}_i^2\mathbf{R}_j^4)+\frac{(2B)^2}{(2B+8p)^4}$$
$$(63(\mathbf{R}_i.\mathbf{R}_j)^2+14\mathbf{R}_i^2\mathbf{R}_j^2+x_i^2x_j^2+y_i^2y_j^2+z_i^2z_j^2)+\frac{35\mathbf{R}_i^2}{(2B+8p)^3},$$

$$D_7(\mathbf{R}_i,\mathbf{R}_j)=\frac{(2B)^4}{(2B+8p)^4}\mathbf{R}_j^2(\mathbf{R}_i.\mathbf{R}_j)^2+\frac{(2B)^2}{(2B+8p)^3}(7(\mathbf{R}_i.\mathbf{R}_j)^2+\mathbf{R}_i^2\mathbf{R}_j^2)+\frac{5\mathbf{R}_i^2}{(2B+8p)^2},$$

$$D_8(\mathbf{R}_j)=\frac{(2B)^2\mathbf{R}_j^4}{(2B+8p)^2}+\frac{\mathbf{R}_j^2}{2B+8p},$$

$$D_9(\mathbf{R}_j)=\frac{35\mathbf{R}_j^2}{(2B+8p)^3}+\frac{(2B)^6}{(2B+8p)^6}\mathbf{R}_j^8+\frac{19(2B)^4}{(2B+8p)^5}\mathbf{R}_j^6+\frac{77(2B)^2}{(2B+8p)^4}\mathbf{R}_j^4,$$

$$D_{10}(\mathbf{R}_j)=\frac{(2B)^4}{(2B+8p)^4}\mathbf{R}_j^6+\frac{(2B)^2}{(2B+8p)^3}\mathbf{R}_j^4+\frac{5}{(2B+8p)^2}\mathbf{R}_j^2,$$

$$D_{11}(\mathbf{R}_i,\mathbf{R}_j)=\frac{(2B)^4}{(2B+8p)^4}\mathbf{R}_j^4(\mathbf{R}_i.\mathbf{R}_j)^2+\frac{(2B)^2}{(2B+8p)^3}(5\mathbf{R}_j^2(\mathbf{R}_i.\mathbf{R}_j)^2+\mathbf{R}_i^2\mathbf{R}_j^4)$$
$$+\frac{1}{(2B+8p)^2}(2(\mathbf{R}_i.\mathbf{R}_j)^2+\mathbf{R}_i^2\mathbf{R}_j^2),\text{ and}$$

$$D_{12}(\mathbf{R}_i,\mathbf{R}_j)=\frac{1}{2048p^3}\Big\{-9975+32768p^5\mathbf{R}_i^4\mathbf{R}_j^4(R_i^2+R_j^2)+40p(287R_i^2+31R_j^2)+$$
$$4096p^4(2R_i^6R_j^2-43R_i^4R_j^4+2R_i^2R_j^6)+512p^3(R_i^2+R_2^j)\big(15R_i^4-14R_i^2R_j^2$$
$$+15R_j^4+16(2(\mathbf{R}_i.\mathbf{R}_j)^2+\mathbf{R}_i^2\mathbf{R}_j^2)\big)-64p^2\Big(287R_i^4-772R_i^2R_j^2+$$
$$287R_j^4+672\big(2(\mathbf{R}_i.\mathbf{R}_j)^2+\mathbf{R}_i^2\mathbf{R}_j^2\big)-1024\big(7\mathbf{R}_i^2\mathbf{R}_j^2+14(\mathbf{R}_i.\mathbf{R}_j)^2\big)\Big)\Big\}.$$

We have eventually replaced $\mathbf{r}_1, \mathbf{r}_2, \mathbf{r}_3, \mathbf{r}_4$ by $\mathbf{R}_1, \mathbf{R}_2, \mathbf{R}_3$, and $\mathbf{R}_c$. With trivial integration on $\mathbf{R}_c$, we have eq.(3.3.2) that is independent of $\mathbf{R}_c$. Now, after the integration on $\mathbf{R}_3$, the above four integral equations (3.4.3-3.4.6) depend only on $\mathbf{R}_1$ and $\mathbf{R}_2$. So every quantity which we want to calculate depends on $\mathbf{R}_1$ and $\mathbf{R}_2$. In eq.(3.4.3-3.4.4), the first two terms containing $\chi_1(\mathbf{R}_1)$ and $\chi_2(\mathbf{R}_2)$ in each equation are for the ground state. It is noted that in these terms, there is no dot product of vectors $\mathbf{R}_1$ and $\mathbf{R}_2$. So the results from these terms should not depend on the angle between $\mathbf{R}_1$ and $\mathbf{R}_2$, that we call θ. The third term in each of eqs.(3.4.3-3.4.4) is due to the gluonic ground and excited states. In these terms dot product of two vectors ($\mathbf{R}_1$ and $\mathbf{R}_2$) appear, so the results from these terms depend on θ.

3.5 Solving the Integral Equations

Now taking the three dimensional Fourier transform of eq.(3.4.3,3.4.5) with respect to $\mathbf{R}_1$ and eq.(3.4.4,3.4.6) with respect to $\mathbf{R}_2$, the integral equations become

$$
\begin{aligned}
&(-E_c - 8Cd^2 - \frac{8}{3}\overline{C} + \frac{P_1^2}{2m} + \frac{3}{2}\omega + 4m)\chi_1(\mathbf{P}_1) + \frac{1}{(2\pi)^{\frac{3}{2}}}\left(\frac{1}{\pi d^2(1+4\bar{k}d^2)}\right)^{\frac{3}{2}}\int d^3\mathbf{R}_1 \\
&d^3\mathbf{R}_2 \exp(i\mathbf{P}_1.\mathbf{R}_1) exp\left(\frac{-(1+8\bar{k}d^2)(\mathbf{R}_1^2+\mathbf{R}_2^2)}{2d^2}\right)\Bigg[-\frac{E_c}{3} - \frac{8Cd^2}{3(1+4\bar{k}d^2)} + \frac{4m}{3} - \\
&\frac{8}{9}\overline{C} + \frac{1+4\bar{k}d^2}{6md^2}\left(\frac{15}{2} - (\mathbf{R}_1^2+\mathbf{R}_2^2)(\frac{1+4\bar{k}d^2}{d^2})\right)\Bigg]\chi_2(\mathbf{R}_2) + \frac{1}{(2\pi)^{\frac{3}{2}}}\int d^3\mathbf{R}_1 d^3\mathbf{R}_2 \\
&\exp(i\mathbf{P}_1.\mathbf{R}_1)\exp(\frac{-\mathbf{R}_2^2}{2d^2})\exp(-2p\mathbf{R}_1^2)\frac{8f^4n^2}{18\sqrt{2}(2\pi d^2)^{\frac{3}{2}}}\Bigg[(\frac{\pi}{\frac{1}{2d^2}+2p})^{\frac{3}{2}}F_1(\mathbf{R}_1,\mathbf{R}_2) \\
&- 2AE(\mathbf{R}_1,\mathbf{R}_2)\Bigg]\chi_2^*(\mathbf{R}_2) = 0,
\end{aligned}
\tag{3.5.1}
$$

$$(-E_c - 8Cd^2 - \frac{8}{3}\overline{C} + \frac{P_2^2}{2m} + \frac{3}{2}\omega + 4m)\chi_2(\mathbf{P}_2) + \frac{1}{(2\pi)^{\frac{3}{2}}}\left(\frac{1}{\pi d^2(1+4\overline{k}d^2)}\right)^{\frac{3}{2}}\int d^3\mathbf{R}_1$$
$$d^3\mathbf{R}_2 \exp(\imath\mathbf{P}_2.\mathbf{R}_2) exp\left(\frac{-(1+8\overline{k}d^2)(\mathbf{R}_1^2+\mathbf{R}_2^2)}{2d^2}\right)[-\frac{E_c}{3} - \frac{8Cd^2}{3(1+4\overline{k}d^2)} + \frac{4m}{3} -$$
$$\frac{8}{9}\overline{C} + \frac{1+4\overline{k}d^2}{6md^2}\left(\frac{15}{2} - (\mathbf{R}_1^2+\mathbf{R}_2^2)(\frac{1+4\overline{k}d^2}{d^2})\right)]\chi_1(\mathbf{R}_1) + \frac{1}{(2\pi)^{\frac{3}{2}}}\int d^3\mathbf{R}_1 d^3\mathbf{R}_2$$
$$\exp(\imath\mathbf{P}_2.\mathbf{R}_2)\exp(\frac{-\mathbf{R}_1^2}{2d^2})\exp(-2p\mathbf{R}_2^2)\frac{8f^4n^2}{18\sqrt{2}(2\pi d^2)^{\frac{3}{2}}}[(\frac{\pi}{\frac{1}{2d^2}+2p})^{\frac{3}{2}}F_1(\mathbf{R}_2,\mathbf{R}_1) -$$
$$2AE(\mathbf{R}_2,\mathbf{R}_1)]\chi_1^*(\mathbf{R}_1) = 0, \tag{3.5.2}$$

$$\left(4m + n^4\{\frac{225E_c}{(4p)^4}(\frac{\pi}{2p})^3 - \frac{\pi^3}{3}\left(\frac{225A}{16(2p+B)^{\frac{7}{2}}(2p)^{\frac{7}{2}}} + \frac{225\overline{c}}{16(2p)^7} + \frac{1575c}{32(2p)^8}\right) + \frac{8}{2m}(\frac{105}{(8p)^3}\right.$$
$$\frac{31}{2} - \frac{15}{64p^2}\frac{299}{16p} + \frac{3}{8p}\frac{685}{256p^2} - \frac{39690}{8p^3} + 32p^2\frac{10395}{(8p)^5} + \frac{315}{p^3} - \frac{6615}{p^4})(\frac{\pi}{4p})^3 - \frac{8P_{1s}^2}{2m}$$
$$\left.\frac{225\pi^3}{16384p^7}\}\right)\chi_1^*(\mathbf{P}_{1s}) + \frac{1}{(2\pi)^{\frac{3}{2}}}\frac{8f^4n^2}{18\sqrt{2}(2\pi d^2)^{\frac{3}{2}}}\int d^3\mathbf{R}_1 d^3\mathbf{R}_2 \exp(\imath\mathbf{P}_{1s}.\mathbf{R}_1)\exp(\frac{-\mathbf{R}_1^2}{2d^2})$$
$$exp(-2p\mathbf{R}_2^2)[.....]\chi_2(\mathbf{R}_2) + \frac{1}{(2\pi)^{\frac{3}{2}}}\frac{8f^4n^4}{3}\int d^3\mathbf{R}_1 d^3\mathbf{R}_2 \exp(\imath\mathbf{P}_{11}.\mathbf{R}_1)\exp(-2p\mathbf{R}_1^2)$$
$$\exp(-2p\mathbf{R}_2^2)[.....]\chi_2^*(\mathbf{R}_2) = 0, \text{ and} \tag{3.5.3}$$

$$\left(4m + n^4\{\frac{225E_c}{(4p)^4}(\frac{\pi}{2p})^3 - \frac{\pi^3}{3}\left(\frac{225A}{16(2p+B)^{\frac{7}{2}}(2p)^{\frac{7}{2}}} + \frac{225\overline{c}}{16(2p)^7} + \frac{1575c}{32(2p)^8}\right) + \frac{8}{2m}(\frac{105}{(8p)^3}\right.$$
$$\frac{31}{2} - \frac{15}{64p^2}\frac{299}{16p} + \frac{3}{8p}\frac{685}{256p^2} - \frac{39690}{8p^3} + 32p^2\frac{10395}{(8p)^5} + \frac{315}{p^3} - \frac{6615}{p^4})(\frac{\pi}{4p})^3 - \frac{8P_{2s}^2}{2m}$$
$$\left.\frac{225\pi^3}{16384p^7}\}\right)\chi_2^*(\mathbf{P}_{2s}) + \frac{1}{(2\pi)^{\frac{3}{2}}}\frac{8f^4n^2}{18\sqrt{2}(2\pi d^2)^{\frac{3}{2}}}\int d^3\mathbf{R}_1 d^3\mathbf{R}_2 \exp(\imath\mathbf{P}_{2s}.\mathbf{R}_2)\exp(\frac{-\mathbf{R}_2^2}{2d^2})$$
$$exp(-2p\mathbf{R}_1^2)[.....]\chi_1(\mathbf{R}_1) + \frac{1}{(2\pi)^{\frac{3}{2}}}\frac{8f^4n^4}{3}\int d^3\mathbf{R}_1 d^3\mathbf{R}_2 \exp(\imath\mathbf{P}_{22}.\mathbf{R}_2)\exp(-2p\mathbf{R}_1^2$$
$$- 2p\mathbf{R}_2^2)[.....]\chi_1^*(\mathbf{R}_1) = 0. \tag{3.5.4}$$

In above $\chi_i(\mathbf{P}_i)$ is the fourier transform of $\chi_i(\mathbf{R}_i)$, and $\chi_i^*(\mathbf{P}_i s)$ is the fourier transform of $\chi_i^*(\mathbf{R}_i)$. The linear momentas P_1,P_2 are conjugate to $\mathbf{R}_1$, $\mathbf{R}_2$ for ground state gluonic field and P_{1s}, P_{2s} are conjugate to $\mathbf{R}_1$, $\mathbf{R}_2$ for excited state gluonic field. The off-diagonal terms of eqs.(3.5.3) and (3.5.4) are too lengthy and not used for results, so dots are used to reduce the length of our equations. The above eqs.(3.5.1-3.5.4) have formal solutions as [26]

$$\chi_1(\mathbf{P}_1) = \delta(P_1 - P_c(1))/P_c^2(1) - \frac{1}{\triangle_1(P_1)}\frac{1}{(2\pi)^{\frac{3}{2}}}\left(\frac{1}{\pi d^2(1+4\bar{k}d^2)}\right)^{\frac{3}{2}}\int d^3\mathbf{R}_1 d^3\mathbf{R}_2$$
$$\exp(\imath\mathbf{P}_1.\mathbf{R}_1)exp\left(\frac{-(1+8\bar{k}d^2)(\mathbf{R}_1^2+\mathbf{R}_2^2)}{2d^2}\right)[-\frac{E_c}{3} - \frac{8Cd^2}{3(1+4\bar{k}d^2)} + \frac{4m}{3} - \frac{8}{9}\overline{C} +$$
$$\frac{1+4\bar{k}d^2}{6md^2}\left(\frac{15}{2} - (\mathbf{R}_1^2+\mathbf{R}_2^2)(\frac{1+4\bar{k}d^2}{d^2})\right)]\chi_2(\mathbf{R}_2) - \frac{1}{\triangle_1(P_1)}\frac{1}{(2\pi)^{\frac{3}{2}}}\int d^3\mathbf{R}_1 d^3\mathbf{R}_2$$
$$\exp(\imath\mathbf{P}_1.\mathbf{R}_1)\quad \exp(\frac{-R_2^2}{2d^2})\quad \exp(-2pR_1^2)\frac{8f^4n^2}{18\sqrt{2}(2\pi d^2)^{\frac{3}{2}}}[(\frac{\pi}{\frac{1}{2d^2}+2p})^{\frac{3}{2}}F_1(\mathbf{R}_1,\mathbf{R}_2)$$
$$-2AE(\mathbf{R}_1,\mathbf{R}_2)]\chi_2^*(\mathbf{R}_2),$$

(3.5.5)

$$\chi_2(P_2) = \delta(P_2 - P_c(2))/P_c^2(2) - \frac{1}{\triangle_2(P_2)}\frac{1}{(2\pi)^{\frac{3}{2}}}\left(\frac{1}{\pi d^2(1+4\bar{k}d^2)}\right)^{\frac{3}{2}}\int d^3\mathbf{R}_1 d^3\mathbf{R}_2$$
$$\exp(\imath\mathbf{P}_2.\mathbf{R}_2)exp\left(\frac{-(1+8\bar{k}d^2)(\mathbf{R}_1^2+\mathbf{R}_2^2)}{2d^2}\right)[-\frac{E_c}{3} - \frac{8Cd^2}{3(1+4\bar{k}d^2)} + \frac{4m}{3} - \frac{8}{9}\overline{C} +$$
$$\frac{1+4\bar{k}d^2}{6md^2}\left(\frac{15}{2} - (\mathbf{R}_1^2+\mathbf{R}_2^2)(\frac{1+4\bar{k}d^2}{d^2})\right)]\chi_1(\mathbf{R}_1) - \frac{1}{\triangle_2(P_2)}\frac{1}{(2\pi)^{\frac{3}{2}}}\int d^3\mathbf{R}_1 d^3\mathbf{R}_2$$
$$\exp(\imath\mathbf{P}_2.\mathbf{R}_2)\quad \exp(\frac{-R_1^2}{2d^2})\quad \exp(-2pR_2^2)\frac{8f^4n^2}{18\sqrt{2}(2\pi d^2)^{\frac{3}{2}}}[(\frac{\pi}{\frac{1}{2d^2}+2p})^{\frac{3}{2}}F_1(\mathbf{R}_2,\mathbf{R}_1)$$
$$-2AE(\mathbf{R}_2,\mathbf{R}_1)]\chi_1^*(\mathbf{R}_1),$$

(3.5.6)

$$\chi_1^*(P_{1s}) = \delta(P_{1s} - P_c(1s))/P_c^2(1s) - \frac{1}{\triangle_1(P_{1s})}\frac{1}{(2\pi)^{\frac{3}{2}}}\frac{8f^4n^2}{18\sqrt{2}(2\pi d^2)^{\frac{3}{2}}}\int d^3\mathbf{R}_1 d^3\mathbf{R}_2$$
$$\exp(\imath\mathbf{P}_{1s}.\mathbf{R}_1)\exp(\frac{-R_1^2}{2d^2})exp(-2pR_2^2)[.....]\chi_2(\mathbf{R}_2) - \frac{1}{\triangle_1(P_{1s})}\frac{8f^4n^4}{3}\frac{1}{(2\pi)^{\frac{3}{2}}}$$
$$\int d^3\mathbf{R}_1 d^3\mathbf{R}_2 \exp(\imath\mathbf{P}_{1s}.\mathbf{R}_1)\exp(-2pR_1^2)\exp(-2pR_2^2)[.....]\chi_2^*(\mathbf{R}_2), \tag{3.5.7}$$

and

$$\chi_2^*(P_{2s}) = \delta(P_{2s} - P_c(2s))/P_c^2(2s) - \frac{1}{\triangle_2(P_{2s})}\frac{1}{(2\pi)^{\frac{3}{2}}}\frac{8f^4n^2}{18\sqrt{2}(2\pi d^2)^{\frac{3}{2}}}\int d^3\mathbf{R}_1 d^3\mathbf{R}_2$$
$$\exp(\imath\mathbf{P}_{2s}.\mathbf{R}_2)\exp(\frac{-R_2^2}{2d^2})exp(-2pR_1^2)[.....]\chi_1(\mathbf{R}_1) - \frac{1}{\triangle_2(Pf_{2s})}\frac{8f^4n^4}{3}\frac{1}{(2\pi)^{\frac{3}{2}}}$$
$$\int d^3\mathbf{R}_1 d^3\mathbf{R}_2 \exp(\imath\mathbf{P}_{2s}.\mathbf{R}_2)\exp(-2pR_2^2)\exp(-2pR_1^2)[.....]\chi_1^*(\mathbf{R}_1). \tag{3.5.8}$$

Here

$$\triangle_1(\mathbf{P}_i) = (-E_c - 8Cd^2 - \frac{8}{3}\overline{C} + \frac{\mathbf{P}_i^2}{2m} + \frac{3}{2}\omega + 4m) - \imath\varepsilon,$$
$$\triangle_2(\mathbf{P}_{is}) = 4m + n^4\{\frac{225E_c}{(4p)^4}(\frac{\pi}{2p})^3 - \frac{\pi^3}{3}\left(\frac{225A}{16(2p+B)^{\frac{7}{2}}(2p)^{\frac{7}{2}}} + \frac{225\overline{c}}{16(2p)^7} + \frac{1575c}{32(2p)^8}\right) +$$
$$\frac{4}{m} - \frac{\pi^3}{3}\left(\frac{225A}{16(2p+B)^{\frac{7}{2}}(2p)^{\frac{7}{2}}} + \frac{225\overline{c}}{16(2p)^7} + \frac{1575c}{32(2p)^8}\right)\left(\frac{105}{(8p)^3}\frac{31}{2} - \frac{15}{64p^2}\frac{299}{16p} + \frac{3}{8p}\right.$$
$$\left.\frac{685}{256p^2} - \frac{39690}{8p^3} + 32p^2\frac{10395}{(8p)^5} + \frac{315}{p^3} - \frac{6615}{(8p)^3}\right)(\frac{\pi}{4p})^3 - \frac{8(\mathbf{P}_{is})^2}{2m}\frac{225\pi^3}{16384p^7}\} - \imath\varepsilon, \tag{3.5.9}$$

and

$$P_c(2) = P_c(1) = \sqrt{2m(E_c - 4m - \frac{3}{md^2} + \frac{8}{3}\overline{C})},$$
$$P_c(2s) = P_c(1s) = \sqrt{2m(E_c - 4m) - \left(0.6667\overline{C} + \frac{1.1667C}{p} + \frac{13.682p^{7/2}}{(0.0657+2p)^{7/2}}\right)m - 64p.} \tag{3.5.10}$$

Because of the coupling to the gluonic excitations, it become difficult to solve above integral equations for non trivial solutions for $\chi_1(\mathbf{P}_1), \chi_2(\mathbf{P}_2), \chi_1^*(\mathbf{P}_{1s})$, and $\chi_2^*(\mathbf{P}_{2s})$

analytically as done in [26, 20]. In [26], the meson wave functions, including gluonic field overlap factor, is separable in $\mathbf{R}_1$, $\mathbf{R}_2$ and hence the integral equations can be solved analytically by replacing χ_1 and χ_2 with solutions obtained by Born Approximation. But in our present work, the meson-meson wave functions are not separable in $\mathbf{R}_1$,$\mathbf{R}_2$. So we use the Born approximation as used in [23] to solve the integral equations for meson-meson scattering) to solve the integral equations. Our results given below also justify our use of the Born Approximation. For using this approximation, we first find the solutions $(\chi_i(\mathbf{R}_i), \chi_i^*(\mathbf{R}_i))$ of eqs.(3.4.3-3.4.6) in absence of interactions (meaning $f = f^a = f^c = 0$). These are

$$\begin{aligned} \chi_1(\mathbf{R}_1) &= \sqrt{\frac{2}{\pi}}\exp(\imath\mathbf{P}_1.\mathbf{R}_1), \\ \chi_2(\mathbf{R}_2) &= \sqrt{\frac{2}{\pi}}\exp(\imath\mathbf{P}_2.\mathbf{R}_2), \\ \chi_1^*(\mathbf{R}_1) &= \sqrt{\frac{2}{\pi}}\exp(\imath\mathbf{P}_{1s}.\mathbf{R}_1), \\ \text{and} \qquad \chi_2^*(\mathbf{R}_2) &= \sqrt{\frac{2}{\pi}}\exp(\imath\mathbf{P}_{2s}.\mathbf{R}_2). \end{aligned} \tag{3.5.11}$$

Here the coefficient of $\exp(\imath\mathbf{P}_i.\mathbf{R}_i)$ is chosen so that it makes $\chi_i(\mathbf{R}_i)$ with $i = 1, 2$ as Fourier transform of $\frac{\delta(P_i - P_c(i))}{P_c^2(i)}$. Similarly the coefficient of $\exp(\imath\mathbf{P}_{is}.\mathbf{R}_i)$ is chosen. Using this approximation, the integrations on $\mathbf{R}_1$ and $\mathbf{R}_2$ in eq.(3.5.5) can be performed

to give

$$\chi_1(\mathbf{P}_1) = \delta(P_1 - P_c(1))/P_c^2(1) - \frac{1}{\triangle_1(P_1)}\left[\frac{1}{3}(\frac{2}{\pi})^{\frac{1}{2}}(\frac{1}{2\pi})^{\frac{3}{2}}\left(\frac{1}{\pi d^2(1+4\bar{k}d^2)}\right)^{\frac{3}{2}}\left(\frac{2\pi d^2}{1+8\bar{k}d^2}\right)^3\right.$$
$$\left.exp\left(-\frac{(p_1^2+p_2^2)d^2}{2(1+8\bar{k}d^2)}\right)\Omega_1\right] - \frac{1}{\triangle_1(P_1)}\frac{1}{3}(\frac{2}{\pi})^{\frac{1}{2}}(\frac{1}{\pi d^2})^{\frac{3}{2}}f^a n^2(\frac{1}{2\pi})^{\frac{3}{2}}\left[\exp(\frac{-P_{1s}^2 d^2}{2})\right.$$
$$(2\pi d^2)^{\frac{3}{2}}\left((\frac{\pi}{2p+\frac{1}{2d^2}})^{\frac{3}{2}}F(p) - \frac{4A}{6\sqrt{2}}F_1(p)\right) - \frac{4A}{6\sqrt{2}}(\frac{\pi}{2p+\frac{1}{2d^2}})^{\frac{3}{2}}\exp(\frac{-p_1^2}{8p+4B})$$
$$(\frac{\pi}{2p+B})^{\frac{3}{2}}(\frac{\pi}{F_2(p)})^{\frac{3}{2}}exp(\frac{(\iota P_{1s} - 4\iota\frac{P_1 B}{8p+4B})^2}{4F_2(p)})\Omega_2 - \frac{4A}{6\sqrt{2}}(\frac{\pi}{2p+\frac{1}{2d^2}})^{\frac{3}{2}}\exp(\frac{-P_1^2}{8p+4B})$$
$$(\frac{\pi}{2p+B})^{\frac{3}{2}}(\frac{\pi}{F_2(p)})^{\frac{3}{2}}\exp(\frac{(\iota P_{1s} + 4\iota\frac{P_1 B}{8p+4B})^2}{4F_2(p)})\Omega_3 + \frac{16A}{3\sqrt{2}}(\frac{\pi}{F_3(p)})^{\frac{3}{2}}\exp(\frac{-P_1^2}{8p})$$
$$\left.(\frac{\pi}{2p})^{\frac{3}{2}}\Omega_4\right](\frac{\pi}{B+\frac{1}{2d^2}-\frac{B^2}{F_3(p)}})^{\frac{3}{2}}\exp(\frac{-P_{1s}^2}{4(B+\frac{1}{2d^2}-\frac{B^2}{F_3(p)})}). \tag{3.5.12}$$

Here,

$$\Omega_1 = -E_c - \frac{8Cd^2}{(1+4\bar{k}d^2)} + \frac{8}{3}C + 4m + \frac{15(1+4\bar{k}d^2)}{4md^2} - (\frac{(1+4\bar{k}d^2)^2}{2md^4})(\frac{-P_1^2 d^4 - P_2^2 d^4}{(1+8\bar{k}d^2)^2}$$
$$+ \frac{6d^2}{1+8\bar{k}d^2})$$

$$\Omega_2 = \left(\frac{-5P_1^2}{4(2p+B)^3} + \frac{15}{4(2p+B)^2} + \frac{15}{4(\frac{1}{2d^2}+2p)^2} - \frac{P_1^2}{4(2p+B)^2(\frac{1}{2d^2}+2p)} + \right.$$
$$\left. \frac{3}{2(2p+B)(\frac{1}{2d^2}+2p)} \right) + \left(\frac{5B^2}{(2p+B)^3} + \frac{4B^2}{4(2p+B)^2(\frac{1}{2d^2}+2p)} \right) \left(\frac{\iota P_{1s} - \frac{4\iota P_1 B}{8p+4B}}{4F_2^2(p)} \right.$$
$$\left. + \frac{3}{2F_2(p)} \right) + \left(\frac{-10\iota B}{4(2p+B)^3} + \frac{2\iota B}{4(2p+B)^2(\frac{1}{2d^2}+2p)} \right) \left(\frac{-2\iota P_1^2 B}{4(2p+B)} + \iota P_1.P_{1s} \right)$$
$$\frac{1}{2F_2(p)} + \frac{1}{16(2p+B)^4} \left\{ P_1^4 + 16B^4 \left(\frac{5(\iota P_{1s} - \frac{4\iota P_1 B}{8p+4B})^2}{4F_2^3(p)} + \frac{(\iota P_{1s} - \frac{4\iota P_1 B}{8p+4B})^4}{16F_2^4(p)} + \right. \right.$$
$$\left. \frac{15}{4F_2^2(p)} \right) - 8B^2 P_1^2 \left(\frac{(\iota P_{1s} - \frac{4\iota P_1 B}{8p+4B})^2}{4F_2^2(p)} + \frac{3}{2F_2(p)} \right) + 8BP_1^2\iota$$
$$\left(\frac{-2\iota P_1^2 \frac{B}{8p+4B} + \iota P_1.P_{1s}}{2F_2(p)} \right) - 32\iota B^3(P_{1x} + P_{1y} + P_{1z}) \left(\left(\frac{\iota B^3 P_1^3}{(2p+B)^3} - \frac{B^2\iota}{(2p+B)^2} \right. \right.$$
$$P_1^2(P_{1sx} + P_{1sy} + P_{1sz}) - 64\frac{B^2\iota}{(8p+4B)^2} P_1(P_1.P_{1s}) + \frac{16\iota B}{8p+4B}(P_1.P_{1s})P_{1s} +$$
$$\left. \frac{4\iota B}{8p+4B}(P_{1x} + P_{1y} + P_{1z})P_{1s}^2 - \iota P_{1s}^3 \right) \frac{1}{8F_2(p)^3} + \frac{(\iota P_{1s} - 4\iota \frac{P_1 B}{8p+4B})}{F_2(p)^2} \Bigg)$$
$$\left. - 16B^2 \left(P_1^2 \frac{(\iota P_{1s} - 4\iota \frac{P_1 B}{8p+4B})^2}{4F_2(p)^2} + \frac{P_1^2}{2F_2(p)} \right) \right\}$$

$$\Omega_3 = \left(\frac{-5P_1^2}{4(2p+B)^3} + \frac{15}{4(2p+B)^2} + \frac{15}{4(\frac{1}{2d^2}+2p)^2} - \frac{P_1^2}{4(2p+B)^2(\frac{1}{2d^2}+2p)} + \frac{3}{2(2p+B)(\frac{1}{2d^2}+2p)}\right) + \left(\frac{5B^2}{(2p+B)^3} + \frac{4B^2}{4(2p+B)^2(\frac{1}{2d^2}+2p)}\right)\left(\frac{\iota P_{1s} + \frac{4\iota P_1 B}{8p+4B}}{4F_2^2(p)} + \frac{3}{2F_2(p)}\right) + \left(\frac{-10\iota B}{4(2p+B)^3} + \frac{2\iota B}{4(2p+B)^2(\frac{1}{2d^2}+2p)}\right)\left(\frac{-2\iota P_1^2 B}{4(2p+B)} + \iota P_1.P_{1s}\right)\frac{1}{2F_2(p)} + \frac{1}{16(2p+B)^4}\left\{P_1^4 + 16B^4\left(\frac{5(\iota P_{1s} + \frac{4\iota P_1 B}{8p+4B})^2}{4F_2^3(p)} + \frac{(\iota P_{1s} + \frac{4\iota P_1 B}{8p+4B})^4}{16F_2^4(p)} + \frac{15}{4F_2^2(p)}\right) - 8B^2P_1^2\left(\frac{(\iota P_{1s} + \frac{4\iota P_1 B}{8p+4B})^2}{4F_2^2(p)} + \frac{3}{2F_2(p)}\right) - 8BP_1^2\iota\left(\frac{2\iota P_1^2\frac{B}{8p+4B} + \iota P_1.P_{1s}}{2F_2(p)}\right) + 32\iota B^3(P_{1x}+P_{1y}+P_{1z})\left(\left(\frac{-\iota B^3P_1^3}{(2p+B)^3} - \frac{B^2\iota}{(2p+B)^2}P_1^2(P_{1sx}+P_{1sy}+P_{1sz}) - 64\frac{B^2\iota}{(8p+4B)^2}P_1(P_1.P_{1s}) - \frac{16\iota B}{8p+4B}(P_1.P_{1s})P_{1s} - \frac{4\iota B}{8p+4B}(P_{1x}+P_{1y}+P_{1z})P_{1s}^2 - \iota P_{1s}^3\right)\frac{1}{8F_2(p)^3} + \frac{(\iota P_{1s} + 4\iota\frac{P_1 B}{8p+4B})}{F_2(p)^2}\right) - 16B^2\left(P_1^2\frac{(\iota P_{1s} + 4\iota\frac{P_1 B}{8p+4B})^2}{4F_2(p)^2} + \frac{P_1^2}{2F_2(p)}\right)\right\}$$

$$\Omega_4 = \frac{15}{2F_3^2(p)} - \frac{10P_1^2}{32p^3} + \frac{2P_1^4}{(4p)^4} + \frac{30}{16p^2} - \frac{2}{F_3(p)}(\frac{-P_1^2}{16p^2} + \frac{3}{4p}) + \left(\frac{10B^2}{F_3^3(p)} - \frac{8B^2}{4pF_3^2(p)}(1 - \frac{P_1^2}{4p}) + \frac{4B^2}{F_3^2(p)}(\frac{-P_1^2}{16p^2} + \frac{3}{4p})\right)\left(\frac{P_{1s}^2}{4B - 4\frac{B^2}{F_3(p)}} + \frac{3}{2B - 2\frac{B^2}{F_3(p)}}\right) + \frac{2B^4}{F_3^4(p)}\left(\frac{5P_{1s}^2}{4(B - \frac{B^2}{F_3(p)})^3} + \frac{P_{1s}^4}{16(B - \frac{B^2}{F_3(p)})^4} + \frac{15}{4(B - \frac{B^2}{F_3(p)})^2}\right)$$

$$F(p) = \Bigg\{ \left(\frac{-5P_1^2}{32p^3} + \frac{P_1^4}{16(2p)^4} + \frac{15}{16p^2} \right) \left(E + \frac{24\bar{c}}{6\sqrt{2}} + \frac{42c}{6\sqrt{2}(\frac{1}{2d^2}+2p)} - \frac{28p}{m} - \frac{3}{2md^2} \right.$$
$$+ \frac{20p^2}{m(\frac{1}{2d^2}+2p)} - \frac{8c}{6\sqrt{2}(\frac{1}{2d^2}+2p)} + (\frac{28c}{6\sqrt{2}} + \frac{1}{2md^4})(-P_{11}^2 d^4 + 3d^2) \Big) +$$
$$\left(\frac{15E}{4(\frac{1}{2d^2}+2p)^2} + \frac{420c}{24\sqrt{2}(\frac{1}{2d^2}+2p)^2}(-P_{1s}^2 d^4 + 3d^2) + \frac{90\bar{c}}{6\sqrt{2}(\frac{1}{2d^2}+2p)^2} + \right.$$
$$\frac{2940c}{48\sqrt{2}(\frac{1}{2d^2}+2p)^3} + \frac{72}{4m(\frac{1}{2d^2}+2p)} - \frac{105p}{m(\frac{1}{2d^2}+2p)^2} + \frac{105p^2}{m(\frac{1}{2d^2}+2p)^3} \Big) +$$
$$\left(\frac{-P_1^2}{16p^2} + \frac{3}{4p} \right) \left(\frac{E}{(\frac{1}{2d^2}+2p)} - \frac{28c}{6\sqrt{2}(\frac{1}{2d^2}+2p)}(-P_{11}^2 d^4 + 3d^2) + \frac{12}{m} + \right.$$
$$\frac{24\bar{c}}{6\sqrt{2}(\frac{1}{2d^2}+2p)} - \frac{120c}{24\sqrt{2}(\frac{1}{2d^2}+2p)^2} + \frac{70c}{6\sqrt{2}(\frac{1}{2d^2}+2p)^2} - \frac{28p}{m(\frac{1}{2d^2}+2p)}$$
$$\left. + \frac{50p^2}{m(\frac{1}{2d^2}+2p)^2} \right) + \left(\frac{8p^2}{m} - \frac{8c}{6\sqrt{2}} \right) \left(- \frac{P_1^6}{(4p)^6} + \frac{21P_1^4}{(4p)^5} + \frac{105}{(4p)^3} - \frac{105P_1^2}{(4p)^4} \right) \Bigg\}$$
$$(\frac{\pi}{2p})^{\frac{3}{2}} \exp(\frac{-P_1^2}{8p}),$$

$$F_1(p) = (\frac{\pi}{\frac{1}{2d^2}+2p+B})^{\frac{3}{2}} (\frac{\pi}{2p+B-\frac{B^2}{(\frac{1}{2d^2}+2p+B)}})^{\frac{3}{2}} \exp(\frac{-P_1^2}{4(2p+B-\frac{B^2}{(\frac{1}{2d^2}+2p+B)})})$$
$$\{(2 + \frac{2B^4}{(\frac{1}{2d^2}+2p+B)^4} - \frac{4B^2}{(\frac{1}{2d^2}+2p+B)^2})(\frac{-5P_1^2}{4(2p+B-\frac{B^2}{(\frac{1}{2d^2}+2p+B)})^3} +$$
$$\frac{P_1^4}{16(2p+B-\frac{B^2}{(\frac{1}{2d^2}+2p+B)})^4} + \frac{15}{4(2p+B-\frac{B^2}{(\frac{1}{2d^2}+2p+B)})^2}) + (\frac{10B^2}{(\frac{1}{2d^2}+2p+B)^3}$$
$$+ \frac{2}{\frac{1}{2d^2}+2p+B})(\frac{-P_1^2}{4(2p+B-\frac{B^2}{(\frac{1}{2d^2}+2p+B)})^2} + \frac{3}{2(2p+B-\frac{B^2}{(\frac{1}{2d^2}+2p+B)})})$$
$$+ \frac{15}{2(\frac{1}{2d^2}+2p+B)^2}\},$$

$F_2(p) = \frac{1}{2d^2} + B - \frac{4B^2}{4(2p+B)}$, and $F_3(p) = \frac{1}{2d^2} + 2p + B$.

Now from this eq.(3.5.12), the elements of transition matrix (T) can be found. As in ref. [28], each of the states with the gluonic excitations are orthogonal to each of the

ground states i.e.

$$\langle 1 \mid 1^* \rangle = \langle 1^* \mid 1 \rangle = \langle 2 \mid 2^* \rangle = \langle 2^* \mid 2 \rangle = 0.$$

This gives

$$T_{11^*} = T_{1^*1} = T_{22^*} = T_{2^*2} = 0.$$

Thus the possible transitions are T_{11}, T_{12}, T_{21}, T_{22}, T_{12^*} and T_{21^*}. As the eq.(3.5.5) and (3.5.6) are similar (interchanging $\mathbf{R}_1$ and $\mathbf{R}_2$ in eq.(3.5.5), it becomes equal to eq.(3.5.6)), so

$$\begin{aligned} T_{11} &= T_{22}, \\ T_{12} &= T_{21}, \end{aligned} \tag{3.5.13}$$

and

$$T_{12^*} = T_{21^*}. \tag{3.5.14}$$

T_{11} can be calculated (as in ref. [26]) by using the coefficient of $\frac{1}{\triangle_1(P_1)}$ containing the $\chi_1(\mathbf{R}_1)$ from eq.(3.5.12). As in this equation, there is no coefficient having $\chi_1(\mathbf{R}_1)$, so it gives $T_{11} = 0$. T_{12} can be calculated by considering the coefficient of $\frac{1}{\triangle_1(P_1)}$ containing the $\chi_2(\mathbf{R}_2)$ from eq.(3.5.12) in the following eq.

$$T_{12} = M\frac{\pi}{2}P_1[coef. \quad of \quad \frac{1}{\triangle_1(P_1)} \quad \text{containing} \quad \chi_2(\mathbf{R}_2)], \tag{3.5.15}$$

with M being the mass of $c\bar{c}$ meson. Similarly T_{12^*} can be calculated by substituting the coefficient of $\frac{1}{\triangle_1(P_1)}$ containing the $\chi_2^*(\mathbf{R}_2)$ from eq.(3.5.12) in the following eq.

$$T_{12^*} = M\frac{\pi}{2}P_{1s}[coef. \quad of\frac{1}{\triangle_1(P_1)} \quad \text{containing} \quad \chi_2^*(\mathbf{R}_2)]. \tag{3.5.16}$$

The relation between T-matrix and S-matrix is written as

$$S = I - 2\imath T, \tag{3.5.17}$$

and the relation between S-matrix and phase shifts is given in ref. [54] and written as

$$S = \exp(2\imath\Delta), \tag{3.5.18}$$

combining the above two eqs.(3.5.17,3.5.18), off-diagonal phase shifts can be calculated by using the following relation

$$I - 2\imath T = \exp(2\imath\Delta), \tag{3.5.19}$$

where S, T, I,and Δ represent 4×4 scattering, transition, identity, and phase shift matrices respectively. As our phase shifts are small, therefore neglecting the higher powers of Δ in the expansion of $\exp(2\imath\Delta)$, the eq.(3.5.19) can be written as

$$S_{ij} = \delta_{ij} - 2\imath T_{ij} = \delta_{ij} + 2\imath\Delta_{ij}. \tag{3.5.20}$$

for $i, j = 1, 2, 1^*, 2^*$. From this eq.(3.5.20), we obtained that the phase shifts are equal to negatve of the transition amplitude, e.g. for $i = 1$, $j = 2$, $\Delta_{12} = \frac{S_{12}}{2\imath} = -T_{12}$.

With the use of transition matrix element, we can also calculate another quantity, energy shift. The energy shift of meson-meson system ($cc\overline{cc}$) can be calculated by using the stationary state perturbation theory, i.e.

$$E_i = E_i^\circ + T_{ii} + \sum_{i \neq j} \int_\circ^\infty \frac{|T_{ij}|^2}{E_i^\circ - E_j^\circ} dP_j, \tag{3.5.21}$$

with the initial state i and intermediate state j. We have considered initial states where the gluonic field should be only in ground state, so $i = 1, 2$, but intermediate gluonic field may be in ground or excited state, i.e. $j = 1, 2, 1^*, 2^*$. Here $T_{ii} = \langle i|T|i\rangle$,

$|T_{ij}|^2 = |\langle j|T|i\rangle|^2$, E_i° is the energy of a ground state (1 or 2) of meson-meson system, and E_j° may be the energy of the other state (meson-meson ground state or an gluonic-excited meson-meson state).

With the use of Born approximation, transition matrix elements (T_{11} and T_{22}) are zero as explained above before eq.(3.5.15). But when we use the unitarity condition ($S^\dagger S = I$), we got non-zero value of T_{11} or T_{22}. This means that Born approximation violates the unitarity condition as written in ref. [55]. To find T_{11}, we can be written T_{11} as

$$T_{11} = ReT_{11} + \iota ImT_{11}$$

To observe the change in the transition probability T_{11} due to the incorporation of excited gluonic field, we used the unitary condition ($SS^\dagger = I$). For this, the $S, S^\dagger, I$ matrices can be written as

$$S = \begin{bmatrix} 1-2\iota T_{11} & -2\iota T_{12} & -2\iota T_{11^*} & -2\iota T_{12^*} \\ -2\iota T_{21} & 1-2\iota T_{22} & -2\iota T_{21^*} & -2\iota T_{22^*} \\ -2\iota T_{1^*1} & -2\iota T_{1^*2} & 1-2\iota T_{1^*1^*} & -2\iota T_{1^*2^*} \\ -2\iota T_{2^*1} & -2\iota T_{2^*2} & -2\iota T_{2^*1^*} & 1-2\iota T_{2^*2^*} \end{bmatrix}, \tag{3.5.22}$$

$$S^\dagger = \begin{bmatrix} 1+2\iota T_{11}^* & 2\iota T_{21}^* & 2\iota T_{1^*1}^* & 2\iota T_{2^*1}^* \\ 2\iota T_{12}^* & 1+2\iota T_{22}^* & 2\iota T_{1^*2}^* & 2\iota T_{2^*2}^* \\ 2\iota T_{11^*}^* & -2\iota T_{21^*}^* & 1+2\iota T_{1^*1^*}^* & -2\iota T_{2^*1^*}^* \\ 2\iota T_{12^*}^* & -2\iota T_{22^*}^* & -2\iota T_{1^*2^*}^* & 1+2\iota T_{2^*2^*}^* \end{bmatrix}, \tag{3.5.23}$$

and

$$I = \begin{bmatrix} 1 & 0 & 0 & 0 \\ 0 & 1 & 0 & 0 \\ 0 & 0 & 1 & 0 \\ 0 & 0 & 0 & 1 \end{bmatrix}. \tag{3.5.24}$$

(As usual, the symbol $*$ is used for complex conjugate.) The 1×2 element of $SS^{\dagger} = I$ gives the following relation

$$2T_{11}T_{21}^{*} + 2T_{12}T_{22}^{*} = -\iota(T_{21}^{*} - T_{12}). \tag{3.5.25}$$

Our results for T_{12} (in chapter 5) show that T_{12} is real, so $T_{12}^{*} = T_{12}$. Using this equality and eqs.(3.5.13,3.5.14), the eq.(3.5.25) gives

$$ReT_{11}(2T_{12}) = 0. \tag{3.5.26}$$

We know that $T_{12} \neq 0$, therefore

$$ReT_{11} = 0. \tag{3.5.27}$$

Hence

$$T_{11} = \iota ImT_{11}. \tag{3.5.28}$$

Now to calculate the imaginary part of T_{11}, the 1×1 element of $SS^{\dagger} = I$ is used. The 1×1 elemet gives the following relation

$$-(\iota T_{11}^{*} - \iota T_{11} + 2T_{11}T_{11}^{*}) = 2T_{12}T_{12}^{*} + 2T_{12'}T_{12'}^{*}. \tag{3.5.29}$$

Using eq.(3.5.28) in eq.3.5.29, we get

$$(ImT_{11})^2 - ImT_{11} + T_{12}T_{12}^{*} + T_{12'}T_{12'}^{*} = 0. \tag{3.5.30}$$

Solving this equation for ImT_{11}, we have

$$ImT_{11} = \frac{1}{2} \pm \frac{1}{2}\sqrt{1 - 4T_{12}T_{12}^{*} - 4T_{12'}T_{12'}^{*}} \tag{3.5.31}$$

Now phase shifts can be calculated by using relation (3.5.20). For $i = j = 1$, we have

$$\Delta_{11} = -T_{11} \tag{3.5.32}$$

Since $T_{11} = T_{22}$, so we have

$$\Delta_{22} = -T_{22} \tag{3.5.33}$$

Chapter 4

Quark Dynamics and Gluonic Excitations in Mesons

In previous chapters, work is done for meson-meson systems including gluonic excitations without spin and flavour basis with $q\bar{q}$ potential in quadratic form. Now, to include the spin, flavour, and realistic coulombic plus linear potential, we study the simpler system of one quark and one anti-quark. For such a simpler system, we study some relevant characteristics like masses, root mean square radii and wave functions at the origin of the conventional and hybrid charmonium mesons through the numerically generated solutions of non-relativistic Schrödinger equation (also used in ref. [19]).

In the quark model, mesons have only certain J^{PC} quantum numbers. Here J is the total angular momentum and is equal to the sum of orbital angular momentum and spin angular momentum, i.e.

$$J = L \oplus S = |L - S|.....|L + S|.$$

The symbol L is used for orbital angular momentum and S is used for spin angular momentum of the quark-antiquark pair. P is the parity of the meson and C is used

for charge conjugation. The parity (P) and charge conjugation (C) are given by

$$P = (-1)^{L+1}, \tag{4.0.1}$$

and

$$C = (-1)^{L+S}. \tag{4.0.2}$$

For $S = 0,1$ and $L = 0,1,2, \ldots$, respectively, the possible J^{PC} states are $0^{-+}, 1^{--}, 1^{+-}$, $0^{++}, 1^{++}, 2^{++}, \ldots\ldots$ The states with $J^{PC} = 0^{+-}, 0^{--}, 1^{-+}, 2^{+-}, 3^{-+}, 4^{+-}, \ldots$ are forbidden in the quark model and are known as exotics (hybrid, glue ball, etc.). Quantum Chromodynamics (QCD), describing the interaction between the quarks and gluonic field, predicts the existence of hybrid mesons which contain the excited gluonic fields.

Thus for understanding of QCD, we need finding experimentally testable predictions of the theory for situations in which the gluonic field between a quark and antiquark is in an excited state. Thus hybrids are an important source of information related to confining properties of QCD, and checking for existence of hybrid mesons is very important objective of particle physics. Reviews of the spectrum of excited gluonic states can be found in refs. [37] [38]. Recently, a resonance is observed at COMPASS [56] with $J^{PC} = 1^{-+}$. Some other groups like VES [57], E852 [58], and the Crystal Barrel collaboration [59] also observed these states. Physicists are working in search of hybrid mesons at PEP2 (BABAR) [60], KEKB (BELLE) [61], Jefferson Lab [62], CLEO-c detector [63], and BES-III detector [64, 65].

Theoretically, hybrid mesons masses have been predicted using different models such as Flux Tube model [17], the lattice gauge theory [66], MIT Bag model [67, 68], the quark model with constituent gluon [69, 70], and QCD sum rules [71].

Using the Born-Oppenheimer expansion, the work of finding implication of QCD

for a meson can be split into first using the numerical lattice simulations of QCD to write down a quark antiquark potential and then using this potential to calculate dynamical implications of the potential. Even a numerically defined potential can be used in this scheme; this is what ref. [19] does. But we write an analytical coulombic plus linear plus exponentially falling expression for the excited state gluonic field potential between a quark and antiquark and fit its parameters to the lattice data for the excited state gluonic field energy values available in ref. [19] for discrete quark antiquark separations.

In this chapter, in section 4.1 below, we write the Hamiltonian for the conventional mesons. Then we describe the shooting method-based numerical procedure to find the solution of the Schrödinger equation for conventional charmonium mesons. The expressions we used to find masses, root mean square radii, and square of radial wave functions at the origin ($|R(0)|^2$) of conventional charmonium mesons are also written in this section. In section 4.2, the Hamiltonian is written for hybrid mesons, and then we redo all the numerical work as done in section 4.1 for hybrids now.

4.1 Characteristics of Conventional Charmonium Mesons

The Potential Model for Conventional Charmonium Mesons

In the potential models, the confining potential for $q\overline{q}$ system in the ground state gluonic field is mostly used in the form of linear plus coulombic potential written in eq.(2.3.17) in chapter 2. It is also mentioned in chapter 2 after eq.(2.3.17) that the coulombic term is due to one gluon exchange and the linear term is linear confining potential [16]. This potential form provides a good fit to the lattice simulations of

refs. [72, 73]. By including the Gaussian-smeared hyperfine interaction [17] [46] and orbital angular momentum (or centrifugal) term, the potential of the $q\overline{q}$ system in the ground state gluonic field have following form

$$V(r) = \frac{-4\alpha_s}{3r} + br + \frac{32\pi\alpha_s}{9m_c^2}(\frac{\sigma}{\sqrt{\pi}})^3 e^{-\sigma^2 r^2} S_c.S_{\overline{c}} + \frac{L(L+1)}{2\mu r^2}, \tag{4.1.1}$$

where

$$S_c.S_{\overline{c}} = \frac{1}{2}\big[S(S+1) - S_c(S_c+1) - S_{\overline{c}}(S_{\overline{c}}+1)\big],$$

S_c and $S_{\overline{c}}$ being the spin quantum numbers of charm quark and anti-quark. S is the total spin quantum number defined as

$$S = S_c + S_{\overline{c}}.$$

As quarks are spin $\frac{1}{2}$ particles, so $S_c = S_{\overline{c}} = \frac{1}{2}$. This results in

$$S_c(S_c+1) = S_{\overline{c}}(S_{\overline{c}}+1) = \frac{3}{4}.$$

Therefore

$$S_c.S_{\overline{c}} = \frac{S(S+1)}{2} - \frac{3}{4}.$$

In eq.(4.1.1), μ is the reduced mass of quark-antiquark, and is defined as

$$\mu = \frac{m_c m_{\overline{c}}}{m_c + m_{\overline{c}}}. \tag{4.1.2}$$

In our case $m_c + m_{\overline{c}} = m$, where m is the mass of charm quark. Therefore,

$$\mu = \frac{m}{2}.$$

For the $c\overline{c}$ mesons, the parameters α_s, b, σ, and m are taken to be 0.5461, 0.1425GeV^2, 1.0946 GeV, and 1.4796 GeV as used in ref. [46]. The quantum numbers (L and S) for some conventional charmonium mesons are reported in Table 4.1.

Table 4.1: Quantum Numbers of some charmonium mesons

Meson	L	S
η_c	0	0
J/ψ	0	1
h_c	1	0
χ_c	1	1

Characteristics of Conventional Charmonium Mesons

A conventional meson can be described by the wave function of the bound quark-antiquark state which satisfies the Schrödinger equation with potential of eq.(4.1.1). Radial Schrödinger equation with wave function $U(r) = rR(r)$ is written (in natural units) as

$$\nabla^2 U(r) + 2\mu(E - V(r))U(r) = 0. \tag{4.1.3}$$

Here R is the radial wave function and r is the interquark distance, E is the sum of kinetic and potential of quark-anti-quark system, and $V(r)$ is defined in eq.(4.1.1) and μ is defined in eq.(4.1.2).

In quark-antiquark bound state, the wave function must satisfy the boundary conditions $U(0) = 0$ and $U(\infty) = 0$. For the numerical solution of the Schrödinger equation for $U(r)$ with the potential of eq.(4.1.1)), we repeated generated energy E from -2 to 2 GeV in steps of 0.1 GeV. For each such trial initial energy, we used the Newton method [74] to select, if any, the energy for which the numerical solution of Schrödinger equation for $U(r)$ became zero at infinity. To obtain these numerical solutions, we used the RK method [75] with using any arbitrary integer value of $U'(0)$. For different values of $U'(0)$, normalized solutions of the Schrödinger equation,

obtained by multiplying the solution with the normalization constant $(\frac{1}{\sqrt{\int U^2(r)dr}})$, remain the same. These energy eigenvalues plus constituent quark masses are taken to be the $c\bar{c}$ mesons masses (in natural units). We found that our results for conventional charmonium meson agree with the Table 1 of ref. [46] which supports the reliability of our method. We also checked the consistency of our method

1) by getting a 100% overlap of HU and EU where H is the Hamiltonian for $q\bar{q}$ system, and

2) by calculating the masses of the conventional mesons listed in Table 4.1 with corresponding quantum numbers by the Crank Nichelson Discritization and finding that masses obtained by both of the methods are identical.

The Figs.(4.1-4.4) show the dependence of η, J/ψ, h_c, and χ_c normalized radial wave functions on the radial separation r between the quark and antiquark. These graphs show that the radial wave functions of η, h_c, χ_c, and J/ψ mesons have the same properties as that of hydrogen atom radial wave function, i.e. they behave as r^L for small inter quark distances and decrease exponentially at large inter quark distances. Figs.(4.1-4.2) are for $L = 0$, so these graphs are similar to $r^0 exp(-r)$. Figs.(4.3-4.4) are for $L = 1$, so these graphs are similar to $r^1 exp(-r)$. As L increases, the wave function's peak goes away from the origin. This means that centrifugal term has more effects on wave function than that of the hyperfine term. One possible reason is that we are dealing with heavy quarks so the $1/m_c^2$ factor (shown in eq.(4.1.1)) of the hyperfine term becomes very small.

The normalized wave function $U(r)$ is used in the further calculations for root mean square radii and radial wave functions at origin. To find the root mean square

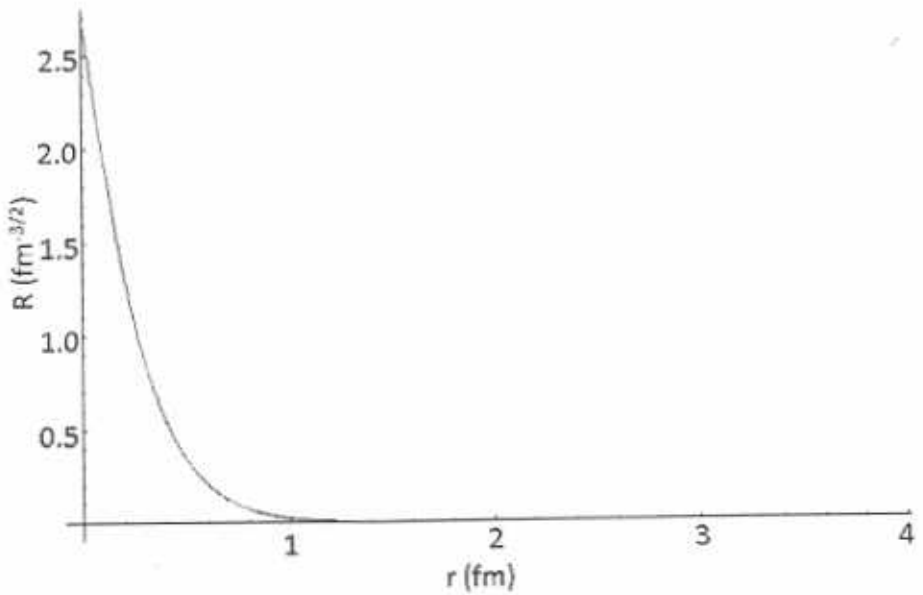

Figure 4.1: The radial part of η meson wave function of r.

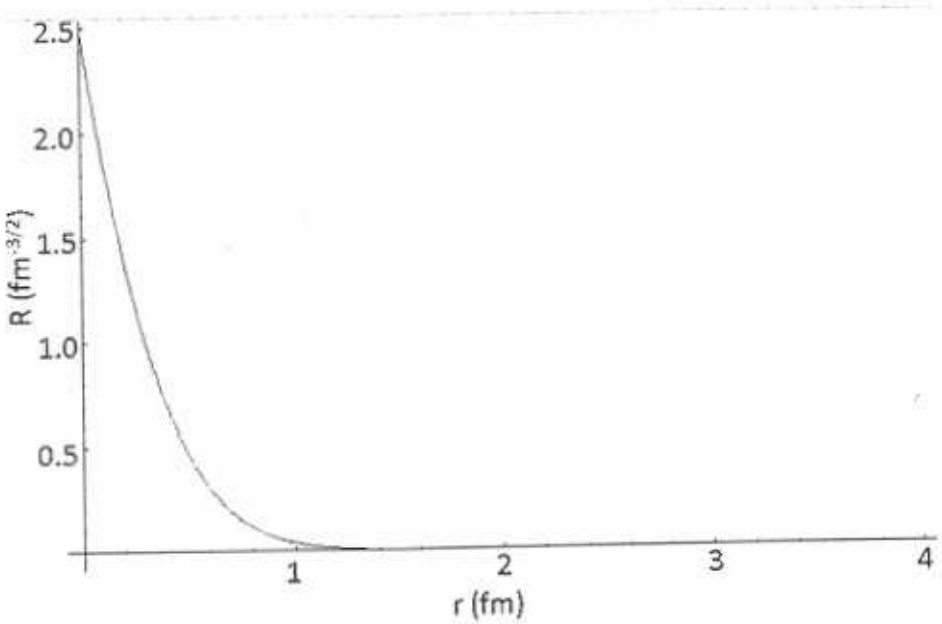

Figure 4.2: The radial part of J/ψ wave function with respect to r.

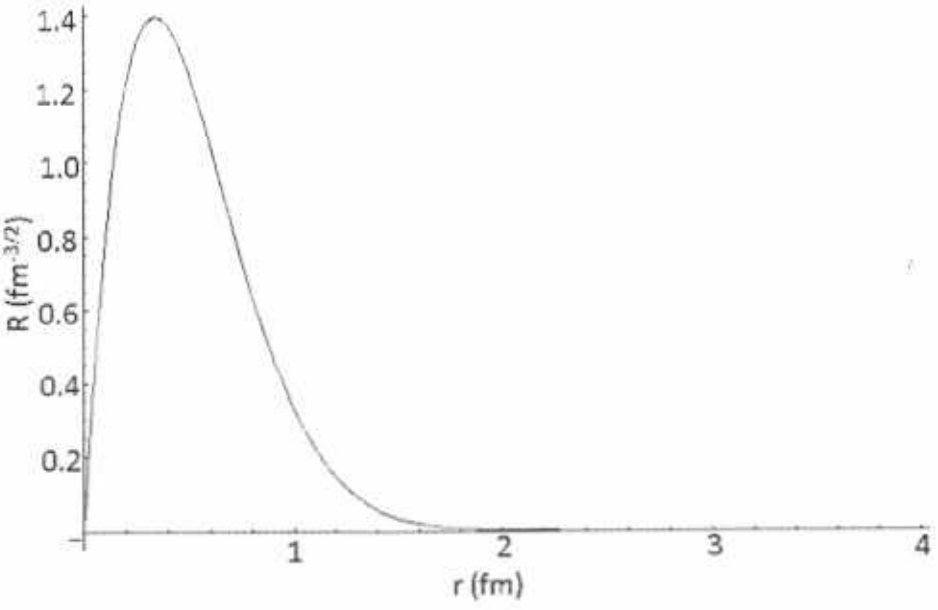

Figure 4.3: The radial part of h_c meson wave function with respect to r.

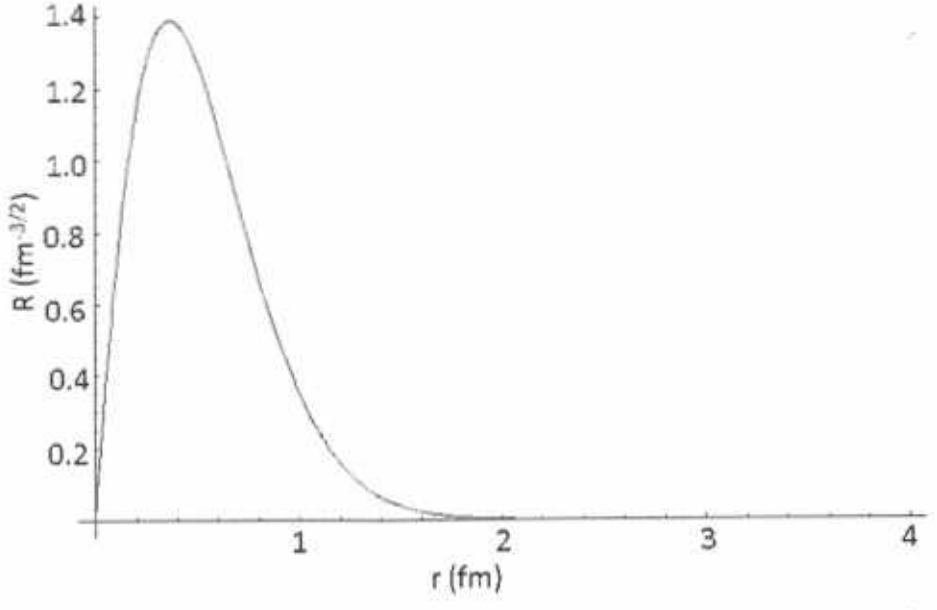

Figure 4.4: The radial part of χ_c meson wave function with respect to r.

radii of the $c\bar{c}$ mesons, we used the following relation:

$$\langle r^2 \rangle = \sqrt{\int U^* r^2 U dr}. \tag{4.1.4}$$

These radii can be used to find scalar form factors [40] for charmonium mesons, along with energy shifts [41] and magnetic polarizabilities [41].

In ref. [76], for normalized wave function

$$U'(0) = R(0) = \sqrt{4\pi}\psi(0) \tag{4.1.5}$$

is used. Thus the derivative of $U(r)$ at $r = 0$ is calculated initially for conventional charmonium mesons to find $|R(0)|^2$ and that is described in this section. $|R(0)|^2$ is used in many applications of high energy physics such as to calculate the decay constants [42], decay rates [42], and differential cross sections [43] for quarkonium states.

4.2 Characteristics of Hybrid Charmonium Mesons

The Potential Model for Hybrid Charmonium Mesons

The centrifugal term for the hybrid mesons replacing the last term of eq.(4.1.1) is written in refs. [77, 33] as

$$\frac{L(L+1) - 2\Lambda^2 + < J_g^2 >}{2\mu r^2}, \tag{4.2.1}$$

where Λ is the projection of the total angular momentum J_g of the gluonic field. The states with $\Lambda = 0, 1, 2, 3, , ...$ are usually represented by the capital greek letters $\Sigma, \Pi, \Delta, \Phi, ...$ respectively. We are interested in finding the masses and root mean square radii of the hybrid states $0^{+-}, 1^{-+}$, and 2^{+-}. In lattice simulations, these

Table 4.2: The quantum numbers of $c\bar{c}$ hybrid mesons with $0^{+-}, 1^{-+}$ and 2^{+-} J^{PC} states.

J^{PC}	L	S	Λ	$< J_g^2 >$
$0^{+-}, 1^{-+}, 2^{+-}$	1	1	1	2
$1^{-+}, 2^{+-}$	2	1	1	2

states can be generated from the Π_u potential. For the Π_u potential, $< J_g^2 >= 2$ and $\Lambda = 1$ [33]. Therefore $-2\Lambda^2 + \langle J_g^2 \rangle = 0$, so centrifugal factor for the hybrid mesons is $L(L+1)/2\mu r^2$. In ref. [33] $J = L \oplus S$, $P = \epsilon(-1)^{L+\Lambda+1}$, and $C = \epsilon\eta(-1)^{L+\Lambda+S}$ with $\epsilon, \eta = \pm 1$. Therefore with same quantum numbers (L,S), different J^{PC} states are possible. L and S for these hybrid J^{PC} states are shown in Table 4.2 (as given in ref. [78]). For the excited part of quark antiquark potential π/r is used in the flux tube model [17]. In this chapter, we also use the chapter 3, *ansätz* of the form $A\exp^{-Br^2}$ for the excited part of the quark antiquark potential; this ansatz is a smeared form of $\frac{constant}{r}$. Detailed description is already given in chapter 3 after eq.(3.1.1), along with the value

$$A = 1.8139266\text{GeV}, \qquad \textit{and} \qquad B = 0.0657212\text{GeV}^2.$$

fitted to the lattice data mentioned there. We calculated χ^2(as defined in eq.(3.1.2)) for $A\exp^{-Br^2}$ and π/r, and found that the χ^2 for Ae^{-Br^2} is lesser than that for π/r. This means that excited state potential in form of $A\exp(-Br^2)$ have a good agreement with QCD simulations [19] as compared to π/r. This new potential form is already used in a more complicated work reported in chapter 3, and ref. [79]. Using this, we

can write the quark antiquark potential in excited state gluonic field as

$$V(r) = \frac{-4\alpha_s}{3r} + br + \frac{32\pi\alpha_s}{9m_c^2}(\frac{\sigma}{\sqrt{\pi}})^3 e^{-\sigma^2 r^2} S_c.S_{\bar{c}} + \frac{L(L+1) - 2\Lambda^2 + < J_g^2 >}{2\mu r^2} + Ae^{-Br^2}. \tag{4.2.2}$$

Characteristics of Hybrid Charmonium Mesons

Using the excited state potential of eq.(4.2.2) along with the above mentioned values (after eq.(4.2.1)) of Λ and $< J_g^2 >$, the energy eigen-values and the corresponding wave functions are found by using the same technique as employed for conventional mesons (mentioned in section 4.1). These eigenvalues plus the constituent quark antiquark masses are taken to be the masses of the hybrid mesons corresponding of Table 4.2 hybrid mesons. Then we normalized the solution of Schrödinger equation and found the root mean square radii of the hybrid mesons by using eq.(4.1.4). The normalized solutions for charmonium hybrid mesons are graphically represented in Fig.4.5,4.6,4.7, and 4.8. In fig.4.5 and 4.7, the wave function is plotted by using the excited state potential in the form of $Aexp(-Br^2)$ used by us. The Fig.4.6 and 4.8 are drawn by using the excited state potential in the form of π/r of the flux tube model.

These figures show the wave function dependence on L and S. Therefore the mass and root mean square radii of $0^{+-}, 1^{-+}$ and 2^{+-} J^{PC} states also depend on the quantum numbers L and S. We also found $|R(0)|^2$ for hybrid mesons using eq.(4.1.5).

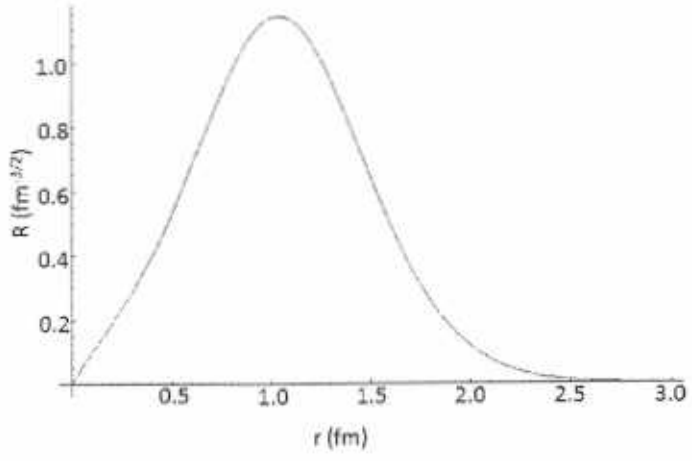

Figure 4.5: Hybrid charmonium meson radial wave function for $0^{+-}, 1^{-+}$ and 2^{+-} J^{PC} states with L=1, S=1 and excited gluonic field potential in the form of $Aexp(-Br^2)$.

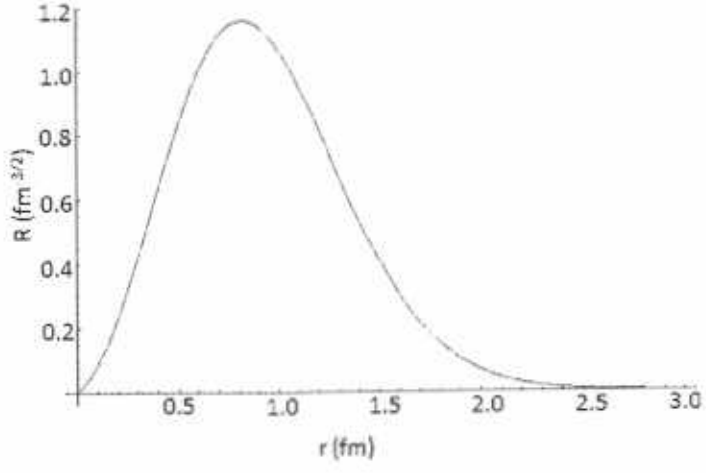

Figure 4.6: Hybrid charmonium meson radial wave function for $0^{+-}, 1^{-+}$ and 2^{+-} J^{PC} states with L=1, S=1 and excited gluonic field potential in the form of π/r.

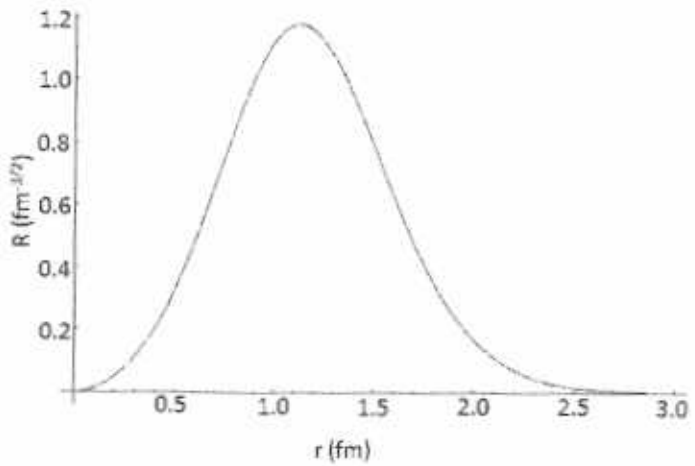

Figure 4.7: Hybrid charmonium meson radial wave function for $0^{+-}, 1^{-+}$ and 2^{+-} J^{PC} states with L = 2 , S = 1 and excited gluonic field potential in the form of $Aexp(-Br^2)$.

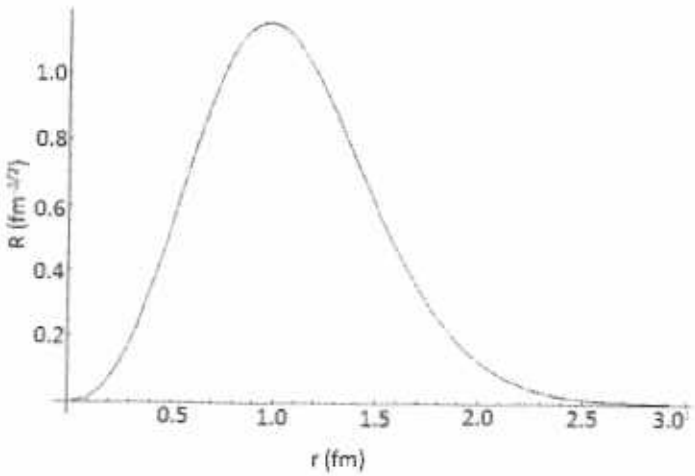

Figure 4.8: Hybrid charmonium meson radial wave function for $0^{+-}, 1^{-+}$ and 2^{+-} J^{PC} states with L=2, S=1 and excited gluonic field potential in the form of π/r.

Chapter 5

Results and Conclusions

In this chapter, results are reported in three sections. In the first section, transition amplitudes, phase shifts, and energy shifts (defined above in eqs(3.5.15,3.5.16,3.5.19,3.5.21)) are reported for the meson-meson system (ignoring the spin) in six basis (three for ground state gluonic field and three for excited state gluonic field) by considering the four static quarks. Magnitudes of phase shifts of eq.(3.5.19) and energy shifts of eq.(3.5.20) averaged over the 0 GeV to 2 GeV center of mass energy range are also reported for the ground state and excited state gluonic field. The comparisons of ground state results (average phase shift and energy shift) with excited state results are also included in this section. As mentioned in chapter 3 after eq.(3.4.6), for ground state gluonic field, the results are independent of θ(the angle between $\mathbf{R}_1$ and $\mathbf{R}_2$) so partial wave analysis are not possible for ground state gluonic field. At the end of this first section partial wave analysis is reported for meson-meson system phase shifts (or negative of transition amplitude) when the gluonic field is in the excited state. As mentioned above in chapter 3, all these quantities are calculated

using the Born Approximation, resulting in $T_{11} = T_{22} = 0$. The Born approximation violates the unitarity condition and if we use the unitarity condition, we got relations reported in eqs.(3.5.27,3.5.31) between off-diagonal and diagonal matrix elements. In section 2, the results for non-zero T_{11} are reported. In section 3, the results for masses, root mean square radii, and $\mid R(0) \mid^2$ of conventional and hybrid charmonium mesons are reported by including the spin and the quark dynamics along with gluon dynamics. Based on these results, we also include some predictions for experimentally measurable quantities.

1-Results for Meson-Meson Systems in Four Basis for Static Quarks

1- The parameters values used in the numerical work are written in Table 5.1. Here d is the size of meson, ω and C related to d as defined above in chapter 2 in paragraph after eq.(2.3.18). The parameters d, ω, C, and $\overline{C}$ are discussed in the paragraph after eq.(2.3.18). The parameters A, B, n, p are related to gluonic excited states discussed after eq.(3.1.1) and eq.(3.1.3).

2-The transition amplitude T_{12}, from one meson-meson ground state to other, are calculated by using eq.(3.5.15) with $k_f = 0.6$ [45](without the incorporation of gluonic excited states). Its dependence on the center of mass kinetic energy is shown in Fig.5.1 below. As it is noted that $-T_{12} = phase \quad shift$ is less than 1, so these results shows the validity of the Born approximation that we have used in chapter 3. In result 4 we compare the phase shifts (in radians) of this many body ground state gluonic field model at $k_f = 0.6$ with the phase shifts obtained from a model that is

Table 5.1: The parameter values used in this work

The parameter	Parameter's used value
d	1.16 GeV^{-1}
m	1.4794 GeV
p	0.048GeV^2
n	0.0036 $GeV^{7/2}$
ω	0.5023 GeV
C	-0.0700 GeV^3
$\overline{C}$	0.5651 GeV
f^c	1
k_f	0.6 or 1.51
b_s	0.18
A	1.8139 GeV
B	0.0657 GeV^2
α_s	0.5461
b	0.1425GeV^2
σ	1.0946 GeV

extended to gluonic excitations along with changing $k_f = 1.51$.

3- The transition matrix element T_{12^*}, for transition from ground state to excited state gluonic field with $k_f = 1.51$, depend on the parameters ϵ of eq.(3.0.6), and f^a of eq.(3.0.3). T_{12^*} also depends on θ (the angle that $\mathbf{P}_1$ makes with $\mathbf{P}_2$ and $\mathbf{P}_{1_s}$ makes with $\mathbf{P}_{2_s}$). We take parameter f^a as a constant as discussed earlier in chapter 3. For $\epsilon = 2$, we take different values of f^a to see the effects of f^a on T_{12^*}. Figs.5.2 to 5.6 show the dependence of T_{12^*} on f^a at angle $\theta = 0$, 30, 60, 75 and 90 degrees respectively. For $\epsilon = 1/2$, the dependence of T^*_{12} on f^a at $\theta = 90°$ is shown in Fig.5.7. And for $\epsilon = 1$, the dependence of T^*_{12} on f^a at $\theta = 90°$ is shown in Fig.5.8. These graphs show that the phase shift (equal to $-T_{12^*}$) is increasing with the increase of f^a.

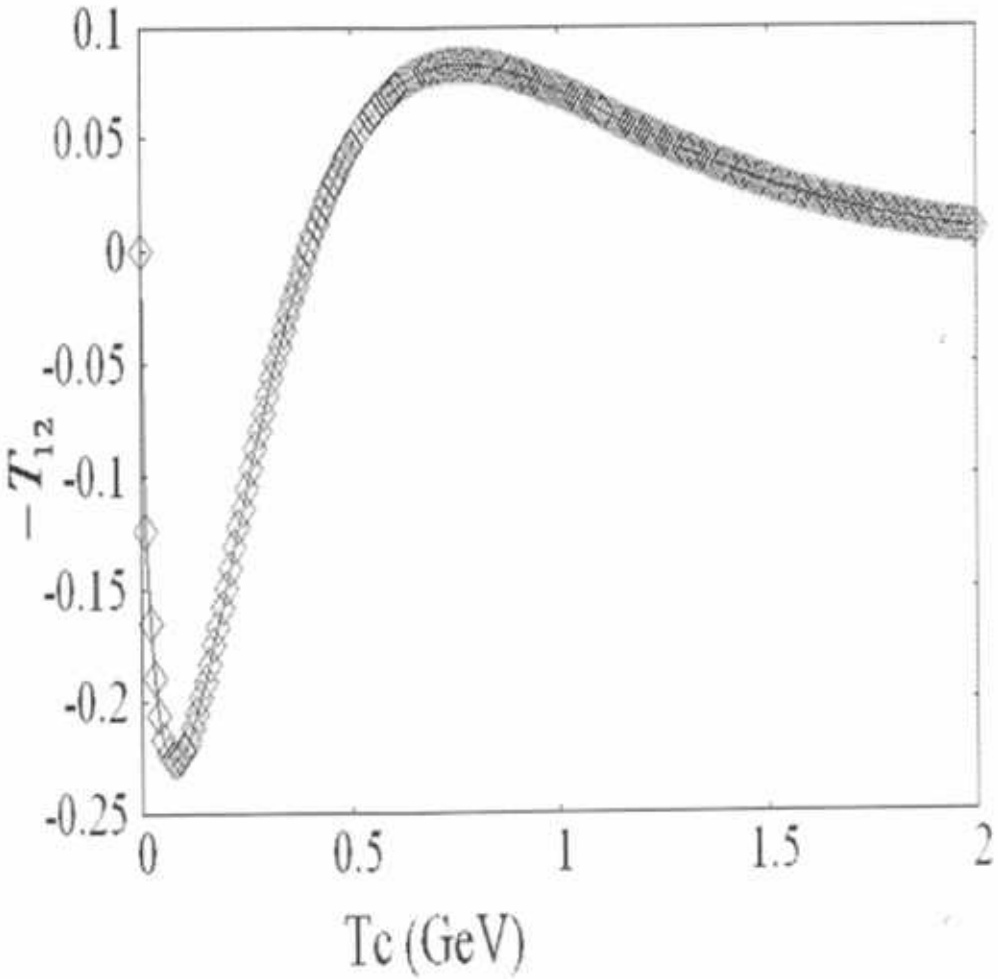

Figure 5.1: A graph between energy and T_{12} for ground state at $k_f = 0.6$.

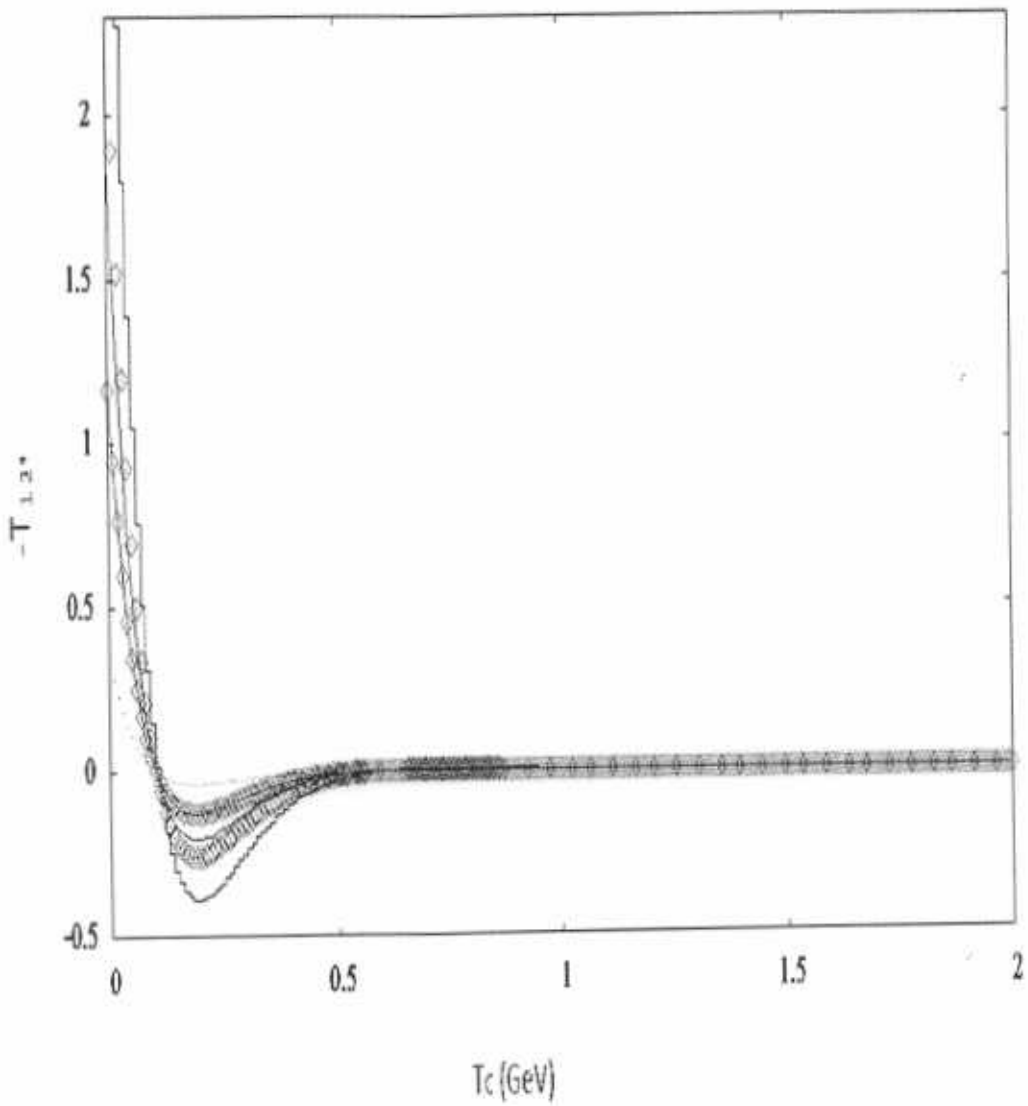

Figure 5.2: A graph between energy and T_{12^*} at $\theta = 0°$ with $\epsilon = 2$ for different values of f^a. The curve with dots is for $f^a = 0.015$, with lines plus points is for $f^a = 0.05$, with lines is for $f^a = 0.08$, with points is for $f^a = 0.1$, and with steps is for $f^a = 0.15$.

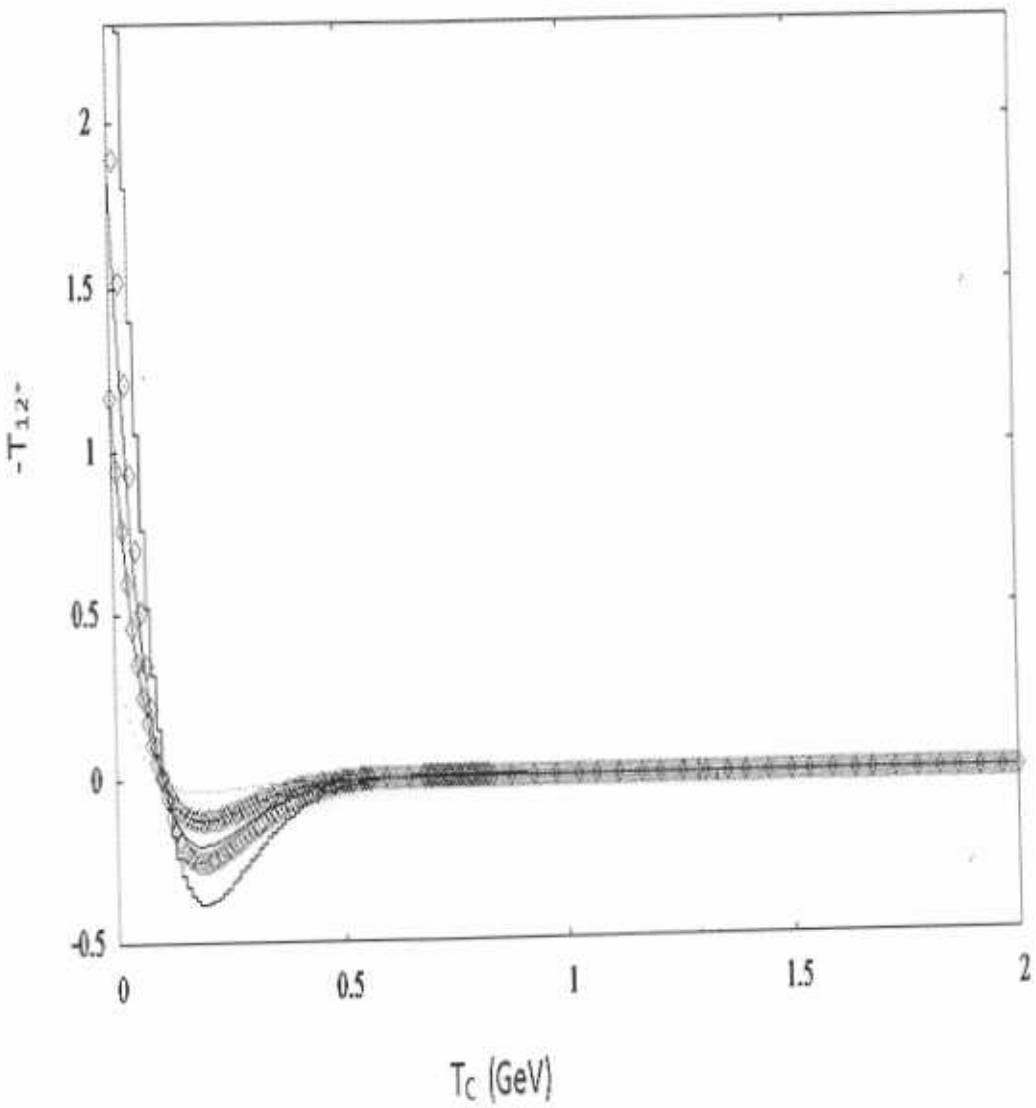

Figure 5.3: The same graph as Fig.5 but with $\theta = 30°$

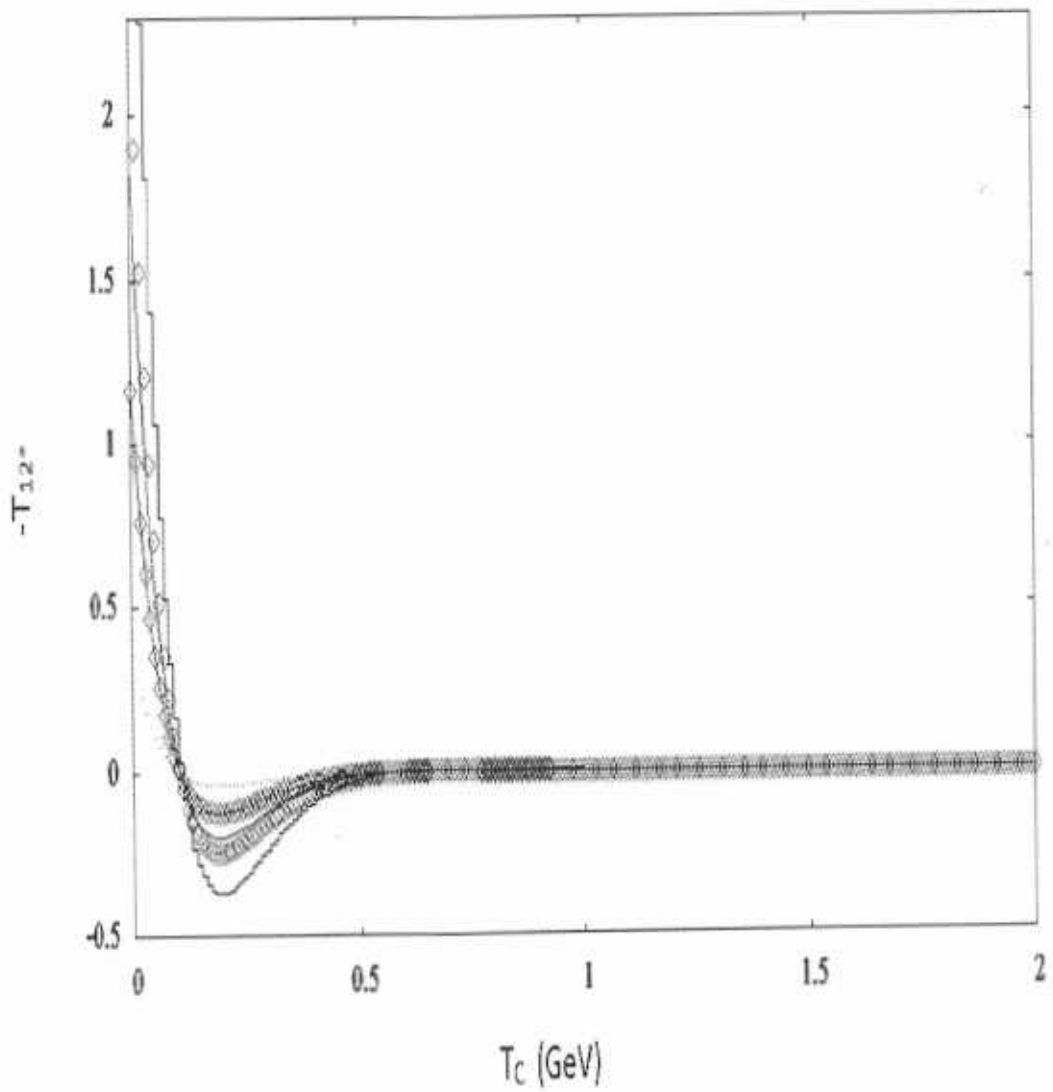

Figure 5.4: The same graph as Fig.5 but with $\theta = 60°$

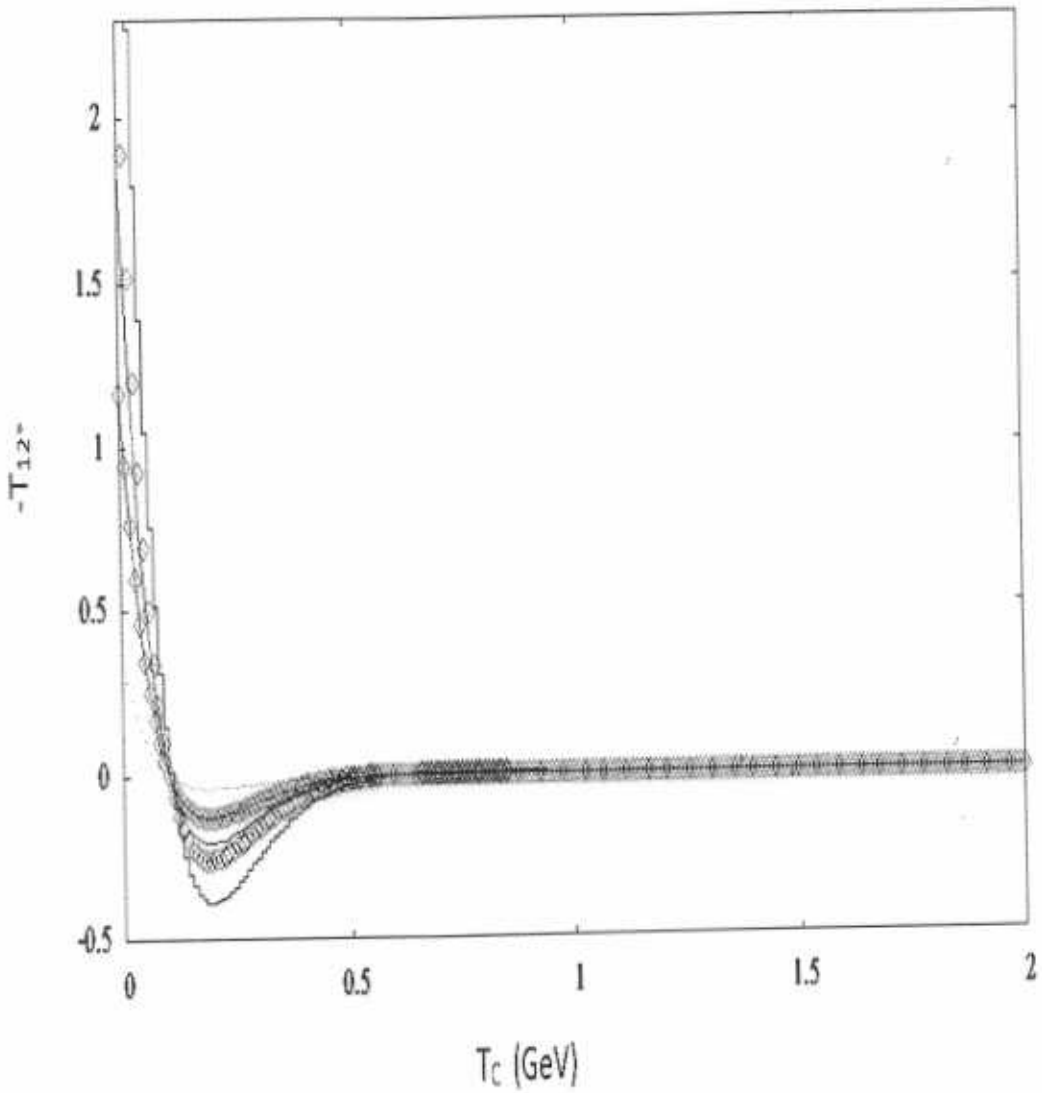

Figure 5.5: The same graph as Fig.5 but with $\theta = 75°$

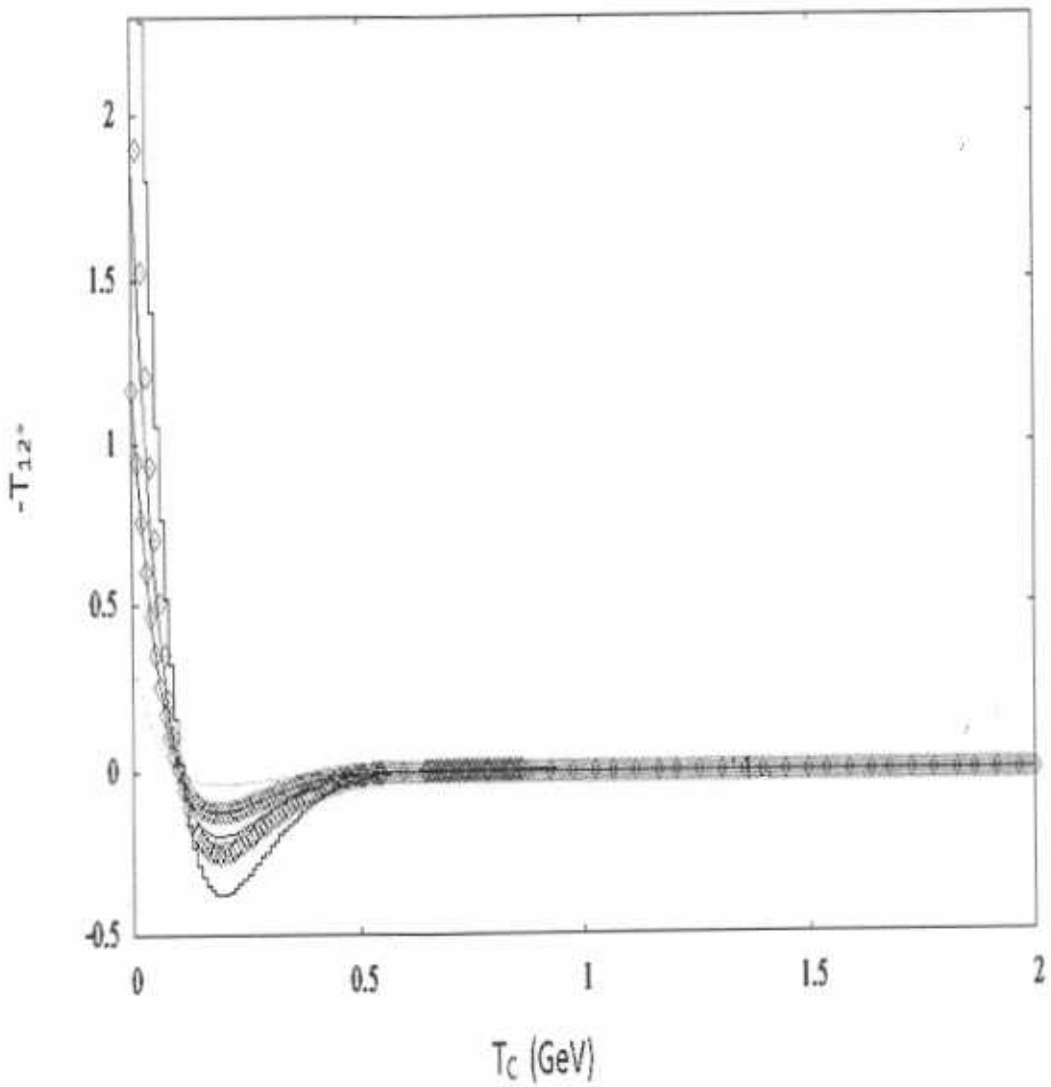

Figure 5.6: The same graph as Fig.5 but with $\theta = 90°$

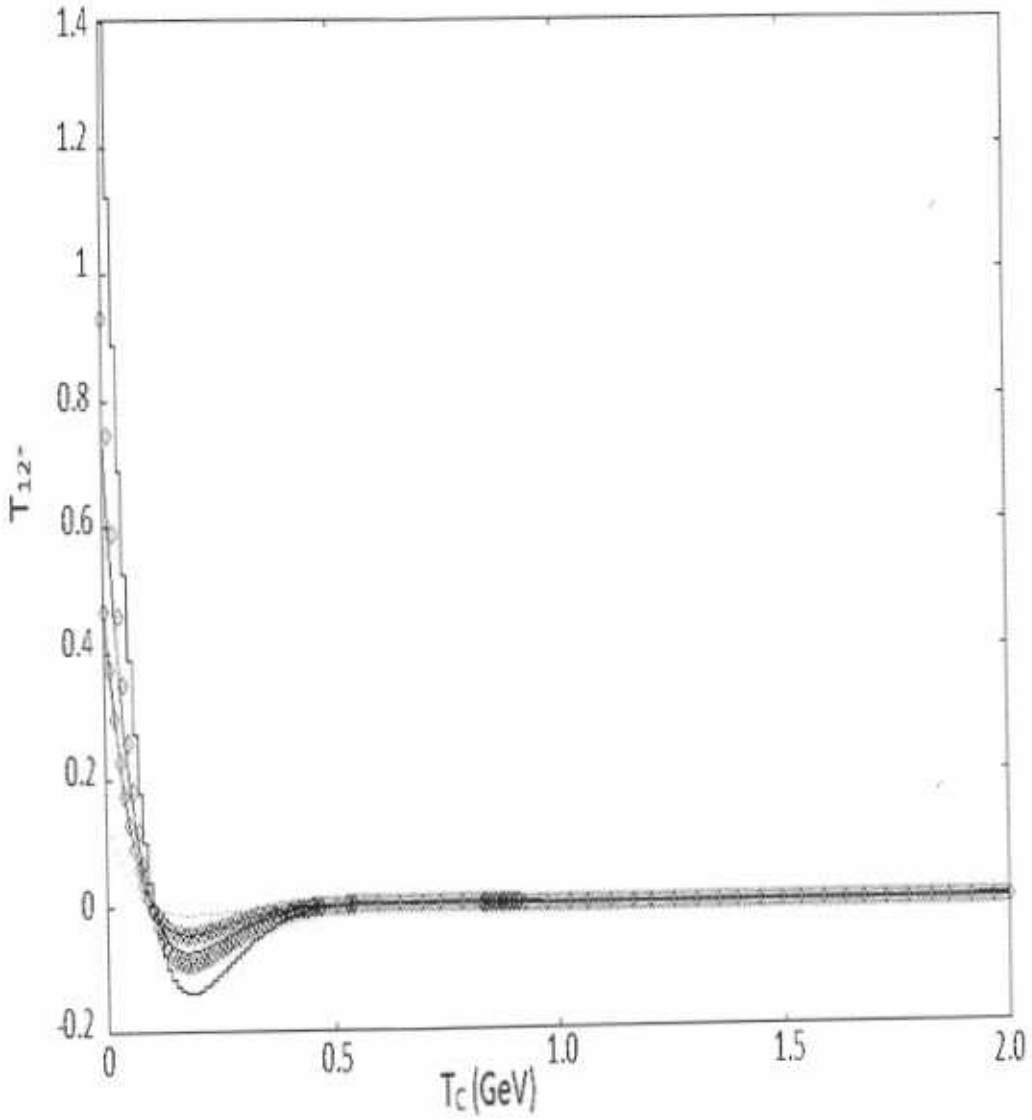

Figure 5.7: A graph between energy and T_{12^*} at $\theta = 90^\circ$ degrees with $\epsilon = 1/2$ for different values of f^a. The curve with dots for $f^a = 0.015$, with lines plus points is for $f^a = 0.05$, with lines is for $f^a = 0.08$, with points is for $f^a = 0.1$, and with steps is for $f^a = 0.15$

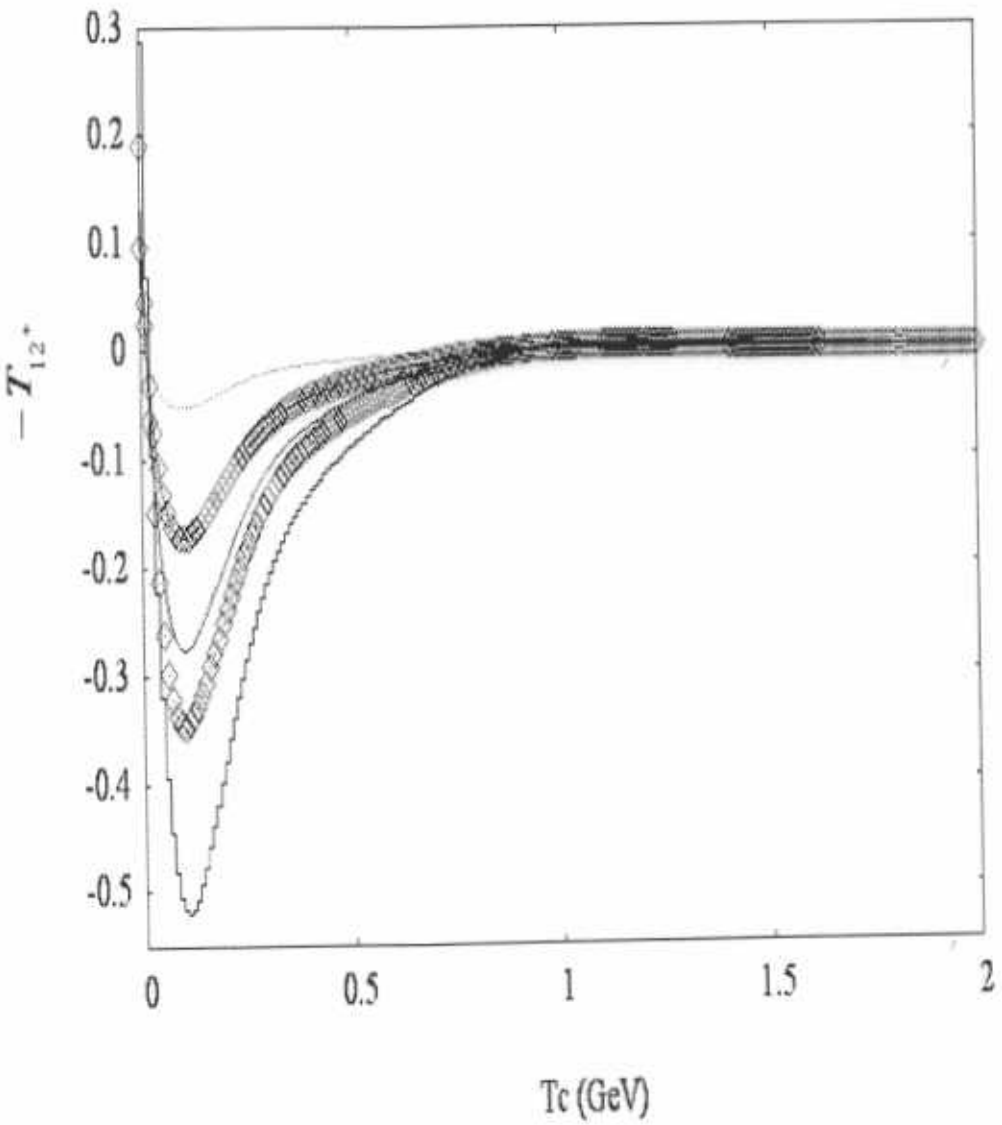

Figure 5.8: The same graph as Fig.10 but with $\epsilon = 1$

4- For the center of mass kinetic energy range 0 to 2 GeV, the average of the modulus of phase shifts (excluding excited states) is equal to -0.0369 radians at $k_f = 0.6$. But if we change the value of k_f from 0.6 to 1.51 and also include the excited state gluonic field, this average meson-meson phase shift again becomes $(-0.0218 - 0.0152)$ radians = -0.0370 radians by choosing $f^a = 0.03$ and $\theta = 90^\circ$ with $\epsilon = 2$. This means that a sum-of-two-body potential model can replace to some extent many-body potential terms in a tetraquark system by including the gluonic excitations. (An exact sum of two body terms would required $f_a = 1$, though.) In above, -0.0218 radians is the phase shift due to ground state gluonic field at $k_f = 1.51$, and -0.0152 radians is the phase shift due to gluonic excited states.

We have also explored the results with $\epsilon = 1/2$ and $\epsilon = 1$. As ϵ is proportional to the potential matrix elements taken between ground and gluonic excited states, when we replace $\epsilon = 2$ with $\epsilon = 1/2$ or 1 , it has no effect on T_{12} and average phase shift. But for $\epsilon = \frac{1}{2}$ with inclusion of gluonic excitations, now the values $f^a = 0.08$ and $\theta = 75^\circ$ almost restore the average phase shifts for $k_f = 1.51$ to $(-0.0218 - 0.0149)$ radians = -0.0367 radians. (The significance of the first and second term is as before). For $\epsilon = 1$, at $f^a = 0.055$ and $\theta = 90^\circ$, the average phase shifts for $k_f = 1.51$ becomes $(-0.0218 - 0.0150)$ radians = -0.0368 radians. This almost restoration again indicates that perhaps we can always choose parameters of the model so that with an inclusion of the gluonic excitations the sum-of-two-body potential model can effectively replace many-body potential terms in a tetraquark system.

5- The effects of meson-meson interaction are also observed through energy shift by using eq.(3.5.21). Here $T_{ii} = 0$ with $i = 1, 2$. In $\int_{i \neq j} \frac{|T_{ij}|^2}{E_i^0 - E_j^0} dP$, we have chosen $E_i^0 = 5.9176$ GeV, the value of energy for which center of mass kinetic energy becomes

zero. The intermediate energy state E_j^0 depends on the state of gluonic field ($|2\rangle, |2^*\rangle$ are only possible states that couple to $|1\rangle$) For the gluonic ground state ($|2\rangle$), $E_j^0 = 5.9176 + 0.3380 P_1^2$ (calculated using eq.(3.5.10) with $P_c^2(1) = P_1^2$); and for the excited state gluonic field ($|2^*\rangle$), $E_j^0 = 5.4638 + 0.3380 P_{1s}^2$ (calculated using (3.5.10) with $P_c^2(1s) = P_{1s}^2$). At $k_f = 0.6$ and $E_c = 5.9176$ (i.e. at the threshold), the shift to the ground state meson-meson energy is found to be $E_i = E_i^0 - 0.7268$ GeV excluding the gluonic excitations. If with increasing k_f to 1.51 as usual and including the coupling to the gluonic-excited meson-meson state, we want to restore the same energy shifts we can get to (with same origin of the first and second correction terms)

$$E_i = E_i^0 + (-0.0950 - 0.6371)\text{GeV} = E_i^0 - 0.7321\text{GeV}$$

if $f^a = 0.14$ is used. This shows that gluonic excitations can effectively replace the many terms for energy shifts as well. We note that the energy shift is independent of θ, the angle between $\mathbf{R}_1$ and $\mathbf{R}_2$ or $\mathbf{P}_1$ and $\mathbf{P}_2$ or $\mathbf{P}_{1s}$ and $\mathbf{P}_{2s}$. The energy shifts we have reported here can be compared with the hadron-loops-generated mass shifts to charmonium states reported in Table III of ref. [80]. It is difficult, though, to conclude anything from this comparison as in ref. [80] the integrand contains squares of the matrix elements of the $^3P_0$ meson decay amplitudes whereas in our integrands in eq.(3.5.21) contain squares of meson-meson couplings. Thus though the intermediate states in both works are respective *hadron loops* $q\bar{q}q\bar{q}$, the initial and final states in ref. [80] are $q\bar{q}$ but in our work initial and final states are also $q\bar{q}q\bar{q}$. Only the glounic-exited intermediate $q\bar{q}q\bar{q}$ state (i.e. the hybrid hadronic loops) is common in the two works. In result 4, it is noted that the average phase shift obtained (for $\epsilon = 2$) by a model that does not include the gluonic excitations is equal to the average phase

shift obtained by including gluonic excitations for $f^a = 0.03$, but the energy shift obtained by both models becomes comparable at $f^a = 0.14$. One possible reason of this difference in the values of f^a could be that the average phase shift is calculated for the center of mass kinetic energy range in between 0 GeV to 2 GeV, but energy shift is calculated at threshold center of mass kinetic energy.

6- For the ground state gluonic field, transition matrix elements are θ independent. But for transition elements to the gluonic-excited meson-meson state depends on θ. We projected this angle dependence on spherical harmonics Y_{lm}. The results of this partial wave analysis are also reported in Figs.(5.9-5.11) for $m = 0$ and $f^a = 0.03$ (this value is used above in result 4). The reason for truncating the spherical expansion to $m = 0$ harmonics is that that we have have no dependence on ϕ, the azimuthal angle. This analysis shows that partial wave amplitudes are decreasing as we go from the coefficient of Y_{00} to that of Y_{50} coefficient i.e. from S-wave to H-wave. Figs.5.9 and 5.10 are for the even wave $(D, G, ...)$ ratios with $S-$wave. S/D ratios are also used in ref. [81, 51]. Our graphs shows that the S/G ratio is too much large as compared to the S/D ratio. It means that $S-$wave is dominant over $G-$wave. In Fig.5.11, ratios of odd waves with $S-$wave are shown. We noted that S/H is too much large as compared to S/P. This shows that $H, J, ...$ waves can be neglected as compared to $S-$wave. The partial wave analysis indicates the presence of P, D, F, G, H waves only when we include the gluonic excitations in combination with essentially sum-of-pair-wise approach. It means that, in the presence of gluonic excitations, an $\ell = 0, 1, 2, 3, ...$ ground state meson-meson system may couple to $\ell = 0, 1, 2, 3, ...$ hybrid hybrid systems as a intermediate states or as final states.

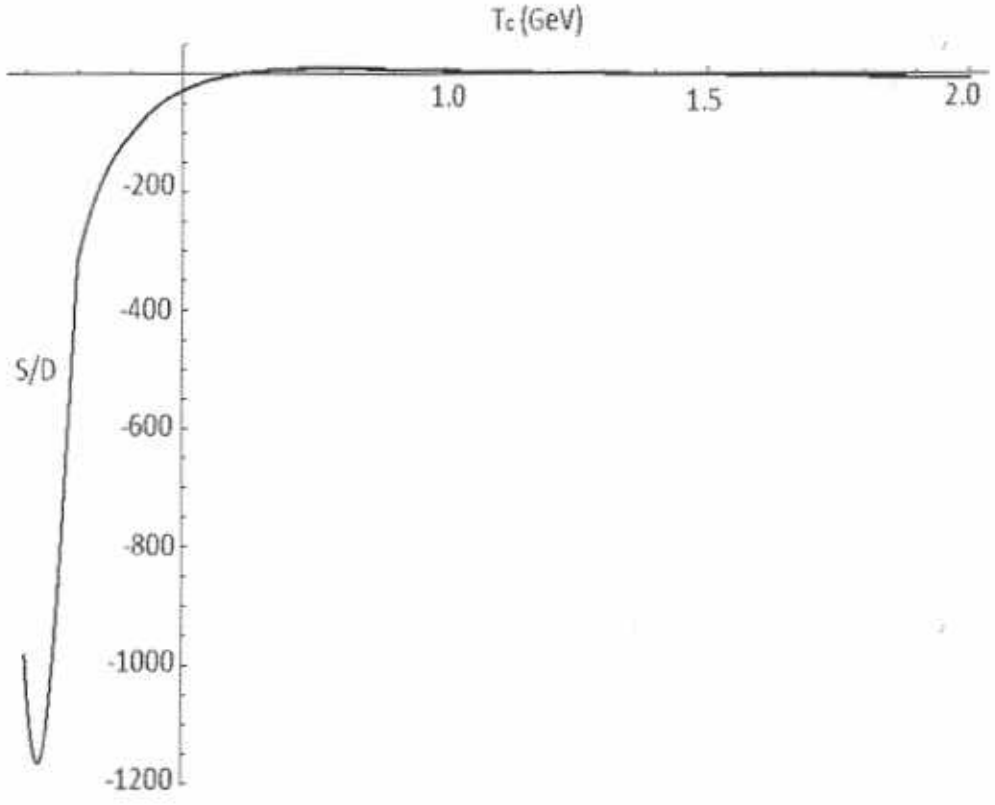

Figure 5.9: A graph between T_c and S/D ratio.

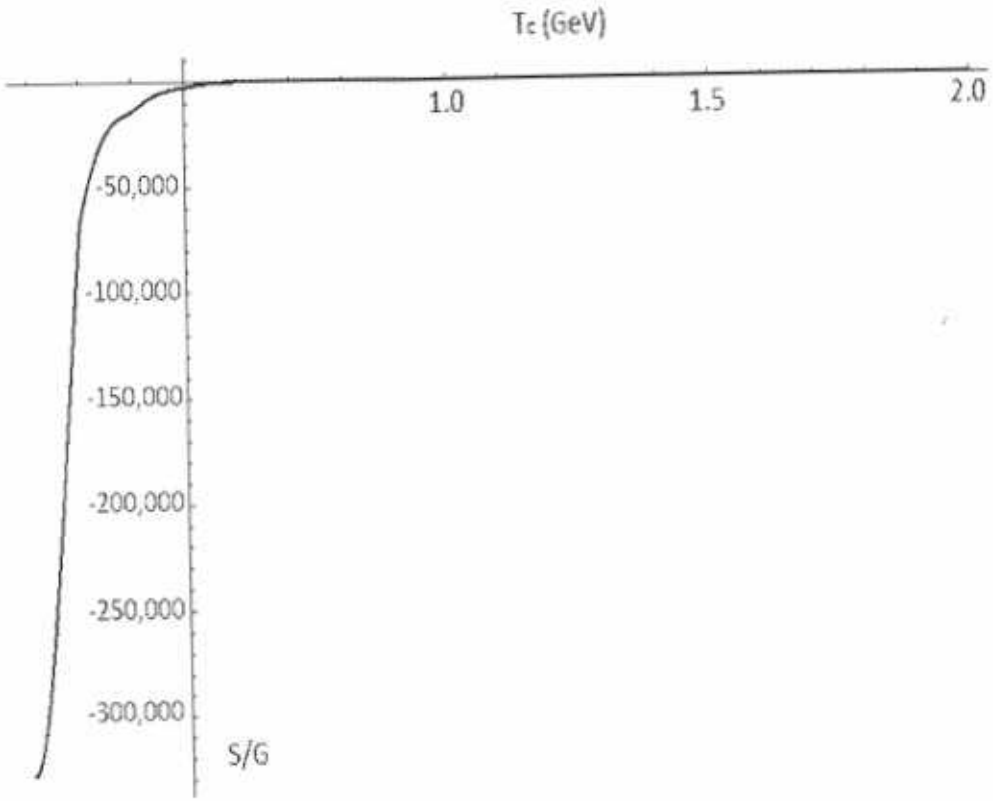

Figure 5.10: A graph between T_c and S/G ratio.

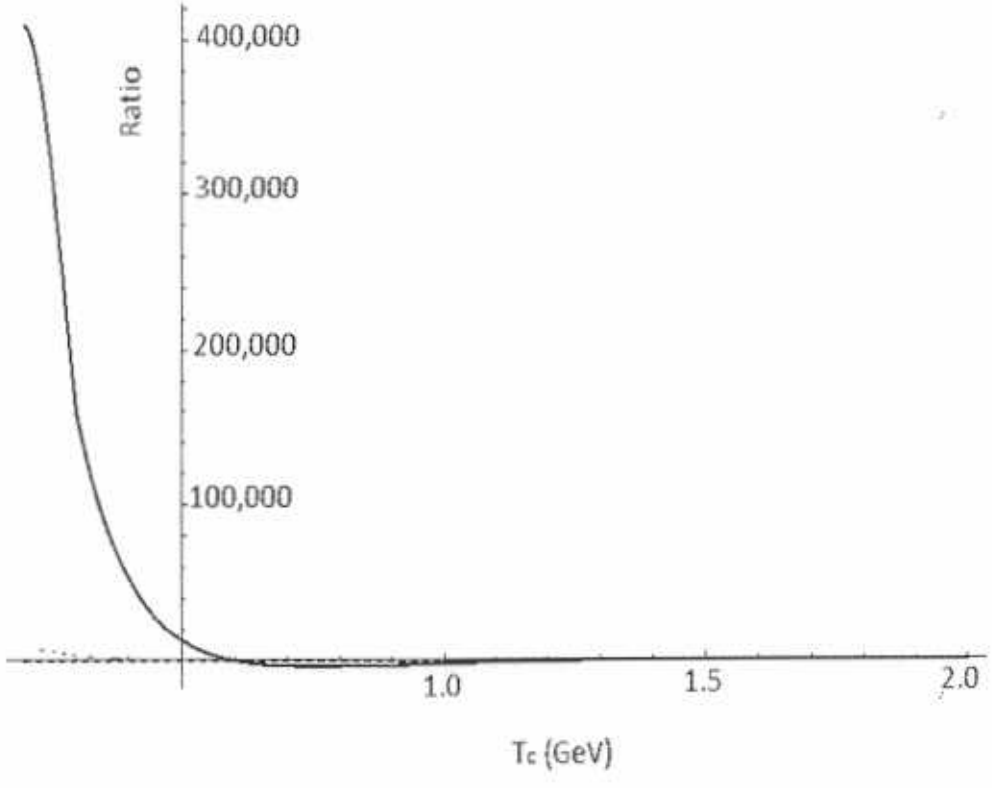

Figure 5.11: A graph between T_c and $S/P, S/F, S/H$ ratios. Dashed line is for S/P, thin solid line is for S/F, and thick solid line is for S/H. S/P and S/F are so small as compared to S/H that the curves for S/P and S/F are lie along horizontal axis.

2- Diagonal elements (T_{11} or T_{22}) and unitarity condition

As $T_{11} = T_{22}$, so the results related to imaginary part of T_{11} are reported here. The same results will be for T_{22}.

1- The real part of $T_{11} = 0$ as given above in chapter 3 in eq.(3.5.27)). To calculate the imaginary part of T_{11}, eq.(3.5.31) is used. For the gluonic field in ground state, the basis states are $\mid 1\rangle, \mid 2\rangle$, so T_{12^*} is zero (as $\mid 2^*\rangle$ not exist for ground state gluonic field). Therefore, eq.(3.5.31) reduces to

$$ImT_{11} = \frac{1}{2} \pm \frac{1}{2}\sqrt{1 - 4T_{12}T_{12}^*}. \tag{5.0.1}$$

Hence for ground state gluonic field T_{11} depends only on T_{12}. T_{12} is calculated by using eq.(3.5.15) with $k_f = 0.6$ [45](without the incorporation of gluonic excited states). Substituting the results for T_{12} in above eq.(5.0.1), we calculated T_{11}. Eq.(5.0.1) shows that for each value of center of mass kinetic energy (T_c), ImT_{11} has two different results; obtained by using the eq.(5.0.1) in the form of

i)

$$ImT_{11} = \frac{1}{2} + \frac{1}{2}\sqrt{1 - 4T_{12}T_{12}^*}, \tag{5.0.2}$$

ii)

$$ImT_{11} = \frac{1}{2} - \frac{1}{2}\sqrt{1 - 4T_{12}T_{12}^*}. \tag{5.0.3}$$

Fig.5.12 shows the dependence of imaginary part of T_{11} on center of mass kinetic energy with using the relation given in eq.(5.0.2) and Fig.5.13 shows the dependence

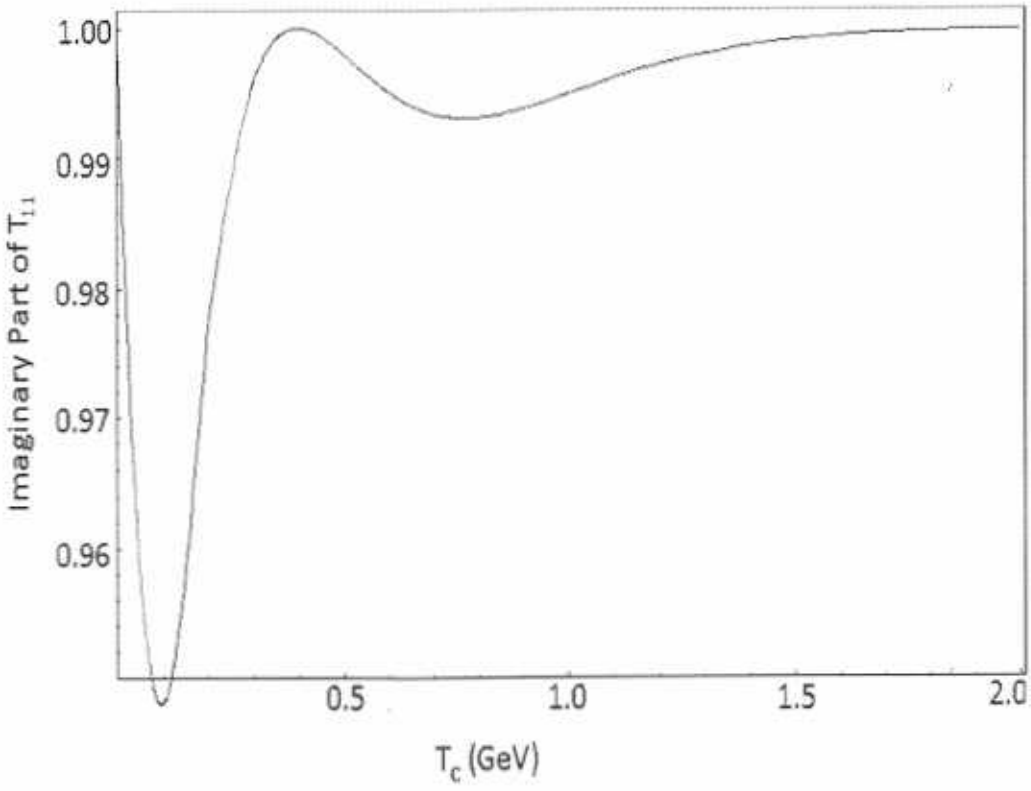

Figure 5.12: a graph between energy and imaginary part of T_{11} for ground state obtained by using the relation given in eq.(5.0.2)

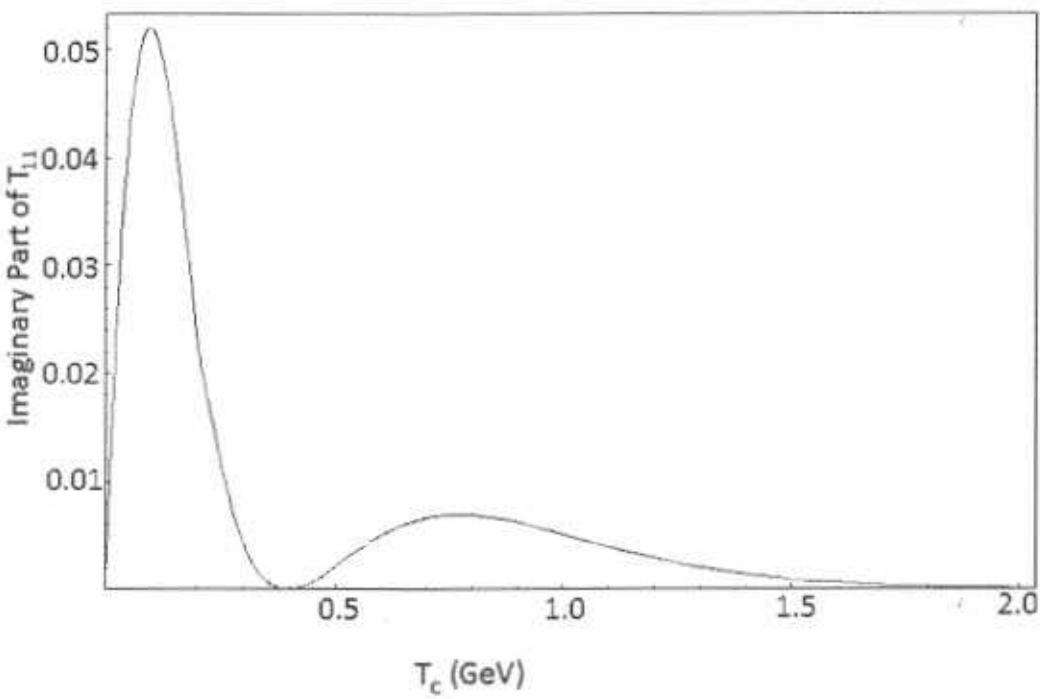

Figure 5.13: The same graph as Fig.5.12 but obtained by using the relation given in eq.(5.0.3)

of imaginary part of T_{11} on center of mass kinetic energy by using the relation given in eq.(5.0.3) for ground state gluonic field.

2- With the incorporation of excited state gluonic field, k_f changes from 0.6 to 1.51, as discussed in section 1 of this chapter. Now using eq.(3.5.31) in the form of

$$ImT_{11} = \frac{1}{2} + \frac{1}{2}\sqrt{1 - 4T_{12}T_{12}^{*} - 4T_{12^{*}}T_{12^{*}}^{*}}, \tag{5.0.4}$$

imaginary part of T_{11} is calculated. Fig.5.14 shows the relation between center of mass kinetic energy and this imaginary part of T_{11} by including the excited state gluonic field. Fig.5.15 shows the relation between center of mass kinetic energy and imaginary part of T_{11} with

$$ImT_{11} = \frac{1}{2} - \frac{1}{2}\sqrt{1 - 4T_{12}T_{12}^{*} - 4T_{12^{*}}T_{12^{*}}^{*}}, \tag{5.0.5}$$

3- The phase shift is calculated for the diagonal element of the transition matrix, T_{11} by using the relations written in eqs.(3.5.32,3.5.33). For the center of mass kinetic energy range 0 to 2 GeV, the average of the modulus of phase shifts (excluding excited states) is equal to -0.0068ι radians at $k_f = 0.6$. But if we change the value of k_f from 0.6 to 1.51 and also include the excited state gluonic field, the average meson-meson phase shift again becomes -0.0068ι radians by choosing $f^a = 0.0258$ and $\theta = 90^{\circ}$ with $\epsilon = 2$. This means that a sum-of-two-body potential model can replace to some extent many-body potential terms in a tetraquark system by including the gluonic excitations even if we not .

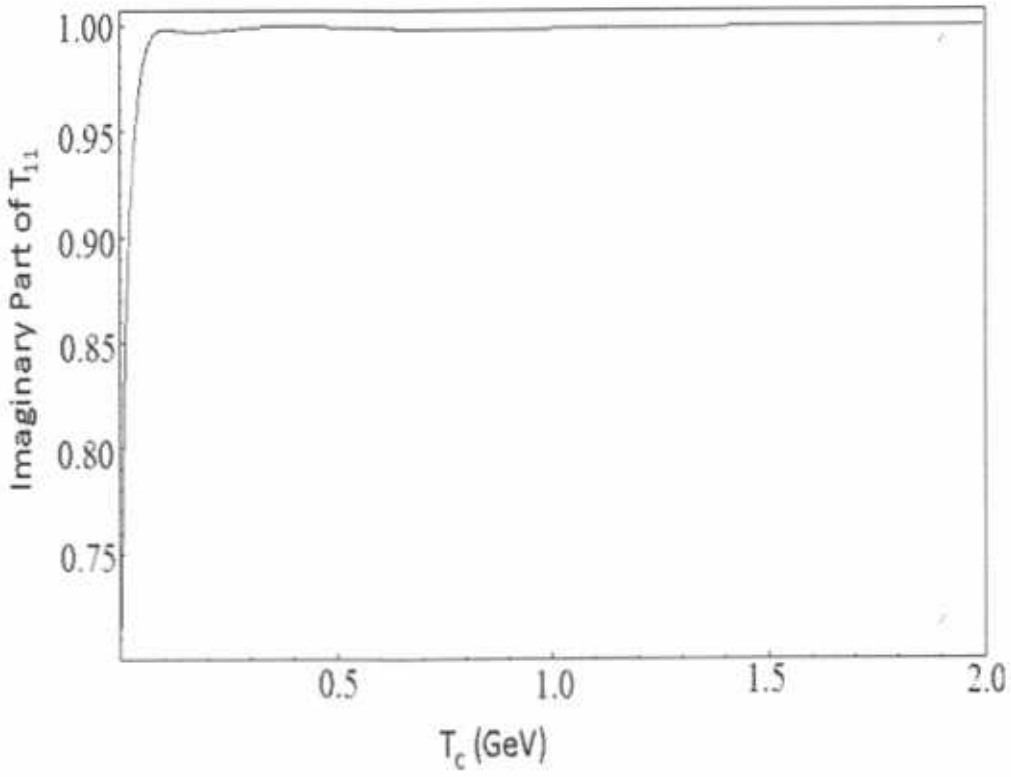

Figure 5.14: a graph between energy and imaginary part of T_{11} for excited state gluonic field obtained by eq.(5.0.4)

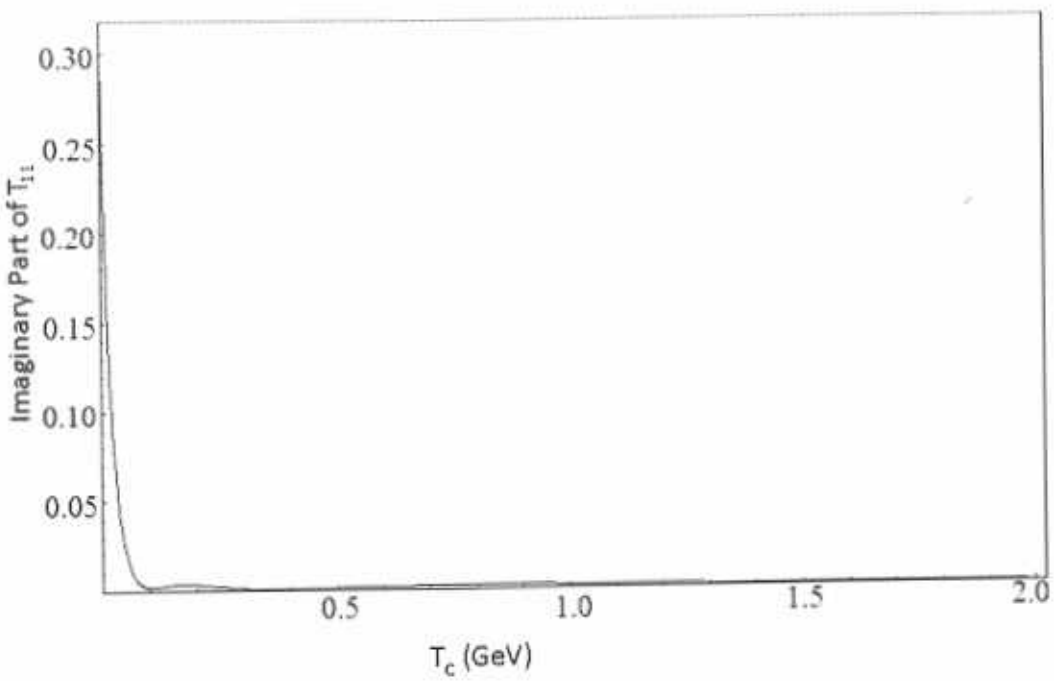

Figure 5.15: The same graph as in Fig.5.14 but obtained by eq.(5.0.5)

3- Properties of charmonium Hybrid mesons

In all above results effects of gluonic excitations are studied for meson-meson systems for static quarks with c-flavour by neglecting the spin. Now following results are obtained by incorporating the spin and quarks dynamics in a meson system composed of quark anti-quark having c-flavour.

1- Our calculated masses and root mean square radii for conventional charmonium mesons obtained by solving the eq.(4.1.3) with potential written in eq.(4.1.1) are reported in Table 5.2 and 5.3 along with the experimental and theoretical predictions of the other works. We observed that our results are in good agreement with the experimental and existing theoretically predicted values, which shows the validity of our method. Quantum mechanically, when L increases, centrifugal barrier increases so particles become less bound implying increased root mean square radii. Our calculated root mean square radii are in agreement with this expectation.

2- With the parameters (given in Table 5.4) for the $0^{+-}, 1^{-+}$ and 2^{+-} J^{PC} states, masses and root mean square radii are calculated for the charmonium hybrid mesons. In Table 5.4, masses of charmonium hybrid meson are calculated for J^{PC} states $0^{+-}, 1^{-+}$ and 2^{+-} using the excited state gluonic field potential in the form of $A\exp(-Br^2)$ and π/r. In Table 5.5, root mean square radii are calculated by taking the excited state potential in the form of $A\exp(-Br^2)$ and π/r. For comparison with earlier works, masses of $c\bar{c}$ hybrid mesons with $0^{+-}, 1^{-+}$ and 2^{+-} J^{PC} states are reported in Table 5.6.

3-For conventional mesons, $|R(0)|^2$ is reported in Table5.7. $|R(0)|^2$ of $c\bar{c}$ hybrid mesons for $0^{+-}, 1^{-+}$ and 2^{+-} J^{PC} states is equal to zero by our calculation and

Table 5.2: The experimental and theoretical masses of some charmonium meson. The experimental mass is the average PDG [46] and rounded to 0.0001 GeV. Our calculated masses are also rounded to 0.0001 GeV.

Meson	L	S	Our calculated mass	Theor. mass [46] with NR potential model	Exp. mass
			GeV	GeV	GeV
η_c	0	0	2.9816	2.982	2.9792 ± 0.0013 [46]
J/ψ	0	1	3.0900	3.090	3.09687 ± 0.00004 [46]
h_c	1	0	3.5156	3.516	3.525 ± 0.00055 [46]
χ_c	1	1	3.5246	3.556	3.55618 ± 0.00013 [82]

Table 5.3: The theoretical root mean square radii of charmonium meson rounded to 0.001 fm.

Meson	L	S	$\langle r^2 \rangle$	Theor. $\langle r^2 \rangle$ [83] with potential model
			fermi	fermi
η_c	0	0	0.365	0.388
J/ψ	0	1	0.414	0.404
h_c	1	0	0.674	0.602
χ_c	1	1	0.685	0.606

Table 5.4: Our calculated masses of $c\bar{c}$ hybrid meson $0^{+-}, 1^{-+}$ and 2^{+-} J^{PC} states

J^{PC}	L	S	Λ	$< J_g^2 >$	Mass with excited potential as $A \times \exp(-Br^2)$	Mass with excited potential as π/r
					GeV	GeV
$0^{+-}, 1^{-+}, 2^{+-}$	1	1	1	2	4.0619	4.3571
$1^{-+}, 2^{+-}$	2	1	1	2	4.1433	4.4632

Table 5.5: Our calculated root mean square radii of $c\bar{c}$ hybrid meson $0^{+-}, 1^{-+}$ and 2^{+-} J^{PC} states

J^{PC}	L	S	Λ	$< J_g^2 >$	$\langle r^2 \rangle$ with excited potential as $A \times \exp(-Br^2)$	$\langle r^2 \rangle$ with excited potential as π/r
					fm	fm
$0^{+-}, 1^{-+}, 2^{+-}$	1	1	1	2	1.2458	1.1061
$1^{-+}, 2^{+-}$	2	1	1	2	1.3203	1.2280

Table 5.6: The mass predictions of $1^{-+}, 0^{+-}$, and 2^{+-} states

Predicted masses (GeV)			models
1^{-+}	0^{+-}	2^{+-}	
≈ 3.9 [85]			bag model
4.2-4.5 [86]			flux tube model
$4.19 \pm sys.error$ [87] [66] 4.7 [89]	≈ 4.5 [88] 4.58 [89]	≈ 4 [88]	heavy quark LGT
4.1-4.5			QCD sum rules
4.369 – 4.420 [90, 91, 92]	4.714(52) [92]	4.895(88) [93]	quenched lattice QCD

this result agrees with ref. [84] which writes "models of hybrids typically expect the wave function at the origin to vanish". We noted that hybrid mesons's masses are greater and radii are lesser when the excited potential is in the form of π/r instead of $A\, exp(-Br^2)$. We also noted that the masses and root mean square radii of the hybrid mesons are greater than ordinary mesons of same flavour and quantum numbers. Since $0^{+-}, 1^{-+}$, 2^{+-} states are not possible with quark model quantum numbers, so we can not compare these J^{PC} states with conventional mesons.

5.1 Conclusions

In this thesis the gluonic excitations are studied

1) by neglecting the spin and using the quadratic potential approximation for

Table 5.7: $|R(0)|^2$ of $c\bar{c}$ meson

Meson	L	S	our predicted normalized $\|R(0)\|^2$ $(\text{fm})^{-3}$
η	0	0	1.9767
J/ψ	0	1	1.10865
h_c	1	0	$< 10^{-10}$
χ_c	1	1	$< 10^{-11}$

meson-meson system, and

2) by introducing spin and using the realistic coulombic plus linear potential for mesons.

The understanding of gluonic excitations is necessary to solve the mysteries of hadron spectroscopy. To understand the quark exchange effects in meson-meson systems (or multi-quark systems), we have used a QCD based potential model. We used a potential model matrix in four basis which at quark level is known to provide a good fit to numerical simulations of a $q^2\bar{q}^2$ system in pure gluonic theory for static quarks in a selection of geometries. Then we have used a formalism of resonating group method and Born approximation to study the interactions of meson-meson systems having dynamics resulting through quark exchange effects using wave functions of a $q\bar{q}$ potential within a cluster. The approximations used in chapter 3 are mentioned in section 3.2. The parameters used in this work are mentioned in Table 5.1.

As mentioned above in results 4 & 5 in section 1, we compare our meson-meson transition amplitudes and polarization potentials (in the respective center of mass energy ranges) in an extended almost sum-of-pair-wise approach and a many-body-term based one. Apparently this comparison has even a qualitative difference in case

of the transition amplitudes (T_{12} and T_{12}^{*}) which have a dependance on the scattering angle (meaning coupling to P and higher orbital excitations in the final channel) if we use gluonic excitation in combination with essentially sum-of-pair-wise approach (can see Figs.(5.2-5.6)) but we get the same transition amplitude for all the scattering angles if we use a many-body potential linking ground-state clusters only. But a recent work [32] indicates that the absence of angle dependence is an artifact of the unjustified overly simple form of the gluonic overlap factor f (defined in eq.(2.3.2)); using a proper lattice-gauge theory-based form of f (defined in eq.(2.3.1)) also results in this angle dependence and the resulting coupling to higher orbital excitations.

The results showed that for ground state basis, the average phase shift and average energy shift are decreasing with the increase of parameter k_f. But if we include the excited states basis, then, by the proper adjustment of parameter f^a, we compensated the decrease in average phase shift and average energy shift. This means that at $k_f = 1.51$, the interaction between ground states decreased and this decrease is compensated by the incorporation of excited states.

The meson-meson to hybrid-hybrid coupling worked out in this thesis may affect properties of any system that is presently understood to be a purely ground-state meson-meson system. This means, in addition to the energy shift of the meson-meson molecules due to coupling to hybrid-hybrid systems, pointing out the possibility of a hybrid-hybrid component in the wave functions of mesons like $X(3872)$, $X(3940)$, $Y(4260)$, and $Z(4433)$ which are considered to have $q^2\bar{q}^2$ components. And in the above paragraph, we indicate that this coupling may also include coupling to orbital excitations. Thus we hope to point out a new dimension in discussions about the structure of scalar mesons as well.

When we concentrated on a $q\overline{q}$ pair but with spin, flavour, and realistic quark anti-quark potential in chapter 4, we concluded that spin angular angular momentum have very little effects on the mass and size of meson as compared to orbital angular momentum. It is also concluded that with the increase of orbital angular momentum, the size and mass of the meson increases. We also noted that hybrid mesons's masses are greater and radii are lesser when the excited potential is in the form of π/r instead of $Aexp(-Br^2)$. We also noted that the masses and root mean square radii of the hybrid mesons are greater than ordinary mesons of same flavour and quantum numbers.

As scalar form factors [40] and energy shifts [41] are proportional to square of root mean square radii and magnetic polarizabilities [41] are proportional to negative of square of root mean square radii, we predict that magnitude of these quantities for hybrids are greater than those for conventional mesons of the same quantum numbers. We also noted that $|R(0)|^2$=0 in case of hybrid mesons. Using this result, we can predict that decay constants [42], decay rates [42], and differential cross sections [43] of hybrid mesons are zero as these quantities are proportional to $|R(0)|^2$.

APPENDIX

In this thesis we use the colour basis given through eqs.(2.1.2,3.0.1). In the notation of Appendix C of ref. [22], the diquark-diantiquark system have colour basis $|\overline{3}_{12}3_{\overline{34}}\rangle$, $|6_{12}\overline{6}_{\overline{34}}\rangle$ and meson-meson system have colour basis $(|1_{1\overline{3}}1_{2\overline{4}}\rangle, |8_{1\overline{3}}8_{2\overline{4}}\rangle)$ or $(|1_{1\overline{4}}1_{2\overline{3}}\rangle, |8_{1\overline{4}}8_{2\overline{3}}\rangle)$. Here $|\overline{3}_{12}3_{\overline{34}}\rangle$ represents that quarks 1 and 2 are in antisymmetric representation $\overline{3}$ of SU(3), and antiquarks 3 and 4 are in antisymmetric representation 3 of SU(3). We use the meson-like base states $(|\overline{3}_{12}3_{\overline{34}}\rangle, |1_{1\overline{3}}1_{2\overline{4}}\rangle, |8_{1\overline{3}}8_{2\overline{4}}\rangle, |8_{1\overline{4}}8_{2\overline{3}}\rangle$. These are written in terms of the orthonormal diquark-diantiquark basis in Appendix C of ref. [22] as

$$|8_{1\overline{3}}8_{2\overline{4}}\rangle = -\sqrt{\frac{2}{3}}|\overline{3}_{12}3_{\overline{34}}\rangle + \sqrt{\frac{1}{3}}|6_{12}\overline{6}_{34}\rangle, \tag{5.1.1}$$

$$|1_{1\overline{3}}1_{2\overline{4}}\rangle = \sqrt{\frac{1}{3}}|\overline{3}_{12}3_{\overline{34}}\rangle + \sqrt{\frac{2}{3}}|6_{12}\overline{6}_{\overline{34}}\rangle, \tag{5.1.2}$$

$$|8_{1\overline{4}}8_{2\overline{3}}\rangle = \sqrt{\frac{8}{9}}|1_{1\overline{3}}1_{2\overline{4}}\rangle - \sqrt{\frac{1}{9}}|8_{1\overline{3}}8_{2\overline{4}}\rangle, \tag{5.1.3}$$

$$|1_{1\overline{4}}1_{2\overline{3}}\rangle = \sqrt{\frac{1}{9}}|\overline{1}_{1\overline{3}}1_{2\overline{4}}\rangle + \sqrt{\frac{8}{9}}|8_{1\overline{3}}8_{2\overline{4}}\rangle. \tag{5.1.4}$$

To calculate the matrix elements of the $F_i.F_j$ operators (introduced above in eq.(3.0.6)), for different values of indices i and j, the results given in the Appendix C of ref. [22] are used along with the above eqs.(5.1.1-5.1.4) and following group theory results

given in [55]

$$|1_{1\bar{4}}1_{2\bar{3}}\rangle = -\sqrt{\frac{1}{3}}|\bar{3}_{12}3_{\bar{3}\bar{4}}\rangle + \sqrt{\frac{2}{3}}|6_{12}\bar{6}_{\bar{3}\bar{4}}\rangle,$$

and

$$\langle 8_{1\bar{3}}8_{2\bar{4}}|\mathbf{F}_i.\mathbf{F}_j|8_{1\bar{3}}8_{2\bar{4}}\rangle = \frac{1}{6}.$$

The matrix elements of the $F_i.F_j$ operators are

$$_c\langle 1| \begin{bmatrix} F_1.F_2 \\ F_1.F_3 \\ F_1.F_4 \\ F_2.F_3 \\ F_2.F_4 \\ F_3.F_4 \end{bmatrix} |1\rangle_c = \begin{bmatrix} 0 \\ -\frac{4}{3} \\ 0 \\ 0 \\ -\frac{4}{3} \\ 0 \end{bmatrix} \tag{5.1.5}$$

As written in chapte 2 that the gluonic state $\mid k\rangle_g$ is a state approaching to colour state $\mid k\rangle_c$ in the limit of quark anti-quark separation approaching to zero.

$$_c\langle 1| \begin{bmatrix} F_1.F_2 \\ F_1.F_3 \\ F_1.F_4 \\ F_2.F_3 \\ F_2.F_4 \\ F_3.F_4 \end{bmatrix} |2\rangle_c =_c \langle 2| \begin{bmatrix} F_1.F_2 \\ F_1.F_3 \\ F_1.F_4 \\ F_2.F_3 \\ F_2.F_4 \\ F_3.F_4 \end{bmatrix} |1\rangle_c = \begin{bmatrix} \frac{4}{9} \\ -\frac{4}{9} \\ -\frac{4}{9} \\ -\frac{4}{9} \\ -\frac{4}{9} \\ \frac{4}{9} \end{bmatrix} \tag{5.1.6}$$

$$_c\langle 1| \begin{bmatrix} F_1.F_2 \\ F_1.F_3 \\ F_1.F_4 \\ F_2.F_3 \\ F_2.F_4 \\ F_3.F_4 \end{bmatrix} |3\rangle_c =_c \langle 1| \begin{bmatrix} F_1.F_2 \\ F_1.F_3 \\ F_1.F_4 \\ F_2.F_3 \\ F_2.F_4 \\ F_3.F_4 \end{bmatrix} |1\rangle_c = \begin{bmatrix} -\frac{2}{3\sqrt{3}} \\ -\frac{4}{3\sqrt{3}} \\ \frac{2}{3\sqrt{3}} \\ \frac{2}{3\sqrt{3}} \\ -\frac{4}{3\sqrt{3}} \\ -\frac{2}{3\sqrt{3}} \end{bmatrix} \tag{5.1.7}$$

$$ {}_c\langle 2| \begin{bmatrix} F_1.F_2 \\ F_1.F_3 \\ F_1.F_4 \\ F_2.F_3 \\ F_2.F_4 \\ F_3.F_4 \end{bmatrix} |2\rangle_c = \begin{bmatrix} 0 \\ 0 \\ -\frac{4}{3} \\ -\frac{4}{3} \\ 0 \\ 0 \end{bmatrix} \tag{5.1.8} $$

$$ {}_c\langle 2| \begin{bmatrix} F_1.F_2 \\ F_1.F_3 \\ F_1.F_4 \\ F_2.F_3 \\ F_2.F_4 \\ F_3.F_4 \end{bmatrix} |3\rangle_c = {}_c\langle 3| \begin{bmatrix} F_1.F_2 \\ F_1.F_3 \\ F_1.F_4 \\ F_2.F_3 \\ F_2.F_4 \\ F_3.F_4 \end{bmatrix} |2\rangle_c = \begin{bmatrix} \frac{?}{3\sqrt{3}} \\ -\frac{2}{3\sqrt{3}} \\ \frac{4}{3\sqrt{3}} \\ \frac{4}{3\sqrt{3}} \\ -\frac{2}{3\sqrt{3}} \\ \frac{2}{3\sqrt{3}} \end{bmatrix} \tag{5.1.9} $$

$$ {}_c\langle 1| \begin{bmatrix} F_1.F_2 \\ F_1.F_3 \\ F_1.F_4 \\ F_2.F_3 \\ F_2.F_4 \\ F_3.F_4 \end{bmatrix} |2^\star\rangle_c = \begin{bmatrix} -\frac{2}{9\sqrt{2}} \\ -\frac{16}{9\sqrt{2}} \\ \frac{2}{9\sqrt{2}} \\ \frac{2}{9\sqrt{2}} \\ -\frac{16}{9\sqrt{2}} \\ -\frac{2}{9\sqrt{2}} \end{bmatrix} \tag{5.1.10} $$

$$ {}_c\langle 2| \begin{bmatrix} F_1.F_2 \\ F_1.F_3 \\ F_1.F_4 \\ F_2.F_3 \\ F_2.F_4 \\ F_3.F_4 \end{bmatrix} |1^\star\rangle_c = \begin{bmatrix} -\frac{2}{9\sqrt{2}} \\ \frac{2}{9\sqrt{2}} \\ \frac{16}{9\sqrt{2}} \\ \frac{16}{9\sqrt{2}} \\ \frac{2}{9\sqrt{2}} \\ -\frac{2}{9\sqrt{2}} \end{bmatrix} \tag{5.1.11} $$

$$ {}_c\langle 1^*| \begin{bmatrix} F_1.F_2 \\ F_1.F_3 \\ F_1.F_4 \\ F_2.F_3 \\ F_2.F_4 \\ F_3.F_4 \end{bmatrix} |2^*\rangle_c = \begin{bmatrix} \frac{10}{18} \\ -\frac{1}{18} \\ -\frac{1}{18} \\ -\frac{1}{18} \\ -\frac{1}{18} \\ \frac{10}{18} \end{bmatrix} \tag{5.1.12} $$

$$ {}_c\langle 1^*| \begin{bmatrix} F_1.F_2 \\ F_1.F_3 \\ F_1.F_4 \\ F_2.F_3 \\ F_2.F_4 \\ F_3.F_4 \end{bmatrix} |1^*\rangle_c = \begin{bmatrix} -\frac{1}{3} \\ \frac{1}{6} \\ \frac{1}{6} \\ \frac{1}{6} \\ \frac{1}{6} \\ -\frac{1}{3} \end{bmatrix} \tag{5.1.13} $$

$$ {}_c\langle 2^*| \begin{bmatrix} F_1.F_2 \\ F_1.F_3 \\ F_1.F_4 \\ F_2.F_3 \\ F_2.F_4 \\ F_3.F_4 \end{bmatrix} |2^*\rangle_c = \begin{bmatrix} -\frac{1}{3} \\ -\frac{7}{6} \\ -\frac{7}{6} \\ -\frac{7}{6} \\ -\frac{7}{6} \\ \frac{1}{3} \end{bmatrix} \tag{5.1.14} $$

The gluonic state $\mid k\rangle_g$ is defined as a state approaching to colour state $\mid k\rangle_c$ in the limit of quark anti-quark separation approaching to zero.

Bibliography

[1] Hedeki Yukawa, *Proceedings of Physico Mathematical Society of Japan*, **17**, 46 (1935)

[2] Powell, C. F. *Report on the Progress of Physics*, **13**, 350 (1950).

[3] M. Gell-Mann, Phys. Lett. **8**, 214 (1964).

[4] C. Zweig, CERN-TH-412, NP=14146, (1964).

[5] O. W. Greenberg, Phys. Rev. Lett. **13**, 598 (1964).

[6] M. Han and Y. Nambu, Phys. Rev. B **139**, 1006 (1965).

[7] C. Morningstar, *What Do We Know about Glueballs and Hybrids from Lattice QCD*? IHEP, Beijing, China, January (2004); C.Michael, *Glueballs and Hybrid Mesons*, Review presented at the Rencontre de Physique 'Results and Perspectives in Particle Physics', La Thuile, hep-ph/9605243.

[8] W. Greiner and A. Schäfer, Quantum Chromodynamics, Springer-Verlag (1994).

[9] J. R. Aitichison and A. J. G. Hey, Gauge Theories in Particle Physics, Vol.1, from Relativistic Quantum Mechanics to QED, (Institute of Physics Publishing), (2003).

[10] D. J. Gross, F. Wilczek, Phys. Rev. Lett. **30**, 1343 (1973).

[11] H. D. Politzer, Phys. Rev. Lett. **30**, 1346 (1973).

[12] K. Wilson, Phys. Rev. D **10**, 2445 (1974).

[13] A. M. Polyakov, Phys. Lett. B **59**, 79 (1975); Phys. Lett. B **59**, 82 (1975).

[14] F. J. Wegner, J. Math. Phys. **12**,2259 (1971).

[15] C. Y. Wong, Phys. Rev. C **69**, 055202 (2004).

[16] D. H. Perkins, *Introduction to High Energy Physics*, Addison-Wesley (1987).

[17] N. Isgur and J. Paton, Phys. Rev. D **31**, 2910 (1985).

[18] J. Kogut and L. Susskind, Phys. Rev. D **11**, 395 (1975); J. Kogut and L. Susskind, Phys. Rev. D **9**, 3501 (1974).

[19] K. J. Juge, J. Kuti, and C. Morningstar, *in Proceedings of AIP Conference*, 2003.

[20] B. Masud , Phys. Rev. D **50**, 6783 (1994).

[21] J. Weinstein and N. Isgur, Phy. Rev. D **27**, 588 (1983).

[22] J. Weinstein and N. Isgur, Phy. Rev. D **41**, 2236 (1990).

[23] T. Barnes and E.S. Swanson, Phys. Rev. D **46** 131 (1992).

[24] T. Barnes,S. Capstick, M. D. Kovarik, and E. S. Swanson, Phy. Rev C **48**, 539 (1993).

[25] O. W. Greenberg and H. J. Lipkin, Nucl. Phys. A **370**, 349 (1981).

[26] B. Masud, J. Paton. A. M. Green, and G. Q. Liu, Nucl. Phy. A **528**, 477 (1991).

[27] K. Widermuth and Y. C. Tang, *A Unified theory of the Nucleus, Vol.1 of Clustering Phenomena in nuclei*(eds. K.Wildermuth and P.Kramer). Vieweg (1997).

[28] A. M. Green and P. Pennanen, Phys. Rev. C **57**, 3384 (1998).

[29] A. M. Green, arXive:nucl-th/0409021v1 (2004).

[30] A. M. Green, J. Lukkarinen, P. Pennanen and C. Michael, Phys. Rev. D **53**, 261 (1996).

[31] P. Pennanen, Nucl. Phys. Proc. Suppl. **53**, 334 (1997).

[32] M. I. Jamil and B. Masud, Eur. Phys. Jour. A **47** (2011).

[33] K. J. Juge, J. Kuti, and C. Morningstar, Nucl. Phys. Proc. Suppl. **63** 326 (1998).

[34] P.Pennanen, Phys. Rev. D **55**, 3958 (1997).

[35] M. Ablikim et el. (BES Collaboration), Phys. Rev. Lett. **97**, 121801 (2006).

[36] M. Ablikim et el. (BES Collaboration), Phys. Lett. B **660**, 315 (2008).

[37] C. McNeile, Nucl. Phys. A **711**, 303 (2002).

[38] C. Michael, hep-ph/0308293.

[39] S. Collins, C. T. H. Davies, G. Bali, Nucl. Phys. Proc. Suppl. **63**, 335 (1998).

[40] B. Ananthanarayan, I. Caprini, G. Colangelo, J. Gasser and H. Leutwyler, Phys. Lett. B **602**, 218 (2004).

[41] S. I. Kruglov, Phys. Rev. D **60**, 116009 (1999).

[42] B. Patel and P. C. Vinodkumar, J. Phys. G **36**, 035003 (2009).

[43] C. H. Chaug, C. F. Qiao, J. X. Wang, Phys. Rev. D **57**, 4035 (1998).

[44] A. M. Green, C. Michael, and J. E. Paton, Nucl. Phys. A **554**, 701 (1993).

[45] A. M. Green, J. Koponen, and P. Pennanen, Phys. Rev. D **61**, 014014 (1999).

[46] T. Barnes, S. Godfrey, and E. S. Swanson, Phys. Rev. D **72**, 054026 (2005).

[47] K. Shimizu, Rep. Prog. Phys., 52:1, (1989).

[48] Y. Suzuki and K. Hecht. Phys. Rev., C 27:299, (1983).

[49] R. R. Schroeder and H. G. Dosch., Nucl. Phys. A **451** :666, (1986).

[50] J. Vijande, A. Valcarce, and J. M. Richard, Phys. Rev. D **76**, 114013 (2007).

[51] E. S. Ackleh, T. Barnes, and E. S. Swanson, Phys. Rev. D **54**, 6811 (1996).

[52] V. G. Bornyakov, P. Yu. Boyko, M. N. Chernodub, and M. I. Polikarpov, arXiv:hep-lat/0508006v1 (2005).

[53] A. M. Green and P. Pennanen, Phys. Lett. B **426**, 243 (1998).

[54] A. M. Green, H. J. Pirnal, G. A. Miller, B. Povh, F. Myhrer, W. Weise, J. A. Niskanen, K. Yazaki, and M. Oka, *Quarks and Nuclei*, edited by W. Weise (World Scientific Publishing Co.Pte Ltd, 1984), Vol. 1, Chap. 6.

[55] John. R. Taylor, Scattering Theory, (John Wiley and Sons, Inc.), (1972).

[56] M. Alekseev et al. [The COMPASS Collaboration], Phys. Rev. Lett. **104**, 241803 (2010); B. Grube et al. [The COMPASS Collaboration], arXiv:1002.1272 [hep-ex] (2010).

[57] Yu. P. Gouz et al. [VES Collaboration.], AIP Conf. Proc. 272, 572 (1993);Yu A.Khokholovetal.[VESCollaboration], Nucl. Phys. A **663**, 596 (2000); A. Zaitsevetal. [VESCollaboration], Nucl. Phys. A **675**, 155c (2000).

[58] G. S. Adams et al. [E852 Collaboration], Phys. Rev. Lett. **81**, 5760 (1998); S. U. Chung et al. [E852 Collaboration], Phys. Rev. D **65**, 072001 (2002); E. I. Ivanovetal.[E852Collaboration], Phys. Rev. Lett. **86**, 3977 (2001); J. Kuhnetal. [E852 Collaboration], Phys. Lett. **B 595**, 109 (2004); M. Luetal. [E852 Collaboration], Phys. Rev. Lett. **94**, 032002 (2005).

[59] C. A. Baker et al., Phys. Lett. B **563**, 140 (2003).

[60] B. Aubert et. al. [BABAR Collaboration], Phys. Rev. D **81**, 092003, (2010).

[61] S. K. Choi et. al. [Belle Collaboration], Phys. Rev. Lett. **100** (2008).

[62] G. S. Adams et al [JLAB], Nucl. Phys. A **680**, 335 (2000).

[63] H. Stock, arXiv:hep-ex/0204015.

[64] Zhang Zhen-Xia, Liu Hong-Bang, Wu Ning, Yu Guo-Wei, Shen Xiao-Yan, and Zheng Han-Qing, Chinese Phys. C **32**, 857, (2008).

[65] S. Jin, Int. J. Mod. Phys. A **20**, 5145 (2005).

[66] S. Perantonis and C. Michael Nucl. Phys. **B 347**, 854 (l990).

[67] A. Chodos, R. L. Jaffe, C.B. Thorne, and V. Weisskopf, Phys. Rev. D **9**, 3471 (1974);

A. Chodos, R. L. Jaffe, C.B. Thorne, and K. Johnson, Phys. Rev. D **10**, 2599 (1974).

[68] T. Barnes and F. E. Close, Phys. Lett. B **ll6**, 365 (1982);

T. Barnes, F. E. Close and F. de Viron, Nucl. Phys. B **224**, 241 (1983).

[69] A. Le Yaouanc, L. Oliver, O. Pene, J. C. Raynal and S. Ono, Z. Phys. C **28**,309 (1985);

F. Iddir, A. Le Yaouanc, L. Oliver, O. Pene, J. C. Raynal and S. Ono, Phys. Lett B **205**, 564 (1988);

S. Ishida, H. Sawazaki, M. Oda and K. Yamada, Phys. Rev. D **47**, 179 (l992).

[70] Yu. S. Kalashnikova, Z. Phys. C **62**(1994);

Proc. of the Int. Conf. on Hadron Spectroscopy, Hadron 95, Manchester July (1995).

[71] Ll. Balitsky, D. I. Dyakonov and A. V. Yung, Z. Phys. C **33**, 265 (1986);

Govaerts, LJ. Reinders, P. Francken, X. Gonze and J. Weeyers, Nucl. Phys. B **284**, 674 (1987).

[72] G. S. Bali, B. Bolder, N. Eicker, T. Lippert, B. Orth, P. Ueberholz, K. Schilling and T. Struckmann, Phys. Rev D **62**, 054503 (2000); G. S. Bali, Phys. Rep. **343**, 1 (2001).

[73] C. Alexandrou, Ph. de Forcrand, and O. John, Nucl. Phys. B **119**, 667 (2003).

[74] C. F. Gerald and P. O. Wheatley, *Applied Numerical Method*, published by Dorling Kindrsley Pvt. Ltd., (1999).

[75] Dr. V. N. Vedamurthy and Dr. N. Ch. Sniyengar, *Applied Numerical Methods*, Published by Vikas publishing House Pvt. Ltd., (1998).

[76] M. M. Feyli, World Academy of Science, Engineering and Technology 71, (2010).

[77] K. J. Juge et. al., Phys. Rev. Lett., **82**, (1999).

[78] E. S. Swanson, talk presented at JLAB/INT Workshop on Gluonic Excitations, (2003).

[79] N. Akbar and B. Masud, arXive: 1102.1690 (2011).

[80] T. Barnes and E. S. Swanson, Phys. Rev. C **77**, 055206 (2008).

[81] P. Geiger, E. Swanson, Phys. Rev. D **50**, 6855 (1994).

[82] K. K. Seth, arXiv:hep-ex/0501022v1 (2005).

[83] Cheuk-Yin-Wong, E. S. Swanson and T. Barnes, Phys. rev. C **65**, 014903 (2001).

[84] S. Godfrey, *Flavor Physics and CP Violation Conference*, Vancouver, (2006).

[85] P. Hasenfratz, R. R. Horgan, J. Kuti and J. M. Richard, Phys. Lett. B **95**, 299 (1980).

[86] J. Merlin and J. Paton, J. Phys. G **11**, 439 (1985);
N. Isgur and J. Paton, Phys. Rev. D **31**, 2910 (1985);
J. Merlin and J. Paton, Phys. Rev. D **35**, 1668 (1987).

[87] L. A. Griffiths, C. Michael, and P. E. L. Rakow, Phys. Lett. B **129**, 351 (1983);
S. Perantonis, C. Michael, Nuc. Phys. B **347**, 854 (1990).

[88] C. J. Morningstar and M. Peardon, Phys. Rev. D **56**, 4043(1997)

[89] F. Iddir and L. Semlala, arxive hep-ph/0611165v2 (2006).

[90] T. Mankeetal, Phys. Rev. Lett.**82**, 4396 (1999).

[91] Z. H. MeiandX., Q. Luo, Int. J. Mod. Phys. A **18**,5713 (2003).

[92] Y. Liu and X. Q. Luo, Phys. Rev. D **73**, 054510 (2006).

[93] X. Liu, T. Manke, hep-lat/0210030.

PUBLICATIONS

Dynamical Implications of Gluonic Excitations in Meson-Meson Systems

Nosheen Akbar *, Bilal Masud †
Centre For High Energy Physics, University of the Punjab University, Lahore-54590, Pakistan.

Abstract

We study meson meson interactions using an extended $q^2\bar{q}^2(g)$ basis that allows calculating coupling of an ordinary meson-meson system to a hybrid-hybrid one. We use a potential model matrix in this extended basis which at quark level is known to provide a good fit to numerical simulations of a $q^2\bar{q}^2$ system in pure gluonic theory for static quarks in a selection of geometries. We use a combination of resonating group method formalism and Born approximation to include the quark motion using wave functions of a $q\bar{q}$ potential within a cluster. This potential is taken to be quadratic for ground states and has an additional smeared $\frac{1}{r}$ (Gaussian) for the matrix elements between hybrid mesons. For the parameters of this potential, we use values chosen to 1) minimize the error resulting from our use of a quadratic potential and 2) best fit the lattice data for difference of Σ_g and Π_u configurations of the gluonic field between a quark and an antiquark. At the quark (static) level, including the gluonic excitation was noted to partially replace the need for introducing many-body terms in a multi-quark potential. We study how successful such a replacement is at the (dynamical) hadronic level of relevance to actual hard experiments. Thus we study effects of both gluonic excitations and many-body terms on mesonic transition amplitudes and the energy shifts resulting from the second order perturbation theory (i.e. from the respective hadron loops). The study suggests introducing both energy and orbital excitations in wave functions of scalar mesons that are modeled as meson-meson molecules or are supposed to have a meson-meson component in their wave functions.

1. INTRODUCTION

Given the availability of both the numbers generated by lattice simulations of quantum chromodynamics and continuum models of the hadronic systems, an effective use of the numbers could be to improve the models through constraints of getting a least chisquare difference with the numbers for the corresponding discrete quarks and antiquarks configurations. Such lattice-improved models can then be reasonably used for all spatial configurations to eventually give dynamical predictions for experimentally measurable quantities like meson masses, meson-meson bindings and cross-sections and shifts (polarization potentials) to meson masses arising through meson-meson loops, etc. For one pair of quark and antiquark, a well established such use of lattice results is substituting in a Schrödinger equation a Coulombic-plus-linear quark-antiquark potential supported by lattice QCD calculations (see ref. [1, 2] and others) for the ground state of the gluonic field between a quark and antiquark. Now that lattice results for excited state of the gluonic field are also available for years, even some dynamical uses of excited state gluonic field potentials have been worked out [3]. So far such uses are either limited to numerical calculations without an explicitly written excited state gluonic field potential or the potential used originate from flux tube [4] or string models [5]. Each of these approaches has its usefulness. What we add, through the present paper, to this series of works is

1) ourselves writing an analytical quadratic plus exponentially falling expression for the excited state gluonic field potential between a quark and antiquark and fit its parameters to the lattice data for the excited state gluonic field values available for discrete quark antiquark separations in [6] , and

2) use models and fits of ref. [7] to extend the model to a system of two quarks and two antiquarks and to its gluonic excitations. Precisely, we replace the numerically fitted $0.562 + 0.0696r - \frac{0.255}{r} - \frac{0.045}{r^2}$ ground state quark antiquark potential used in ref. [7] by a constant plus quadratic confining potential

*e mail: noshinakbar@yahoo.com
†e mail: bilalmasud@chep.pu.edu.pk

term and the *additional* $\frac{\pi}{r} - \frac{4.24}{r^2} + \frac{3.983}{r^4}$ potential for the $q\bar{q}$ gluonic excitation by one of the form $Aexp(-Br^2)$. We have to do this, because we are doing a full meson level dynamical calculations for transition amplitudes from one set of quark-antiquark clusterings (mesons) to the other. From these amplitudes we also calculate polarization potentials for a meson-meson system. Thus we incorporate quark motion (precisely, wave functions for different $qq\bar{q}\bar{q}$ spatial configurations) as well, whereas the model of ref. [7] specializes to a fixed configuration of the two quarks and two antiquarks. We have to replace the resulting potential formulas of ref. [7] by simpler ones that can be symbolically integrated a later stage, after necessary multiplications by wave functions of $qq\bar{q}\bar{q}$ positions, to complete the adiabatic-approximation-based treatment of a $qq\bar{q}\bar{q}$ system.

Being not limited by such demands of later integrations, the form and then parameters values of the continuum $qq\bar{q}\bar{q}$ model proposed in ref. [7] were chosen to simply minimize

$$\chi^2_A = \frac{1}{N(G)} \sum_{i=1}^{N(G)} (E_i - M_i)^2 / \triangle E_i, \tag{1}$$

where $N(G)$ is the number of data points for geometry G. The $qq\bar{q}\bar{q}$ geometries ref. [7] numerically worked on were (quarks at the corners of) squares, rectangles, tetrahedra and some other less symmetric geometries Q, N, P and L (linear). For each data point i , the lattice energy E_i was extracted by solving the following eigenvalue equation

$$W^T_{ikl} a^T_{il} = \lambda^{(T)}_i W^{T-1}_{ikl} a^T_{il} \tag{2}$$

for $\lambda^{(T)}_i$ that approaches to $\exp(-V_i)$ as (Euclidean time) $T \to \infty$, and then subtracting the energy of two separated $q\bar{q}$ clusters from the V_i to get the lattice-generated $qq\bar{q}\bar{q}$ binding energy E_i for the data point. The values of the $\lambda^{(T)}_i$, and thus of E_i, depend only on the numerical values of the elements W^T_{ikl} of the matrix of the Wilson loops. The values of k and l depend on the number of Wilson loops evaluated; for the $qq\bar{q}\bar{q}$ system these were taken to be 1 and 2. Two of the corresponding Wilson operators (whose vacuum expectation values are the Wilson loops W^T_{kl}) are shown for example in Fig. 1.5 of [8]. Knowing the Wilson loops, the procedure of getting V_i can be found for example in eqs. 4, 11, 12 and 15 of ref. [9]. The arguments for continuum limits being achieved before extracting E_i are given in ref. [10].

The M_i in eq.(1) are obtained by subtracting the energy of two separated $q\bar{q}$ clusters from the eigenvalues of a matrix obtained through a *model* of the $qq\bar{q}\bar{q}$ system. For this, the model has to give a basis and an operator $\widehat{V}$ whose representation with respect to the basis gives a potential matrix V. M_i are obtained by setting the determinant of $V - (M_i + V_{11})N$ equal to zero, with V_{11} being the energy of two separated $q\bar{q}$ clusters and N the (overlap) matrix of an identity operator in the basis. Searching for the model, the simplest way to extend a two-particle potential model to a few-body is to use the potential for each pair of particles in the few-body system and simply add up such two-body potentials. This approach has been successful in atomic and many-nucleon systems; the corresponding two-body interaction being described by Coulombic and Yukawa potential, for example. For a hadron (or a system of hadrons) composed of many quarks, antiquarks and the gluonic field, the lowest order perturbative Feynman amplitudes are of this sum-of-pair-wise form. Though Feynman diagrams themselves become impractical for typical hadronic energies because of larger couplings, models have been tried which simply replace the two-body Coulombic potential (essentially a Fourier transform of the Gluonic propagator) by more general Coulombic-plus-linear form; see ref. [11]. This approach is not free of problems; for example it leads to inverse power van der Waals' potentials [12] between separated color-singlet hadrons which are in contradiction with experimental data. But this model has many phenomenological successes and it is worthwhile inquiring if

1) it provides a basis and operator to generate a potential matrix, and

2) how good is the chisquare if the eigenvalues of the resulting matrix are used as M_i in eq.(1).

The answer provided by ref. [7] and earlier related works is that the model does generate a matrix of the required kind. But the resulting chisquare, defined by eq.(1), is too bad; see Fig.4 of ref.[13]. To refine the model we can improve the basis beyond the $\{|1\rangle, |2\rangle, |3\rangle\}$ defined as [7, 14]

$$|1\rangle = (q_1 q_3)(q_2 q_4), \quad |2\rangle = (q_1 q_4)(q_2 q_3), \text{ and } \quad |3\rangle = (q_1 q_2)(q_3 q_4), \tag{3}$$

and the operator beyond

$$H = -\sum_{i=1}^{4} [m_i + \frac{\widehat{P}^2_i}{2m_i}] + \sum_{i<j} v_{ij} \mathbf{F}_i . \mathbf{F}_j, \tag{4}$$

with v_{ij} being is the potential energy of a $q\bar{q}$ pair with the gluonic field between them in the ground state. Or both the basis and the operator can be improved. What ref. [7] does is to improve directly the matrix (representation) after writing down the underlying basis. They do this in a number of ways. One model, termed model II, uses the same $\{|1\rangle, |2\rangle, |3\rangle\}$ basis but multiplies the off-diagonal elements of the overlap and potential energy matrices (that is, the representations of the identity and potential operators

$$\sum_{i<j} v_{ij} \mathbf{F}_i.\mathbf{F}_j$$

respectively) by a few-body gluonic field overlap factor $f = \exp(-b_s k_f S)$ with b_s as the tension of the string connecting a quark with an antiquark, S the area of a surface bounded by external four lines connecting two quarks and two antiquark and $k_f = 0.5$ approximately; theoretical arguments suggest S should be the area of the corresponding minimal surface, though in ref. [7] half of a sum of four triangles was used instead for numerical convenience. This model II was noted to much reduce, at the quark level the chisquare of eq.(1). This model has been worked out in [15, 16, 17] till meson-level transition amplitudes. The dynamical calculations require a kinetic energy term as well. As that is taken, apart from some technical considerations of hermicity, proportional to the overlap matrix and hence its off-diagonal elements are also multiplied by the overlap f factor. Thus f provides one parametrization that connect QCD simulations with hard experiments.

But model II is not the best model of ref. [7]; the paper continues to then improve the basis by including the gluonic excitations as well. That is, it extends the $\{|1\rangle, |2\rangle, |3\rangle\}$ basis by including the states

$$|1^*\rangle = (q_1q_3)_g(q_2q_4)_g, \quad |2^*\rangle = (q_1q_4)_g(q_2q_3)_g, \text{ and } \quad |3^*\rangle = (q_1q_2)_g(q_3q_4)_g. \tag{5}$$

Here $(q_1q_3)_g$ denotes a state where the gluon field is *excited* to the lowest state. (The excited states of gluonic field can, for example, be seen in the QCD numerical simulations; see ref.[18, 6] and others). When the overlap, potential and kinetic energy matrices are written in this extended basis, their order increases to 6×6 rather than previous 3×3. If in addition, we introduce many body terms in this extended model, new kind of gluonic field overlap factors (f^a, f^c) appear in the off diagonal terms resulting in what ref. [7] terms model III giving the least chisqure in ref. [7]; (see eq.(15) below); our truncation to 4×4 matrices is explained before this equation. As mentioned above, the purpose of our present paper is to work out this improved model III of ref. [7] till the meson-meson scattering amplitudes and energy shifts. As this improved model III includes the gluonic excitations, it consider transitions from four ground state quark states to the one having gluonic excitations. And by adding to it the quark motion (wave functions) to reach the hadron level, we are now able to study transitions from ground state meson-meson systems to hybrid-hybrid systems.

A worth-mentioning aspect we have studied is the hadron-level implications of the differences of the gluonic-excitation-including model III and the sum-of-pair-wise approach. The quark-level work in ref. [7] can be interpreted to mean that with suitable extensions and modifications something like a sum-of-pairs approach can be a good approximation for a tetraquark system as well. It writes "At the shortest distances, upto about 0.2fm, perturbation theory is reasonable with the binding being given mainly by the $|1\rangle$, $|2\rangle$, and $|3\rangle$ states inter-acting simply through the two-quark potentials with little effect from four-quark potentials". However, ref. [7] tells, "for large inter-quark distance (greater than 0.5 fermi), quark-pair creation can no longer be neglected. However, in the intermediate energy range, from about 0.2 to 0.5 fm, the four-quark potentials act in such a way as to reduce the effect of the $|1\rangle$, $|2\rangle$, and $|3\rangle$ states so that the binding is dominated by the $|1^*\rangle$, $|2^*\rangle$, and $|3^*\rangle$ states, which now interact among themselves again simply through the two-quark potentials with little effect from four-quark potentials." This suggests that models involving only two-quark potentials could be justified provided excited gluon states (such as $|1^*\rangle$, $|2^*\rangle$, $|3^*\rangle$) are included on the same footing as the standard states $|1\rangle$, $|2\rangle$,$|3\rangle$. We have checked if such features survive at the experimentally meaningful hadron level, by comparing the dynamical implications of

(1) a model extended to the gluonic excitations but otherwise sharing many features with the sum-of-pair-wise approach, with

(2) a model that includes explicit many-body terms but does not include gluonic excitations.

Thus we report if after including the gluonic excitations a sum-of-two-body potential model can replace to some extent many-body potential terms in a tetraquark system *even at a hadronic level*. Specifically, we have calculated in both kind of models meson-meson transition amplitudes T_{ij} from (i) a ground state

meson-meson clustering to (j) a different ground-state clustering and to a clustering of gluonic-excited mesons. T_{ij} are elements of the meson-meson scattering theory T-matrix, can be termed as phase shifts, transition potentials or meson-meson coupling, and their absolute squares give meson-meson differential cross sections [11]. Moreover, using these transition amplitudes in the second order perturbation theory we calculate shifts in a ground state meson-meson energy due to coupling to a different ground-state clustering and to an excited state meson-meson system (i.e. to *hybrid loops*). These energy shifts are what are also termed polarization potentials [19].

To reach the hadronic level, we have included the quark motion through quark wave functions. To solve for quark position wave functions, there are a number of methods used such as variational method [20, 21], Born-order diagrams [11], and resonating group method [22]. Variational approach is used by Weinstein and Isgur [20, 21] to optimize a meson meson wave function in a quadratic (and later coulomb plus linear) potential and a hyperfine term combined with a sum-of-two-body approach. Then they projected the meson meson state onto free meson wave functions to estimate a relative two meson wave function which gives the equivalent meson meson potential and obtained the meson meson phase shifts. The similar results can be obtained by using Born-order quark exchange diagrams [11] in a non-relativistic potential model to describe low energy scattering of $q\bar{q}$ mesons. In the present paper, we have used a formalism of the resonating method as used in [15]. In the resonating group method, the dependence on the internal co-ordinates of the system is specified before solving the problem to integrate out the degrees of freedom corresponding to the internal coordinates of clusters of the system. At a later stage, because of the complexity of the calculations we also specify the dependence on the vectors connecting the centers of masses of our mesonic clusters, something that is done in a Born approximation. Moreover, we have not included in our basis an explicit diquark-diantiquark state. In the weak coupling limit such a state is a linear combination of the meson-meson states and thus cannot be included in a basis. Away from the weak coupling this can be included. But its inclusion in the basis did not affect the lattice simulations reported in ref. [7] and thus we have expanded our two-quark two antiquark wave function in a basis that is limited to four meson-meson states: ground and excited states for each of the two possible $q\bar{q}q\bar{q}$ clusterings.

In this exploratory work, we have taken all the constituent quark masses to be same as that of a charm quark and we have taken all the spin overlaps to be 1 without calculating them. Without incorporating flavor and spin dependence, we basically want to study certain features of including the gluonic excitations in our basis. In section 2, the potential model in the extended basis in the pure gluonic theory is introduced for the static quarks. Basically, in this section we tell where does the model of ref.[7] fits in our full scheme that incorporates the quark motion through a resonating group method formalism which means pre-specifying quark-antiquark wave functions within $q\bar{q}$ clusters. The coupled integral equations for the remaining inter-cluster wave function $\chi_K(\mathbf{R}_K)$ are written in section 3. In section 4, these integral equations are solved to calculate the transition amplitudes and energy shifts. The numerical results for meson meson system transition amplitudes and energy shifts with concluding remarks are given in section 5. The partial wave analysis results are also reported in section 5.

2. $q^2\overline{q}^2$ POTENTIAL MODEL (IN THE EXTENDED BASIS)

Using the adiabatic approximation, the total state vector of a system containing two quarks, two anti-quarks and the gluonic field between them can be written as sum of product of quark position dependence function $\phi_K(\mathbf{r}_1, \mathbf{r}_2, \mathbf{r}_{\overline{3}}, \mathbf{r}_{\overline{4}})$ and the gluonic field state $\mid k\rangle_g$. (The gluonic state $\mid k\rangle_g$ is defined as a state approaching to color state $\mid k\rangle_c$ in the limit of quark anti-quark separation approaching to zero. Here $k = 1, 2, 3, 1^*, 2^*, 3^*$.) The function $\phi_K(\mathbf{r}_1, \mathbf{r}_2, \mathbf{r}_{\overline{3}}, \mathbf{r}_{\overline{4}})$ can be written as

$$\phi_K(\mathbf{r}_1, \mathbf{r}_2, \mathbf{r}_{\overline{3}}, \mathbf{r}_{\overline{4}}) = \phi_K(\mathbf{R}_c, \mathbf{R}_K, \mathbf{y}_K, \mathbf{z}_K),$$

with $K = 1, 2, 3$. R_c is the overall center of mass co-ordinate of the whole system.

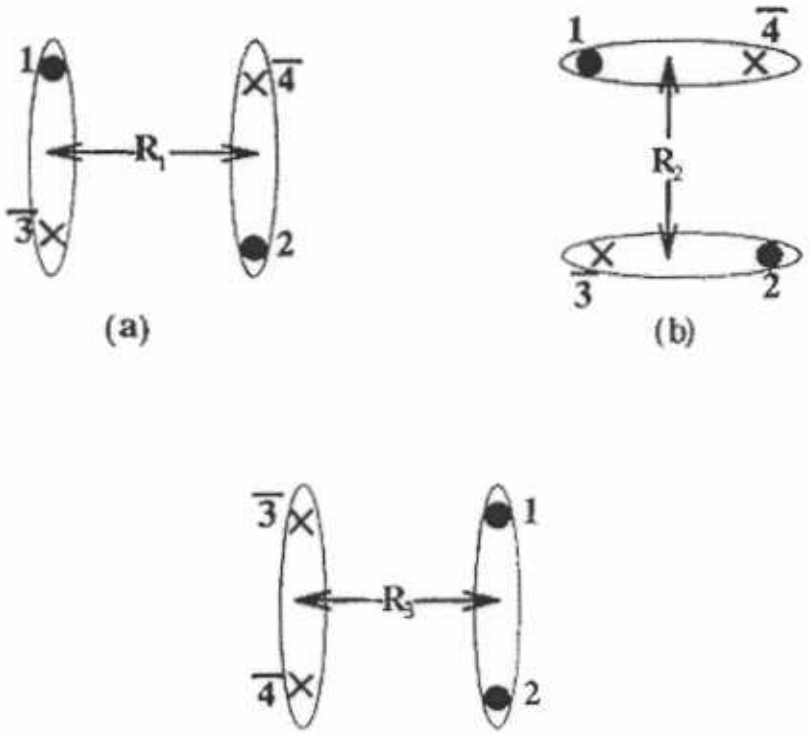

Figure 1: Three different topologies of diquark and diantiquark

With the notation of Fig.1, the relative co-ordinates $\mathbf{R}_1, \mathbf{R}_2$, and $\mathbf{R}_3$ are defined as

$$\mathbf{R}_1 = \frac{1}{2}(\mathbf{r}_1 + \mathbf{r}_{\overline{3}} - \mathbf{r}_2 - \mathbf{r}_{\overline{4}}), \mathbf{y}_1 = \mathbf{r}_1 - \mathbf{r}_{\overline{3}}, \mathbf{z}_1 = \mathbf{r}_2 - \mathbf{r}_{\overline{4}}$$
$$\mathbf{R}_2 = \frac{1}{2}(\mathbf{r}_1 + \mathbf{r}_{\overline{4}} - \mathbf{r}_2 - \mathbf{r}_{\overline{3}}), \mathbf{y}_2 = \mathbf{r}_1 - \mathbf{r}_{\overline{4}}, \mathbf{z}_2 = \mathbf{r}_2 - \mathbf{r}_{\overline{3}}$$
$$\mathbf{R}_3 = \frac{1}{2}(\mathbf{r}_1 + \mathbf{r}_2 - \mathbf{r}_{\overline{3}} - \mathbf{r}_{\overline{4}}), \mathbf{y}_3 = \mathbf{r}_1 - \mathbf{r}_2, \mathbf{z}_3 = \mathbf{r}_{\overline{3}} - \mathbf{r}_{\overline{4}},$$

$\mathbf{R}_1$ being the vector joining the centers of mass of the mesonic clusters $(1, \overline{3})$ and $(2, \overline{4})$; similarly about $\mathbf{R}_2$ and $\mathbf{R}_3$. Now using the resonating group method, the quark position dependence function can be written as a product of function of known dependence on $\mathbf{R}_c$,$\mathbf{y}_K$,$\mathbf{z}_K$ and of unknown dependence on $\mathbf{R}_K$. i.e.

$$\phi_K(\mathbf{R}_c, \mathbf{R}_K, \mathbf{y}_K, \mathbf{z}_K) = \psi_c(\mathbf{R}_c)\chi_K(\mathbf{R}_K)\psi_K(\mathbf{y}_K, \mathbf{z}_K). \tag{6}$$

Thus, the two quarks two antiquarks state vector can be written as

$$\mid \Psi(q_1 q_2 q_3 q_{\overline{4}})\rangle = \sum_k \mid k\rangle_g \psi_c(\mathbf{R}_c)\chi_k(\mathbf{R}_K)\psi_k(\mathbf{y}_K, \mathbf{z}_K), \tag{7}$$

where

$$\psi_k(\mathbf{y}_K, \mathbf{z}_K) = \xi_k(\mathbf{y}_K)\xi_k(\mathbf{z}_K),$$

$\xi_k(\mathbf{y}_K)$ and $\xi_k(\mathbf{z}_K)$ being the normalized solutions of the Schrödinger equation for quadratic confining potential (written in eq.(10)) for a pair of quark-anti-quark within a cluster. We take

$$\xi_K(\mathbf{y}_K) = \frac{1}{(2\pi d^2)^{\frac{3}{4}}}\exp(-\frac{y_K^2}{4d^2}),$$
$$\xi_K(\mathbf{z}_K) = \frac{1}{(2\pi d^2)^{\frac{3}{4}}}\exp(-\frac{z_K^2}{4d^2}). \tag{8}$$

Here d is the size of meson (detail is written after eq.(10)) and m being the constitute quark mass. In our case, m is the mass of c-quark and equal to 1.4794 GeV as used in [23].

After writing the form of the wave vector, we describe our Hamiltonian, starting with the limit when each gluonic field overlap factor $f = f^a = f^c = 1$. In this limit, the Hamiltonian whose representation matrices in the basis $\{|1\rangle, |2\rangle, |3\rangle, |1^*\rangle, |2^*\rangle, |3^*\rangle\}$ would become those in ref. [7] is

$$H = -\sum_{i=1}^{4}\left[m_i + \frac{\widehat{P}_i^2}{2m_i}\right] + \sum_{i<j}(v_{ij} + \epsilon\triangle v_{ij}^*)\mathbf{F}_i.\mathbf{F}_j, \tag{9}$$

where v_{ij} is the potential energy of meson for the ground state gluonic field and $\triangle v_{ij}^*$ is the difference between ground state and excited state gluonic field potential. We take the kinetic energy in the non-relativistic limits. This limit is also used in a recent work by Vijande ref. [24] that deals with multiquark system (two quarks and two antiquarks) to study the spectrum using a string model for the potential. In ref. [7], potential energy matrix elements are written so that the potential energy for each pair ij is equal to v_{ij} for the matrix elements of the Hamiltonian between gluonic ground states, and it is equal to $v_{ij} + \triangle v_{ij}^*$ for the matrix elements between the gluonic-excited states. We have modeled these two forms by taking $\epsilon = 0$ for the ground state matrix elements and $\epsilon = 1$ for the elements between gluonic-excited states. For the elements between ground and excited state gluonic field, the ϵ value that results from their parameter a_0 being fitted to 4 (in their Table 1) is surprisingly 2 and not any value between 0 and 1. A possibility is that this is a result of them taking the area S, we mentioned above in our introduction, in the form of average of the sum of triangle areas instead of the theoretically motivated minimal surface area. Thus we have somewhat explored $\epsilon = \frac{1}{2}$ between 0 and 1 and $\epsilon = 1$ in addition to $\epsilon = 2$ which we have mainly studied.

In the above equation, $\mathbf{F}_i$ (operating on i_{th} particle) has eight components. Each component is equal to $\frac{\lambda_i}{2}$, where λ_i are the Gell-Mann matrices. We used the potential with the color structure of one gluon exchange in the form given in ref. [7]. With the use of ground state potential v_{ij} in the realistic coulombic plus linear form, it becomes impossible for us to solve the integral equations appearing below in eqs.(21-24). Therefore we used the parametrization of the static pairwise two quark potential as

$$v_{ij} = Cr_{ij}^2 + \overline{C}, \qquad \text{with} \quad i,j = 1,2,\overline{3},\overline{4}. \tag{10}$$

In this simple harmonic potential, the parameters C and ω are related to size (d) of wavefunction (ξ_k) through the relations $\omega = \frac{1}{md^2}$ and $C = -\frac{3}{16}m\omega^2$, and for consistency of the diagonal term of the integral eq.(21) $\overline{C} = \frac{3}{8}(4m + 3\omega - 2M)$ GeV [15] with $M = 2m = 2.9588$GeV being the mass of a charmonium meson. The parameter d is chosen in such a way to reduce the error resulting from a use of this quadratic potential instead of the realistic one. The error may be both in the wave functions of the distance between a quark and antiquark within cluster and those of the vector joining the centers of masses of the two clusters. As for the first dependence, we found that the maximum overlap integral of each of the wave functions $\xi_K(\mathbf{y}_K)$ and $\xi_K(\mathbf{z}_K)$ of the quadratic potential and that of a more realistic coulombic plus linear potential is 99% at $d = 1.16\text{GeV}^{-1}$. (For the parameters of the realistic potential we used values $\alpha_s = 0.5461$GeV [23] and $b_s = 0.1425$GeV [23] for mesons composed of charm quarks.) This overlap is shown in Fig.2. A similar work was done in ref. [25] for lighter quarks. They found that the overlap wave function of SHO (quadratic potential) and that of coulombic plus linear can be made as large as 99.4% with the suitable adjustment of parameters.

For the additional term in the $q\bar{q}$ potential for the gluonic excitation, the usual flux tube $(\pi/r$ [4]) or string based analytical expressions become impractical for us, as mentioned in the introduction. Thus for that we tried an *ansätz* of the form of

$$\triangle v_{ij}^* = Ae^{-Br_{ij}^2}. \tag{11}$$

This gaussian gluonic potential $(A\exp(-Br_{ij}^2))$ is a smeared form of $\frac{constant}{r}$ as written in appendix of ref. [21]. From the Fig.3 of [6], we get the potential energy difference ε_i between ground and excited states for different r values (r_i). We choose A and B for which χ^2 becomes minimum. χ^2 is defined as

$$\chi^2 = \sum_{i=1}^{n}(\varepsilon_i - A\exp[-Br_{ij}^2])^2,$$

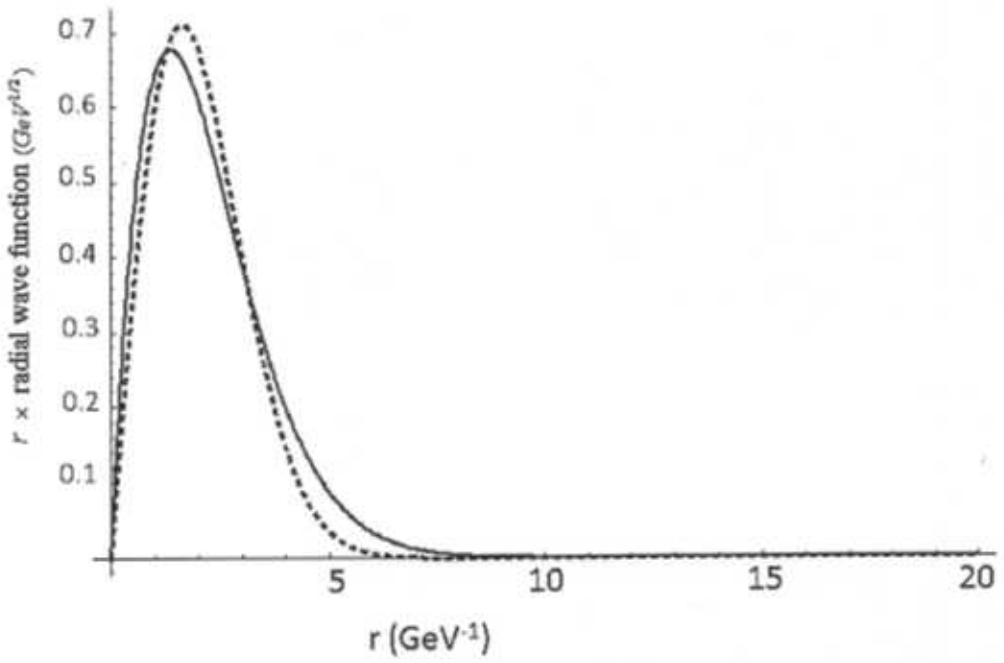

Figure 2: Overlap of the (ground state) wave function of the realistic linear plus Coulombic potential and that of the quadratic potential. The solid line represents linear plus coulombic potential wave function and the dashed line represents quadratic potential wave function.

with n being the number of data points. This gives

$$A = 1.8139\text{GeV}, \qquad B = 0.0657\text{GeV}^2.$$

For finding the wave function corresponding to our total potential $Cr_{ij}^2 + \overline{C} + Ae^{-Br_{ij}^2}$, we used the variational method with an *ansätz* wave function

$$\xi_K^*(\mathbf{y}_K) = ny_K^2 \exp(-py_K^2). \tag{12}$$

The normalization of this $\xi_K^*(\mathbf{y}_K)$ w.r.t y_K gives

$$n = (42^{\frac{3}{4}} p^{\frac{7}{4}})(15^{\frac{1}{4}} \pi^{\frac{3}{4}}).$$

This leaves us with one variational parameter p chosen to minimize the expectation value of the two body Hamiltonian in the excited state gluonic field wave function. This gave $p = 0.048GeV^2$. For this value of p, the overlap of wave function of the quadratic potential plus Δv_{ij}^* and that of coulombic plus linear plus Δv_{ij}^* within a hybrid cluster became 99.9%. Both wave functions are shown in in Fig.3. Having much reduced the errors in the in-cluster factors of the total wave function, the question remains how much the inter-cluster factors of the (terms of the) total state vector are affected by our use of convenient but not realistic $q\bar{q}$ potentials. For the inter-cluster wave functions, eventually we use below in eq. (25) plane wave forms which get their justifications from the validity of Born approximation for our problem regardless of potential expressions we use. This plane wave form has only one usual parameter (the wave number) and eq.(C10) below relates its value for the ground as well as excited state inter-cluster waves to the very good values of d and p that almost give realistic ground state and excited state wave functions within $q\bar{q}$ clusters. But the relations between the inter-cluster wave numbers and the d and p do assume a quadratic confinement and this may affect our numerical results but hopefully not at least the qualitative features we are pointing out. Perhaps it is worth mentioning here that properties of $q^2\bar{q}^2$ systems were calculated using quadratic confinement in ref. [20], and then with the realistic potential in ref. [21] and both the works favored the existence of meson-meson molecules.

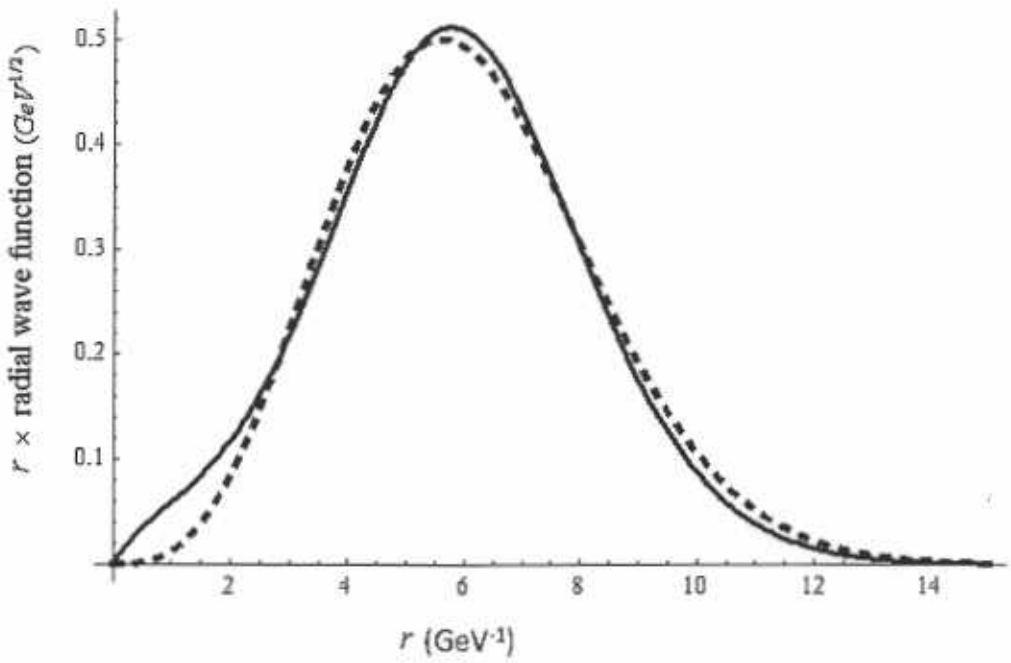

Figure 3: Overlap of the (excited state) wave function of the realistic Coulombnic plus linear plus $A\exp(-Br^2)$ potential and that of the quadratic plus $A\exp(-Br^2)$ potential. The solid line represents linear plus coulombic plus $A\exp(-Br^2)$ potential wave function and the dashed line represents quadratic plus $A\exp(-Br^2)$ potential wave function.

Now we combined our Hamiltonian and all the wave functions we have mentioned in the Schrödinger equation for the meson-meson system, which means that the overlap of $(\mathbf{H}-E_c)\mid\Psi\rangle$ with an arbitrary variation $\mid\delta\Psi\rangle$ of state vector $\mid\Psi\rangle$ vanishes where $\mid\Psi\rangle$ is the state vector of the whole $q^2\bar{q}^2$ system. In $\mid\delta\Psi\rangle$, we considered only the variation in χ_k (see eq.(7)), as in the resonating group method. Thus we wrote

$$\begin{aligned}\langle\delta\Psi\mid\mathbf{H}-E_c\mid\Psi\rangle=\sum_{k,l}\int d^3R_c d^3R_K d^3y_K d^3z_K\psi_c(\mathbf{R}_c)\delta\chi_k(\mathbf{R}_K)\xi_k(\mathbf{y}_K)\xi_k(\mathbf{z}_K)_g\\ \langle k\mid\mathbf{H}-E_c\mid l\rangle_g\psi_c(\mathbf{R}_c)\chi_l(\mathbf{R}_L)\xi_l(\mathbf{y}_L)\xi_l(\mathbf{z}_L)=0\end{aligned}\tag{13}$$

for$k,l=1,2,3,1^*,2^*,3\star$ and $K,L=1,2,3$. The arbitrary variations $\delta\chi_k(\mathbf{R}_K)$'s for different values of R_K are linearly independent and hence their co-efficient in eq.(13) should be zero. With the trivial R_c integration performed to give a finite result, this leads to

$$\sum_l\int d^3y_K d^3z_K\xi_k(\mathbf{y}_K)\xi_k(\mathbf{z}_K)_g\langle k\mid\mathbf{H}-E_c\mid l\rangle_g\chi_l(\mathbf{R}_L)\xi_l(\mathbf{y}_L)\xi_l(\mathbf{z}_L)=0,\tag{14}$$

where

$$_g\langle k\mid\mathbf{H}-E_c\mid l\rangle_g=_g\langle k\mid KE+V+4m-E_c\mid l\rangle_g.$$

Elements of V and KE matrices are defined below in eq.(17) and eq.(18). In ref. [7] it is stated that, in the lattice QCD simulations, it was found that the energy of the lowest state was always the same in both a 2×2 and 3×3 description, provided $\mid1\rangle$ or $\mid2\rangle$ had the lowest energy. In addition the energy of the second state was, in most cases,more or less the same. Two level approximation is also used in a later work [26] of the tetraquark system. Considering this, we include only two topologies(1,2), meaning four states($\mid1\rangle,\mid2\rangle,\mid1^*\rangle,\mid2^*\rangle$). According to the model of ref. [7] the overlap matrix N in this truncated

4-basis is given by

$$N =_g \langle k \mid l \rangle_g = \begin{bmatrix} 1 & f/3 & 0 & -f^a/3 \\ f/3 & 1 & -f^a/3 & 0 \\ 0 & -f^a/3 & 1 & -f^c/3 \\ -f^a/3 & 0 & -f^c/3 & 1 \end{bmatrix}. \tag{15}$$

And the potential matrix $V(f)$ is

$$V =_g \langle k \mid V \mid l \rangle_g = \begin{bmatrix} V_{11} & V_{12} & V_{11^\bullet} & V_{12^\bullet} \\ V_{21} & V_{22} & V_{21^\bullet} & V_{22^\bullet} \\ V_{1^\bullet 1} & V_{1^\bullet 2} & V_{1^\bullet 1^\bullet} & V_{1^\bullet 2^\bullet} \\ V_{2^\bullet 1} & V_{2^\bullet 2} & V_{2^\bullet 1^\bullet} & V_{2^\bullet 2^\bullet} \end{bmatrix}. \tag{16}$$

Here,

$$\begin{aligned}
V_{11} &= -\frac{4}{3}(v_{1\bar{3}} + v_{2\bar{4}}) \\
V_{12} = V_{21} &= \frac{4}{9} f(v_{12} + v_{\bar{3}\bar{4}} - v_{1\bar{3}} - v_{2\bar{4}} - v_{1\bar{4}} - v_{2\bar{3}}) \\
V_{22} &= -\frac{4}{3}(v_{1\bar{4}} + v_{2\bar{3}}) \\
V_{21^\bullet} = V_{2^\bullet 1} &= -\frac{f^a}{18}\left(\sqrt{2}(v^*_{1\bar{3}} + v^*_{2\bar{4}}) - \frac{16}{\sqrt{2}}(v^*_{1\bar{4}} + v^*_{2\bar{3}}) - \sqrt{2}(-v^*_{12} - v^*_{\bar{3}\bar{4}})\right) \\
V_{1^\bullet 2} = V_{12^\bullet} &= -\frac{f^a}{18}\left(\sqrt{2}(v^*_{1\bar{4}} + v^*_{2\bar{3}}) - \frac{16}{\sqrt{2}}(v^*_{1\bar{3}} + v^*_{2\bar{4}}) - \sqrt{2}(-v^*_{12} - v^*_{\bar{3}\bar{4}})\right) \\
V_{1^\bullet 1^\bullet} &= \frac{1}{6}(v^*_{1\bar{3}} + v^*_{2\bar{4}}) \\
V_{1^\bullet 2^\bullet} = V_{2^\bullet 1^\bullet} &= -\frac{1}{18} f^c\Big(- (v^*_{1\bar{3}} + v^*_{2\bar{4}} + v^*_{1\bar{4}} + v^*_{2\bar{3}}) + 10(v^*_{12} + v^*_{\bar{3}\bar{4}})\Big) \\
V_{2^\bullet 2^\bullet} &= \frac{1}{6}(v^*_{1\bar{4}} + v^*_{2\bar{3}}) \\
V_{1^\bullet 1} = V_{11^\bullet} &= V_{2^\bullet 2} = V_{22^\bullet} = 0,
\end{aligned} \tag{17}$$

with $v^*_{ij} = v_{ij} + \epsilon \triangle v^*_{ij}$, ϵ being defined above (after eq.(9)). The coefficients of v_{ij} and v^*_{ij}, resulting from the $\mathbf{F}.\mathbf{F}$ operator, are given in Table 1 in the Appendix A. The kinetic energy matrix of the two quarks two anti-quarks is taken to be

$$KE =_g \langle k \mid KE \mid l \rangle_g = N(f)^{\frac{1}{2}}_{k,l}\left(\frac{-1}{2m}\sum_{i=1}^{4}\nabla_i^2\right)N(f)^{\frac{1}{2}}_{k,l}. \tag{18}$$

The kinetic energy in the same form is also used in ref. [15].

The gluonic field overlap factor, f, as written in Introduction, is suggested by ref. [7] as

$$f = \exp[-b_s k_f S], \tag{19}$$

with $b_s = 0.18 GeV^2$ [4]. In ref. [27] the gluonic field overlap factor f is used in the Gaussian form as

$$f = \exp[-k_f b_s \sum_{i<j} r_{ij}^2], \tag{20}$$

employed in $SU(3)_c$ for interpreting the results in terms of the potential for the corresponding single heavy-light meson. In ref. [27], the simulations that are fitted by using f are for the configurations when the gluonic field is in the ground state i.e. overlap matrix is a 2×2 matrix. In ref. [7], simulations are reported with 2-color approximation. But in ref. [27], lattice simulations done for $SU(3)_c$ are reported. Our overlap, potential and kinetic energy matrices are also written in $SU(3)_c$, so we use the k_f multiplying sum of area form of f (written in eq.(20)) with $k_f = 0.6$ (as used in [27]) for numerical convenience and not used the minimal area form. When we are observing the dynamical effects for the ground state, our overlap, potential and kinetic energy matrices are 2×2 matrices and we use f with $k_f = 0.6$. But when

we incorporate the excited state gluonic field our overlap, potential and kinetic energy matrices become 4×4 matrices, in the upper left 2×2 block of these matrices, the form of f remains the same but the value of k_f is changed to 1.51 according to the conclusion of ref. [7]. In the other blocks f^a, f^c [7] [14] are also used. If we take f^a as a function of area as defined in [7], it becomes unmanageable to solve the integral equations (21-24) and hence we have taken f^a to be a constant but have tried a variety of its values to explore how much our conclusions depend on it value. As for f^c, the fit in ref. [14] [7] of the model to the lattice data favors $k_c = 0$ which implies that $f^c = 1$ i.e. the excited configurations interact amongst themselves in the way expected from perturbation theory. Thus we have used $f^c = 1$.

3. COUPLED INTEGRAL EQUATIONS

Using "N", "V" and "KE" elements in eq.(14), we got four integral equations for four different values of k or l. Then we do $\mathbf{y}_K$ and $\mathbf{z}_K$ integrations. All the integrations required are in the Gaussian form or modified Gaussian form (with a polynomial in the integrand multiplying the Gaussian exponential) and we integrate analytically. For $K = L = 1, 2$, in eq.(14), $\chi_l(\mathbf{R}_L)$ is independent of $\mathbf{y}_K$ and $\mathbf{z}_K$ and, thus, can be taken out of integrations. After the integration, the result is $\mathbf{R}_K$ dependent co-efficient of $\chi_k(\mathbf{R}_K)$. For $K \neq L$, $\mathbf{y}_K$ and $\mathbf{z}_K$ are replaced by their linear combinations with one of them as identical to $\mathbf{R}_L$ and other one independent of it as $\mathbf{R}_3$. The jacobian of transformation is equal to 8. Then we integrate the equation w.r.t $\mathbf{R}_3$. Integration leaves the following four equations:

$$\Delta_1(\mathbf{R}_1)\chi_1(\mathbf{R}_1) + \left(\frac{1}{\pi d^2(1+4\bar{k}d^2)}\right)^{\frac{3}{2}} \int d^3\mathbf{R}_2 \exp\left(\frac{-(1+8\bar{k}d^2)(\mathbf{R}_1^2+\mathbf{R}_2^2)}{2d^2}\right)\left[-\frac{E_c}{3} - \frac{8Cd^2}{3(1+4\bar{k}d^2)} + \frac{4m}{3}\right.$$
$$\left. - \frac{8}{9}\overline{C} + \frac{1+4\bar{k}d^2}{6md^2}\left(\frac{15}{2} - (\mathbf{R}_1^2+\mathbf{R}_2^2)\left(\frac{1+4\bar{k}d^2}{d^2}\right)\right)\right]\chi_2(\mathbf{R}_2) + \frac{8f^a n^2}{18\sqrt{2}(2\pi d^2)^{\frac{3}{2}}} \int d^3\mathbf{R}_2 \exp\left(\frac{-\mathbf{R}_2^2}{2d^2}\right)$$
$$\exp(-2p\mathbf{R}_1^2)\left[\left(\frac{\pi}{\frac{1}{2d^2}+2p}\right)^{\frac{3}{2}} F_1(\mathbf{R}_1,\mathbf{R}_2) - 2AE(\mathbf{R}_1,\mathbf{R}_2)\right]\chi_2^*(\mathbf{R}_2) = 0 \tag{21}$$

$$\Delta_2(\mathbf{R}_2)\chi_2(\mathbf{R}_2) + \left(\frac{1}{\pi d^2(1+4\bar{k}d^2)}\right)^{\frac{3}{2}} \int d^3\mathbf{R}_1 \exp\left(\frac{-(1+8\bar{k}d^2)(\mathbf{R}_1^2+\mathbf{R}_2^2)}{2d^2}\right)\left[-\frac{E_c}{3} - \frac{8Cd^2}{3(1+4\bar{k}d^2)} + \frac{4m}{3}\right.$$
$$\left. - \frac{8}{9}\overline{C} + \frac{1+4\bar{k}d^2}{6md^2}\left(\frac{15}{2} - (\mathbf{R}_1^2+\mathbf{R}_2^2)\left(\frac{1+4\bar{k}d^2}{d^2}\right)\right)\right]\chi_1(\mathbf{R}_1) + \frac{8f^a n^2}{18\sqrt{2}(2\pi d^2)^{\frac{3}{2}}} \int d^3\mathbf{R}_1 \exp\left(\frac{-\mathbf{R}_1^2}{2d^2}\right)$$
$$\exp(-2p\mathbf{R}_2^2)\left[\left(\frac{\pi}{\frac{1}{2d^2}+2p}\right)^{\frac{3}{2}} F_1(\mathbf{R}_2,\mathbf{R}_1) - 2AE(\mathbf{R}_2,\mathbf{R}_1)\right]\chi_1^*(\mathbf{R}_1) = 0 \tag{22}$$

$$F_4(\mathbf{R}_1)\chi_1^*(\mathbf{R}_1) + \frac{8f^a n^2}{18\sqrt{2}(2\pi d^2)^{\frac{3}{2}}} \int d^3\mathbf{R}_2 \exp\left(\frac{-\mathbf{R}_1^2}{2d^2}\right)\exp(-2p\mathbf{R}_2^2)\left[\left(\frac{\pi}{\frac{1}{2d^2}+2p}\right)^{\frac{3}{2}} F_3(\mathbf{R}_1,\mathbf{R}_2) - 2AE(\mathbf{R}_2,\mathbf{R}_1)\right]$$
$$\chi_2(\mathbf{R}_2) + \frac{8n^4 f^c}{3} \int d^3\mathbf{R}_2 \exp(-2p\mathbf{R}_1^2 - 2p\mathbf{R}_2^2)\left[\left(\frac{\pi}{4p}\right)^{\frac{3}{2}}\left(E_c F_5(\mathbf{R}_1,\mathbf{R}_2) + F_6(\mathbf{R}_1,\mathbf{R}_2)\right) + 2A\right.$$
$$\left[\exp(-B\mathbf{R}_2^2)\{D(\mathbf{R}_1,\mathbf{R}_2)D_1(\mathbf{R}_2) + \mathbf{R}_1^4\mathbf{R}_2^4 + 2(\mathbf{R}_1^6 + \mathbf{R}_1^4\mathbf{R}_2^2)D_2(\mathbf{R}_1) + 2(\mathbf{R}_1^2+\mathbf{R}_2^2)D_3(\mathbf{R}_2) + \right.$$
$$D_4(\mathbf{R}_2) - 4\mathbf{R}_2^4 D_5(\mathbf{R}_1,\mathbf{R}_2) - 4D_6(\mathbf{R}_1,\mathbf{R}_2) - 8\mathbf{R}_2^2 D_7(\mathbf{R}_1,\mathbf{R}_2) - 4\mathbf{R}_1^4 D_8(\mathbf{R}_2) - 4D_9(\mathbf{R}_2) - 8\mathbf{R}_1^2$$
$$D_{10}(\mathbf{R}_2) + 16D_{11}(\mathbf{R}_1,\mathbf{R}_2)\}\exp\left(\frac{(2B)^2\mathbf{R}_2^2}{4(B+4p)}\right) + \exp(-B\mathbf{R}_1^2)\{D(\mathbf{R}_1,\mathbf{R}_2)D_1(\mathbf{R}_1) + \mathbf{R}_1^4\mathbf{R}_2^4 +$$
$$2(\mathbf{R}_1^6 + \mathbf{R}_1^4\mathbf{R}_2^2)D_2(\mathbf{R}_1) + 2(\mathbf{R}_1^2+\mathbf{R}_2^2)D_3(\mathbf{R}_1) + D_4(\mathbf{R}_1) - 4\mathbf{R}_1^4 D_5(\mathbf{R}_2,\mathbf{R}_1) - 4D_6(\mathbf{R}_2,\mathbf{R}_1) -$$
$$8\mathbf{R}_1^2 D_7(\mathbf{R}_2,\mathbf{R}_1) - 4\mathbf{R}_1^4 D_8(\mathbf{R}_1) - 4D_9(\mathbf{R}_1) - 8\mathbf{R}_2^2 D_{10}(\mathbf{R}_1) + 16D_{11}(\mathbf{R}_2,\mathbf{R}_1)\}\exp\left(\frac{(2B)^2\mathbf{R}_1^2}{4(B+4p)}\right)]$$
$$\left. + \frac{1}{2m}\left(\frac{\pi}{4p}\right)^{\frac{3}{2}} D_{12}(\mathbf{R}_1,\mathbf{R}_2)\right]\chi_2^*(\mathbf{R}_2) = 0 \tag{23}$$

$$F_4(\mathbf{R}_2)\chi_2^*(\mathbf{R}_2) + \frac{8f^a n^2}{18\sqrt{2}(2\pi d^2)^{\frac{3}{2}}}\int d^3\mathbf{R}_1 \exp(\frac{-\mathbf{R}_2^2}{2d^2})\exp(-2p\mathbf{R}_1^2)[(\frac{\pi}{\frac{1}{2d^2}+2p})^{\frac{3}{2}}F_3(\mathbf{R}_2,\mathbf{R}_1) - 2AE(\mathbf{R}_1,\mathbf{R}_2)]$$

$$\chi_1(\mathbf{R}_1) + \frac{8f^a n^4}{3}\int d^3\mathbf{R}_1 \exp(-2p\mathbf{R}_2^2 - 2p\mathbf{R}_1^2)\Big[(\frac{\pi}{4p})^{\frac{3}{2}}\left(E_c F_5(\mathbf{R}_2,\mathbf{R}_1) + F_6(\mathbf{R}_2,\mathbf{R}_1)\right) + 2A$$

$$[\exp(-B\mathbf{R}_2^1)\{D(\mathbf{R}_2,\mathbf{R}_1)D_1(\mathbf{R}_1) + \mathbf{R}_2^4\mathbf{R}_1^4 + 2(\mathbf{R}_2^6 + \mathbf{R}_2^4\mathbf{R}_1^2)D_2(\mathbf{R}_2) + 2(\mathbf{R}_2^2 + \mathbf{R}_1^2)D_3(\mathbf{R}_1) +$$

$$D_4(\mathbf{R}_1) - 4\mathbf{R}_1^4 D_5(\mathbf{R}_2,\mathbf{R}_1) - 4D_6(\mathbf{R}_2,\mathbf{R}_1) - 8\mathbf{R}_1^2 D_7(\mathbf{R}_2,\mathbf{R}_1) - 4\mathbf{R}_2^4 D_8(\mathbf{R}_1) - 4D_9(\mathbf{R}_1) - 8\mathbf{R}_2^2$$

$$D_{10}(\mathbf{R}_1) + 16D_{11}(\mathbf{R}_2,\mathbf{R}_1)\}\exp(\frac{(2B)^2\mathbf{R}_2^2}{4(B+4p)}) + \exp(-B\mathbf{R}_2^2)\{D(\mathbf{R}_2,\mathbf{R}_1)D_1(\mathbf{R}_2) + \mathbf{R}_2^4\mathbf{R}_1^4$$

$$+ 2(\mathbf{R}_2^6 + \mathbf{R}_2^4\mathbf{R}_1^2)D_2(\mathbf{R}_2) + 2(\mathbf{R}_2^2 + \mathbf{R}_1^2)D_3(\mathbf{R}_2) + D_4(\mathbf{R}_2) - 4\mathbf{R}_2^4 D_5(\mathbf{R}_1,\mathbf{R}_2) - 4D_6(\mathbf{R}_1,\mathbf{R}_2)$$

$$- 8\mathbf{R}_2^2 D_7(\mathbf{R}_1,\mathbf{R}_2) - 4\mathbf{R}_2^4 D_8(\mathbf{R}_2) - 4D_9(\mathbf{R}_2) - 8\mathbf{R}_1^2 D_{10}(\mathbf{R}_2) + 16D_{11}(\mathbf{R}_1,\mathbf{R}_2)\}\exp(\frac{(2B)^2\mathbf{R}_1^2}{4(B+4p)})]$$

$$(\frac{\pi}{B+4p})^{\frac{3}{2}} + \frac{1}{2m}(\frac{\pi}{4p})^{\frac{3}{2}}D_{12}(\mathbf{R}_2,\mathbf{R}_1)\Big]\chi_1^*(\mathbf{R}_1) = 0. \tag{24}$$

The symbols are defined in the appendix B. We have eventually replaced $\mathbf{r}_1, \mathbf{r}_2, \mathbf{r}_3, \mathbf{r}_4$ by $\mathbf{R}_1, \mathbf{R}_2, \mathbf{R}_3$, and $\mathbf{R}_c$. With trivial integration on $\mathbf{R}_c$, we have eq.(14) that is independent of $\mathbf{R}_c$. Now, after the integration on $\mathbf{R}_3$, the above four integral equations (21-24) depend only on $\mathbf{R}_1$ and $\mathbf{R}_2$. So every quantity which we want to calculate depends on $\mathbf{R}_1$ and $\mathbf{R}_2$. In eq.(21-22), the first two terms in each equation containing $\chi_1(\mathbf{R}_1)$ and $\chi_2(\mathbf{R}_2)$ are for the ground state. It is noted that in these terms, there is no dot product of vectors $\mathbf{R}_1$ and $\mathbf{R}_2$. So the results from these terms should not depend on the angle between $\mathbf{R}_1$ and $\mathbf{R}_2$, called θ. The third term of eq.(21-22) is due to the gluonic ground and excited states. In these terms dot product of two vectors ($\mathbf{R}_1$ and $\mathbf{R}_2$) appear, so the results from these terms depend on θ.

4. SOLVING THE INTEGRAL EQUATIONS

Now taking the three dimensional Fourier transform of eq.(21,23) with respect to $\mathbf{R}_1$ and eq.(22-24) with respect to $\mathbf{R}_2$, we get formal solutions $\chi_1(\mathbf{P}_1)$, $\chi_2(\mathbf{P}_2)$, $\chi_1^*(\mathbf{P}_{1s})$, and $\chi_1^*(\mathbf{P}_{1s})$ as shown in appendix C. Because of the coupling to the gluonic excitations, it become difficult to solve the integral equations for non trivial solutions for $\chi_1(\mathbf{P}_1), \chi_2(\mathbf{P}_2), \chi_1^*(\mathbf{P}_{1s})$, and $\chi_2^*(\mathbf{P}_{2s})$ analytically as done in [15, 16]. In [15], the meson wave functions, including the gluonic field overlap factor, is $\mathbf{R}_1$, $\mathbf{R}_2$ separable. So there the integral equations can be solved analytically by replacing χ_1 and χ_2. But in our present work, the meson meson wave functions are not separable in $\mathbf{R}_1$,$\mathbf{R}_2$. So we use the Born approximation (as used in [11] for meson meson scattering) to solve the integral equations. Our results given below also justify our use of the Born Approximation. For using this approximation, we use the solutions $(\chi_i(\mathbf{R}_i), \chi_i^*(\mathbf{R}_i))$ of eqs.(21-24) in absence of interactions (meaning $f = f^a = f^c = 0$)

$$\chi_i(\mathbf{R}_i) = \sqrt{\frac{2}{\pi}}\quad \exp(\imath\mathbf{P}_i.\mathbf{R}_i),$$
$$\text{and} \qquad \chi_i^*(\mathbf{R}_i) = \sqrt{\frac{2}{\pi}}\quad \exp(\imath\mathbf{P}_{is}.\mathbf{R}_i) \tag{25}$$

for $i = 1, 2$. Here the coefficient of $\exp(\imath\mathbf{P}_i.\mathbf{R}_i)$ is chosen so that it makes $\chi(\mathbf{R}_i)$ as Fourier transform of $\frac{\delta(P_i - P_c(i))}{P_c^2(i)}$. Similarly the coefficient of $\exp(\imath\mathbf{P}_{is}.\mathbf{R}_i)$ is chosen. Using this approximation, the integration on $\mathbf{R}_1$ and $\mathbf{R}_2$ can be performed to get $\chi_1(\mathbf{P}_1)$ (written in eq.(C11)).

T_{11} can be calculated (as in ref. [15]) by considering the coefficient of $\frac{1}{\Delta_1(P_1)}$ containing the $\chi_1(\mathbf{R}_1)$ from eq.(C11). As in this equation, there is no coefficient having $\chi_1(\mathbf{R}_1)$, so it gives $T_{11} = 0$. T_{12} can be calculated by considering the coefficient of $\frac{1}{\Delta_1(P_1)}$ containing the $\chi_2(\mathbf{R}_2)$ from eq.(C11) in the following eq.

$$T_{12} = M\frac{\pi}{2}P_1[\text{coef. of } \frac{1}{\Delta_1(P_1)} \text{ containing } \chi_2(\mathbf{R}_2)], \tag{26}$$

with M being the mass of $c\bar{c}$ meson. Similarly T_{12^*} can be calculated by considering the coefficient of $\frac{1}{\Delta_1(P_1)}$ containing the $\chi_2^*(\mathbf{R}_2)$ from eq.(C11)

$$T_{12^*} = M\frac{\pi}{2}P_{1s}[\text{coef. of}\frac{1}{\Delta_1(P_1)} \text{ containing } \chi_2^*(\mathbf{R}_2)]. \tag{27}$$

Off-diagonal phase shift can be calculated by using the following relation given in ref. [28]

$$S = I - 2\imath T = \exp(2\imath\Delta), \tag{28}$$

where S, T, I,and Δ represent 4×4 scattering, transition, identity, and phase shift matrices respectively. By neglecting the higher powers of Δ in the expansion of $\exp(2\imath\Delta)$, the eq.(28) can be written as

$$S_{ij} = \delta_{ij} - 2\imath T_{ij} = \delta_{ij} + 2\imath\Delta_{ij}. \tag{29}$$

for $i,j = 1,2,1^*,2^*$. From this eq.(29), we obtained that the phase shifts are equal to -ve of the transition amplitude, e.g. for $i=1$, $j=2$, $\Delta_{12} = \frac{S_{12}}{2\imath} = -T_{12}$. Using the transition matrix elements, the energy shift of meson meson system ($cc\bar{c}\bar{c}$) can be calculated by using the stationary state perturbation theory, i.e.

$$E_i = E_i^0 + T_{ii} + \sum_{i\neq j}\int_0^\infty \frac{|T_{ij}|^2}{E_i^0 - E_j^0}dP_j, \tag{30}$$

with the initial state i and intermediate state j. We have considered initial states where the gluonic field should is in ground state, so $i=1,2$, but intermediate $j = 1,2,1^*,2^*$. Here $T_{ii} = \langle i|T|i\rangle$, $|T_{ij}|^2 = |\langle j|T|i\rangle|^2$, E_i^0 is the energy of a ground state (1 or 2) of meson meson system, and E_j^0 may be the energy of the other meson meson ground state or that of an gluonic-excited meson meson state.

5. RESULTS AND CONCLUSIONS

1-The transition amplitude T_{12}, from one meson-meson ground state to other, are calculated by using eq.(26) with $k_f = 0.6$ [27](without the incorporation of gluonic excited states). Its dependence on the center of mass kinetic energy is shown in Fig.4 below. As it is noted that $-T_{12} = phase\ \ shift$ is less than 1, so these results shows the validity of Born approximation. In result 3 we compare the phase shifts (in radians) of this many body ground state gluonic field model at $k_f = 0.6$ with the phase shifts obtained from a model that is extended to gluonic excitations along with changing $k_f = 1.51$.

2- The transition matrix element T_{12^*}, for transition from ground state to excited state gluonic field with $k_f = 1.51$, depend on the parameters ϵ, and f^a. T_{12^*} also depends on θ (the angle that $\mathbf{P}_1$ makes with $\mathbf{P}_2$ and $\mathbf{P}_{1s}$ makes with $\mathbf{P}_{2s}$). We take parameter f^a as a constant as discussed earlier in section 2. For $\epsilon = 2$, we take different values of f^a to see the effects of f^a on T_{12^*}. Figs.5,6,7,8 and 9 show the dependence of T_{12^*} on f^a at angles 0, 30, 60, 75 and 90 respectively. For $\epsilon = 1/2$, the dependence of T_{12}^* on f^a at $\theta = 90$ is shown in Fig.10. And for $\epsilon = 1$, the dependence of T_{12}^* on f^a at $\theta = 90$ is shown in Fig.11. These graphs show that the phase shift (equal to $-T_{12^*}$) is increasing with the increase of f^a.

3- For the center of mass kinetic energy range 0 to 2 GeV, the average of the modulus of phase shifts (excluding excited states) is equal to -0.0369 radians at $k_f = 0.6$. But if we change the value of k_f from 0.6 to 1.51 and also include the excited state gluonic field, the average meson-meson phase shift again becomes $(-0.0218 - 0.0152)$ radians = -0.0370 radians by choosing $f^a = 0.03$ and $\theta = 90$ with $\epsilon = 2$. This means that a sum-of-two-body potential model can replace to some extent many-body potential terms in a tetraquark system by including the gluonic excitations. (An exact sum of two body terms would required $f_a = 1$ though). In above, -0.0218 radians is the phase shift due to ground state gluonic field at $k_f = 1.51$, and -0.0152 radians is the phase shift due to gluonic excited states.

We have also explored the results with $\epsilon = 1/2$ and $\epsilon = 1$. As ϵ is proportional to the potential matrix elements taken between ground and gluonic excited states, when we replace $\epsilon = 2$ with $\epsilon = 1/2$ or 1, it has no effect on T_{12} and average phase shift. But for $\epsilon = \frac{1}{2}$ with inclusion of gluonic excitations, now the values $f^a = 0.08$ and $\theta = 75$ almost restore the average phase shifts for $k_f = 1.51$ to $(-0.0218 - 0.0149)$

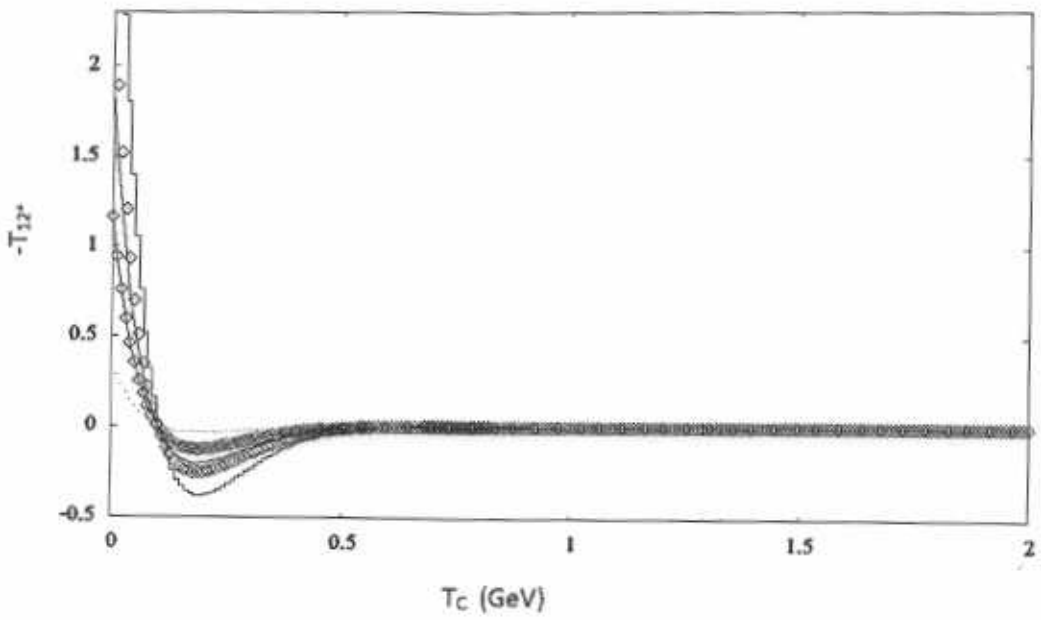

Figure 6: The same graph as Fig.5 but with $\theta = 30$

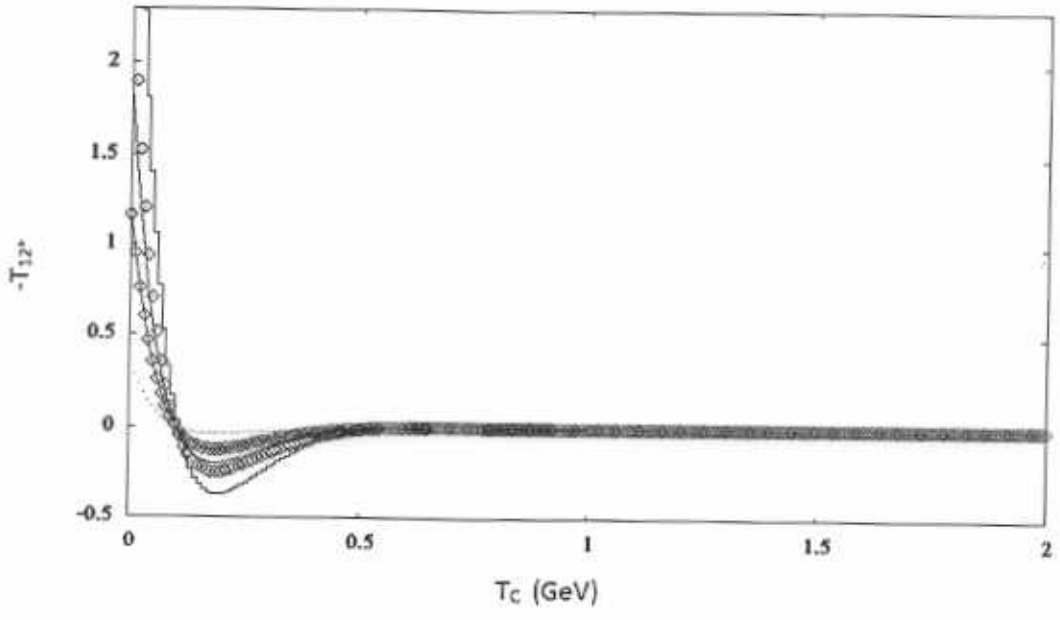

Figure 7: The same graph as Fig.5 but with $\theta = 60$

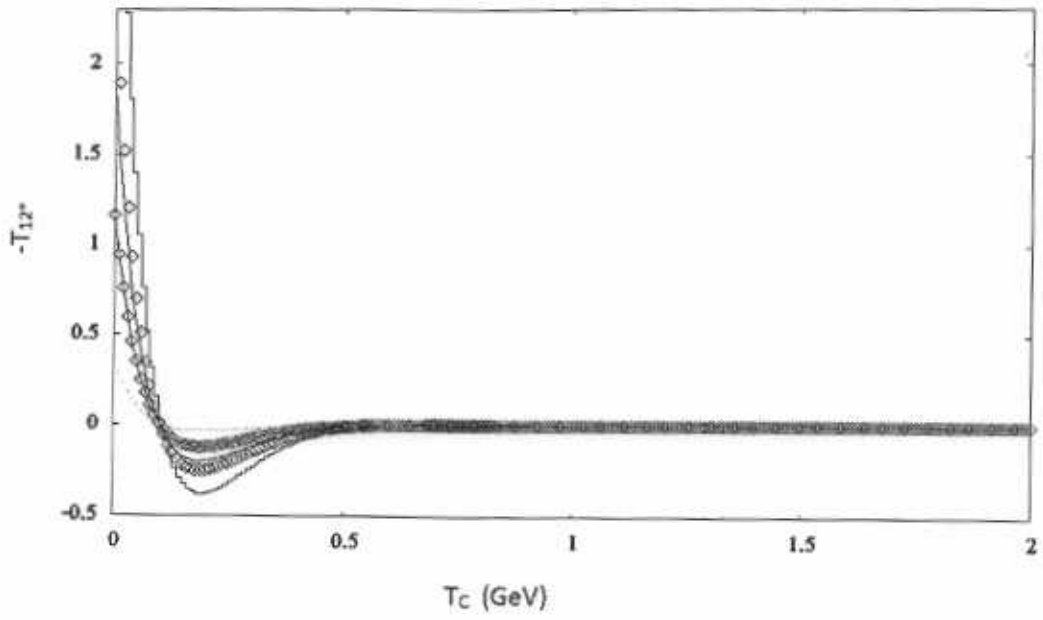

Figure 6: The same graph as Fig.5 but with $\theta = 30$

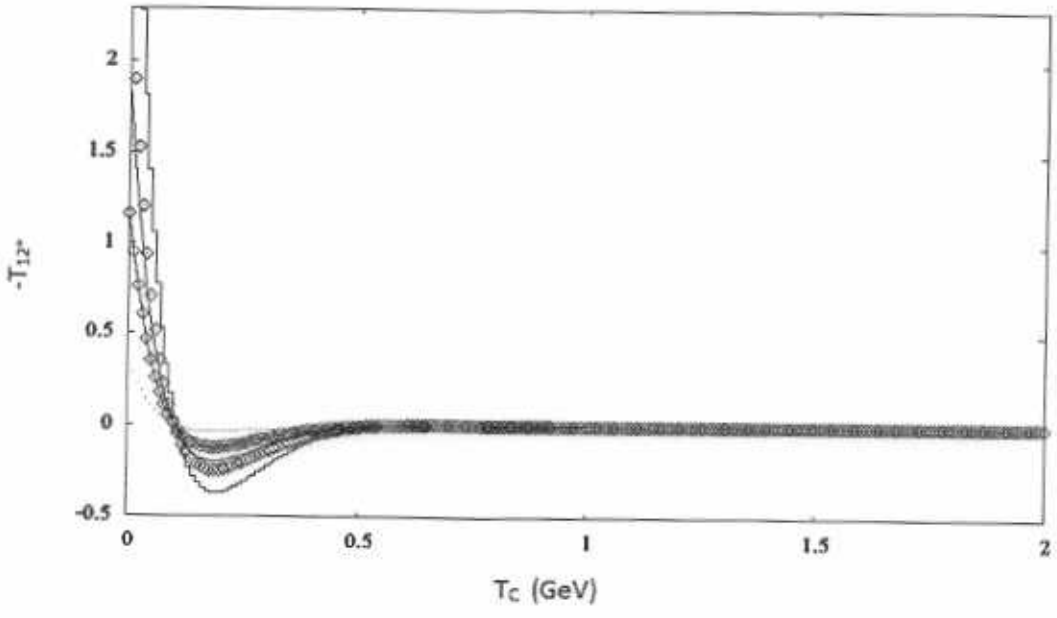

Figure 7: The same graph as Fig.5 but with $\theta = 60$

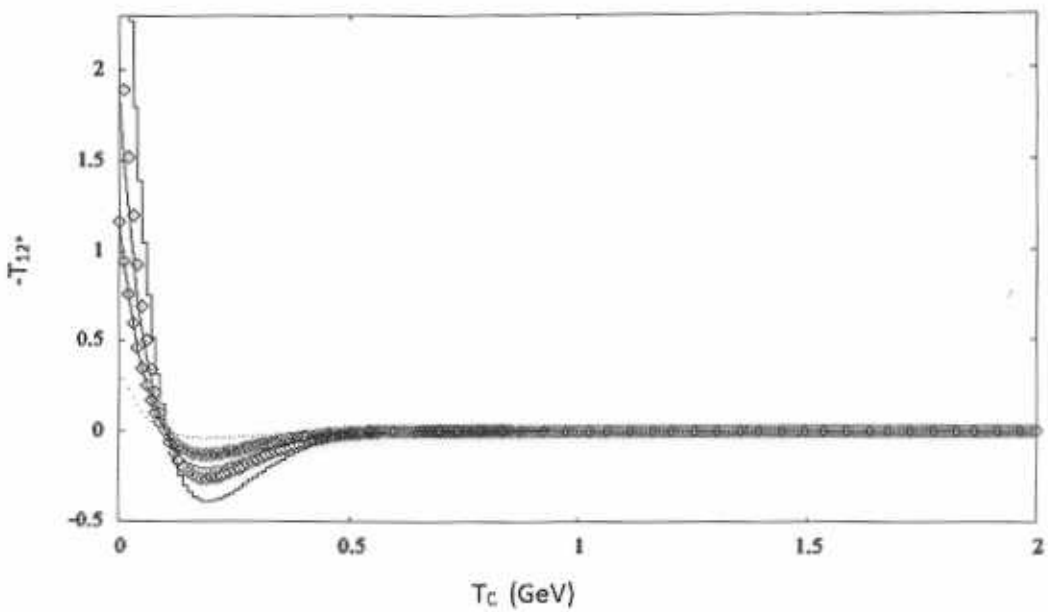

Figure 8: The same graph as Fig.5 but with $\theta = 75$

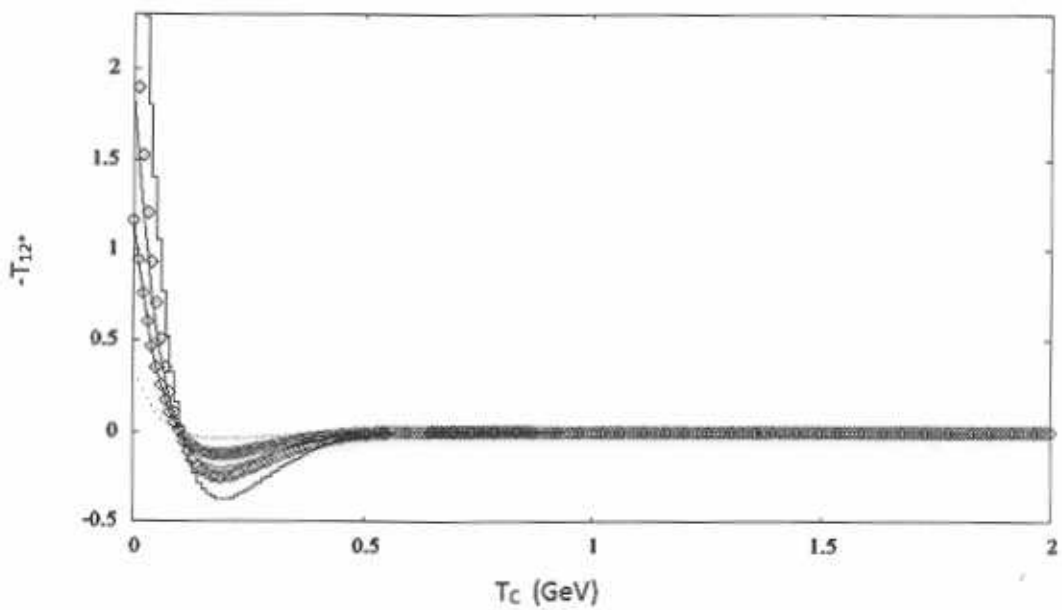

Figure 9: The same graph as Fig.5 but with $\theta = 90$

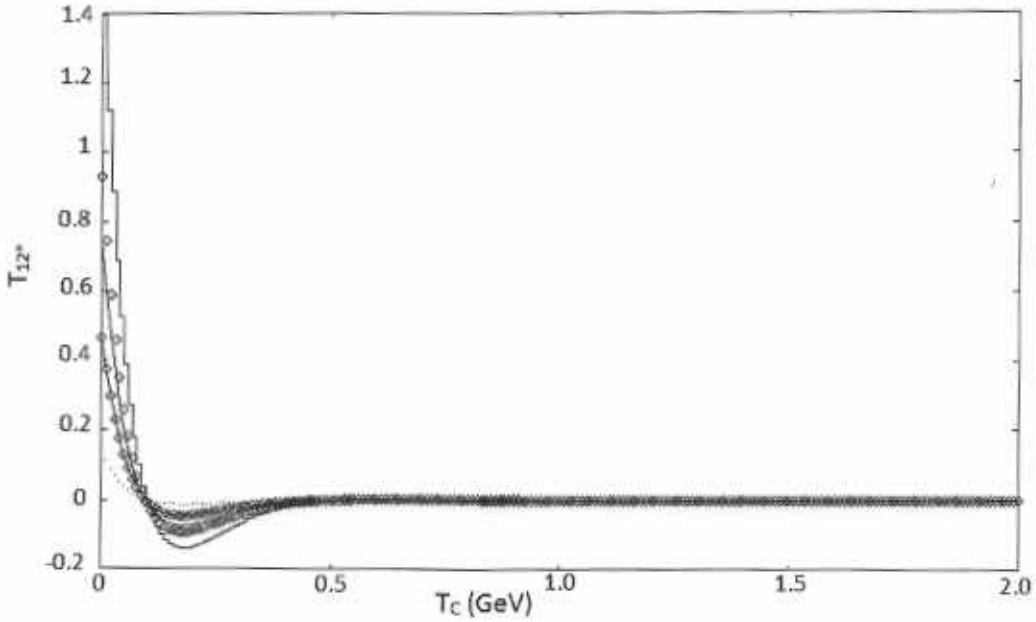

Figure 10: A graph between energy and T_{12^*} at $\theta = 90$ degrees with $\epsilon = 1/2$ for different values of f^a. The curve with dots for $f^a = 0.015$, with lines plus points is for $f^a = 0.05$, with lines is for $f^a = 0.08$, with points is for $f^a = 0.1$, and with steps is for $f^a = 0.15$

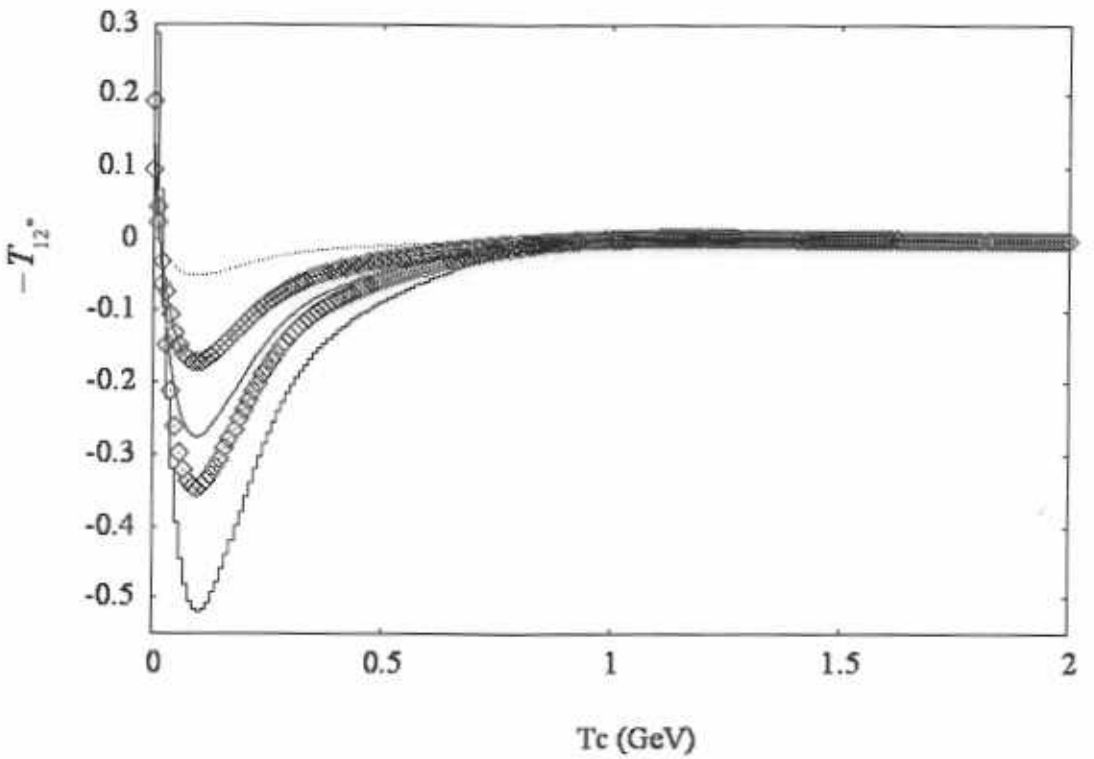

Figure 11: The same graph as Fig.10 but with $\epsilon = 1$

radians = -0.0367 radians. (The significance of the first and second term is as before). For $\epsilon = 1$, at $f^a = 0.055$ and $\theta = 90$, the average phase shifts for $k_f = 1.51$ becomes $(-0.0218 - 0.0150)$ radians = -0.0368 radians. This almost restoration again indicates that perhaps we can always choose parameters etc. so that with an inclusion of the gluonic excitations the sum-of-two-body potential model can replace many-body potential terms in a tetraquark system.

4- The effects of interaction are also observed through energy shift by using eq.(30). Here $T_{ii} = 0$ with $i = 1, 2$. In $\int_{i\neq j} \frac{|T_{ij}|^2}{E_i^0 - E_j^0} dP$, we have chosen $E_i^0 = 5.9176$ GeV, the value of energy for which center of mass kinetic energy becomes zero. The intermediate energy state E_j^0 depends on the state of gluonic field ($|2\rangle, |2^*\rangle$ are only possible states that couple to $|1\rangle$). For the gluonic ground state ($|2\rangle$), $E_j^0 = 5.9176 + 0.3380 P_1^2$ (calculated using eq.(C10) with $P_c^2(1) = P_1^2$); and for the excited state gluonic field ($|2^*\rangle$), $E_j^0 = 5.4638 + 0.3380 P_{1s}^2$ (calculated using eq.(C10) with $P_c^2(1s) = P_{1s}^2$). At $k_f = 0.6$ and $E_c = 5.9176$ (i.e. at the threshold), the shift to the ground state meson-meson energy is found to be $E_i = E_i^0 - 0.7268$ GeV excluding the gluonic excitations. If with increasing k_f to 1.51 as usual and including the coupling to the gluonic-excited meson meson state, we want to restore the same energy shifts we can get to (with same origin of the first and second correction terms)

$$E_i = E_i^0 + (-0.0950 - 0.6371)\text{GeV} = E_i^0 - 0.7321\text{GeV}$$

if $f^a = 0.14$ is used. This shows that gluonic excitations can replace the many terms for energy shifts as well. We note that the energy shift is independent of θ, the angle between $\mathbf{R}_1$ and $\mathbf{R}_2$. The energy shifts we have reported here can be compared with the hadron-loops-generated mass shifts to charmonium states reported in Table III of ref. It is difficult, though, to conclude anything from this comparison as in ref. [29] the integrand contains squares of the matrix elements of the $^3P_0$ meson decay amplitudes whereas in our integrands in eq.(30) contain squares of meson-meson couplings. Thus though the intermediate states in both works are respective *hadron loops* $q\bar{q}q\bar{q}$, the initial and final states in ref. [29] are $q\bar{q}$ but in our work initial and final states are also $q\bar{q}q\bar{q}$. Only we include the glounic-exited intermediate $q\bar{q}q\bar{q}$ state (i.e. the hybrid hadronic loops) for our problem. In result 3, it is noted that the average phase shift obtained (for $\epsilon = 2$) by a model that does not include the gluonic excitations is equal to the average phase shift obtained by including gluonic excitations for $f^a = 0.03$, but the energy shift obtained by both models becomes comparable at $f^a = 0.14$. One possible reason of this difference in the values of f^a could be that the average phase shift is calculated for the center of mass kinetic energy range in between 0 GeV to 2 GeV, but energy shift is calculated at threshold center of mass kinetic energy.

5- For the ground state gluonic field, transition matrix elements are θ independent. But for transition elements to the gluonic-excited meson-meson state depends on θ. We projected this angle dependence on spherical harmonics Y_{lm}. The results of this partial wave analysis are also reported in Figs. (12-14) for $m = 0$ and $f^a = 0.03$ (this value is used above in result 3). The reason for truncating the spherical expansion to $m = 0$ harmonics is that that we have have no dependence on ϕ, the azimuthal. These analysis shows that partial wave amplitudes are decreasing as we go from Y_{00} the coefficient to the Y_{50} coefficient i.e. from S-wave to H-wave. Figs. 12 and 13 are for the even wave $(D, G, ...)$ ratios with $S-$wave. S/D ratios are also used in ref. [30, 25]. These graphs shows that the S/G ratio is too much large as compared to the S/D ratio. It means that $S-$wave is dominant over $G-$wave. In Fig.14, ratios of odd waves with $S-$wave are shown. We noted that S/H is too much large as compared to S/P. This shows that $H, J, ...$ waves can be neglected as compared to $S-$wave. The partial wave analysis indicates the presence of P, D, F, G, H waves only when we include the gluonic excitations in combination with essentially sum-of-pair-wise approach. It means that, in the presence of gluonic excitations, an $\ell = 0, 1, 2, 3, ...$ ground state meson meson system may couple to $\ell = 0, 1, 2, 3, ...$ hybrid hybrid systems as a intermediate states or as final states.

As mentioned above in result 3,4, we compare our meson-meson transition amplitudes and polarization potentials (in the respective center of mass energy ranges) in an extended almost sum-of-pair-wise approach and a many-body-term based one. Apparently this comparison has even a qualitative difference in case of the transition amplitudes (T_{12} and T_{12}^*) which have a dependance on the scattering angle (meaning coupling to P and higher orbital excitations in the final channel) if we use gluonic excitation in combination with essentially sum-of-pair-wise approach (can see fig.(5-9)) but we get the same transition amplitude for all the scattering angles if we use a many-body potential linking ground-state clusters only. But a recent work [17] indicates that the absence of angle dependence is an artifact of the unjustified overly simple form of the gluonic overlap factor f (defined in eq.(20)); using a proper lattice-gauge theory-based form of f (defined in eq.(19)) also results in this angle dependence and the resulting coupling to

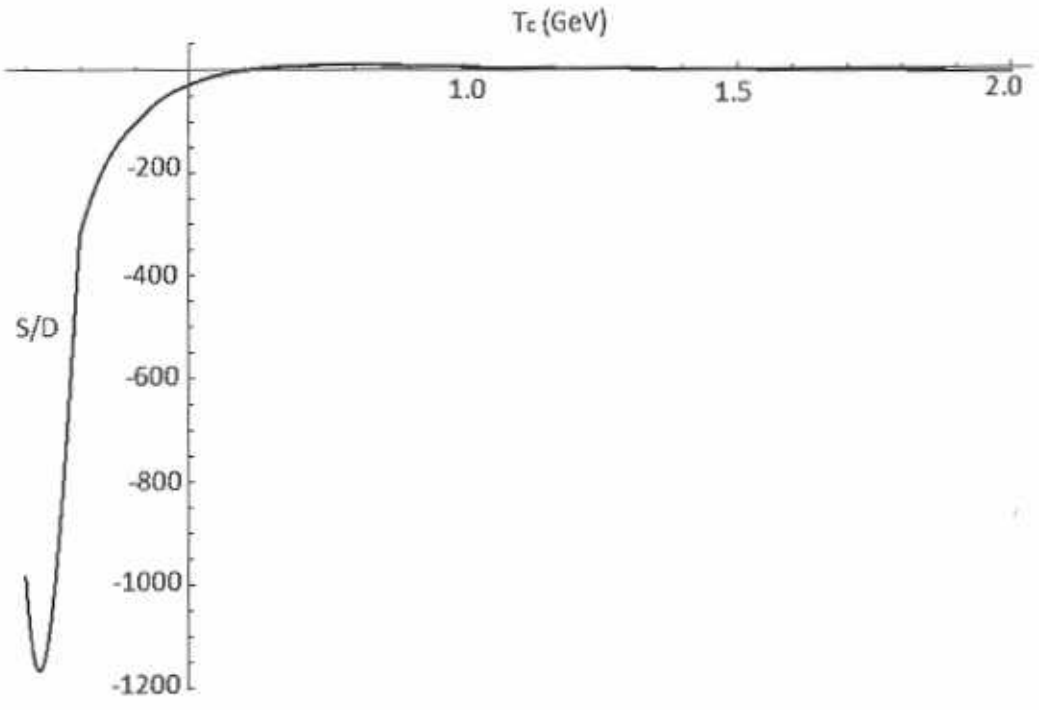

Figure 12: A graph between T_c and S/D ratio.

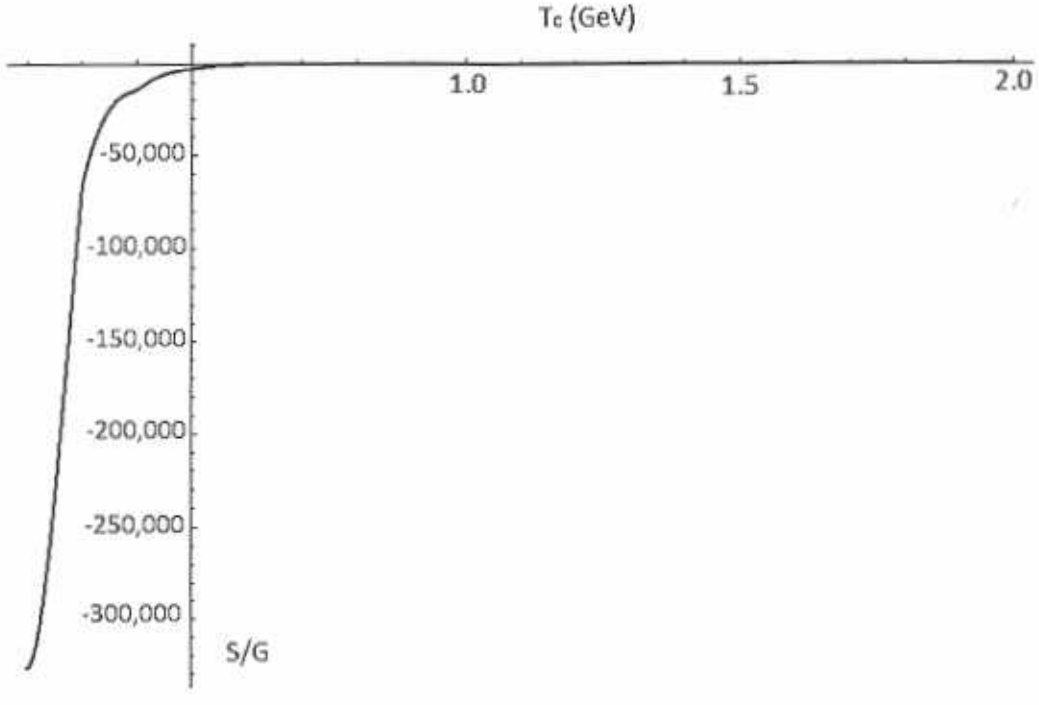

Figure 13: A graph between T_c and S/G ratio.

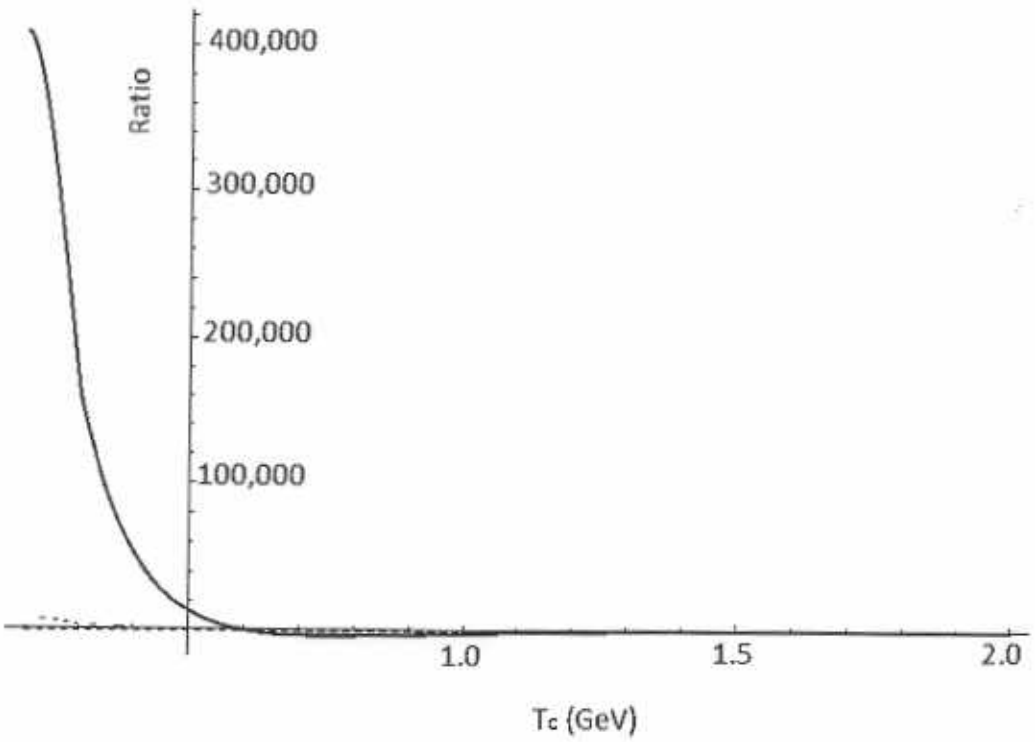

Figure 14: A graph between T_c and $S/P, S/F, S/H$ ratios. Dashed line is for S/P, thin solid line is for S/F, and thick solid line is for S/H. S/P and S/F are so small as compared to S/H that the curves for S/P and S/F are lie along horizontal axis.

Table 1: The matrix elements of the $F_i.F_j$ operators

	$<1\|..\|1>$	$<1\|..\|2>$	$<2\|..\|2>$	$<1\|..\|2^*>$	$<2\|..\|1^*>$	$<1^*\|..\|2^*>$	$<1^*\|..\|1^*>$	$<2^*\|..\|2^*>$
$F_1.F_2$	0	$\frac{4}{9}$	0	$-\frac{2}{9\sqrt{2}}$	$-\frac{2}{9\sqrt{2}}$	$\frac{10}{18}$	$-\frac{1}{3}$	$-\frac{1}{3}$
$F_1.F_3$	$-\frac{4}{3}$	$-\frac{4}{9}$	0	$-\frac{16}{9\sqrt{2}}$	$\frac{2}{9\sqrt{2}}$	$-\frac{1}{18}$	$\frac{1}{6}$	$-\frac{7}{6}$
$F_1.F_4$	0	$-\frac{4}{9}$	$-\frac{4}{3}$	$\frac{2}{9\sqrt{2}}$	$-\frac{16}{9\sqrt{2}}$	$-\frac{1}{18}$	$-\frac{7}{6}$	$\frac{1}{6}$
$F_2.F_3$	0	$-\frac{4}{9}$	$-\frac{4}{3}$	$\frac{2}{9\sqrt{2}}$	$-\frac{16}{9\sqrt{2}}$	$-\frac{1}{18}$	$-\frac{7}{6}$	$\frac{1}{6}$
$F_2.F_4$	$-\frac{4}{3}$	$-\frac{4}{9}$	0	$-\frac{16}{9\sqrt{2}}$	$\frac{2}{9\sqrt{2}}$	$-\frac{1}{18}$	$\frac{1}{6}$	$-\frac{7}{6}$
$F_3.F_4$	0	$\frac{4}{9}$	0	$-\frac{2}{9\sqrt{2}}$	$-\frac{2}{9\sqrt{2}}$	$\frac{10}{18}$	$-\frac{1}{3}$	$-\frac{1}{3}$

higher orbital excitations.

The meson-meson to hybrid coupling worked out in this paper may affect properties of any system that is presently understood to be a purely ground-state meson-meson system. This means, in addition to the energy shift of the meson-meson molecules due to coupling to hybrid-hybrid systems, pointing out the possibility of a hybrid-hybrid component in the wave functions of mesons like $X(3872)$, $X(3940)$, $Y(4260)$, and $Z(4433)$ which are considered to have $q^2\bar{q}^2$ components. And in the above paragraph, we indicate that this coupling may also include coupling to orbital excitations. Thus we hope to point out a new dimension in discussions about the structure of scalar mesons as well.

ACKNOWLEDGEMENT

We are grateful to Higher education Commission of Pakistan for their financial support no.17-5-3 (Ps3-212) HEC/Sch/2006.

APPENDIX A

Table 1 is used for the matrix elements of the $F_i.F_j$ operators (introduced above in eq.(9)), for different values of indices i and j. In this table ground state elements (with out star) are taken from [15] and excited state elements (with star) are calculated by using the following group theory results:

$$|8_{1\bar{3}}8_{2\bar{4}}>=-\sqrt{\frac{2}{3}}|\bar{3}_{12}3_{\bar{3}\bar{4}}>+\sqrt{\frac{1}{3}}|6_{12}\bar{6}_{34}>$$

$$|1_{1\bar{3}}1_{2\bar{4}}>=\sqrt{\frac{1}{3}}|\bar{3}_{12}3_{\bar{3}\bar{4}}>+\sqrt{\frac{2}{3}}|6_{12}\bar{6}_{\bar{3}\bar{4}}>$$

$$|8_{1\bar{4}}8_{2\bar{3}}>=\sqrt{\frac{8}{9}}|1_{1\bar{3}}1_{2\bar{4}}>-\sqrt{\frac{1}{9}}|8_{1\bar{3}}8_{2\bar{4}}>$$

$$|1_{1\bar{4}}1_{2\bar{3}}>=\sqrt{\frac{1}{9}}|\bar{1}_{1\bar{3}}1_{2\bar{4}}>+\sqrt{\frac{8}{9}}|8_{1\bar{3}}8_{2\bar{4}}>$$

$$=-\sqrt{\frac{1}{3}}|\bar{3}_{12}3_{\bar{3}\bar{4}}>+\sqrt{\frac{2}{3}}|6_{12}\bar{6}_{\bar{3}\bar{4}}>$$

and

$$<8_{1\bar{3}}8_{2\bar{4}}|\mathbf{F}_i.\mathbf{F}_j|8_{1\bar{3}}8_{2\bar{4}}>=\frac{1}{6}.$$

APPENDIX B

The terms used in eqs.(21-24) are defined as

$$\Delta_i(\mathbf{R}_i) = -E_c - 8Cd^2 - \frac{8}{3}\overline{C} - \frac{\nabla^2_{\mathbf{R}_i}}{2m} + \frac{3}{2}\omega + 4m,$$

$$F_1(\mathbf{R}_i,\mathbf{R}_j) = (\mathbf{R}_i^4 + \frac{15}{4(\frac{1}{2d^2}+2p)^2} + \frac{\mathbf{R}_i^2}{\frac{1}{2d^2}+2p})\{E_c - 24\overline{C} - 28C\mathbf{R}_j^2 - 28C\frac{3}{2(\frac{1}{2d^2}+2p)} + 2A$$
$$\exp(-B\mathbf{R}_i^2 - B\mathbf{R}_j^2) + 2A\exp(-B\mathbf{R}_i^2 + B\mathbf{R}_j^2)\} - 28C(\frac{3\mathbf{R}_i^4}{2(\frac{1}{2d^2}+2p)} + \frac{105}{8(\frac{1}{2d^2}+2p)^3}$$
$$+ \frac{5\mathbf{R}_i^2}{2(\frac{1}{2d^2}+2p)^2}) + \frac{1}{2m}\{24\mathbf{R}_i^2 - 56p\mathbf{R}_i^4 + 16p^2\mathbf{R}_i^6 - R_i^4(\frac{3}{d^2} + \frac{\mathbf{R}_j^2}{d^4}) + \frac{1}{2(\frac{1}{2d^2}+2p)}(72 -$$
$$112p\mathbf{R}_i^2 + 80p^2\mathbf{R}_i^4) + \frac{1}{(\frac{1}{2d^2}+2p)^2}(400p^2\mathbf{R}_i^2 - 840p) + \frac{1680p^2}{8(\frac{1}{2d^2}+2p)^3}\},$$

$$E(\mathbf{R}_i) = \exp(-B\mathbf{R}_i^2)\exp(\frac{B^2\mathbf{R}_i^2}{\frac{1}{2d^2}+2p+B}),$$

$$F_2(\mathbf{R}_i,\mathbf{R}_j) = 2\mathbf{R}_i^4 + \frac{10B^2\mathbf{R}_j^2}{(\frac{1}{2d^2}+2p+B)^3} + \frac{2B^4\mathbf{R}_j^4}{(\frac{1}{2d^2}+2p+B)^4} + \frac{15}{2(\frac{1}{2d^2}+2p+B)^2} + \frac{4B^2\mathbf{R}_i^2\mathbf{R}_j^2}{(\frac{1}{2d^2}+2p+B)^2}$$
$$+ \frac{2(\mathbf{R}_i^2)}{(\frac{1}{2d^2}+2p+B)} - \frac{8B^2(\mathbf{R}_i.\mathbf{R}_j)^2}{(\frac{1}{2d^2}+2p+B)^2},$$

$$E(\mathbf{R}_i,\mathbf{R}_j) = (\frac{\pi}{\frac{1}{2d^2}+2p+B})^{\frac{3}{2}}\{16E(\mathbf{R}_j)F_2(\mathbf{R}_i,\mathbf{R}_j) + 2E(\mathbf{R}_i)F_2(\mathbf{R}_i,\mathbf{R}_i)\},$$

$$F_3(\mathbf{R}_i,\mathbf{R}_j) = (\mathbf{R}_j^4 + \frac{15}{4(\frac{1}{2d^2}+2p)^2} + \frac{\mathbf{R}_j^2}{\frac{1}{2d^2}+2p})\{E_c - 24\overline{C} - 28C\mathbf{R}_i^2 - 28C\frac{3}{2(\frac{1}{2d^2}+2p)} + 2A$$
$$\exp(-B\mathbf{R}_i^2 - B\mathbf{R}_j^2) + 2A\exp(-B\mathbf{R}_i^2 + B\mathbf{R}_j^2)\} - 28C(\frac{3\mathbf{R}_j^4}{2(\frac{1}{2d^2}+2p)} + \frac{105}{8(\frac{1}{2d^2}+2p)^3} + \frac{5\mathbf{R}_j^2}{2(\frac{1}{2d^2}+2p)^2})$$
$$+ \frac{1}{2m}\{20\mathbf{R}_j^2 - 44p\mathbf{R}_j^4 + 16p^2\mathbf{R}_j^6 - \frac{6\mathbf{R}_j^4}{d^2} + \frac{\mathbf{R}_j^4\mathbf{R}_i^2}{d^4} + \frac{3}{2(\frac{1}{2d^2}+2p)}(42 - 56p\mathbf{R}_j^2 + 32p^2\mathbf{R}_j^4 - \frac{12R_j^2}{d^2}$$
$$+ \frac{2R_j^2R_i^2}{d^4} + \frac{R_2^4}{d^4}) + \frac{15}{4(\frac{1}{2d^2}+2p)^2}(-12p + 16p^2\mathbf{R}_j^2 - \frac{6}{d^2} + \frac{\mathbf{R}_j^2}{d^4} + \frac{2\mathbf{R}_j^2}{d^4}) + \frac{1}{d^4}\frac{35\times 3}{(\frac{1}{2d^2}+2p)^3} + (112p$$
$$- 64p^2\mathbf{R}_j^2 + \frac{24}{d^2} - \frac{4\mathbf{R}_i^2}{d^4})\frac{\mathbf{R}_j^2}{2(\frac{1}{2d^2}+2p)} - \frac{20\mathbf{R}_j^2}{d^4(\frac{1}{2d^2}+2p)^2}\},$$

$$F_4(\mathbf{R}_i) = 4m + n^4\{\frac{225E_c}{(4p)^4}(\frac{\pi}{2p})^3 - \frac{\pi^3}{3}\left(\frac{225A}{16(2p+B)^{\frac{7}{2}}(2p)^{\frac{7}{2}}} + \frac{225\overline{c}}{16(2p)^7} + \frac{1575c}{32(2p)^8}\right) + \frac{8}{2m}\left(\frac{105}{(8p)^3}\frac{31}{2} -$$
$$\frac{15}{64p^2}\frac{299}{16p} + \frac{3}{8p}\frac{685}{256p^2} - \frac{39690}{8p^3} + 32p^2\frac{10395}{(8p)^5} + \frac{315}{p^3} - \frac{6615}{(8p)^3}\right)(\frac{\pi}{4p})^3 + \frac{8\nabla^2_{\mathbf{R}_i}}{2m}\frac{225\pi^3}{16384p^7}\},$$

$$F_5(\mathbf{R}_i,\mathbf{R}_j) = \mathbf{R}_i^4\mathbf{R}_j^4 + \frac{945}{(8p)^4} + \frac{1}{(8p)^2}(15\mathbf{R}_i^4 + 15\mathbf{R}_j^4 - 36\mathbf{R}_i^2\mathbf{R}_j^2 - 32(\mathbf{R}_i.\mathbf{R}_j)^2) + \frac{1}{8p}(2\mathbf{R}_j^4\mathbf{R}_i^2$$
$$+ 2\mathbf{R}_i^4\mathbf{R}_j^2) + \frac{70}{(8p)^3}(\mathbf{R}_i^2 + \mathbf{R}_j^2),$$

$$F_6(\mathbf{R}_i,\mathbf{R}_j) = (-10A\exp(-B\overline{\mathbf{R}_i + \mathbf{R}_j}^2) - 10A\exp(-B\overline{\mathbf{R}_i - \mathbf{R}_j}^2))\{\frac{15}{(8p)^2}(\mathbf{R}_j^4 + \mathbf{R}_i^4 + 4\mathbf{R}_i^2\mathbf{R}_j^2)$$
$$+ \mathbf{R}_i^4\mathbf{R}_j^4 + \frac{6}{8p}(\mathbf{R}_i^6 + \mathbf{R}_i^4\mathbf{R}_j^2) + \frac{210}{(8p)^3}(\mathbf{R}_i^2 + \mathbf{R}_j^2) + \frac{945}{(8p)^4} - \frac{\mathbf{R}_j^4\mathbf{R}_i^2}{2p} - \frac{140\mathbf{R}_i^2}{(8p)^3} - 80\frac{\mathbf{R}_i^2\mathbf{R}_j^2}{(8p)^2}$$
$$- \frac{\mathbf{R}_i^4\mathbf{R}_j^2}{2p} - \frac{140\mathbf{R}_j^2}{(8p)^3} + \frac{32(\mathbf{R}_i.\mathbf{R}_j)^2}{(8p)^2} + \frac{16R_i^2R_j^2}{(8p)^2}\},$$

$$D(\mathbf{R}_i,\mathbf{R}_j)=\mathbf{R}_j^4+\mathbf{R}_i^4+4\mathbf{R}_i^2\mathbf{R}_j^2$$

$$D_1(\mathbf{R}_j)=\frac{10(2B\mathbf{R}_j)^2}{(2B+8p)^3}+\frac{(2B\mathbf{R}_j)^4}{(2B+8p)^4}+\frac{15}{(2B+8p)^2}$$

$$D_2(\mathbf{R}_i)=\frac{(2B\mathbf{R}_i)^2}{(2B+8p)^2}+\frac{3}{(2B+8p)}$$

$$D_3(\mathbf{R}_i)=\frac{(2B\mathbf{R}_i)^6}{(2B+8p)^6}+\frac{21(2B\mathbf{R}_i)^4}{(2B+8p)^5}+\frac{105}{(2B+8p)^3}+\frac{105(2B\mathbf{R}_i)^2}{(2B+8p)^4}$$

$$D_4(\mathbf{R}_i)=\frac{(2B\mathbf{R}_i)^8}{(2B+8p)^8}+\frac{36(2B\mathbf{R}_i)^6}{(2B+8p)^7}+\frac{378(2B\mathbf{R}_i)^4}{(2B+8p)^6}+\frac{1260(2B\mathbf{R}_i)^2}{(2B+8p)^5}+\frac{945}{(2B+8p)^4}$$

$$D_5(\mathbf{R}_i,\mathbf{R}_j)=\frac{(2B)^2(\mathbf{R}_i.\mathbf{R}_j)^2}{(2B+8p)^2}+\frac{3\mathbf{R}_i^2}{(2B+8p)}$$

$$D_6(\mathbf{R}_i,\mathbf{R}_j)=\frac{(2B)^6(\mathbf{R}_i.\mathbf{R}_j)^2\mathbf{R}_j^4}{(2B+8p)^6}+\frac{(2B)^4}{(2B+8p)^5}(18\mathbf{R}_j^2(\mathbf{R}_i.\mathbf{R}_j)^2+\mathbf{R}_i^2\mathbf{R}_j^4)+\frac{(2B)^2}{(2B+8p)^4}(63(\mathbf{R}_i.\mathbf{R}_j)^2$$
$$+14\mathbf{R}_i^2\mathbf{R}_j^2+x_i^2x_j^2+y_i^2y_j^2+z_i^2z_j^2)+\frac{35\mathbf{R}_i^2}{(2B+8p)^3}$$

$$D_7(\mathbf{R}_i,\mathbf{R}_j)=\frac{(2B)^4}{(2B+8p)^4}\mathbf{R}_j^2(\mathbf{R}_i.\mathbf{R}_j)^2+\frac{(2B)^2}{(2B+8p)^3}(7(\mathbf{R}_i.\mathbf{R}_j)^2+\mathbf{R}_i^2\mathbf{R}_j^2)+\frac{5\mathbf{R}_i^2}{(2B+8p)^2}$$

$$D_8(\mathbf{R}_j)=\frac{(2B)^2\mathbf{R}_j^4}{(2B+8p)^2}+\frac{\mathbf{R}_j^2}{2B+8p}$$

$$D_9(\mathbf{R}_j)=\frac{35\mathbf{R}_j^2}{(2B+8p)^3}+\frac{(2B)^6}{(2B+8p)^6}\mathbf{R}_j^8+\frac{19(2B)^4}{(2B+8p)^5}\mathbf{R}_j^6+\frac{77(2B)^2}{(2B+8p)^4}\mathbf{R}_j^4$$

$$D_{10}(\mathbf{R}_j)=\frac{(2B)^4}{(2B+8p)^4}\mathbf{R}_j^6+\frac{(2B)^2}{(2B+8p)^3}\mathbf{R}_j^4+\frac{5}{(2B+8p)^2}\mathbf{R}_j^2$$

$$D_{11}(\mathbf{R}_i,\mathbf{R}_j)=\frac{(2B)^4}{(2B+8p)^4}\mathbf{R}_j^4(\mathbf{R}_i.\mathbf{R}_j)^2+\frac{(2B)^2}{(2B+8p)^3}(5\mathbf{R}_j^2(\mathbf{R}_i.\mathbf{R}_j)^2+\mathbf{R}_i^2\mathbf{R}_j^4)$$
$$+\frac{1}{(2B+8p)^2}(2(\mathbf{R}_i.\mathbf{R}_j)^2+\mathbf{R}_i^2\mathbf{R}_j^2)$$

$$D_{12}(\mathbf{R}_i,\mathbf{R}_j)=\frac{1}{2048p^3}\Big\{-9975+32768p^5\mathbf{R}_i^4\mathbf{R}_j^4(R_i^2+R_j^2)+40p(287R_i^2+31R_j^2)+4096p^4(2R_i^6R_j^2-$$
$$43R_i^4R_j^4+2R_i^2R_j^6)+512p^3(R_i^2+R_2^j)(15R_i^4-14R_i^2R_j^2+15R_j^4+16(2(\mathbf{R}_i.\mathbf{R}_j)^2+\mathbf{R}_i^2\mathbf{R}_j^2))-$$
$$64p^2\Big(287R_i^4-772R_i^2R_j^2+287R_j^4+672\big(2(\mathbf{R}_i.\mathbf{R}_j)^2+\mathbf{R}_i^2\mathbf{R}_j^2\big)-1024\big(7\mathbf{R}_i^2\mathbf{R}_j^2+14(\mathbf{R}_i.\mathbf{R}_j)^2\big)\Big)\Big\}.$$

APPENDIX C

Solving the Integral Equation

By taking the three dimensional Fourier transform of eqs.(21,23) with respect to $\mathbf{R}_1$ and eqs.(22,24) with respect to $\mathbf{R}_2$, these integral equations become

$$(-E_c-8Cd^2-\frac{8}{3}\overline{C}+\frac{P_1^2}{2m}+\frac{3}{2}\omega+4m)\chi_1(\mathbf{P}_1)+\frac{1}{(2\pi)^{\frac{3}{2}}}\Big(\frac{1}{\pi d^2(1+4\bar{k}d^2)}\Big)^{\frac{3}{2}}\int d^3\mathbf{R}_1d^3\mathbf{R}_2\exp(\imath\mathbf{P}_1.\mathbf{R}_1)$$
$$\exp\Big(\frac{-(1+8\bar{k}d^2)(\mathbf{R}_1^2+\mathbf{R}_2^2)}{2d^2}\Big)[-\frac{E_c}{3}-\frac{8Cd^2}{3(1+4\bar{k}d^2)}+\frac{4m}{3}-\frac{8}{9}\overline{C}+\frac{1+4\bar{k}d^2}{6md^2}\Big(\frac{15}{2}-(\mathbf{R}_1^2+\mathbf{R}_2^2)$$
$$(\frac{1+4\bar{k}d^2}{d^2})\Big)]\chi_2(\mathbf{R}_2)+\frac{1}{(2\pi)^{\frac{3}{2}}}\int d^3\mathbf{R}_1d^3\mathbf{R}_2\exp(\imath\mathbf{P}_1.\mathbf{R}_1)\exp(\frac{-\mathbf{R}_2^2}{2d^2})\exp(-2p\mathbf{R}_1^2)\frac{8f^6n^2}{18\sqrt{2}(2\pi d^2)^{\frac{3}{2}}}$$
$$[(\frac{\pi}{\frac{1}{2d^2}+2p})^{\frac{3}{2}}F_1(\mathbf{R}_1,\mathbf{R}_2)-2\Lambda E(\mathbf{R}_1,\mathbf{R}_2)]\chi_2^*(\mathbf{R}_2)=0, \tag{C1}$$

$$(-E_c - 8Cd^2 - \frac{8}{3}\overline{C} + \frac{P_2^2}{2m} + \frac{3}{2}\omega + 4m)\chi_2(\mathbf{P}_2) + \frac{1}{(2\pi)^{\frac{3}{2}}}\left(\frac{1}{\pi d^2(1+4\overline{k}d^2)}\right)^{\frac{3}{2}}\int d^3\mathbf{R}_1 d^3\mathbf{R}_2 \exp(\imath\mathbf{P}_2.\mathbf{R}_2)$$
$$\exp\left(\frac{-(1+8\overline{k}d^2)(\mathbf{R}_1^2+\mathbf{R}_2^2)}{2d^2}\right)[-\frac{E_c}{3} - \frac{8Cd^2}{3(1+4\overline{k}d^2)} + \frac{4m}{3} - \frac{8}{9}\overline{C} + \frac{1+4\overline{k}d^2}{6md^2}\left(\frac{15}{2} - (\mathbf{R}_1^2+\mathbf{R}_2^2)\right.$$
$$\left.(\frac{1+4\overline{k}d^2}{d^2})\right)]\chi_1(\mathbf{R}_1) + \frac{1}{(2\pi)^{\frac{3}{2}}}\int d^3\mathbf{R}_1 d^3\mathbf{R}_2 \exp(\imath\mathbf{P}_2.\mathbf{R}_2)\exp(\frac{-\mathbf{R}_1^2}{2d^2})\exp(-2p\mathbf{R}_2^2)\frac{8f^4n^2}{18\sqrt{2}(2\pi d^2)^{\frac{3}{2}}}$$
$$[(\frac{\pi}{\frac{1}{2d^2}+2p})^{\frac{3}{2}}F_1(\mathbf{R}_2,\mathbf{R}_1) - 2AE(\mathbf{R}_2,\mathbf{R}_1)]\chi_1^*(\mathbf{R}_1) = 0, \tag{C2}$$

$$\left(4m + n^4\{\frac{225E_c}{(4p)^4}(\frac{\pi}{2p})^3 - \frac{\pi^3}{3}\left(\frac{225A}{16(2p+B)^{\frac{7}{2}}(2p)^{\frac{7}{2}}} + \frac{225\overline{c}}{16(2p)^7} + \frac{1575c}{32(2p)^8}\right) + \frac{8}{2m}(\frac{105}{(8p)^3}\frac{31}{2} - \frac{15}{64p^2}\frac{299}{16p}\right.$$
$$\left. + \frac{3}{8p}\frac{685}{256p^2} - \frac{39690}{8p^3} + 32p^2\frac{10395}{(8p)^5} + \frac{315}{p^3} - \frac{6615}{p^4})(\frac{\pi}{4p})^3 - \frac{8P_{1s}^2}{2m}\frac{225\pi^3}{16384p^7}\}\right)\chi_1^*(\mathbf{P}_{1s})$$
$$+ \frac{1}{(2\pi)^{\frac{3}{2}}}\frac{8f^4n^2}{18\sqrt{2}(2\pi d^2)^{\frac{3}{2}}}\int d^3\mathbf{R}_1 d^3\mathbf{R}_2 \exp(\imath\mathbf{P}_{1s}.\mathbf{R}_1)\exp(\frac{-\mathbf{R}_1^2}{2d^2})\exp(-2p\mathbf{R}_2^2)[.....]\chi_2(\mathbf{R}_2)$$
$$+ \frac{1}{(2\pi)^{\frac{3}{2}}}\frac{8f^4n^4}{3}\int d^3\mathbf{R}_1 d^3\mathbf{R}_2 \exp(\imath\mathbf{P}_{11}.\mathbf{R}_1)\exp(-2p\mathbf{R}_1^2)\exp(-2p\mathbf{R}_2^2)[.....]\chi_2^*(\mathbf{R}_2) = 0, \tag{C3}$$

$$\left(4m + n^4\{\frac{225E_c}{(4p)^4}(\frac{\pi}{2p})^3 - \frac{\pi^3}{3}\left(\frac{225A}{16(2p+B)^{\frac{7}{2}}(2p)^{\frac{7}{2}}} + \frac{225\overline{c}}{16(2p)^7} + \frac{1575c}{32(2p)^8}\right) + \frac{8}{2m}(\frac{105}{(8p)^3}\frac{31}{2} - \frac{15}{64p^2}\frac{299}{16p}\right.$$
$$\left. + \frac{3}{8p}\frac{685}{256p^2} - \frac{39690}{8p^3} + 32p^2\frac{10395}{(8p)^5} + \frac{315}{p^3} - \frac{6615}{p^4})(\frac{\pi}{4p})^3 - \frac{8P_{2s}^2}{2m}\frac{225\pi^3}{16384p^7}\}\right)\chi_2^*(\mathbf{P}_{2s})$$
$$+ \frac{1}{(2\pi)^{\frac{3}{2}}}\frac{8f^4n^2}{18\sqrt{2}(2\pi d^2)^{\frac{3}{2}}}\int d^3\mathbf{R}_1 d^3\mathbf{R}_2 \exp(\imath\mathbf{P}_{2s}.\mathbf{R}_2)\exp(\frac{-\mathbf{R}_2^2}{2d^2})\exp(-2p\mathbf{R}_1^2)[.....]\chi_1(\mathbf{R}_1)$$
$$+ \frac{1}{(2\pi)^{\frac{3}{2}}}\frac{8f^4n^4}{3}\int d^3\mathbf{R}_1 d^3\mathbf{R}_2 \exp(\imath\mathbf{P}_{22}.\mathbf{R}_2)\exp(-2p\mathbf{R}_1^2 - 2p\mathbf{R}_2^2)[.....]\chi_1^*(\mathbf{R}_1) = 0, \tag{C4}$$

where $\chi(\mathbf{P})$ is the fourier transform of $\chi(\mathbf{R})$. P_1,P_2 are conjugate to R_1, R_2 for ground state gluonic field and P_{1s}, P_{2s} are conjugate to R_1, R_2 for excited state gluonic field. The off-diagonal terms of eq.(C3) and (C4) are too lengthy and not used for results, so dots are used to reduce the length of equations. The above eqs.(C1-C4) have formal solutions as [15]

$$\chi_1(\mathbf{P}_1) = \delta(P_1 - P_c(1))/P_c^2(1) - \frac{1}{\triangle_1(P_1)}\frac{1}{(2\pi)^{\frac{3}{2}}}\left(\frac{1}{\pi d^2(1+4\overline{k}d^2)}\right)^{\frac{3}{2}}\int d^3\mathbf{R}_1 d^3\mathbf{R}_2 \quad \exp(\imath\mathbf{P}_1.\mathbf{R}_1)$$
$$\exp\left(\frac{-(1+8\overline{k}d^2)(\mathbf{R}_1^2+\mathbf{R}_2^2)}{2d^2}\right)[-\frac{E_c}{3} - \frac{8Cd^2}{3(1+4\overline{k}d^2)} + \frac{4m}{3} - \frac{8}{9}\overline{C} + \frac{1+4\overline{k}d^2}{6md^2}\left(\frac{15}{2} - (\mathbf{R}_1^2+\mathbf{R}_2^2)\right.$$
$$\left.(\frac{1+4\overline{k}d^2}{d^2})\right)]\chi_2(\mathbf{R}_2) - \frac{1}{\triangle_1(P_1)}\frac{1}{(2\pi)^{\frac{3}{2}}}\int d^3\mathbf{R}_1 d^3\mathbf{R}_2 \exp(\imath\mathbf{P}_1.\mathbf{R}_1) \quad \exp(\frac{-R_2^2}{2d^2}) \quad \exp(-2pR_1^2)$$
$$\frac{8f^4n^2}{18\sqrt{2}(2\pi d^2)^{\frac{3}{2}}}[(\frac{\pi}{\frac{1}{2d^2}+2p})^{\frac{3}{2}}F_1(\mathbf{R}_1,\mathbf{R}_2) - 2AE(\mathbf{R}_1,\mathbf{R}_2)]\chi_2^*(\mathbf{R}_2), \tag{C5}$$

$$\chi_2(P_2) = \delta(P_2 - P_c(2))/P_c^2(2) - \frac{1}{\triangle_2(P_2)}\frac{1}{(2\pi)^{\frac{3}{2}}}\left(\frac{1}{\pi d^2(1+4\bar{k}d^2)}\right)^{\frac{3}{2}}\int d^3\mathbf{R}_1 d^3\mathbf{R}_2 \quad \exp(\imath\mathbf{P}_2.\mathbf{R}_2)$$
$$\exp\left(\frac{-(1+8\bar{k}d^2)(\mathbf{R}_1^2+\mathbf{R}_2^2)}{2d^2}\right)[-\frac{E_c}{3} - \frac{8Cd^2}{3(1+4\bar{k}d^2)} + \frac{4m}{3} - \frac{8}{9}\bar{C} + \frac{1+4\bar{k}d^2}{6md^2}\left(\frac{15}{2} - (\mathbf{R}_1^2+\mathbf{R}_2^2)\right.$$
$$\left.(\frac{1+4\bar{k}d^2}{d^2})\right)]\chi_1(\mathbf{R}_1) - \frac{1}{\triangle_2(P_2)}\frac{1}{(2\pi)^{\frac{3}{2}}}\int d^3\mathbf{R}_1 d^3\mathbf{R}_2 \exp(\imath\mathbf{P}_2.\mathbf{R}_2) \quad \exp(\frac{-R_1^2}{2d^2}) \quad \exp(-2pR_2^2)$$
$$\frac{8f^n n^2}{18\sqrt{2}(2\pi d^2)^{\frac{3}{2}}}[(\frac{\pi}{\frac{1}{2d^2}+2p})^{\frac{3}{2}}F_1(\mathbf{R}_2,\mathbf{R}_1) - 2AE(\mathbf{R}_2,\mathbf{R}_1)]\chi_1^*(\mathbf{R}_1), \tag{C6}$$

$$\chi_1^*(P_{1s}) = \delta(P_{1s} - P_c(1s))/P_c^2(1s) - \frac{1}{\triangle_1(P_{1s})}\frac{1}{(2\pi)^{\frac{3}{2}}}\frac{8f^n n^2}{18\sqrt{2}(2\pi d^2)^{\frac{3}{2}}}\int d^3\mathbf{R}_1 d^3\mathbf{R}_2 \exp(\imath\mathbf{P}_{1s}.\mathbf{R}_1)$$
$$\exp(\frac{-R_1^2}{2d^2})\exp(-2pR_2^2)[.....]\chi_2(\mathbf{R}_2) - \frac{1}{\triangle_1(P_{1s})}\frac{8f^n n^4}{3}\frac{1}{(2\pi)^{\frac{3}{2}}}\int d^3\mathbf{R}_1 d^3\mathbf{R}_2 \exp(\imath\mathbf{P}_{1s}.\mathbf{R}_1) \tag{C7}$$
$$\exp(-2pR_1^2)\exp(-2pR_2^2)[.....]\chi_2^*(\mathbf{R}_2),$$

$$\chi_2^*(P_{2s}) = \delta(P_{2s} - P_c(2s))/P_c^2(2s) - \frac{1}{\triangle_2(P_{2s})}\frac{1}{(2\pi)^{\frac{3}{2}}}\frac{8f^n n^2}{18\sqrt{2}(2\pi d^2)^{\frac{3}{2}}}\int d^3\mathbf{R}_1 d^3\mathbf{R}_2 \exp(\imath\mathbf{P}_{2s}.\mathbf{R}_2)$$
$$\exp(\frac{-R_2^2}{2d^2})\exp(-2pR_1^2)[.....]\chi_1(\mathbf{R}_1) - \frac{1}{\triangle_2(Pf_{2s})}\frac{8f^n n^4}{3}\frac{1}{(2\pi)^{\frac{3}{2}}}\int d^3\mathbf{R}_1 d^3\mathbf{R}_2 \exp(\imath\mathbf{P}_{2s}.\mathbf{R}_2) \tag{C8}$$
$$\exp(-2pR_2^2)\exp(-2pR_1^2)[.....]\chi_1^*(\mathbf{R}_1),$$

where

$$\triangle_1(\mathbf{P}_i) = (-E_c - 8Cd^2 - \frac{8}{3}\bar{C} + \frac{\mathbf{P}_i^2}{2m} + \frac{3}{2}\omega + 4m) - \imath\varepsilon,$$
$$\triangle_2(\mathbf{P}_{1s}) = 4m + n^4\{\frac{225E_c}{(4p)^4}(\frac{\pi}{2p})^3 - \frac{\pi^3}{3}\left(\frac{225A}{16(2p+B)^{\frac{7}{2}}(2p)^{\frac{7}{2}}} + \frac{225\bar{c}}{16(2p)^7} + \frac{1575c}{32(2p)^8}\right) + \frac{4}{m}\left(\frac{105}{(8p)^3}\frac{31}{2} -\right.$$
$$\left.\frac{15}{64p^2}\frac{299}{16p} + \frac{3}{8p}\frac{685}{256p^2} - \frac{39690}{8p^3} + 32p^2\frac{10395}{(8p)^5} + \frac{315}{p^3} - \frac{6615}{(8p)^3}\right)(\frac{\pi}{4p})^3 - \frac{8(\mathbf{P}_{1s})^2}{2m}\frac{225\pi^3}{16384p^7}\} - \imath\varepsilon, \tag{C9}$$

and

$$P_c(2) = P_c(1) = \sqrt{2m(E_c - 4m - \frac{3}{md^2} + \frac{8}{3}\bar{C})},$$
$$P_c(2s) = P_c(1s) = \sqrt{2m(E_c - 4m) - \left(0.6667\bar{C} + \frac{1.1667C}{p} + \frac{13.682p^{7/2}}{(0.0657+2p)^{7/2}}\right)m - 64p.} \tag{C10}$$

Using the Born approximation, the integration on $\mathbf{R}_1$ and $\mathbf{R}_2$ in eq.(C5) can be performed to give

$$\chi_1(\mathbf{P}_1) = \delta(P_1 - P_c(1))/P_c^2(1) - \frac{1}{\triangle_1(P_1)}\left[\frac{1}{3}(\frac{2}{\pi})^{\frac{1}{2}}(\frac{1}{2\pi})^{\frac{3}{2}}\left(\frac{1}{\pi d^2(1+4\bar{k}d^2)}\right)^{\frac{3}{2}}\left(\frac{2\pi d^2}{1+8\bar{k}d^2}\right)^3\exp\left(-\frac{(p_1^2+p_2^2)d^2}{2(1+8\bar{k}d^2)}\right)\right.$$
$$\left.\Omega_1\right] - \frac{1}{\triangle_1(P_1)}\frac{1}{3}(\frac{2}{\pi})^{\frac{1}{2}}(\frac{1}{\pi d^2})^{\frac{3}{2}}f^a n^2(\frac{1}{2\pi})^{\frac{3}{2}}\left[\exp(\frac{-P_{1s}^2 d^2}{2})(2\pi d^2)^{\frac{3}{2}}\left((\frac{\pi}{2p+\frac{1}{2d^2}})^{\frac{3}{2}}F(p) - \frac{4A}{6\sqrt{2}}F_1(p)\right)\right.$$
$$- \frac{4A}{6\sqrt{2}}(\frac{\pi}{2p+\frac{1}{2d^2}})^{\frac{3}{2}}\exp(\frac{-p_1^2}{8p+4B})(\frac{\pi}{2p+B})^{\frac{3}{2}}(\frac{\pi}{F_2(p)})^{\frac{3}{2}}\exp(\frac{(\imath P_{1s} - 4\imath\frac{P_1 B}{8p+4B})^2}{4F_2(p)})\Omega_2 - \frac{4A}{6\sqrt{2}}(\frac{\pi}{2p+\frac{1}{2d^2}})^{\frac{3}{2}}$$
$$\exp(\frac{-P_1^2}{8p+4B})(\frac{\pi}{2p+B})^{\frac{3}{2}}(\frac{\pi}{F_2(p)})^{\frac{3}{2}}\exp(\frac{(\imath P_{1s} + 4\imath\frac{P_1 B}{8p+4B})^2}{4F_2(p)})\Omega_3 + \frac{16A}{3\sqrt{2}}(\frac{\pi}{F_3(p)})^{\frac{3}{2}}\exp(\frac{-P_1^2}{8p})(\frac{\pi}{2p})^{\frac{3}{2}}\Omega_4\Big]$$
$$(\frac{\pi}{B+\frac{1}{2d^2}-\frac{B^2}{F_3(p)}})^{\frac{3}{2}}\exp(\frac{-P_{1s}^2}{4(B+\frac{1}{2d^2}-\frac{B^2}{F_3(p)})}). \tag{C11}$$

Here,

$$\Omega_1 = -E_c - \frac{8Cd^2}{(1+4\bar{k}d^2)} + \frac{8}{3}C + 4m + \frac{15(1+4\bar{k}d^2)}{4md^2} - (\frac{(1+4\bar{k}d^2)^2}{2md^4})(\frac{-P_1^2d^4 - P_2^2d^4}{(1+8\bar{k}d^2)^2} + \frac{6d^2}{1+8\bar{k}d^2})$$

$$\Omega_2 = \left(\frac{-5P_1^2}{4(2p+B)^3} + \frac{15}{4(2p+B)^2} + \frac{15}{4(\frac{1}{2d^2}+2p)^2} - \frac{P_1^2}{4(2p+B)^2(\frac{1}{2d^2}+2p)} + \frac{3}{2(2p+B)(\frac{1}{2d^2}+2p)}\right) +$$
$$\left(\frac{5B^2}{(2p+B)^3} + \frac{4B^2}{4(2p+B)^2(\frac{1}{2d^2}+2p)}\right)\left(\frac{\iota P_{1s} - \frac{4\iota P_1 B}{8p+4B}}{4F_2^2(p)} + \frac{3}{2F_2(p)}\right) + \left(\frac{-10\iota B}{4(2p+B)^3} + \right.$$
$$\left.\frac{2\iota B}{4(2p+B)^2(\frac{1}{2d^2}+2p)}\right)\left(\frac{-2\iota P_1^2 B}{4(2p+B)} + \iota P_1.P_{1s}\right)\frac{1}{2F_2(p)} + \frac{1}{16(2p+B)^4}\left\{P_1^4 + 16B^4\left(\frac{5(\iota P_{1s} - \frac{4\iota P_1 B}{8p+4B})^2}{4F_2^3(p)}\right.\right.$$
$$\left.+ \frac{(\iota P_{1s} - \frac{4\iota P_1 B}{8p+4B})^4}{16F_2^4(p)} + \frac{15}{4F_2^2(p)}\right) - 8B^2P_1^2\left(\frac{(\iota P_{1s} - \frac{4\iota P_1 B}{8p+4B})^2}{4F_2^2(p)} + \frac{3}{2F_2(p)}\right) + 8BP_1^2\iota$$
$$\left(\frac{-2\iota P_1^2\frac{B}{8p+4B} + \iota P_1.P_{1s}}{2F_2(p)}\right) - 32\iota B^3(P_{1x}+P_{1y}+P_{1z})\left(\left(\frac{\iota B^3P_1^3}{(2p+B)^3} - \frac{B^2\iota}{(2p+B)^2}P_1^2(P_{1sx}+P_{1sy}+P_{1sz})\right.\right.$$
$$- 64\frac{B^2\iota}{(8p+4B)^2}P_1(P_1.P_{1s}) + \frac{16\iota B}{8p+4B}(P_1.P_{1s})P_{1s} + \frac{4\iota B}{8p+4B}(P_{1x}+P_{1y}+P_{1z})P_{1s}^2 - \iota P_{1s}^3\Big)\frac{1}{8F_2(p)^3}$$
$$\left.\left.+ \frac{(\iota P_{1s} - 4\iota\frac{P_1 B}{8p+4B})}{F_2(p)^2}\right) - 16B^2\left(P_1^2\frac{(\iota P_{1s} - 4\iota\frac{P_1 B}{8p+4B})^2}{4F_2(p)^2} + \frac{P_1^2}{2F_2(p)}\right)\right\}$$

$$\Omega_3 = \left(\frac{-5P_1^2}{4(2p+B)^3} + \frac{15}{4(2p+B)^2} + \frac{15}{4(\frac{1}{2d^2}+2p)^2} - \frac{P_1^2}{4(2p+B)^2(\frac{1}{2d^2}+2p)}\right.$$
$$\left.+ \frac{3}{2(2p+B)(\frac{1}{2d^2}+2p)}\right) + \left(\frac{5B^2}{(2p+B)^3} + \frac{4B^2}{4(2p+B)^2(\frac{1}{2d^2}+2p)}\right)\left(\frac{\iota P_{1s} + \frac{4\iota P_1 B}{8p+4B}}{4F_2^2(p)} + \frac{3}{2F_2(p)}\right)$$
$$+ \left(\frac{-10\iota B}{4(2p+B)^3} + \frac{2\iota B}{4(2p+B)^2(\frac{1}{2d^2}+2p)}\right)\left(\frac{-2\iota P_1^2 B}{4(2p+B)} + \iota P_1.P_{1s}\right)\frac{1}{2F_2(p)} + \frac{1}{16(2p+B)^4}\left\{P_1^4\right.$$
$$+ 16B^4\left(\frac{5(\iota P_{1s} + \frac{4\iota P_1 B}{8p+4B})^2}{4F_2^3(p)} + \frac{(\iota P_{1s} + \frac{4\iota P_1 B}{8p+4B})^4}{16F_2^4(p)} + \frac{15}{4F_2^2(p)}\right) - 8B^2P_1^2\left(\frac{(\iota P_{1s} + \frac{4\iota P_1 B}{8p+4B})^2}{4F_2^2(p)} + \frac{3}{2F_2(p)}\right)$$
$$- 8BP_1^2\iota\left(\frac{2\iota P_1^2\frac{B}{8p+4B} + \iota P_1.P_{1s}}{2F_2(p)}\right) + 32\iota B^3(P_{1x}+P_{1y}+P_{1z})\left(\left(\frac{-\iota B^3P_1^3}{(2p+B)^3} - \frac{B^2\iota}{(2p+B)^2}P_1^2(P_{1sx}\right.\right.$$
$$+ P_{1sy} + P_{1sz}) - 64\frac{B^2\iota}{(8p+4B)^2}P_1(P_1.P_{1s}) - \frac{16\iota B}{8p+4B}(P_1.P_{1s})P_{1s} - \frac{4\iota B}{8p+4B}(P_{1x}+P_{1y}+P_{1z})P_{1s}^2$$
$$\left.\left.- \iota P_{1s}^3\right)\frac{1}{8F_2(p)^3} + \frac{(\iota P_{1s} + 4\iota\frac{P_1 B}{8p+4B})}{F_2(p)^2}\right) - 16B^2\left(P_1^2\frac{(\iota P_{1s} + 4\iota\frac{P_1 B}{8p+4B})^2}{4F_2(p)^2} + \frac{P_1^2}{2F_2(p)}\right)\right\}$$

$$\Omega_4 = \frac{15}{2F_3^2(p)} - \frac{10P_1^2}{32p^3} + \frac{2P_1^4}{(4p)^4} + \frac{30}{16p^2} - \frac{2}{F_3(p)}(\frac{-P_1^2}{16p^2} + \frac{3}{4p}) + \left(\frac{10B^2}{F_3^3(p)} - \frac{8B^2}{4pF_3^2(p)}\right.$$
$$\left.(1 - \frac{P_1^2}{4p}) + \frac{4B^2}{F_3^2(p)}(\frac{-P_1^2}{16p^2} + \frac{3}{4p})\right)\left(\frac{P_{1s}^2}{4B - 4\frac{B^2}{F_3(p)}} + \frac{3}{2B - 2\frac{B^2}{F_3(p)}}\right) + \frac{2B^4}{F_3^4(p)}\left(\frac{5P_{1s}^2}{4(B - \frac{B^2}{F_3(p)})^3}\right.$$
$$\left.+ \frac{P_{1s}^4}{16(B - \frac{B^2}{F_3(p)})^4} + \frac{15}{4(B - \frac{B^2}{F_3(p)})^2}\right)$$

$$F(p) = \Big\{\Big(\frac{-5P_1^2}{32p^3} + \frac{P_1^4}{16(2p)^4} + \frac{15}{16p^2}\Big)\Big(E + \frac{24\bar{c}}{6\sqrt{2}} + \frac{42c}{6\sqrt{2}(\frac{1}{2d^2}+2p)} - \frac{28p}{m} - \frac{3}{2md^2} + \frac{20p^2}{m(\frac{1}{2d^2}+2p)}$$
$$- \frac{8c}{6\sqrt{2}(\frac{1}{2d^2}+2p)} + (\frac{28c}{6\sqrt{2}} + \frac{1}{2md^4})(-P_{11}^2d^4 + 3d^2)\Big) + \Big(\frac{15E}{4(\frac{1}{2d^2}+2p)^2} + \frac{420c}{24\sqrt{2}(\frac{1}{2d^2}+2p)^2}$$
$$(-P_{1s}^2d^4 + 3d^2) + \frac{90\bar{c}}{6\sqrt{2}(\frac{1}{2d^2}+2p)^2} + \frac{2940c}{48\sqrt{2}(\frac{1}{2d^2}+2p)^3} + \frac{72}{4m(\frac{1}{2d^2}+2p)} - \frac{105p}{m(\frac{1}{2d^2}+2p)^2}$$
$$+ \frac{105p^2}{m(\frac{1}{2d^2}+2p)^3}\Big) + \Big(\frac{-P_1^2}{16p^2} + \frac{3}{4p}\Big)\Big(\frac{E}{(\frac{1}{2d^2}+2p)} - \frac{28c}{6\sqrt{2}(\frac{1}{2d^2}+2p)}(-P_{11}^2d^4 + 3d^2) + \frac{12}{m}$$
$$+ \frac{24\bar{c}}{6\sqrt{2}(\frac{1}{2d^2}+2p)} - \frac{120c}{24\sqrt{2}(\frac{1}{2d^2}+2p)^2} + \frac{70c}{6\sqrt{2}(\frac{1}{2d^2}+2p)^2} - \frac{28p}{m(\frac{1}{2d^2}+2p)} + \frac{50p^2}{m(\frac{1}{2d^2}+2p)^2}\Big)$$
$$+ \Big(\frac{8p^2}{m} - \frac{8c}{6\sqrt{2}}\Big)\Big(-\frac{P_1^6}{(4p)^6} + \frac{21P_1^4}{(4p)^5} + \frac{105}{(4p)^3} - \frac{105P_1^2}{(4p)^4}\Big)\Big\}(\frac{\pi}{2p})^{\frac{3}{2}}\exp(\frac{-P_1^2}{8p}),$$

$$F_1(p) = (\frac{\pi}{\frac{1}{2d^2}+2p+B})^{\frac{3}{2}}(\frac{\pi}{2p+B-\frac{B^2}{(\frac{1}{2d^2}+2p+B)}})^{\frac{3}{2}}\exp(\frac{-P_1^2}{4(2p+B-\frac{B^2}{(\frac{1}{2d^2}+2p+B)})})$$
$$\{(2 + \frac{2B^4}{(\frac{1}{2d^2}+2p+B)^4} - \frac{4B^2}{(\frac{1}{2d^2}+2p+B)^2})(\frac{-5P_1^2}{4(2p+B-\frac{B^2}{(\frac{1}{2d^2}+2p+B)})^3} + \frac{P_1^4}{16(2p+B-\frac{B^2}{(\frac{1}{2d^2}+2p+B)})^4}$$
$$+ \frac{15}{4(2p+B-\frac{B^2}{(\frac{1}{2d^2}+2p+B)})^2}) + (\frac{10B^2}{(\frac{1}{2d^2}+2p+B)^3} + \frac{2}{\frac{1}{2d^2}+2p+B})(\frac{-P_1^2}{4(2p+B-\frac{B^2}{(\frac{1}{2d^2}+2p+B)})^2}$$
$$+ \frac{3}{2(2p+B-\frac{B^2}{(\frac{1}{2d^2}+2p+B)})}) + \frac{15}{2(\frac{1}{2d^2}+2p+B)^2}\}, \quad \text{with}$$

$F_2(p) = \frac{1}{2d^2} + B - \frac{4B^2}{4(2p+B)}$, and $F_3(p) = \frac{1}{2d^2} + 2p + B$.
Now from this eq.(C11) the elements of transition matrix (T) can be found. As shown in ref. [14], the gluonic excitations are orthogonal to the ground states i.e.

$$\langle 1 \mid 1^* \rangle = \langle 1^* \mid 1 \rangle = \langle 2 \mid 2^* \rangle = \langle 2^* \mid 2 \rangle = 0.$$

This gives

$$T_{11^*} = T_{1^*1} = T_{22^*} = T_{2^*2} = 0.$$

Thus the only possible transition amplitudes are T_{11}, T_{12}, T_{21}, T_{22}, T_{12^*} and T_{21^*}. As the eq.(C5) and (C6) are similar (interchanging $\mathbf{R}_1$ and $\mathbf{R}_2$ in eq.(C5) gives eq.(C6)), so

$$T_{11} = T_{22},$$
$$T_{12} = T_{21},$$

and

$$T_{12^*} = T_{21^*}.$$

References

[1] G. S. Bali, B. Bolder, N. Eicker, T. Lippert, B. Orth, P. Ueberholz, K. Schilling and T. Struckmann, Phys. Rev D **62**, 054503 (2000); G. S. Bali, Phys. Rep. **343**, 1 (2001).

[2] C. Alexandrou, Ph. de Forcrand, and O. John, Nucl. Phys. B **119**, 667 (2003).

[3] C. J. Morningstar, K. J. Juge, and J. Kuti, Nucl. Phys. Proc. Suppl. **73**, 590 (1999); K. J. Juge, J. Kuti, and C. Morningstar, Phys. Rev. Lett. **90**, 161601 (2003).

[4] N. Isgur and J. Paton, Phys. Rev. D **31**, 2910 (1985).

[5] J. F. Arvis, Phys. Lett. B **127**, 106 (1983); M. Luscher and P. Weisz, Jour. High Energy Phys. **07**, 014 (2004).

[6] K. J. Juge, J. Kuti, and C. Morningstar, in *Proceedings of AIP Conference*, 2003.

[7] A. M. Green and P. Pennanen, Phys. Rev. C **57**, 3384 (1998).

[8] A. M. Green, arXive:nucl-th/0409021v1 (2004).

[9] A. M. Green, J. Lukkarinen, P. Pennanen and C. Michael, Phys. Rev. D **53**, 261 (1996).

[10] P. Pennanen, Nucl. Phys. Proc. Suppl. **53**, 334 (1997).

[11] T. Barnes and E. S. Swanson, Phys. Rev. D **46**, 131 (1992).

[12] O. W. Greenberg and H. J. Lipkin, Nucl. Phys. A **370**, 349 (1981).

[13] A. M. Green, C. Michael, and J. E. Paton, Nucl. Phys. A **554**, 701 (1993).

[14] A. M. Green and P. Pennanen, Phys. Lett. B **426**, 243 (1998).

[15] B. Masud, J. Paton. A. M. Green, and G. Q. Liu, Nucl. Phy. A **528**, 477 (1991).

[16] B. Masud , Phys. Rev. D **50**, 6783 (1994).

[17] M. I. Jamil and B. Masud, Eur. Phys. Jour. A **47** (2011).

[18] K. J. Juge, J. Kuti, and C. Morningstar, Nucl. Phys. Proc. Suppl. **63** 326 (1998).

[19] C. Y. Wong, Phys. Rev. C **69**, 055202 (2004).

[20] J. Weinstein and N. Isgur, Phy. Rev. D **27**, 588 (1983).

[21] J. Weinstein and N. Isgur, Phy. Rev. D **41**, 2236 (1990).

[22] D. J. Gross and F. Wilczek, Phys. Rev. Lett. **30**, 1343 (1973).

[23] T. Barnes, S. Godfrey, and E. S. Swanson, Phys. Rev. D **72**, 054026 (2005).

[24] J. Vijande, A. Valcarce, and J. M. Richard, Phys. Rev. D **76**, 114013 (2007).

[25] E. S. Ackleh, T. Barnes, and E. S. Swanson, Phys. Rev. D **54**, 6811 (1996).

[26] V. G. Bornyakov, P. Yu. Boyko, M. N. Chernodub, and M. I. Polikarpov, arXiv:hep-lat/0508006v1 (2005).

[27] A. M. Green, J. Koponen, and P. Pennanen, Phys. Rev. D **61**, 014014 (1999).

[28] A. M. Green, H. J. Pirnal, G. A. Miller, B. Povh, F. Myhrer, W. Weise, J. A. Niskanen, K. Yazaki, and M. Oka, *Quarks and Nuclei*, edited by W. Weise (World Scientific Publishing Co.Pte Ltd, 1984), Vol. 1, Chap. 6.

[29] T. Barnes and E. S. Swanson, Phys. Rev. C **77**, 055206 (2008).

[30] P. Geiger, E. Swanson, Phys. Rev. D **50**, 6855 (1994)

Wave Function Based Characteristics of Hybrid Mesons

Nosheen Akbar* , Bilal Masud† , Saba Noor‡
Centre For High Energy Physics, University of the Punjab, Lahore(54590), Pakistan.

Abstract

We use an extension (fitted to the lattice data) of the quark potential model to hybrids for the purpose of calculating the masses, root mean square radii and radial wave functions at the origin of the conventional and hybrid charmonium mesons. We treat the ground and excited gluonic field between a quark and an antiquark as in the Born-Oppenheimer expansion, and use the shooting method to numerically solve the required Schrödinger equation for the radial wave functions. From these we calculate the above mentioned quantities; for masses we also check through a Crank Nichelson discretization. For hybrid charmonium mesons, we consider the exotic quantum number states with $J^{PC} = 0^{+-}, 1^{-+}$ and 2^{+-}. We also compare our results with the experimentally observed masses and theoretically predicted results of the other models. Our results have implications for scalar form factors, energy shifts, magnetic polarizabilities, decay constants, decay widths and differential cross sections of conventional and hybrid mesons; we accordingly include some results that can help in experimentally recognizing the hybrid mesons.

I. Introduction

A number of hadron properties are well described by the quark model where mesons have quantum numbers $J = L \oplus S$, $P = (-1)^{L+1}$, and $C = (-1)^{L+S}$, L and S being the quantum numbers for orbital angular momentum and spin angular momentum respectively. The states with $J^{PC} = 0^{+-}, 1^{-+}, 2^{+-}$ (for the lowest lying hybrids in the flux tube model) can not be formed from a $q\overline{q}$ pair and hence are not allowed in the quark model. These states are signals for a exotic mesons (hybrids, glueballs, etc). Quantum Chromodynamics (QCD), describing the interaction between the quarks and gluonic field, predicts the existence of hybrid mesons which contain the excited gluonic fields. Thus for understanding of QCD, we need finding experimentally testable predictions of the theory for situations in which the gluonic field between a quark and antiquark is in an excited state. Thus hybrids are an important source of information related to confining properties of QCD, and checking for existence of hybrid mesons is very important objective of particle physics. Reviews of the spectrum of excited gluonic states can be found in refs. [1] [2]. Recently, a resonance is observed at COMPASS [3] with $J^{PC} = 1^{-+}$. Some other groups like VES [4], E852 [5], and the Crystal Barrel collaboration [6] also observed these states. Using the Born-Oppenheimer expansion, the work of finding implication of QCD for a meson can be split into first using the numerical lattice simulations of QCD to write down a quark antiquark potential and then using this potential to calculate its dynamical implications. Even a numerically defined potential can be used in this scheme; this is what ref. [7] does. But we write an analytical coulombic plus linear plus exponentially falling expression for the excited state gluonic field potential between a quark and antiquark and fit its parameters to the lattice data for the excited state gluonic field energy values available in ref. [7] for discrete quark antiquark separations.

In the present paper, some characteristics (masses, root mean square radii and wave functions at the origin) obtainable through the numerically generated solutions of non-relativistic Schrödinger equation (also used in ref. [7]) for conventional and hybrid mesons are studied. An advantage of considering the charmonium mesons is indicated in ref. [8] as

> " The best systems for a hybrid search may be $c\overline{c}$ or $b\overline{b}$ where there is a large gap between the lowest states and the $D\overline{D}$ and $B\overline{B}$ threshod respectively."

*e mail: noshinakbar@yahoo.com
†e mail: bilalmasud@chep.pu.edu.pk
‡e mail: sabanoor87@gmail.com

To find the wave functions of conventional charmonium mesons, we use the realistic columbic plus linear potential model to solve the Schrödinger equation numerically by taking the corresponding quantum numbers of mesons. To study hybrids, we repeat the numerical work with the above mentioned columbic plus linear potential plus exponentially falling potential. From the numerically found wave functions, we calculate the root mean square radii. These radii can be used to find scalar form factors [9] for charmonium mesons, along with energy shifts [10] and magnetic polarizabilities [10]. Thus we have reported some predictions about these quantities for conventional and hybrid charmonium mesons. We have also found the numerical value of radial wave function at the origin ($|R(0)|^2$), which can be used to calculate the decay constants [11], decay rates [11], and differential cross sections [12] for quarkonium states. The predictions about these quantities are also reported for conventional and hybrid charmonium meson.

In the section II below, we write the Hamiltonian for the conventional mesons. Then we describe the shooting method-based numerical procedure to find the solution of the Schrödinger equation for conventional charmonium mesons. The expressions we used to find masses, root mean square radii, and square of radial wave functions at the origin ($|R(0)|^2$) of conventional charmonium mesons are also written in this section. In section III, the Hamiltonian is written for hybrid mesons, and then we redo all the numerical work as done in section II for hybrids now. Results for the masses, root mean square radii and $|R(0)|^2$ of conventional and hybrid mesons are reported in section IV for systems composed of charm quarks and antiquarks. Based on these results, we also include some results related to experimentally measurable quantities.

II. Characteristics of Conventional charmonium mesons

The Potential Model for Conventional Charmonium Meson

In the potential models, the confining potential for $Q\overline{Q}$ system in the the ground state gluonic field is mostly used in the form of

$$\frac{-4\alpha_s}{3r} + br + c, \tag{1}$$

with inter-quark distance r. Here, $-4/3$ is due to the color factor, α_s is the quark-gluon coupling, b is the string tension, and c is a constant. In above equation, the first term is due to one gluon exchange and the second term is the linear confining potential [13]. This potential form provides a good fit to the lattice simulations of refs. [14, 15]. By including the Gaussian-smeared hyperfine interaction [16] and orbital angular momentum (or centrifugal) term, the potential of the $Q\overline{Q}$ system in the ground state gluonic field have following form

$$V(r) = \frac{-4\alpha_s}{3r} + br + \frac{32\pi\alpha_s}{9m_c^2}(\frac{\sigma}{\sqrt{\pi}})^3 e^{-\sigma^2 r^2} S_c.S_{\overline{c}} + \frac{L(L+1)}{2\mu r^2}, \tag{2}$$

where $S_c.S_{\overline{c}} = \frac{S(S+1)}{2} - \frac{3}{4}$, μ is the reduced mass of the quark and antiquark, and m_c is the mass of the charm quark. For the $c\overline{c}$ mesons, the parameters α_s, b, σ, and m_c are taken to be 0.5461, 0.1425GeV^2, 1.0946 GeV, and 1.4796 GeV as in ref. [16]. The quantum numbers for the conventional charmonium mesons we choose for our study are reported below in Table 1.

Characteristics of conventional charmonium mesons

A conventional meson can be described by the wave function of the bound quark-antiquark state which satisfies the Schrödinger equation with potential of eq.(2). Radial Schrödinger equation with wave function $U(r) = rR(r)$ is written (in natural units) as

$$\nabla^2 U(r) + 2\mu(E - V(r))U(r) = 0. \tag{3}$$

R is the radial wave function and r is the interquark distance. Here E is the sum of kinetic and potential of quark-anti-quark system, and $V(r)$ and μ are defined above just after eq.(2).

In quark-antiquark bound state, the wave function must satisfy the boundary conditions $U(0) = 0$ and $U(\infty) = 0$. For the numerical solution of the Schrödinger equation with the potential of eq.(2)), energy E was repeatedly generated from -2 to 2 GeV in steps of 0.1 GeV. For each such trial initial energy, we

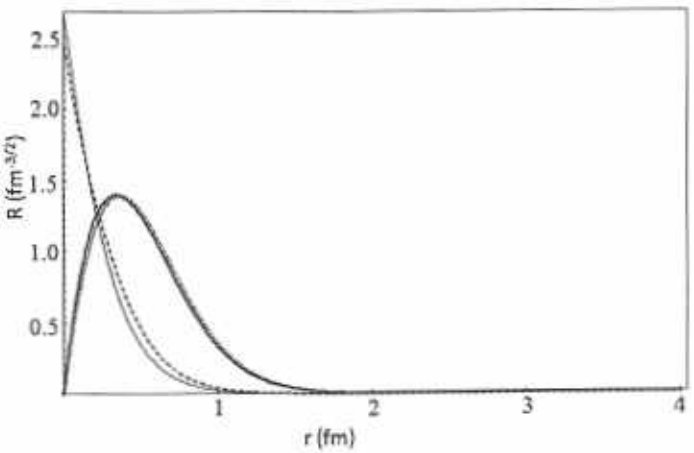

Figure 1: The radial part of η,J/ψ,h_c, and χ_c meson wave functions as functions of r. Thin solid line represents the η wave function, dashed line represents the J/ψ wave function, thick solid line represents the h_c wave function, and points represent the χ_c wave function.

used the Newton method [17] to select, if any, the energy for which the numerical solution of Schrödinger equation became zero at infinity. To obtain these numerical solutions, we used the RK method [18] with using any arbitrary integer value of $U'(0)$. For different values of $U'(0)$, normalized solutions of the Schrödinger equation, by multiplying the solution with the normalization constant $(\frac{1}{\sqrt{\int U^2(r)dr}})$, remain the same. These energy eigenvalues plus constituent quark masses are taken to be the $c\bar{c}$ mesons masses (in natural units). It is found that our results for conventional charmonium meson agree with the Table 1 of ref. [16] which support the reliability of our method. We also checked the consistency of our method by getting a 100% overlap of HU and EU and by calculating the masses of conventional meson by the Crank Nichelson Discritization and finding that masses obtained by both of the methods are identical. The Fig.1 shows the dependence of η, J/ψ, h_c, and χ_c normalized radial wave functions on the radial separation r. The quantum numbers (L and S) for these particles are given below in Table 1. These graphs show that the radial wave functions of η, h_c, χ_c, and J/ψ have the same properties as that of hydrogen atom radial wave function, i.e. they behave as r^L for small inter quark distances and decrease exponentially at large inter quark distances. Thin solid and Dashed lines graphs are for $L = 0$, so these graphs are similar to $r^0 exp(-r)$. Thick solid and points are for $L = 1$, so these graphs are similar to $r^1 exp(-r)$. As L increases, the wave function's peak goes away from the origin. This means that centrifugal term has more effects on wave function that that of the hyperfine term. One possible reason is that we are dealing with heavy quarks so the $1/m_c^2$ factor (shown in eq.(2)) of the hyperfine term becomes very small.

The normalized wave function is used in the further calculations for root mean square radii and radial wave functions at origin. To find the root mean square radii of the $c\bar{c}$ mesons, we used the following relation:

$$\langle r^2 \rangle = \sqrt{\int U^* r^2 U dr}. \tag{4}$$

In ref. [19], for normalized wave function

$$U'(0) = R(0) = \sqrt{4\pi}\psi(0) \tag{5}$$

is used. Thus the derivative of $U(r)$ at $r = 0$ is calculated for conventional charmonium mesons to find $|R(0)|^2$. $|R(0)|^2$ is used in many applications of high energy physics as mentioned in section I.

III. Characteristics of Hybrid Charmonium mesons

The Potential Model for Hybrid Charmonium Meson

The centrifugal factor for the hybrid mesons is written in refs. [20, 21] as

$$\frac{L(L+1) - 2\Lambda^2 + < J_g^2 >}{2\mu r^2} \tag{6}$$

where Λ is the projection of the total angular momentum J_g of the gluonic field. The states with $\Lambda = 0, 1, 2, 3, , ...$ are usually represented by the capital greek letters $\Sigma, \Pi, \Delta, \Phi, ...$ respectively. We are interested in finding the masses and root mean square radii of the hybrid states $0^{+-}, 1^{-+}$, and 2^{+-}. These states can be generated from the Π_u potential. For the Π_u potential, $< J_g^2 >= 2$ and $\Lambda = 1$ [21]. Therefore $-2\Lambda^2 + \langle J_g^2 \rangle = 0$, so centrifugal factor for the hybrid mesons is $L(L+1)/2mr^2$. In ref. [21] $J = L \oplus S$, $P = \epsilon(-1)^{L+\Lambda+1}$, and $C = \epsilon\eta(-1)^{L+\Lambda+S}$ with $\epsilon, \eta = \pm 1$. Therefore with same quantum numbers (L,S), different J^{PC} states are possible. L and S for these hybrid J^{PC} states are shown in Table 2 (as given in ref. [22]).

For the excited part of quark antiquark potential π/r is used in the flux tube model [23]. In the present work, an *ansätz* of the form Ae^{-Br^2} is also used for the excited part of the quark antiquark potential. This gaussian gluonic potential is a smeared form of $\frac{constant}{r}$, as written in appendix of ref. [24]. From the lattice simulation reported in Fig. 3 of ref. [7], we get the potential energy difference (ε_i) between ground and excited states for different r_i values. Using this data, we found A and B for which χ^2 becomes minimum. χ^2 is defined as

$$\chi^2 = \sum_{i=1}^{n} (\varepsilon_i - Aexp[-Br_i^2])^2, \tag{7}$$

with $i = 1, 2, 3, ..., n$ being no.of data points. This gives

$$A = 1.8139266\text{GeV}, \qquad B = 0.0657212\text{GeV}^2.$$

We calculated χ^2 for Ae^{-Br^2} and π/r, and found that the χ^2 for Ae^{-Br^2} is lesser than that for π/r. This new potential form is already used in a more complicated work in ref. [25]. Using this, we can write the quark antiquark potential in excited state gluonic field as

$$V(r) = \frac{-4\alpha_s}{3r} + br + \frac{32\pi\alpha_s}{9m_c^2}(\frac{\sigma}{\sqrt{\pi}})^3 e^{-\sigma^2 r^2} S_c.S_{\overline{c}} + \frac{L(L+1) - 2\Lambda^2 + < J_g^2 >}{2\mu r^2} + Ae^{-Br^2}. \tag{8}$$

Characteristics of Hybrid Charmonium mesons

Using the excited state potential of eq.(8) along with the above mentioned values (after eq.(6)) of Λ and $< J_g^2 >$, the energy eigen-values and the corresponding wave functions are found by using the same technique as employed for conventional mesons (mentioned in section II). These eigenvalues plus constitutent quark antiquark masses are taken to be the masses of hybrid mesons. Then we normalized the solutions and found the root mean square radii of hybrid mesons by using eq.(4). The normalized solutions for charmonium hybrid mesons are graphically represented in Fig.2 and Fig.3. These figures show the wave function dependence on L and S. Therefore the mass and root mean square radii of $0^{+-}, 1^{-+}$ and 2^{+-} J^{PC} states also depend on the quantum numbers L and S. $|R(0)|^2$ is found for hybrid mesons using eq.(5).

IV. Results and Conclusions

1- Our calculated masses and root mean square radii are reported in Table 1 along with the experimental and theoretical predictions of the other works. We observed that our results are in good agreement with the experimental and existing theoretically predicted values, which shows the validity of our method. Quantum mechanically, when L increases, centrifugal barrier increases so particles become less bound implying increased root mean square radii. Our calculated root mean square radii are in agreement with this expectation.

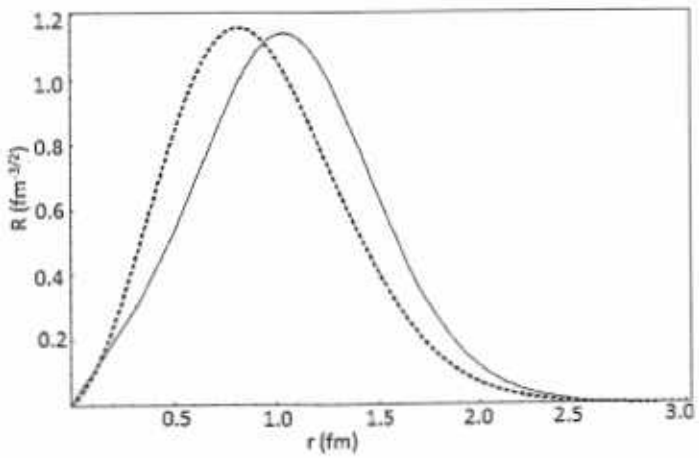

Figure 2: Hybrid charmonium meson radial wave functions for $0^{+-}, 1^{-+}$ and 2^{+-} J^{PC} states at L=1 and S=1. The wave function with potential in the form of coulombic plus linear plus $Aexp(-Br^2)$ is represented by solid lines and and wave function with potential in the form of coulombic plus linear plus π/r is represented by dashed line.

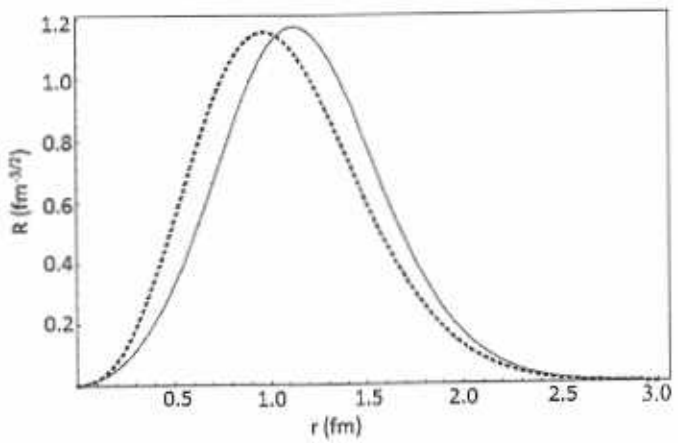

Figure 3: The same figure as Fig.2 but with L = 2 and S = 1.

Table 1: The experimental and theoretical masses and theoretical root mean square radii of some charmonium mesons. The experimental mass is the average PDG [16] and rounded to 0.001 GeV. Our calculated masses are rounded to 0.0001 GeV.

Meson	L	S	Our calculated mass	Theor. mass [16] with NR potential model	Exp. mass	our calculated $\sqrt{\langle r^2 \rangle}$	Theor. $\sqrt{\langle r^2 \rangle}$ [26] with potential model
			GeV	GeV	GeV	fermi	fermi
η_c	0	0	2.9816	2.982	2.9792 ± 0.0013 [16]	0.365	0.388
J/ψ	0	1	3.0900	3.090	3.09687 ± 0.00004 [16]	0.414	0.404
h_c	1	0	3.5156	3.516	3.525 ± 0.00055 [16]	0.674	0.602
χ_c	1	1	3.5246	3.556	3.55618 ± 0.00013 [27]	0.685	0.606

Table 2: Our calculated masses and root mean square radii of $c\bar{c}$ hybrid meson $0^{+-}, 1^{-+}$ and 2^{+-} J^{PC} states.

J^{PC}	L	S	Λ	$< J_g^2 >$	Mass with excited potential as $A \times \exp(-Br^2)$	mean square radii $\langle r^2 \rangle$	Mass with excited potential as π/r	$\sqrt{\langle r^2 \rangle}$
					GeV	fm	GeV	fm
$0^{+-}, 1^{-+}, 2^{+-}$	1	1	1	2	4.0619	1.2458	4.3571	1.1061
$1^{-+}, 2^{+-}$	2	1	1	2	4.1433	1.3203	4.4632	1.2280

2- With the parameters (given in Table 2) for the $0^{+-}, 1^{-+}$ and 2^{+-} J^{PC} states, masses and root mean square radii are calculated for the charmonium hybrid mesons. In Column 6-7 of this Table, masses and root mean square radii are calculated using the excited state gluonic field potential in the form of $A\,exp(-Br^2)$. But in column 8-9, masses and root mean square radii are calculated by taking the excited state potential in the form of π/r. For comparison with earlier works, masses of $c\bar{c}$ hybrid mesons with $0^{+-}, 1^{-+}$ and 2^{+-} J^{PC} states are given in Table 3.

3-For conventional mesons $|R(0)|^2$ is reported in Table 4. Each of $|R(0)|^2$ of $c\bar{c}$ hybrid mesons for $0^{+-}, 1^{-+}$ and 2^{+-} J^{PC} states is equal to zero by our calculation and this result agrees with ref. [38] which writes "models of hybrids typically expect the wave function at the origin to vanish". We noted that hybrid mesons's masses are greater and radii are lesser when the excited potential is in the form of π/r instead of $Aexp(-Br^2)$. We also noted that the masses and root mean square radii of the hybrid mesons are greater than ordinary mesons of same flavour and quantum numbers. Since $0^{+-}, 1^{-+}$, 2^{+-} states are not possible with quark model quantum numbers, so we can not compare these J^{PC} states with conventional mesons.

As scalar form factors [9] and energy shifts [10] are proportional to square of root mean square radii and magnetic polarizabilities [10] are proportional to negative of square of root mean square radii, we predict that magnitude of these quantities for hybrids are greater than those for conventional mesons of the same quantum numbers. We also noted that $|R(0)|^2$=0 in case of hybrid mesons. Using this result, we can predict that decay constants [11], decay rates [11], and differential cross sections [12] of hybrid mesons are zero as these quantities are proportional to $|R(0)|^2$.

Acknowledgement

We are grateful to Higher education Commission of Pakistan for their financial support no.17-5-3 (Ps3-212) HEC/Sch/2006.

Table 3: The mass predictions of $1^{-+}, 0^{+-}$, and 2^{+-} states

Predicted masses (GeV)			models
1^{-+}	0^{+-}	2^{+-}	
≈ 3.9 [28]			bag model
4.2-4.5 [29]			flux tube model
$4.19 \pm sys.error$ [30] [31] 4.7 [33]	≈ 4.5 [32] 4.58 [33]	≈ 4 [32]	heavy quark LGT
4.1-4.5			QCD sum rules
4.369 – 4.420 [34, 35, 36]	4.714(52) [36]	4.895(88) [37]	quenched lattice QCD

Table 4: $|R(0)|^2$ of $c\bar{c}$ meson

Meson	L	S	our calculated normalized $\|R(0)\|^2$ $(\text{fm})^{-3}$
η	0	0	1.9767
J/ψ	0	1	1.10865
h_c	1	0	$< 10^{-10}$
χ_c	1	1	$< 10^{-11}$

References

[1] C. McNeile, Nucl. Phys. A **711**, 303 (2002).

[2] C. Michael, arXive:hep-ph/0308293.

[3] M. Alekseev et al. [The COMPASS Collaboration], Phys. Rev. Lett. **104**, 241803 (2010); B. Grube et al. [The COMPASS Collaboration], arXiv:1002.1272 [hep-ex] (2010).

[4] Yu. P. Gouz et al. [VES Collaboration.], AIP Conf. Proc. 272, 572 (1993);Yu A.Khokholovetal.[VESCollaboration], Nucl. Phys. A **663**, 596 (2000); A. Zaitsevetal. [VESCollaboration], Nucl. Phys. A **675**, 155c (2000).

[5]] G. S. Adams et al. [E852 Collaboration], Phys. Rev. Lett. 81, 5760 (1998); S. U. Chung et al. [E852 Collaboration], Phys. Rev. D65, 072001 (2002); E. I. Ivanovetal.[E852Collaboration], Phys. Rev. Lett. 86, 3977 (2001); J. Kuhnetal. [E852 Collaboration], Phys. Lett. **B** 595, 109 (2004); M. Luetal. [E852 Collaboration], Phys. Rev. Lett. 94, 032002 (2005).

[6] C. A. Baker et al., Phys. Lett. B563, 140 (2003).

[7] K. J. Juge, J. Kuti and C. Morningstar, AIP Conf. Proc. **688**, 193 (2003).

[8] S. Collins, C. T. H. Davies, G. Bali, Nucl. Phys. Proc. Suppl. **63**, 335 (1998).

[9] B. Ananthanarayan, I. Caprini, G. Colangelo, J. Gasser and H. Leutwyler, Phys. Lett. B **602**, 218 (2004).

[10] S. I. Kruglov, Phys. Rev. D **60**, 116009 (1999).

[11] B. Patel and P. C. Vinodkumar, J. Phys. G **36**, 035003 (2009).

[12] C. H. Chaug, C. F. Qiao, J. X. Wang, Phys. Rev. D **57**, 4035 (1998).

[13] D. H. Perkins, *Introduction to High Energy Physics*, Addison-Wesley (1987).

[14] Bali G S et al. , Phys. Rev **D62**, 054503 (2000).
Bali G S, Phys. Rep.**343**, 1 (2001).

[15] Alexandrou C, de Forcrand P and John O, Nucl. Phys. **B119**, 667 (2003).

[16] T. Barnes, S. Godfrey, and E. S. Swanson, Phys. Rev. D **72**, 054026 (2005).

[17] C. F. Gerald and P. O. Wheatley, *Applied Numerical Method*, published by Dorling Kindrsley Pvt. Ltd., (1999).

[18] Dr. V. N. Vedamurthy and Dr. N. Ch. Sniyengar, *Applied Numerical Methods*, Published by Vikas publishing House Pvt. Ltd., (1998).

[19] M. M. Feyli, World Academy of Science, Engineering and Technology 71, (2010).

[20] K. J. Juge, J. Kuti, and C. J. Morningstar, Phys. Rev. Lett., **82**, 4400 (1999).

[21] K. J. Juge, J. Kuti and C. J. Morningstar, Nucl. Phys. Proc. Suppl. **63**, 326 (1998).

[22] E. S. Swanson, talk presented at JLAB/INT Workshop on Gluonic Excitations, (2003).

[23] N. Isgur and J. Paton, Phys. Rev. D **31** 2910 (1985).

[24] J. Weinstein and N. Isgur, Phy. Rev. D **41**, 2236 (1990).

[25] N. Akbar and B. Masud, arXive: 1102.1690 (2011).

[26] Cheuk-Yin Wong, E. S. Swanson, and T. Barnes, Phys. Rev. **C 65**, 014903 (2002).

[27] K. K. Seth, Jour. Phys. Conf. Ser. **9**, 32 (2005).

[28] P. Hasenfratz, R. R. Horgan, J. Kuti and J. M. Richard, Phys. Lett. B **95**, 299 (1980).

[29] J. Merlin and J. Paton, J. Phys. G **11**, 439 (1985);
N. Isgur and J. Paton, Phys. Rev. D **31**, 2910 (1985);
J. Merlin and J. Paton, Phys. Rev. D **35**, 1668 (1987).

[30] L. A. Griffiths, C. Michael, and P. E. L. Rakow, Phys. Lett. B **129**, 351 (1983);
S.Perantonis, C. Michael, Nuc. Phys. B **347**, 854 (1990).

[31] S. Perantonis and C. Michael Nucl. Phys. B **347**, 854 (1990).

[32] C. J. Morningstar and M. Peardon, Phys. Rev. D **56**, 4043 (1997).

[33] F. Iddir and L. Semlala, arxive hep-ph/0611165v2 (2006)

[34] T. Mankeetal., Phys. Rev. Lett.**82**, 4396 (1999).

[35] Z. H. MeiandX., Q. Luo, Int. J. Mod. Phys. A **18**,5713 (2003).

[36] Y. Liu and X. Q. Luo, Phys. Rev. D **73**, 054510 (2006).

[37] X. Liu, T. Manke, arXive:hep-lat/0210030.

[38] S. Godfrey, Flavor Physics and CP Violation Conference, Vancouver, (2006).

Eur. Phys. J. A (2011) 47: 124
DOI 10.1140/epja/i2011-11124-2

THE EUROPEAN PHYSICAL JOURNAL A

Regular Article – Theoretical Physics

Wave-function–based characteristics of hybrid mesons

Nosheen Akbar[a], Bilal Masud[b], and Saba Noor[c]

Centre For High Energy Physics, University of the Punjab, Lahore (54590), Pakistan

Received: 21 June 2011 / Revised: 6 September 2011
Published online: 21 October 2011 – © Società Italiana di Fisica / Springer-Verlag 2011
Communicated by H. Witting

Abstract. We propose some extensions of the quark potential model to hybrids, fit them to the lattice data and use them for the purpose of calculating the masses, root mean square radii and wave functions at the origin of the conventional and hybrid charmonium mesons. We treat the ground and excited gluonic field between a quark and an antiquark as in the Born-Oppenheimer expansion, and use the shooting method to numerically solve the required Schrödinger equation for the radial wave functions; from these wave functions we calculate the mesonic properties. For masses we also check through a Crank Nichelson discretization. For hybrid charmonium mesons, we consider the exotic quantum number states with $J^{PC} = 0^{+-}, 1^{-+}$ and 2^{+-}. We also compare our results with the experimentally observed masses and theoretically predicted results of the other models. Our results have implications for scalar form factors, energy shifts, magnetic polarizabilities, decay constants, decay widths and differential cross-sections of conventional and hybrid mesons.

1 Introduction

A number of hadron properties are well described by the quark model where mesons have quantum numbers $J = L \oplus S$, $P = (-1)^{L+1}$ and $C = (-1)^{L+S}$, L and S being the quantum numbers for the quark-antiquark orbital angular momentum and their net spin angular momentum, respectively. The states with $J^{PC} = 0^{+-}, 1^{-+}, 2^{+-}$ (for the lowest lying hybrids in the flux tube model) can not be formed from a $q\bar{q}$ pair and hence are not allowed in the quark model. These states are signals for exotic mesons (hybrids, glueballs, etc). Quantum Chromodynamics (QCD), describing the interaction between quarks and gluonic field, predicts the existence of hybrid mesons containing the excited gluonic field. Thus for understanding QCD, we need to find experimentally testable predictions of the theory for situations in which the gluonic field between a quark and an antiquark is in an excited state. Thus hybrids are an important source of information related to the confining properties of QCD, and checking for the existence of hybrid mesons is a very important objective of particle physics. Reviews of the spectrum of the excited gluonic states can be found in ref. [1]. Recently, a resonance is observed at COMPASS [2] with $J^{PC} = 1^{-+}$. Some other groups like VES [3–5], E852 [6–10], and the Crystal Barrel Collaboration [11] also observed these states.

Using the Born-Oppenheimer approach, the work of finding implications of QCD for a meson can be split into first using the numerical lattice simulations of QCD to fit parameters of a quark-antiquark potential and then using this potential to calculate its dynamical implications. Even a numerically defined potential can be used in this scheme, as in refs. [12,13]. These works use some potentials to calculate hybrid masses and few radial probability graphs (but presents no $q\bar{q}$ wave function expressions or uses). What we add to this work is that now we suggest a number of analytical expressions for the excited state gluonic field potential between a quark and antiquark and fit their parameters to the lattice data for the ground and excited state gluonic field energy values available in ref. [12] for discrete quark antiquark separations. For each case, we report a dimensionless chisquare and other measures directly telling how much fractional error each model has in fitting. We use this variety of potentials to indicate suitable ones for different applications, for example for analytical calculations of expectation values in few-body wave functions where a numerical approach may have convergence problems. Our full list of chisquare and other error measures tells how much extra error is generated in preferring the flux tube model and other integrable forms over the ones that can be only numerically used but fit better. After using these potentials to find the quark-antiquark wave functions, we also calculate a number of conventional and hybrid meson rms radii and square of radial wave functions at the origin. We continue till writing some implications of these for scalar form factors, energy shifts,

[a] e-mail: noshinakbar@yahoo.com
[b] e-mail: bilalmasud.chep@pu.edu.pk
[c] e-mail: sabanoor87@gmail.com

magnetic polarizabilities, decay constants, decay widths and differential cross-sections of conventional and hybrid mesons. All this is an addition to our own results for meson masses and radial probabilities that are in agreement to those reported in ref. [12] for the height of the single peak of the probability graph.

In the present paper, we apply our techniques to charmonium mesons. An advantage of considering them is indicated in ref. [14] as

" The best systems for a hybrid search may be $c\bar{c}$ or $b\bar{b}$ where there is a large gap between the lowest states and the $D\overline{D}$ and $B\overline{B}$ threshod respectively."

To find the wave functions of conventional charmonium mesons, we use the realistic Columbic plus linear potential model to solve the Schrödinger equation numerically by using the corresponding quantum numbers of the mesons. To study hybrids, we repeat the numerical work with the models of the gluonic excitation energy mentioned in sect. 3. From the numerically found wave functions, we calculate the root mean square radii. These radii can be used to find scalar form factors [15] for charmonium mesons, along with energy shifts [16] and magnetic polarizabilities [16]. Thus we have reported some predictions about these quantities for conventional and hybrid charmonium mesons. We have also found the numerical values of square of radial wave functions at the origin ($|R(0)|^2$), which can be used to calculate the decay constants [17], decay rates [17], and differential cross-sections [18] for quarkonium states. The predictions about these quantities are also reported for conventional and hybrid charmonium mesons.

In sect. 2 below, we write the Hamiltonian for the conventional mesons. Then we describe the shooting method-based numerical procedure to find the solution of the radial Schrödinger equation for conventional charmonium mesons. The expressions to find masses, root mean square radii, and squares of radial wave functions at the origin ($|R(0)|^2$) of conventional charmonium mesons are also written in this section. In sect. 3, the Hamiltonian is written for hybrid mesons, and then we redo all the numerical work as done in sect. 2 for hybrids now. The χ^2 and other error measures for different forms of the potential difference between ground and excited state are also written in sect. 3. Results for the masses, root mean square radii and $|R(0)|^2$ of conventional and hybrid mesons are reported in sect. 4 for systems composed of charm quarks and antiquarks. Based on these results, we also include some results related to experimentally measurable quantities.

2 Characteristics of conventional charmonium mesons

2.1 The potential model for conventional charmonium mesons

In the potential models, the confining potential for $Q\overline{Q}$ system in the ground-state gluonic field is mostly used in the form of

$$\frac{-4\alpha_s}{3r} + br + c, \tag{1}$$

with inter-quark distance r. Here, $-4/3$ is due to the colour factor, α_s is the quark-gluon coupling, b is the string tension and c is a constant. In the above equation, the first term is due to one-gluon exchange and the second term is the linear confining potential [19]. This potential form provides a good fit to the lattice simulations of refs. [20–22]. By including the Gaussian-smeared hyperfine interaction [23] and the orbital-angular-momentum (or centrifugal) term, the potential of the $Q\overline{Q}$ system for the ground-state gluonic field has following form:

$$V(r) = \frac{-4\alpha_s}{3r} + br + \frac{32\pi\alpha_s}{9m_c^2}\left(\frac{\sigma}{\sqrt{\pi}}\right)^3 e^{-\sigma^2 r^2} S_c \cdot S_{\overline{c}} + \frac{L(L+1)}{2\mu r^2}, \tag{2}$$

where $S_c \cdot S_{\overline{c}} = \frac{S(S+1)}{2} - \frac{3}{4}$, μ is the reduced mass of the quark and antiquark, m_c is the mass of the charm quark, and S is the total spin quantum number of the meson. For the $c\bar{c}$ mesons, the parameters α_s, b, σ, and m_c are taken to be 0.5461, 0.1425 GeV^2, 1.0946 GeV and 1.4796 GeV, respectively as in ref. [23]. The quantum numbers for the conventional charmonium mesons we choose for our study are reported below in table 5.

2.2 Wave functions and radii of conventional charmonium mesons

A conventional meson can be described by the wave function of the bound quark-antiquark state which satisfies the Schrödinger equation with the potential of eq. (2). The radial Schrödinger equation with wave function $U(r) = rR(r)$ is written (in natural units) as

$$\nabla^2 U(r) + 2\mu(E - V(r))U(r) = 0. \tag{3}$$

Here $R(r)$ is the radial wave function, r is the interquark distance, E is the sum of the kinetic and potential energy of the quark-antiquark system, and $V(r)$ and μ are defined above through eq. (2).

In the quark-antiquark bound state, the wave function must satisfy the boundary conditions $U(0) = 0$ and $U(\infty) = 0$. For the numerical solution of the Schrödinger equation with the potential of eq. (2), we repeatedly generated the energy E from -2 to 2 GeV in steps of 0.1 GeV. For each such trial initial energy, we used the Newton method [24] to select, if any, the energy for which the numerical solution of the Schrödinger equation became zero at infinity. To obtain these numerical solutions, we used the RK method [25] with using any arbitrary integer value of $U'(0)$. For different values of $U'(0)$, normalized solutions of the Schrödinger equation, obtained by multiplying the solution with the normalization constant $\left(\frac{1}{\sqrt{\int U^2(r)\mathrm{d}r}}\right)$, remain the same. These energy eigenvalues plus constituent-quark masses are taken to be the $c\bar{c}$ mesons masses (in natural units). It is found that our results for conventional charmonium mesons agree with table 1 of ref. [23]. This supports the reliability of our

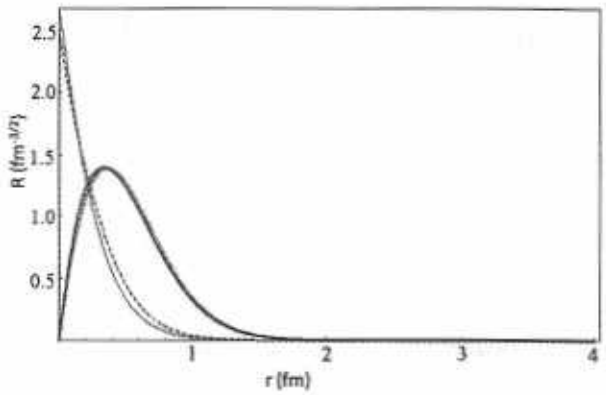

Fig. 1. The radial parts of η, J/ψ, h_c, and χ_c meson wave functions as functions of r. Thin solid line represents the η wave function, dashed line represents the J/ψ wave function, thick solid line represents the h_c wave function and points represent the χ_c wave function.

method. We also checked the consistency of our method by 1) getting a 100% overlap of our *HU* and *EU* and 2) by calculating the masses of the conventional mesons by the Crank-Nicholson Discritization and finding that the masses obtained by both the methods are identical. Figure 1 shows the dependence of η, J/ψ, h_c, and χ_c normalized radial wave functions on the radial separation r. The quantum numbers (L and S) for these particles are given below in table 5. These graphs show that the radial wave functions of η, h_c, χ_c, and J/ψ have the same properties as those of the hydrogen atom radial wave functions, i.e. they behave as r^L for small interquark distances and decrease exponentially at large interquark distances. Thin solid and dashed lines graphs are for $L = 0$, so these graphs are similar to $r^0 \exp(-r)$. Thick solid line and points are for $L = 1$, so these graphs are similar to $r^1 \exp(-r)$. As L increases, the wave function's peak goes away from the origin. This means that the centrifugal term has more effect on the wave function than of the hyperfine term. One possible reason is that we are dealing with heavy quarks so the $1/m_c^2$ factor (shown in eq. (2)) of the hyperfine term becomes very small.

The normalized wave functions are used in the further calculations of root mean square radii and square of radial wave functions at the origin. To find the root mean square radii of the $c\bar{c}$ mesons, we used the following relation:

$$\langle r^2 \rangle = \sqrt{\int U^* r^2 U \mathrm{d}r}. \tag{4}$$

In ref. [26], for normalized wave function

$$U'(0) = R(0) = \sqrt{4\pi}\,\psi(0) \tag{5}$$

is used and we use this prescription. Thus the derivative of $U(r)$ at $r = 0$ is calculated to find $|R(0)|^2$. $|R(0)|^2$ is used in many applications of high-energy physics as mentioned in sect. 1.

3 Characteristics of hybrid charmonium mesons

3.1 The potential model for hybrid charmonium mesons

The centrifugal factor for the hybrid mesons is written in refs. [27,28] as

$$\frac{L(L+1) - 2\Lambda^2 + \langle J_g^2 \rangle}{2\mu r^2}, \tag{6}$$

where Λ is the projection of the total angular momentum J_g of the gluonic field. The states with $\Lambda = 0, 1, 2, 3, \ldots$ are usually represented by the capital greek letters $\Sigma, \Pi, \Delta, \Phi, \ldots$, respectively. We are interested in finding the masses and root mean square radii of the hybrid states $0^{+-}, 1^{-+}$, and 2^{+-}. These states can be generated from the Π_u potential. For the Π_u potential, $\langle J_g^2 \rangle = 2$ and $\Lambda = 1$ [28]. Therefore $-2\Lambda^2 + \langle J_g^2 \rangle = 0$, so the centrifugal factor for the hybrid mesons is $L(L+1)/2mr^2$. In ref. [28] $J = L \oplus S$, $P = \epsilon(-1)^{L+\Lambda+1}$, and $C = \epsilon\eta(-1)^{L+\Lambda+S}$ with $\epsilon, \eta = \pm 1$. Therefore with the same quantum numbers (L, S), different J^{PC} states are possible. L and S for these hybrid J^{PC} states are shown in table 6 (as given in ref. [29]). For the excited part of the quark-antiquark potential π/r is used in the flux tube model [30]. This form of excitation energy is only valid at large interquark distances. In comparison, we suggest and evaluate the excited potential energy in forms which are valid for smaller distances as well. For this purpose, we get the potential energy differences (ε_i) between ground and excited states for different r_i values from the lattice simulation reported in fig. 3 of ref. [12], and calculate χ^2 with a variety (π/r, $A \times \exp(-Br^2)$, $A \times \exp(-Br^{0.1897})$, $\frac{c}{r} + A \times \exp(-Br^2)$, and $\frac{c}{r} + A \times \exp(-Br^{0.3723})$) of *ansatz* by fitting parameters appearing in each *ansatz*. Dimensionless χ^2 is defined as

$$\chi^2 = \frac{\sum_{i=1}^{n} (\varepsilon_i - V_g(r_i))^2}{\sum_{i=1}^{n} \varepsilon_i^2}, \tag{7}$$

with $i = 1, 2, 3, \ldots, n$ being the number of data points. Here $V_g(r)$ is a model of the potential energy difference between the ground and excited state. We tried

$V_g(r) = \pi/r$,
$V_g(r) = A \times \exp(-Br^2)$,
$V_g(r) = A \times \exp(-Br^\gamma)$,
$V_g(r) = \frac{c}{r} + A \times \exp(-Br)$, and
$V_g(r) = \frac{c}{r} + A \times \exp(-Br^\gamma)$.

The parameters A, B, c, and γ are found by fitting these models ($V_g(r)$) with the potential difference data of ref. [12], and reported in table 1. χ^2, χ^2/D and χ are also reported in table 1 with $\chi^2/D = \chi^2/(\text{number of data points})$ and $\chi = \frac{\sum_{i=1}^{n} |(\varepsilon_i - V_g(r))|}{\sum_{i=1}^{n} |\varepsilon_i|}$.

It is noted that the χ^2 for π/r is greater than all other potential difference forms. Figure 2, representing

Table 1. Our calculated χ^2 for the data of potential difference to our suggested models ($V_9(r)$) with best fit parameter's values.

Ansatz	χ^2	χ^2/D (GeV^2)	χ	Parameters			
				A (GeV)	B (GeV)	c	γ
π/r	0.2305	0.3268	0.5285	–	–	–	–
$A \times \exp(-Br^\gamma)$	0.0857	0.1215	0.2773	1.8139	0.0657	–	2
$A \times \exp(-Br^\gamma)$	0.0004	0.0005	0.0205	17.9325	2.5195	–	0.1897
$\frac{c}{r} + A \times \exp(-Br^\gamma)$	0.0012	0.0017	0.0331	1.2448	0.1771	0.3583	1
$\frac{c}{r} + A \times \exp(-Br^\gamma)$	0.0003	0.0004	0.0132	3.4693	1.0110	0.1745	0.3723

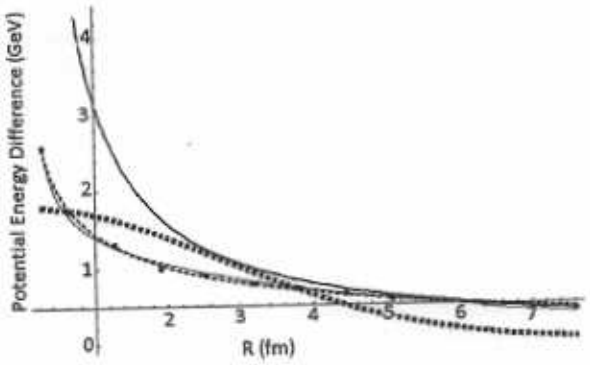

Fig. 2. Graphs of potential energy differences between ground and excited state. Points represent the data taken from ref. [12], thick solid line represents the potential difference model $\frac{\pi}{r}$, thin solid line represents the potential energy difference $\frac{c}{r} + A \times \exp(-Br)$, dashed line represents the potential difference $A \times \exp(-Br^{0.1897})$, and squared points represents the potential energy difference $A \times \exp(-Br^2)$.

the graphs for different forms of potential difference, also shows the same behaviour. The χ^2 of the gaussian gluonic potential ($A \times \exp(-Br^2)$) is less than $\frac{\pi}{r}$, but larger than all other forms. $A \times \exp(-Br^2)$ is a smeared form of $\frac{\text{constant}}{r}$, as written in appendix of ref. [31]. The potential difference in this form ($A \times \exp(-Br^2)$) has an advantage that it can be easily used in dynamical applications. For example, the expectation value of this part of the potential energy in a Gaussian wave function of the quadratic confining potential is given in terms of error function differences even if one uses antiderivatives to evaluate the definite integrals in it. Or, for usual infinite limits it simply multiplies in the integrand with already Gaussian meson wave functions to keep the integrand as Gaussian, whose well-known integral can be written by inspection. (The expression for the expectation value can be minimized with respect to the chosen parameters of the wave function to find the ground-state energy and wave function using the variational method.) This calculational advantage may be trivial for a two-body problem. But if one has to evaluate an expectation value for few or many-body problem (or for a minor variant used in the resonating group method based treatment [32,33] of a system of two quark and two antiquarks), we have to evaluate an integral of a high order whose direct numerical evaluation may have convergence problems as in ref. [33] and a Gaussian integration by inspection may well be the only practical option. The need to keep the multi-dimensional integrals as Gaussian, giving importance to the $A \times \exp(-Br^2)$ form, becomes even more prominent when wave functions of the conventional mesons are replaced for the respective problems by those of the hybrids as in ref. [32].

The analytic Gaussian expectation value of $A \times \exp(-Br)$ term is similarly given in terms of error function differences. (Or, its product in integrand with Gaussian wave functions can be converted to a new Gaussian integrand using a completing of square.) The χ^2 for the potential difference in form of $\frac{c}{r} + A \times \exp(-Br^{0.3723})$ is much less. The $\frac{c}{r}$ term in this form can be used for analytical expressions of expectation values in the above-mentioned Gaussian quark-antiquark wave functions of quadratic potential, resulting in differences of the exponential integral functions for the most analytical way of finding the expectation values and integrals of resonating group method [32,33]. But a similar fully analytical route for Gaussian expectation values and resonating group integrals of the $A \times \exp(-Br^\gamma)$, for $\gamma =$ non-integer number, is not available, and this can lead to convergence problems [33] when we integrate numerically integrals of high dimensions.

In ref. [13,28] excited-state potential (*not* the difference) is used in the form of

$$c_0 + \sqrt{b_0 + b_1 r + b_2 r^2}. \tag{8}$$

By fitting this potential with data of first excited potential taken from fig. 3 of ref. [12], we calculated the parameters b_0, b_1, b_2, c_0. We also calculated χ^2, χ and χ^2/D and reported in table 2 along with the parameter values. The fit of the data with this excited state potential is shown in our fig. 3. As for the analytical calculations (for finding expectation values etc.), these are also not possible with this potential form and thus for many applications it has to be replaced by others of higher chisquare.

Figure 4 shows the behaviour of string potential [34]

$$\sqrt{\sigma^2 r^2 + 2\pi\sigma\left(N + \frac{3}{2}\right) + w_q} \tag{9}$$

Table 2. Our calculated χ^2 for the first excited state data of ref. [12] to the model used in ref. [13] with best fit parameter's values.

Excited potential	χ^2	χ^2/D (GeV^2)	χ	Parameters			
				b_0 (GeV^2)	b_1 (GeV^3)	b_2 (GeV^4)	c_0 (GeV)
$c_0+\sqrt{b_0+b_1r+b_2r^2}$	0.00096	0.0030	0.0226	58.0016	4.4896×10^{-10}	0.2859	−6.1814

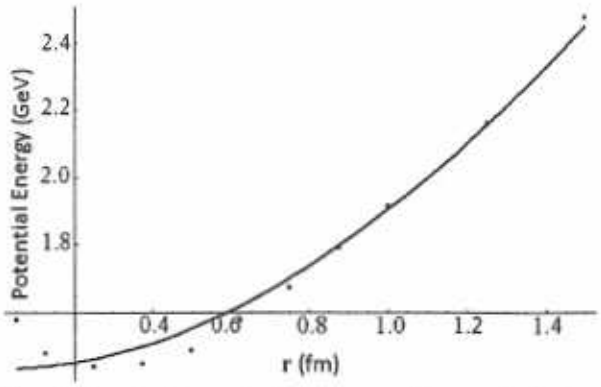

Fig. 3. Graphs of the excited-state potential energy in the form of $c_0+\sqrt{b_0+b_1r+b_2r^2}$ along with data of ref. [12]. Solid line is for the potential $c_0+\sqrt{b_0+b_1r+b_2r^2}$ and dots are for data of ref. [12].

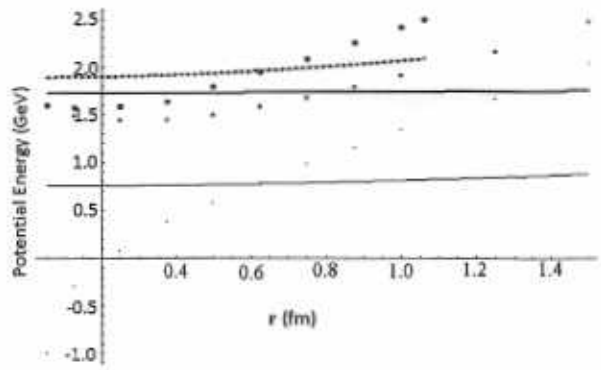

Fig. 4. Graphs of potential energy in the form of $\sqrt{\sigma^2r^2+2\pi\sigma(N+\frac{3}{2})}+w_0$. The solid line is for $N=0$ and small points are for $N=0$ data of ref. [12]. Thick solid line is for $N=1$ and medium size points are for $N=1$ data of ref. [12]. Dashed line is for the $N=2$ and large size points are for the $N=2$ data of ref. [12].

with $N=0,1,2$. In this figure, the points represent the data taken from ref. [12]. The parameter's values, χ^2 and other error measures of the string potential with the data (of excited potential) of ref. [12] is reported in table 3. The parameter's values are calculated by fitting the data of excited potential with the string potential. The analytical calculations (for finding expectation values) are not possible with this string potential form as well.

3.2 Wave functions and radii of hybrid charmonium mesons

Now, we can write the quark-antiquark potential in excited state gluonic field as

$$V(r)=\frac{-4\alpha_s}{3r}+br+\frac{32\pi\alpha_s}{9m_c^2}\left(\frac{\sigma}{\sqrt{\pi}}\right)^3 e^{-\sigma^2r^2}S_c\cdot S_{\bar{c}} + \frac{L(L+1)-2\Lambda^2+\langle J_g^2\rangle}{2\mu r^2}+V_g(r); \tag{10}$$

$V_g(r)$ is defined above after eq. (7).

Using this excited-state potential of eq. (10) along with the above-mentioned values (after eq. (6)) of Λ and $\langle J_g^2\rangle$, the energy eigenvalues and the corresponding wave functions are found by using the same technique as employed for conventional mesons (mentioned in sect. 2). As before, these eigenvalues plus constituent quark-antiquark masses are taken to be the masses of hybrid mesons. Then we normalized the wave functions and found the root mean square radii of hybrid mesons by using eq. (4). The normalized radial wave functions for charmonium hybrid mesons are graphically represented in fig. 5 and fig. 6. The overlaps of our numerically calculated radial wave functions ($U=rR$) for the excited states and a modified Gaussian wave function ansatz

$$\psi=n\,r^2\exp(-pr^2) \tag{11}$$

multiplied by $\sqrt{4\pi}r$ are written in table 4 in such a way that $U=rR=\sqrt{4\pi}r\psi$.

The normalization of the Gaussian wave function gives

$$n=\left(42^{\frac{3}{4}}p^{\frac{7}{4}}\right)\left(15^{\frac{1}{4}}\pi^{\frac{3}{4}}\right). \tag{12}$$

The numerical value of p is found by fitting this function with the data of numerically calculated wave function, and written in table 4.

Figures 5 and 6 show the wave function dependence on L and S. Therefore the masses and root mean square radii of $0^{+-}, 1^{-+}$ and 2^{+-} J^{PC} states also depend on the quantum numbers L and S. $|R(0)|^2$ is found for hybrid mesons using eq. (5). Figures 5 and 6 also show that the peaks of the graphs for radial probability density are in agreement with the peak of the radial probability curve drawn in ref. [12].

Table 3. Our calculated χ^2 with best fit parameter's values.

Excited potential	χ^2	χ^2/D (GeV^2)	χ (GeV)	Parameters N –	w_q (GeV^2)	σ (GeV^4)
$\sqrt{\sigma^2 r^2 + 2\pi\sigma(N+\frac{3}{2}) + w_q}$	0.5536	0.6633	0.6932	0	5.9884×10^{-9}	0.0601
	0.0112	0.0348	0.0899	1	3.5044×10^{-7}	0.1629
	0.0190	0.0740	0.1259	2	1.0531×10^{-5}	0.1627

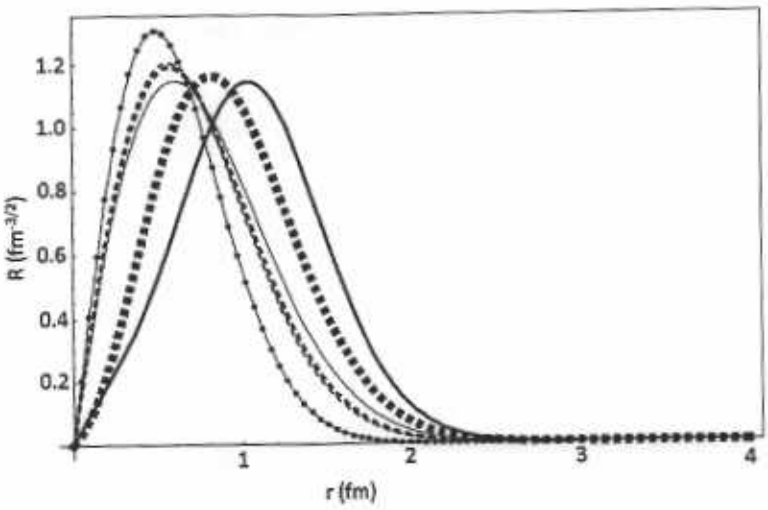

Fig. 5. Hybrid charmonium meson radial wave functions for $0^{+-}, 1^{-+}$ and 2^{+-} J^{PC} states for $L = 1$ and $S = 1$. The wave function with potential in the form of Coulombic plus linear plus $A\exp(-Br^2)$ is represented by the solid line. The wave function with Coulombic plus linear plus π/r potential is represented by square points. The wave function with Coulombic plus linear plus $A\times\exp(-B\,r^{0.1896})$ potential is represented by dashed line. The wave function with Coulombic plus linear plus $\frac{c}{r}+A\times\exp(-B\,r)$ potential is represented by thin solid line. The wave function with Coulombic plus linear plus $\frac{c}{r}+A\times\exp(-B\,r^{0.3723})$ potential is represented by thick dashed line, and the wave function with excited potential in the form of $c_0+\sqrt{b_0+b_1 r+b_2 r^2}$ is represented by points with lines.

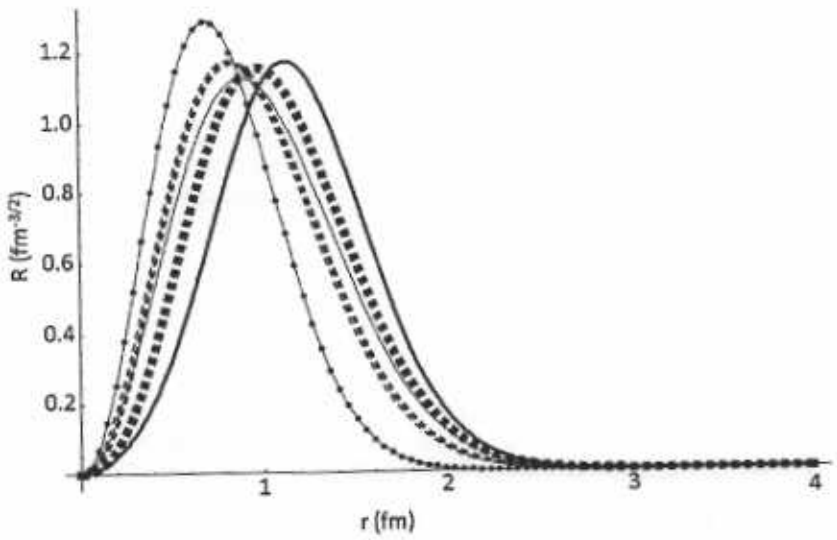

Fig. 6. The same as fig. 4 but with $L = 2$ and $S = 1$.

Table 4. Our best fit parameter's values and overlaps of numerically solved wave functions to the wave function form written in eq. (11).

Ansatz	$L=1$ and $S=1$ Parameters of the excited-state function written in eq. (11)		Overlap	$L=2$ and $S=1$ Parameters of the excited-state function written in eq. (11)		Overlap
	n	p		n	p	
π/r	0.0047	0.0556	0.9997	0.0032	0.0451	0.9989
$A\times\exp(-Br^2)$	0.0031	0.0439	0.9964	0.0025	0.0391	0.9905
$A\times\exp(-Br^{0.1897})$	0.0093	0.0822	0.9903	0.0048	0.0565	0.9998
$\frac{c}{r}+A\times\exp(-Br)$	0.0070	0.0698	0.9899	0.0036	0.0482	0.9999
$\frac{c}{r}+A\times\exp(-Br^{0.3723})$	0.0087	0.0794	0.9903	0.0045	0.0547	0.9998
$c_0+\sqrt{b_0+b_1r+b_2r^2}$	0.0163	0.1135	0.9921	0.0090	0.0807	0.9999

Table 5. The experimental and theoretical masses and theoretical root mean square radii of some conventional charmonium mesons. The experimental mass is the average PDG [23] and rounded to 0.001 GeV. Our calculated masses are rounded to 0.0001 GeV.

Meson	L	S	Our calculated mass (GeV)	Theoretical mass [23] with NR potential model (GeV)	Experimental mass (GeV)	Our calculated $\sqrt{\langle r^2\rangle}$ (fm)	Theoretical $\sqrt{\langle r^2\rangle}$ [35] with potential model (fm)
η_c	0	0	2.9816	2.982	2.9792 ± 0.0013 [23]	0.365	0.388
J/ψ	0	1	3.0900	3.090	3.09687 ± 0.00004 [23]	0.414	0.404
h_c	1	0	3.5156	3.516	3.525 ± 0.00055 [23]	0.674	0.602
χ_c	1	1	3.5246	3.556	3.55618 ± 0.00013 [36]	0.685	0.606

4 Results and conclusions

1) For conventional mesons, our calculated masses and root mean square radii are reported in table 5 along with the experimental and theoretical predictions of the other works. We observed that our results are in good agreement with the experimental and existing theoretically predicted values, which shows the validity of our method. Quantum mechanically, when L increases, the centrifugal barrier increases so particles become less bound implying increased root mean square radii. Our calculated root mean square radii are in agreement with this expectation.

2) With the parameters (given in table 6) for the 0^{+-}, 1^{-+} and 2^{+-} J^{PC} states, masses and root mean square radii are calculated for the charmonium hybrid mesons. In table 6, masses are calculated using the excited state gluonic field potential in the above-mentioned forms. For comparison with earlier works, masses of $c\bar{c}$ hybrid mesons with $0^{+-}, 1^{-+}$ and 2^{+-} J^{PC} states are given in table 7. In table 8, root mean square radii are calculated by taking the excited-state potential in the coulomb plus linear plus additional excited potential. In table 9, masses and root mean square radii are reported for the excited potential in the form of $c_0+\sqrt{b_0+b_1r+b_2r^2}$.

3) For conventional mesons $|R(0)|^2$ is reported in table 10. Each $|R(0)|^2$ of the $c\bar{c}$ hybrid mesons for 0^{+-}, 1^{-+} and 2^{+-} J^{PC} states is equal to zero by our calculation and this result agrees with ref. [37] which writes "models of hybrids typically expect the wave function at the origin to vanish". We also noted that the masses and root mean square radii of the hybrid mesons are greater than ordinary mesons with the same flavour and quantum numbers (L and S). Since $0^{+-}, 1^{-+}$, 2^{+-} states are not possible with quark model quantum numbers, we cannot compare these J^{PC} states with conventional mesons.

In ref. [15], the scalar form factor is written as

$$\overline{\Gamma}_\pi(t)=1+\frac{1}{6}\langle r^2\rangle_s^\pi t+o(t^2). \tag{13}$$

In ref. [16], energy shift and magnetic polarizability are written as

$$\Delta E_n=\left\langle n\left|\frac{eH}{8\mu}L_3+\left(\frac{e^2}{4\widetilde{\mu}}+\frac{q^2}{\mu_1+\mu_2}\right)\frac{H^2r^2\sin^2\theta}{32}\right|n'\right\rangle +\Sigma_n'\frac{|\langle n'|eHL_3/8\widetilde{\mu}|n\rangle|^2}{E_n-E_{n'}}. \tag{14}$$

Here the symbols L_3, H, e, m are used for the angular momentum, magnetic field, charge and mass of the quark, $\widetilde{\mu}=\frac{\mu}{2}$, θ is the angle between H and relative coordinate r, $q=e_1-e_2$, and $e=e_1+e_2$. In the above equation, the term having $\langle n|\frac{H^2r^2\sin^2\theta}{32}|n'\rangle$ is related to the square of root mean square radii:

$$\beta=-\frac{1}{24}\left(\frac{e^2}{4\widetilde{\mu}}+\frac{q^2}{\mu_1+\mu_2}\right)\langle r^2\rangle. \tag{15}$$

Table 6. Our calculated masses of $c\bar{c}$ hybrid meson $0^{+-}, 1^{-+}$ and 2^{+-} J^{PC} states.

J^{PC}	L	S	Λ	$\langle J_g^2 \rangle$	Excited potential as Coulombic plus linear plus				
					π/r (GeV)	$A \times \exp(-Br^2)$ (GeV)	$A \times \exp(-Br^{0.1897})$ (GeV)	$\frac{c}{r} + A \times \exp(-Br)$ (GeV)	$\frac{c}{r} + A \times \exp(-Br^{0.3723})$ (GeV)
$0^{+-}, 1^{-+}, 2^{+-}$	1	1	1	2	4.3571	4.0619	4.2680	4.2733	4.2694
$1^{-+}, 2^{+-}$	2	1	1	2	4.4632	4.1433	4.4632	4.4258	4.40796

Table 7. The mass predictions of $1^{-+}, 0^{+-}$ and 2^{+-} states of other works.

Predicted masses (GeV)			Models
1^{-+}	0^{+-}	2^{+-}	
≈ 3.9 [38]			bag model
4.2-4.5 [39–41]			flux tube model
$4.19 \pm$ sys. error [42,43] 4.7 [44]	≈ 4.5 [13] 4.58 [44]	≈ 4 [13]	heavy quark LGT
4.1-4.5			QCD sum rules
4.369 – 4.420 [45–47]	4.714(52) [47]	4.895(88) [48]	quenched lattice QCD

Table 8. Our calculated root mean square radii of $c\bar{c}$ hybrid meson $0^{+-}, 1^{-+}$ and 2^{+-} J^{PC} states.

J^{PC}	L	S	Λ	$\langle J_g^2 \rangle$	$\sqrt{\langle r^2 \rangle}$ with excited potential as Coulombic plus linear plus				
					π/r (fm)	$A \times \exp(-Br^2)$ (fm)	$A \times \exp(-Br^{0.1897})$ (fm)	$\frac{c}{r} + A \times \exp(-Br)$ (fm)	$\frac{c}{r} + A \times \exp(-Br^{0.3723})$ (fm)
$0^{+-}, 1^{-+}, 2^{+-}$	1	1	1	2	1.1061	1.2458	0.9110	0.9881	0.9272
$1^{-+}, 2^{+-}$	2	1	1	2	1.2280	1.3203	1.0988	1.1883	1.1160

Table 9. Our calculated masses and root mean square radii with excited potential $c_0 + \sqrt{b_0 + b_1 r + b_2 r^2}$ of $c\bar{c}$ hybrid meson with $0^{+-}, 1^{-+}, 2^{+-}$ J^{PC} states.

J^{PC}	L	S	Λ	$\langle J_g^2 \rangle$	Masses (GeV)	$\sqrt{\langle r^2 \rangle}$ (fm)
$0^{+-}, 1^{-+}, 2^{+-}$	1	1	1	2	4.9503	0.7748
$1^{-+}, 2^{+-}$	2	1	1	2	5.1693	0.9185

Table 10. $|R(0)|^2$ of $c\bar{c}$ mesons.

Meson	L	S	Our calculated normalized $\lvert R(0)\rvert^2$ $(\text{fm})^{-3}$
η	0	0	2.5910
J/ψ	0	1	2.1789
h_c	1	0	$< 10^{-10}$
χ_c	1	1	$< 10^{-11}$

In the above equations (13)–(15) the root mean square radii is in the numerator, therefore we predict that the magnitudes of the scalar form factor [15], energy shift [16], and magnetic polarizability [16] for hybrids are greater than those for conventional mesons with the same quantum numbers (L and S).

By parametrizing the excited-state wave function written above in eq. (11), we get

$$\langle r^2 \rangle = \int \psi^* r^2 \psi \, dr = \frac{15n^2\sqrt{\pi/2}}{128p^{7/2}}. \tag{16}$$

Here n is a function of p, as given by eq. (12). Substituting the result of eq. (16) in eqs. (13) and (15), the scalar form factor and magnetic polarizability become

$$T_\pi(t) = 1 + \frac{1}{6}\frac{15n^2\sqrt{\pi/2}}{128p^{7/2}}t + o(t^2), \tag{17}$$

$$\beta = -\frac{1}{24}\left(\frac{e^2}{4\bar{\mu}} + \frac{q^2}{\mu_1 + \mu_2}\right)\frac{15n^2\sqrt{\pi/2}}{128p^{7/2}}. \tag{18}$$

Numerically calculated values of n and p are written in table 4 for different forms of the excited-state potentials for different L and S.

As we mentioned above, $|R(0)|^2$ is equal to zero for hybrid mesons. Using this result, we can predict that decay constants [17], decay rates [17], and differential cross-sections [18] of hybrid mesons are zero as these quantities are proportional to $|R(0)|^2$ as written in these references.

We are grateful to the Higher education Commission of Pakistan for their financial support no. 17-5-3 (Ps3-212) HEC/Sch/2006.

References

1. C. McNeile, Nucl. Phys. A **711**, 303 (2002).
2. The COMPASS Collaboration (M. Alekseev *et al.*), Phys. Rev. Lett. **104**, 241803 (2010) The COMPASS Collaboration (B. Grube *et al.*), arXiv:1002.1272 [hep-ex] (2010).
3. VES Collaboration (Yu.P. Gouz *et al.*), AIP Conf. Proc. **272**, 572 (1993).
4. VES Collaboration (Yu.A. Khokholov *et al.*), Nucl. Phys. A **663**, 596 (2000).
5. VES Collaboration (A. Zaitsev *et al.*), Nucl. Phys. A **675**, 155c (2000).
6. E852 Collaboration (G.S. Adams *et al.*), Phys. Rev. Lett. **81**, 5760 (1998).
7. E852 Collaboration (S.U. Chung *et al.*), Phys. Rev. D **65**, 072001 (2002).
8. E852 Collaboration (E.I. Ivanov *et al.*), Phys. Rev. Lett. **86**, 3977 (2001).
9. E852 Collaboration (J. Kuhn *et al.*), Phys. Lett. B **595**, 109 (2004).
10. E852 Collaboration (M. Lu *et al.*), Phys. Rev. Lett. **94**, 032002 (2005).
11. C.A. Baker *et al.*, Phys. Lett. B **563**, 140 (2003).
12. K.J. Juge, J. Kuti, C. Morningstar, AIP Conf. Proc. **688**, 193 (2003).
13. C.J. Morningstar, M. Peardon, Phys. Rev. D **56**, 4043 (1997).
14. S. Collins, C.T.H. Davies, G. Bali, Nucl. Phys. Proc. Suppl. **63**, 335 (1998).
15. B. Ananthanarayan, I. Caprini, G. Colangelo, J. Gasser, H. Leutwyler, Phys. Lett. B **602**, 218 (2004).
16. S.I. Kruglov, Phys. Rev. D **60**, 116009 (1999).
17. B. Patel, P.C. Vinodkumar, J. Phys. G **36**, 035003 (2009).
18. C.H. Chaug, C.F. Qiao, J.X. Wang, Phys. Rev. D **57**, 4035 (1998).
19. D.H. Perkins, *Introduction to High Energy Physics* (Addison-Wesley, 1987).
20. G.S. Bali *et al.*, Phys. Rev. D **62**, 054503 (2000).
21. G.S. Bali, Phys. Rep. **343**, 1 (2001).
22. C. Alexandrou, P. de Forcrand, O. John, Nucl. Phys. B **119**, 667 (2003).
23. T. Barnes, S. Godfrey, E.S. Swanson, Phys. Rev. D **72**, 054026 (2005).
24. C.F. Gerald, P.O. Wheatley, *Applied Numerical Method* (Dorling Kindrsley Pvt. Ltd., 1999).
25. Dr. V.N. Vedamurthy, Dr. N.Ch. Sniyengar, *Applied Numerical Methods* (Vikas Publishing House Pvt. Ltd., 1998).
26. M.M. Feyli, Proc. World Acad. Sci. Eng. Technol. **71**, 565 (2010).
27. K.J. Juge, J. Kuti, C.J. Morningstar, Phys. Rev. Lett. **82**, 4400 (1999).
28. K.J. Juge, J. Kuti, C.J. Morningstar, Nucl. Phys. Proc. Suppl. **63**, 326 (1998).
29. E.S. Swanson, talk presented at *JLAB/INT Workshop on Gluonic Excitations, Newport News, Virgina* (2003) arXiv:hep-ph/0605152.
30. N. Isgur, J. Paton, Phys. Rev. D **31**, 2910 (1985).
31. J. Weinstein, N. Isgur, Phys. Rev. D **41**, 2236 (1990).
32. N. Akbar, B. Masud, arXive: 1102.1690 (2011).
33. M.I. Jamil, B. Masud, Eur. Phys. J. A **47**, 33 (2011).
34. F. Buisseretа, V. Mathieua, C. Semaya, B. Silvestre-Brac, Eur. Phys. J. A **32**, 123 (2007).
35. Cheuk-Yin Wong, E.S. Swanson, T. Barnes, Phys. Rev. C **65**, 014903 (2002).
36. K.K. Seth, J. Phys. Conf. Ser. **9**, 32 (2005).
37. S. Godfrey, *Flavor Physics and CP Violation Conference, Vancouver*, ECONF C 060409:015 (2006), arXiv:hep-ph/0605152.
38. P. Hasenfratz, R.R. Horgan, J. Kuti, J.M. Richard, Phys. Lett. B **95**, 299 (1980).
39. J. Merlin, J. Paton, J. Phys. G **11**, 439 (1985).
40. N. Isgur, J. Paton, Phys. Rev. D **31**, 2910 (1985).
41. J. Merlin, J. Paton, Phys. Rev. D **35**, 1668 (1987).
42. L.A. Griffiths, C. Michael, P.E.L. Rakow, Phys. Lett. B **129**, 351 (1983).
43. S. Perantonis, C. Michael, Nucl. Phys. B **347**, 854 (1990).
44. F. Iddir, L. Semlala, arxive hep-ph/0611165v2 (2006).
45. T. Manke *et al.*, Phys. Rev. Lett. **82**, 4396 (1999).
46. Z.H. Mei, X.Q. Luo, Int. J. Mod. Phys. A **18**, 5713 (2003).
47. Y. Liu, X.Q. Luo, Phys. Rev. D **73**, 054510 (2006).
48. X. Liu, T. Manke, arXive:hep-lat/0210030.